Boltzmann approach to the transversal spin Seebeck effect

Im Fachbereich Physik der
Freien Universität Berlin
eingereichte

Dissertation

von

Francis Benjamin Wilken

Berlin, im Juni 2016

1. Gutachterin: Prof. Dr. Tamara S. Nunner
2. Gutachter: Prof. Dr. Piet W. Brouwer

Tag der Einreichung: 9. Juni 2016
Tag der Disputation: 18. Juli 2016

Selbstständigkeitserklärung

Hiermit versichere ich, dass ich in meiner Dissertation alle Hilfsmittel und Hilfen angegeben habe, und auf dieser Grundlage die Arbeit selbstständig verfasst habe. Diese Arbeit habe ich nicht schon einmal in einem früheren Promotionsverfahren eingereicht.

Berlin, 8. Juni 2016

Contents

1 Introduction

1.1 Spintronics

"Spintronic" is a compound word out of "spin" and "electronic". In regular electronic devices, the information is transported and stored by electronic charge. In the field of spintronic devices, the information is transported and stored by spin (or magnetization) and no longer by electronic charge. One benefit of this technology is that one needs less energy to transport information by spin than by electronic charge. A requirement of this technology is, that one has to find materials in which the electronic spin is stable for a long time and does not flip to equilibrium. A spin current can be generated in a conductor or semiconductor, when more electrons with spin up than with spin down move to one direction. Thus, the current for spin up electrons and the current for spin down electrons are different. Hence, there is a net spin current.

One milestone in the field of spintronic research was the discovery of the giant magneto resistance as reported in between 1986 and 1989 [1, 2, 3]. In 2007, Albert Fert and Peter Grünberg got the Nobel price for the parallel discovery. Here, one considers a junction out of a normal metal, a ferromagnet, a normal metal, another ferromagnet and again a normal metal. For electrons with a spin polarization parallel to the majority electron spin orientation in the ferromagnets, the resistance is small, and large for antiparallel configuration. One has to mention that the magnetic moment of the electrons is anti parallel to the spin orientation. Thus, when both magnets are polarized in the same direction, the resistance is small, because the electrons with parallel spin orientation are able to propagate easily through both of the magnets. If the magnets are polarized antiparallel, for every electron there is a magnet with a high resistivity and the entire resistivity is very large. Without an external magnetic field, the magnetization of the magnets tends to be anti parallel. On the other hand, the magnetization of the magnets becomes parallel by an applied external magnetic field. The difference between the resistance in these two cases divided by the resistance without a magnetic field is called giant magneto resistance (GMR). The GMR-effect is used in hard disk drives or in sensors for magnetic fields.

The discovery of the Spin Hall effect marks another milestone in the field of spintronic research. If one applies an electric field on a conductor or a semiconductor, an electrical current will be induced. When the spin polarization is perpendicular to the current direction, a spin current will be induced in perpendicular direction because of spin-orbit interaction. The spin current direction is perpendicular to the electrical current and perpendicular to the spin-polarization. This effect was theoretically predicted in 1971 by M. I. D'yakonov and V. I. Perel' [4, 5]. In 1999, J. E. Hirsch gave the name to this effect [6]. The first observation of the Spin Hall effect at 30 Kelvin was reported in 2004 by Kato *et al.* [7]. Later, in 2005, other experiments from Wunderlich *et al.* [8] and Sih *et al.* [9] confirmed the existence of the Spin Hall effect. It is also able to invert the Spin Hall effect, called inverse Spin Hall effect. If there is a spin current with perpendicular spin-polarization, a charge current will be induced perpendicular to the direction of the spin current and perpendicular to the polarization of the spin current. This effect was first observed in 1984 by Bakun *et al.* [10]. Later, there were several measurements of the Spin Hall effect as well as of the inverse Spin Hall effect in semiconductors [11] and in metals [12, 13, 14]. The inverse spin Hall effect will be important in this thesis. Besides, the spin Hall effect is used in spin batteries and in spin transistors.

1.2 Spin Caloritronics and Spin Seebeck effect

1.2.1 Seebeck effect

In 1822, Thomas Johann Seebeck developed the thermoelectric effect or Seebeck effect [15] [16, p. 2 ff]. If one applies a temperature gradient to a conducting material, an electrical voltage U can be measured between the hot end and the cold end of the material. It is

$$U = S \cdot \Delta T \,, \tag{1.1}$$

where ΔT denotes the temperature difference between the two ends of the material and S denotes the material and size dependent Seebeck coefficient.

At first, there is a diffusion contribution to the Seebeck effect. The distribution of the charge carriers in general follows a Fermi-Dirac distribution (cf. Eq. (2.2)). On the hot end, in comparison to the cold end, there are more electrons with higher energy as well as there are less electrons with lower energy. There is a spatial diffusion of the charge carriers between the hot end and the cold end. Charge carriers with high energy also keep a higher kinetic energy and thus, the diffusion proceeds faster than for charge carriers with low kinetic energy. In the net effect, there are more charge carriers traveling from the hot end to the cold end than in the opposite direction. This force is called electromotoric force. Thus, if the charge carriers are not able to leave the material, there will be a charge accumulation. If the charge carriers are negatively charged electrons, there will be negative charge at the cold end and positive charge at the hot end. This will induce an electric field, driving against the electromotoric force until an equilibrium is reached.

Additionally, there is another effect, which drives the Seebeck voltage. This is a phonon drag contribution. When the temperature difference is applied, phonons are propagating from the hot end to the cold end. When they scatter with electrons, momentum and energy will be transfered to the electrons. Thus, the electrons also start to propagate in the direction of the cold end. Similarly, there will be a charge accumulation at the cold end and a lack of charge at the hot end.

In practical experiments, one takes two different metals as shown in figure 1a and connects them thermally at the hot end. The two cold ends will be at the same temperature and the voltage is measured between the cold ends. Thus, one is measuring the difference of the Seebeck voltage in metal A and the Seebeck voltage in metal B. The benefit of this measuring method is, that the two ends of the voltmeter are at the same temperature.

1.2.2 Spin Seebeck effect

In the same way as for the Hall effect, there exists a spin dependent version for the Seebeck effect, called Spin Seebeck effect. This effect was first observed by Uchida *et al.* at 300 K as reported in 2008 [17] and later in 2010 [18]. The setup for this experiment is depicted in figure 1b. Since there are different Seebeck coefficients for spin down and spin up conduction electrons, the net electromotoric force will be different for spin up and spin down electrons. Thus, a spin up accumulation will be found at the one end and a spin down accumulation at the other end. The chemical potential is a measure for the number of charge carriers. Thus, the chemical potentials for spin up electrons and for spin down electrons differ from each other at the ends of the magnet. The spin Seebeck coefficient is defined as [19]

$$S_{\mathrm{xy}} = \frac{E_{\mathrm{y}}}{\nabla_{\mathrm{x}} T} \,. \tag{1.2}$$

The value of this coefficient for a ferromagnetic semiconductor can be found in figure 2e of Ref. [19]. There is a behavior as a hyperbolic sine dependent on the position of the ferromagnetic stripe. A review of the experiments and theories reported until end of 2011 was written by Uchida *et al.* [20].

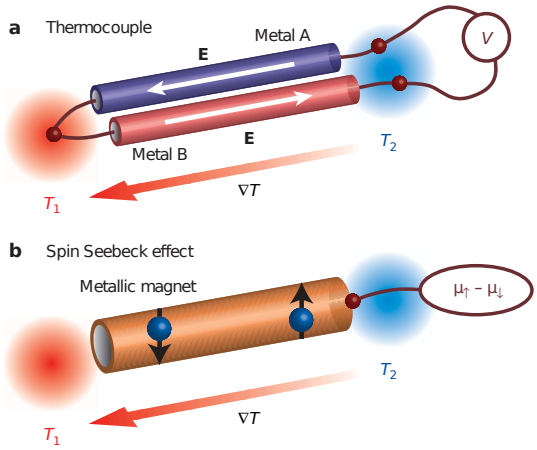

Figure 1: Figure taken from Uchida *et al.* [17]. (a) A thermocouple consists of two different metals, which are connected at the hot end at temperature T_1. The two cold ends are both at temperature T_2 and a voltage is measured between them. The resulting voltage is the difference between the Seebeck voltage of metal A and B. (b) Here, a temperature gradient is applied to a metallic ferromagnet resulting in a difference for the spin dependent chemical potentials.

Experimentally, the spin accumulation at the ends of the metal is detected via the inverse spin Hall effect. In figure 2a, the setup of the experiment by Uchida *et al.* in 2008 [17] including platinum stripes for the measurement of the inverse spin Hall voltage is shown. On top of the sapphire substrate, there is a ferromagnetic film, which consists of $Ni_{81}Fe_{19}$ (permalloy). In addition, on top of the ferromagnet, there are two platinum stripes. The experimental setup, where the generated spin current is perpendicular to the applied temperature gradient, is called transverse spin Seebeck effect. When it is parallel to the applied temperature gradient, it is called longitudinal spin Seebeck effect. In case of the transverse spin Seebeck effect, there will be a spin down accumulation at the one end and a spin up accumulation at the other end. Uchida *et al.* state that the outcome of this accumulation is a spin current from the metallic magnet into the platinum. This spin current induces a charge current via the inverse spin Hall effect. Thus, there will be an electric field E_{SHE} along the platinum stripe which is perpendicular to the spin current and to the polarization σ of the electrons. This electric field induces an electric voltage which can be measured. In figure 2b the chemical potential for spin up and spin down electrons is shown.

The spin current, which flows from the ferromagnet into the platinum, is dependent on the difference of the chemical potential for spin up electrons and spin down electrons. In figure 2b, one finds a linear behavior and a sign change in the middle of the sample. Since this chemical potential difference is proportional to the inverse spin Hall voltage, the behavior remains in the inverse spin Hall voltage as one can find in figure 3. Uchida *et al.* also found a linear spatial variation and a sign change in the middle of the setup. The magnitude of the observed Spin Seebeck voltage increases when the applied temperature difference is enhanced. One has to emphasize, that the resulting transverse spin Seebeck voltage is at the order of microvolts. This is roughly the same order as for the normal Seebeck effect.

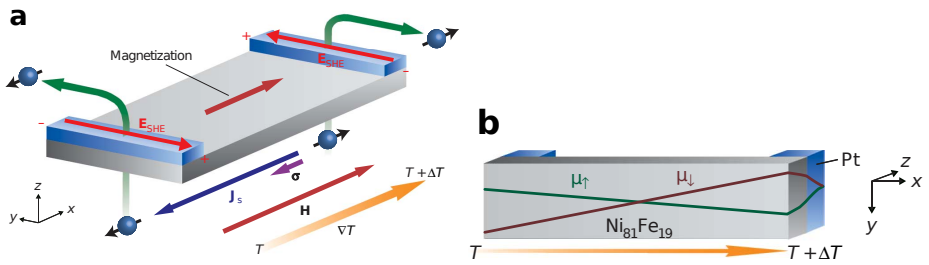

Figure 2: Figure taken from Uchida *et al.* [17]. (a) The experimental setup is shown in this figure. The external field H drives the magnetization of the ferromagnet. The spin current from the metal (gray) into the platinum (blue) induces an electric field E_{SHE} via the inverse spin Hall effect. The dimensions of the ferromagnet are $d_{\mathsf{FM}} = 20$ nm thickness, $L_{\mathsf{FM}} = 6$ mm length and $w_{\mathsf{FM}} = 4$ mm width. The platinum stripes are $d_{\mathsf{Pt}} = 10$ nm thick, $L_{\mathsf{Pt}} = 100$ µm long and $w_{\mathsf{Pt}} = 4$ mm wide. (b) The space dependent chemical potential is plotted for spin up electrons and spin down electrons.

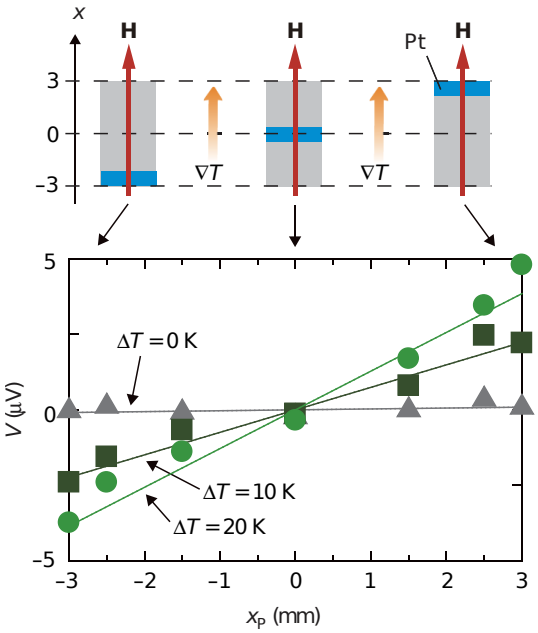

Figure 3: Figure taken from Uchida *et al.* [17]. Here, one finds the voltage V from the inverse spin Hall effect dependent on the position x_p of the platinum stripe on the magnet and for different applied temperature differences. The larger the temperature difference is the larger the inverse spin Hall voltage is.

At the same time, as reported in 2010, Uchida *et al.* [21] made measurements on the transverse spin Seebeck effect using an insulating ferrimagnet. It is remarkable, that the transverse spin Seebeck effect is also present in ferrimagnetic insulators. The ferrimagnet consists of $LaY_2Fe_5O_{12}$, wherein only phonons and magnons are able to propagate. Thus, the effect can not be caused by a difference in the spin chemical potential for spin up and spin down electrons. It must be mediated by magnons in the ferrimagnet. This was unexpected until then. Electrons are not able to propagate. As the substrate, they used $Gd_3Ga_5O_{12}$, which is insulating and non magnetic. Thus, only phonons are able to propagate in the substrate. On top of the $LaY_2Fe_5O_{12}$-film, there are stripes of platinum for detecting the spin Seebeck voltage. The setup of the experiment is shown in figure 4. In this figure,

the conversion mechanism is shown. The magnetization of the $LaY_2Fe_5O_{12}$ is directed into the negative x-direction. Since the magnetization of magnons is polarized into the opposite direction, here their magnetization is polarized into the positive x-direction. The magnetic moment is transfered to the electrons in the platinum. Since the magnetic moment of the electron is antiparallel to their spin, the spin of the electrons is polarized in the negative x-direction, propagating in the z-direction. Via the inverse spin Hall effect, the electrons in the platinum are driving into the negative y-direction. Thus, an electric field will build up in the positive y-direction as shown in figure 4.

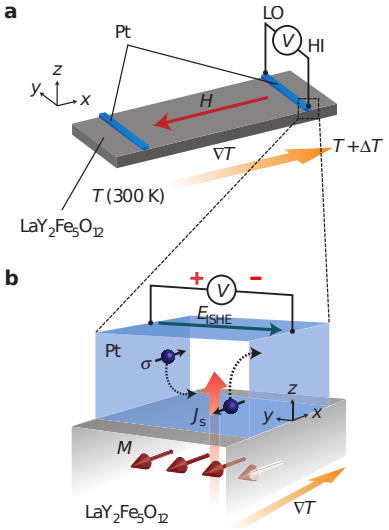

Figure 4: Figure taken from Uchida *et al.* [21] and modified. This is a schematical setup for measuring the transverse spin Seebeck effect by using an insulating material as ferrimagnet (here $LaY_2Fe_5O_{12}$). On top, there is a platinum stripe. The spin current is sketched and the transformation to the transverse spin Seebeck voltage via the inverse spin Hall effect is shown. The dimensions of the ferrimagnet are $d_{\mathrm{FM}} = 3.9$ µm thickness, $L_{\mathrm{FM}} = 8$ mm length and $w_{\mathrm{FM}} = 4$ mm width. The platinum stripes are $d_{\mathrm{Pt}} = 15$ nm thick, $L_{\mathrm{Pt}} = 0.1$ mm long and $w_{\mathrm{Pt}} = 4$ mm wide.

Later, as reported in 2010, the transverse spin Seebeck effect was also observed in ferromagnetic semiconductors by Jaworski *et al.* [19]. Here, they took $Ga_{1-s}Ms_sAs$ as magnetic semiconductor and semi insulating GaAs as substrate. In order to obtain some information about the mechanism of the Spin Seebeck effect, Jaworski *et al.* made a scratch on the ferromagnetic semiconductor as shown in figure 5a. The scratch is only present in the ferromagnetic insulator and not present in the substrate. In figure 5b, the spin Seebeck coefficient with and without the scratch is shown. The difference in the results is small, which is at first glance inconsistent to explanations to previous experiments. Jaworski *et al.* explained the effect, either there is a magnetic dipole coupling over the scratch or there is a coupling via the phonons in the substrate. This is a first hint, that the substrate is very important for the explanation of the transverse spin Seebeck effect, as we will see later. In the present thesis, we will explicitly consider the role of the substrate for the Spin Seebeck effect. In chapter 3 we will calculate the phonon temperature distribution in the substrate and then analyze the local influence on the magnon temperature distribution in an insulating ferrimagnet in chapter 4.

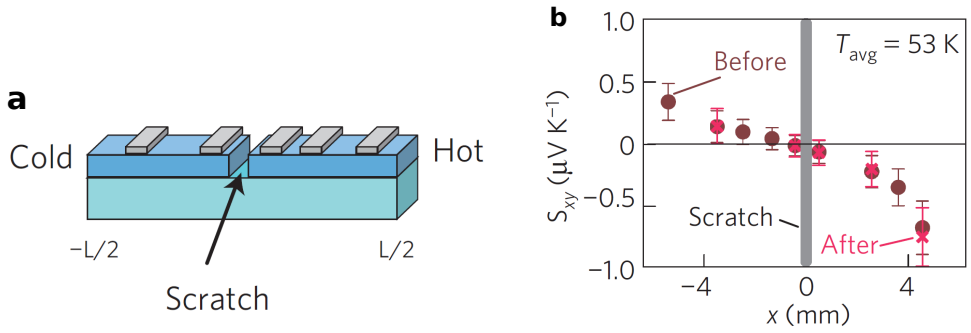

Figure 5: Figure taken from Jaworski *et al.* [19]. (a) This is a setup of the experiment including a scratch on the ferromagnetic semiconductor. The scratch is not present in the substrate. The dimensions of the ferromagnet is $d_{\mathrm{FM}} = 30$ nm thickness, $L_{\mathrm{FM}} = 10 - 25$ mm length and $w_{\mathrm{FM}} = 3 - 5$ mm width. The platinum stripes are $d_{\mathrm{Pt}} = 20$ nm thick, $L_{\mathrm{Pt}} = 0.25$ mm long and $w_{\mathrm{Pt}} = 3 - 5$ mm wide. (b) Spatial variation for the spin Seebeck coefficient without (Before) and with (After) the scratch. The gray line represents the scratch area.

As discussed above, Jaworski *et al.* [19] investigated the transverse spin Seebeck effect and made a scratch in the ferromagnetic layer. There were no differences in the results with and without the scratch. This initiated Uchida *et al.* [22] to make measurements, where the ferromagnetic film has the same small surface as the platinum stripe. In figure 6 one finds the setup of their experiment. They again used conducting $Ni_{81}Fe_{19}$ as the ferromagnetic layer and sapphire as substrate.

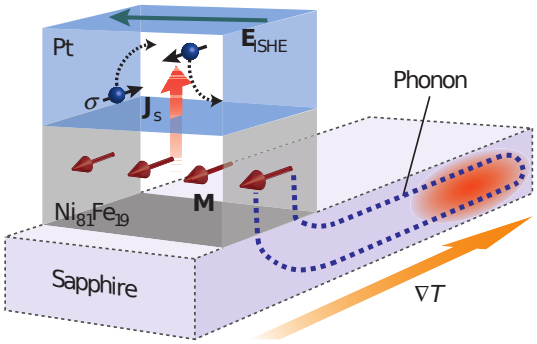

Figure 6: Figure taken from Uchida *et al.* [22]. This is a setup of the experiment, while the stripe of the conducting ferromagnet $Ni_{81}Fe_{19}$ has the same area as the platinum stripe on top of it. The length of the sapphire is much larger than the length of the $Ni_{81}Fe_{19}$ and the platinum. The substrate is $L_{\mathrm{sp}} = 10$ mm long, $w_{\mathrm{sp}} = 3$ mm wide and $d_{\mathrm{sp}} = 0.5$ mm thick. The length of the ferromagnet and the platinum is $L_{\mathrm{FM}} = L_{\mathrm{Pt}} = 0.1$ mm, its width is $w_{\mathrm{FM}} = w_{\mathrm{Pt}} = 3$ mm. The thickness of the ferromagnet is $d_{\mathrm{FM}} = 20$ nm and the thickness of the platinum is $d_{\mathrm{Pt}} = 10$ nm, respectively.

If they compare their result [22] with previous work [17] with a setup as in figure 2, they found a 10 times smaller result for the spin Seebeck voltage, but they are still finite. Additionally, they performed the same experiment again and replaced the substrate by glass. There, they found nearly no spin Seebeck voltage (cf. figure 3c of Ref. [22]). This is an important hint that the substrate plays an important role for the transverse spin Seebeck

effect.

In figure 3 of Ref. [21], the results for the transverse spin Seebeck voltage V are shown dependent on the position x_{Pt} of the platinum stripe on the $LaY_2Fe_5O_{12}$-film. Uchida *et al.* [21] also found a linear behavior and the sign change in the middle of the setup. The larger the applied temperature difference is, the larger the spin Seebeck voltage is.

As reported in 2010, Xiao *et al.* [23] formulated a first theory for explaining the transverse spin Seebeck effect. They considered a setup where a ferrimagnetic insulator of length L is positioned between two insulating and non-magnetic normal metals. Thus, magnons are only allowed to propagate in the ferrimagnet. In the calculation, one does not have to include conduction electrons. In all setups for the transverse Spin Seebeck effect, magnons are able to propagate in the magnet. On top of the magnet, there is a platinum stripe, while the width w of the insulating ferrimagnet and the platinum stripe are the same. The length L_{Pt} of the stripe is much smaller than the length of the insulating ferrimagnet ($L_{\mathrm{Pt}} < L$). In figure 1 of Ref. [23] one can find a figure of the setup. They made use of the Landau-Lifschitz-Gilbert equation and considered first the contact between the insulating ferrimagnet and the platinum stripe. Due to spin pumping there is a spin current from the ferrimagnet into the normal metal (platinum). Contrary, there is a fluctuation spin current in the opposite direction. Xiao *et al.* calculated the net spin current $\langle I_z \rangle$ and found the relation [23]

$$\langle I_z \rangle = L_s'(T_{\mathrm{F}}^{\mathrm{m}} - T_{\mathrm{N}})\,, \tag{1.3}$$

where L_s' denotes a material dependent parameter. Details to L_s' can be found in Ref. [23]. Furthermore, T_{N} denotes the temperature of the electrons in the normal metal (platinum), which is assumed to be equal to the phonon temperature due to strong electron-phonon coupling. Additionally, $T_{\mathrm{F}}^{\mathrm{m}}$ denotes the temperature of the magnons in the ferrimagnet. Xiao *et al.* assumed a strong coupling between the phonons in the ferrimagnet and the phonons in the platinum. Thus, their temperatures are equal and only the magnon temperature in the ferrimagnet deviates. The main result is, that the spin current is dependent on the temperature difference of magnons in the ferrimagnet and the electrons in the normal metal.

Subsequently, they considered the ferrimagnetic insulator of length L to be positioned between two insulating and non-magnetic normal metals. Extending the calculation of D. J. Sanders and D. Walton [24] and Xiao *et al.* [23], one finds

$$\Delta T_{\mathrm{mp}}(z) = \eta \frac{\sinh \frac{z}{\lambda}}{\sinh \frac{L}{2\lambda}} \Delta T \tag{1.4}$$

$$V_H = \xi \frac{\sinh \frac{z_c}{\lambda}}{\sinh \frac{L}{2\lambda}} \Delta T\,, \tag{1.5}$$

where $\Delta T_{\mathrm{mp}}(z)$ denotes the z-dependent ($-L/2 < z < L/2$) difference between magnon temperature and phonon temperature. The spin Seebeck voltage is denoted by V_H, while the platinum stripe sits at position z_c ($-L/2 < z_c < L/2$). The contact to the heat reservoirs are located at $z = \pm L/2$. ΔT is the phonon temperature difference between the left and right contact. The parameters ξ, η and λ are material dependent and the expressions can be found in Ref. [23]. The authors claim, that λ is in the order of millimeters (0.85 mm - 8.5 mm). This theory from Xiao *et al.* [23] is able to explain the experiments of Uchida *et al.* [17, 18, 21]. But in the experiment of Jaworski *et al.* [19], they made a scratch in the ferromagnetic film. Additionally, Uchida *et al.* [22] considered a very short ferromagnetic film. In both cases, this theory is not able to explain the measured transverse Spin Seebeck voltage, because they need a magnon push parallel to the z-axis. Later, there will be other

experiments which cannot be explained by this theory. This motivates us, to find a theory which is valid by including the scratch.

Adachi *et al.* [25, 26] formulated a linear response theory for an insulating ferrimagnet for the transverse spin Seebeck effect without a scratch. They found that the phonon contribution to the spin current I_s^{drag} is proportional to the phonon lifetime τ_{ph}

$$I_s^{\mathrm{drag}} \propto \tau_{\mathrm{ph}} \,. \tag{1.6}$$

This gives a hint to the discrepance of the spin Seebeck results for sapphire and glass as a substrate. The thermal phonon conductivity is proportional to the phonon lifetime. Thus, the curve progression of the spin Seebeck voltage follows the curve progression of the thermal phonon conductivity (cf. figure 3 of Ref. [25]). One has to mention, that the boundaries of the substrate and the ferrimagnetic film play an important role in their modeling. This motivates us to consider the boundaries as perfect heat reservoirs in our calculations in chapter 3. Adachi *et al.* also give a thought, how a finite spin Seebeck voltage will be generated, if one makes a scratch in the ferromagnetic film. Then, the phonon mediated effect will also be present in this case.

In 2011 Ohe *et al.* [27] reported about numerical calculations on the transverse spin Seebeck effect with a large film of a ferromagnetic insulator. They made use of the Landau-Lifshitz-Gilbert equation and found a linear spin Seebeck voltage with a sign change in the middle of the setup.

Uchida *et al.* [22, 28, 29] also investigated another setup of experiment. Here, the temperature gradient is perpendicular to the boundary surface area. The induced spin current in the platinum film is parallel to the temperature gradient. This effect in this configuration is called longitudinal spin Seebeck effect. The temperature gradient is created by two thermal heat baths with a different temperature [28, 29]. In another experiment Uchida *et al.* [22] used a piezoelectric actuator for producing phonons. The longitudinal spin Seebeck effect is better understood and more stable than the transverse Spin Seebeck effect. Thus, we concentrate on the transverse Spin Seebeck effect in this thesis.

As reported in 2011, Jaworski *et al.* [30] made measurements on the transverse spin Seebeck effect using a magnetic semiconductor (GaMnAs) film without a scratch. If one compares the temperature dependence of the spin Seebeck coefficient with the temperature dependence of the thermal conductivity of the insulating and non magnetic substrate (GaAs), one finds qualitatively the same curve progression. This is again a hint, that the effect is mainly influenced by the phonons of the substrate and we will analyze this in chapter 3.

As reported in 2013, Agrawal *et al.* [31] made a direct measurement of the magnon temperature in the transversal Spin Seebeck effect setup. They used the insulating and non magnetic gallium gadolinium garnet (GGG) as a substrate and yttrium iron garnet (YIG) as the ferrimagnetic and insulating film. A picture of the setup can be found in figure 1 of Ref. [31]. There are no platinum stripes on top of it. Both ends of the substrate are connected to Peltier elements, which generate the temperature difference and thus the temperature gradient. The equilibrium distribution of magnons is determined by the Bose-Einstein distribution (cf. Eq. (2.8)). Thus, when the temperature of the magnons becomes larger, there are more magnons present in the analyzed area. The presence of one magnon reduces the magnetization of the ferrimagnet by one Bohr magneton.

The magnon temperature is measured by using Brillouin light scattering. There, a laser light is spotted on the position, where one wants to measure the magnon temperature. One photon of the laser light absorbs one magnon out of the magnetic film and will be reflected. By measuring the frequency of the reflected photon, one can conclude how large

the temperature is, because the dispersion relation of the magnons is temperature dependent. In figure 7 one finds the results for the measured phonon and magnon temperature.

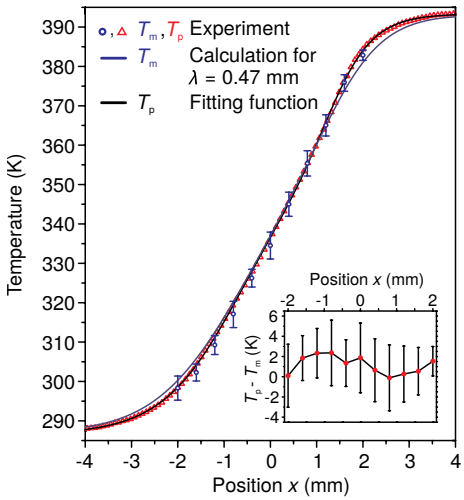

Figure 7: Figure taken from Agrawal *et al.* [31]. The measured phonon and magnon temperature dependent on the position at the sample are plotted. Additionally, the fit curve of the phonon temperature data is plotted. They calculated and plotted the magnon temperature by using the model out or Ref. [23] and used $\lambda = 0.47$ mm. The length of YIG-film and GGG substrate are $L_{\mathrm{YIG}} = L_{\mathrm{GGG}} = 10$ mm, its width are $w_{\mathrm{YIG}} = w_{\mathrm{GGG}} = 3$ mm. The thickness of the GGG-substrate is $d_{\mathrm{GGG}} = 0.5$ mm, while the thickness of the YIG-film is $d_{\mathrm{YIG}} = 6.7$ µm.

Surprisingly, the difference between magnon and phonon temperature is much smaller than predicted by Xiao *et al.* [23]. Xiao *et al.* predicted that λ is in the order of millimeters (0.85 mm - 8.5 mm). Here, they found a maximal value of $\lambda = 0.47$ mm, which is one magnitude smaller. If one would set in this measured parameter by Agrawal *et al.* into Eq. (25) of Ref. [23], one would find a voltage, which is more than one magnitude smaller and has a different curve progression than measured in experiments by Uchida *et al.* with a magnetic insulator [21]. This motivates us to neglect the effect described by Xiao *et al.* [23] or by D. J. Sanders and D. Walton [24] and search for other contributions to the transversal spin Seebeck effect.

Agrawal *et al.* [31] state, that their method is only applicable to detect short wavelength magnons ($k_m \gtrsim 10^6$ rad cm^{-1}). They cannot detect the temperature for long wavelength magnons ($k_m < 10^5$ rad cm^{-1}), which could be different to the short wavelength magnons and may drive the spin Seebeck voltage. This motivates us to analyze the wave-vector dependent phonon temperature in chapter 3. After that in chapter 4 and 5 we will analyze how the magnons are influenced by the phonons. There, we will find that long wavelength phonons will have a different temperature than short wavelength phonons. This influences the magnons, that long wavelength magnons will have a different temperature than short wavelength magnons. Hence, our calculations will qualitatively agree with the measurement of Agrawal *et al.*.

The role of the substrate is very important, just as reported by Tikhonov *et al.* [32] in 2013. They investigated the transverse spin Seebeck effect and made the first wave vector dependent calculations. A spatial non uniform phonon distribution in the substrate was found, which leads to a spatial non uniform temperature distribution. This non uniformity holds in the proximity of the heat bath reservoirs and leads to a finite longitudinal spin

Seebeck voltage. They estimated the transverse spin Seebeck voltage to be at the order of microvolts. Again, this is a hint that we have to consider the role of the substrate.

As reported in 2013, Schmid *et al.* [33] made measurements on the transverse spin Seebeck effect. Their results are at the order of nanovolts, which is much smaller than microvolts measured by Uchida *et al.* in Ref. [17, 22]. Among other things, they used permalloy ($Ni_{80}Fe_{20}$) as conducting ferromagnet onto insulating and non magnetic GaAs or MgO as substrate. On figure 4 of Ref. [33] one finds the results for the spin Seebeck voltage. Furthermore Schmid *et al.* found finite values when there is no temperature difference applied to the substrate. Thus, they claim, there must be a different thermoelectric mechanism, which explains the result.

To investigate the role of the substrate, Schmid *et al.* made the same measurements with GaAs as a substrate and taking the same size for the substrate (see supplemental material of Ref. [33]). The results for the spin Seebeck voltage are not different to using MgO as a substrate. Additionally they made measurements on MgO as a substrate, but with copper stripes in lieu of platinum stripes (see supplemental material of Ref. [33]). Copper has a much lower spin Hall angle, why one would expect a much smaller signal for the spin Seebeck voltage. But again, they found the same magnitude and behavior in the spin Seebeck voltage. This emphasizes, that there must be a different thermoelectric mechanism, which explains the behavior of the result. Schmid *et al.* state [33], that the transversal spin Seebeck effect cannot be detected in their detection limit. This contradiction to previous measurements motivates us to investigate the transversal spin Seebeck effect theoretically.

Actually, there are more publications reporting a small or a vanishing transverse spin Seebeck voltage. Huang *et al.* [34] did not reproduce the results in a metal from Uchida *et al.* [17]. They found, that the voltage is strongly dependent on the distance to the heater. This approves us to include the heat baths in our calculation and we will model them as perfect heat reservoirs.

Avery *et al.* [35] claim, that their transverse spin Seebeck voltage in a permalloy and nickel films is at least one order of magnitudes smaller than measured in experiments before. Meier *et al.* [36] made measurements with metallic and ferromagnetic permalloy ($Ni_{80}Fe_{20}$) film on insulating MgO or sapphire as substrate. In the platinum stripes on top, they just found a voltage which can be attributed to the planar Nernst effect and not to the transverse Spin Seebeck effect. Beyond, they found when there is a temperature gradient which is perpendicular to the permalloy area, then there will be a finite voltage. Bui *et al.* [37] investigated the transverse spin Seebeck effect by using half-metallic and ferromagnetic $La_{2/3}Sr_{1/3}MnO_3$ and $SrTiO_3$ as a substrate (see supplemental material of Ref. [37]). Only the planar and anomalous Nernst effect was observed in their experiments. They claim, that they did not find a contribution from the transverse spin Seebeck effect. The transverse spin Seebeck effect with semi-conductors (GaMnAs) was also investigated by Soldatov *et al.* [38]. Here, GaAs is used as a substrate. On top, there are platinum stripes. They claim, that the contribution from the transverse spin Seebeck effect to the measured voltage is negligible.

Meier *et al.* [39] investigated the transverse spin Seebeck effect by using ferrimagnetic and insulating YIG ($Y_3Fe_5O_{12}$) as well as NFO ($NiFe_2O_4$). Here, GGG ($Gd_3Ga_5O_{12}$) is used as a substrate. First, they made measurements by using gold bonding wires which is 25 µm thin to detect the spin Seebeck voltage. Then, no signal was found in the order of microvolts. After that, they used wolfram needles with a contact area of 0.003 mm^2 for detecting the spin Seebeck voltage. Again, there was no spin Seebeck voltage in the order of microvolts. Surprisingly, when they increased the contact area of the wolfram needles up to 0.27 mm^2, there was a voltage measured in the order of microvolts. Meier *et al.* [39] found, that the

signal becomes larger, when the temperature difference of the contact needles is larger as well as the signal also becomes larger, when the contact area of the wolfram needles is increased. Because the wolfram needles have a temperature other than that in the substrate, there is a temperature gradient perpendicular to the area of the ferromagnet. This temperature gradient influences a longitudinal spin Seebeck effect, which then can be measured. The signature of the measured signal can look like a transverse spin Seebeck effect. Besides, one has to mention, that this effect would hold, if one makes a scratch into the ferromagnetic film. Thus, one really should be careful when interpreting spin Seebeck voltage signals.

Shestakov *et al.* [40] investigated the transversal spin Seebeck effect and found that a parasitic external magnetic field leads to a signature which can be wrongly interpreted as transverse spin Seebeck signal. Normally in the experiment, the direction of the external magnetic field is fixed. Starting at a large positive magnetic field intensity, the intensity will be reduced, passing through the zero and finishing at a large negative magnetic field intensity and an antiparallel direction. When there is an additional magnetic field showing in a fixed direction and not varied in the field strength, the summation of both fields is not passing through the zero. In addition the starting direction of the summation fields is not antiparallel to the summation of the finishing field.

The contradictory measurements of the transverse spin Seebeck voltage in experiments motivate us, to find a theory which clarifies the contradictions. There are also theories, which only explain a part of the experiments. Here, we want to fill the gap. This we do by using the Boltzmann equation.

The theories of Sanders and Walton [24] and Xiao *et al.* [23] only explain the effect with a continuous film of ferromagnet as done by Uchida *et al.* [17, 18, 21]. Their theories do not explain the transverse spin Seebeck voltage if one makes a scratch in the ferromagnetic film as done by Jaworski *et al.* [19] and later in similar ways by Uchida *et al.* [22]. Additionally, measurements of Agrawal *et al.* [31] claim the effect to be small. In reports of Schmid *et al.* [33] and in other reports, the measured transverse spin Seebeck effect is small. This is a contradiction to the experiments of Uchida *et al.* [17, 18, 21]. Because of that, we want to develop a theory to find out, how large the transverse spin Seebeck voltage should be.

1.3 Outline of this thesis

In chapter 2, we present methods of transport theory, which we will use in this thesis. The method of quasi particles and the Boltzmann equation are introduced. After that, we present the relaxation time approximation, which is a useful approximation to solve the Boltzmann equation. We will use these methods in chapter 3, where we will investigate the pure phonon problem. There, a temperature difference is applied to a insulating and non-magnetic substrate and we will calculate the space dependent temperature and phonon density. In chapter 4, we will investigate a thin and insulating but ferrimagnetic film (out of $Y_3Fe_5O_{12}$) on top of the substrate. Since the ferrimagnetic film is thin compared to the substrate, we claim that the phonons are approximately not influenced by the magnons. Instead, the magnons are influenced by the phonons via phonon-magnon interaction. This influence will be calculated in chapter 4. Beyond, we will add the magnon-magnon interaction. Its influence will be calculated in chapter 5. In chapter 6, we will investigate a junction out of a ferrimagnet and a normal metal. The spin current will be calculated, which is created by magnons at a different temperature. The results are presented and discussed in chapter 7. Finally in chapter 8, we will summarize the results and give an outlook on potential future research related to the content of this thesis.

2 Methods of transport theory

2.1 Method of quasi particles

In the entire thesis we work with the Boltzmann equation. The Boltzmann equation is a statistical equation and describes the evolution of the phase space density inside a medium and finds application in many fields of physical research. Especially, the Boltzmann equation is appropriate to describe transport phenomena of quasi particles in solids. A quasi particle is a theoretical exemplary description of an elementary excitation in a many-body-system, for instance inside a solid. The benefit of quasi particles is, that you can describe them as classical particles. They exhibit a quasi particle mass and are able to scatter with other particles and quasi particles. Additionally in these scattering events, conservation of energy and momentum needs to be fulfilled like in classical mechanics. But for some quasi particles, there is a small difference in momentum conservation. The quasi particle momentum conservation needs to be fulfilled up to a reciprocal lattice vector. Quasi particles also exhibit a dispersion relation, which can be different for different types of quasi particles. Lew Dawidowitsch Landau was the first physicist, who introduced the concept of quasi particles.

In the thesis, we will work with electrons, phonons and magnons. Electrons will be described with the theory of the free electron gas. In this theory, which is appropriate for a metallic conductor, the solid is composed out of metal ions and valence electrons. The ions are fixed and the valence electrons are able to propagate through the solid like free particles. A homogeneous background charge is created by the ions. The valence electrons have an energy level close to the Fermi energy. In the model, the electrons have a quadratic energy dispersion relation

$$\epsilon_{\vec{k}} = \frac{|\vec{p}|^2}{2m^*} = \frac{\hbar^2 |\vec{k}|^2}{2m^*}\,, \tag{2.1}$$

while $\vec{p}$ denotes the momentum of the electron and $\vec{k} = \vec{p}/\hbar$ the corresponding De Broglie wave vector of the electron. The reduced mass is described by m^* and is a model parameter depending on the specific band structure of the metal. This parameter will be fixed in that way, that electrons close to the Fermi surface are well described. In statistics, electrons will be described by the Fermi-Dirac distribution for fermions. This reads

$$f_{\vec{k}}^{(0)} = \frac{1}{e^{(\epsilon_{\vec{k}} - \mu)/(k_\mathrm{B} T_0)} + 1}\,, \tag{2.2}$$

while $f_{\vec{k}}^{(0)}$ is the equilibrium electron particle density, μ denotes the chemical potential, k_B the Boltzmann constant and T_0 the average temperature for the electrons. The energy $\epsilon_{\vec{k}}$ is taken from Eq. (2.1).

Phonons are described by the method of quasi particles. In a solid, the atoms are arranged in a lattice structure, which is repetitive. Thus, the atoms are able to oscillate around their position in the lattice structure. These oscillation can be described by a quantum mechanical harmonic oscillator. In this model, the excitation energy is quantized. A phonon describes elementary excitation of a wave, which propagates through the solid using the atoms as a medium. In that way, energy, heat and sound can be transported through the solid. In our calculations, we are working with a simple dispersion relation. It is

$$\omega_{\vec{p}} = c_\mathrm{Ph}\,|\vec{p}|\,, \tag{2.3}$$

where $\vec{p}$ denotes the wave vector and c_Ph denotes the sound velocity. This linearity is true, as long as excitations are low enough. The statistics of the phonon is described by the

Bose-Einstein distribution for bosons. This reads

$$n_{\vec{p}}^{(0)} = \frac{1}{e^{\omega_{\vec{p}}/(k_\mathrm{B}T_0)} - 1}\,, \tag{2.4}$$

where $n_{\vec{p}}^{(0)}$ is the equilibrium phonon particle density and T_0 the average temperature for the phonons. For a deeper study of phonons, we refer to the book by G. P. Srivastava [41], especially to the chapter two, or the book by N. W. Ashcroft and N. D. Mermin [42].

In the model, every atom of the ferromagnet, ferrimagnet or other magnets carries a spin, which has an orientation. The spins are coupled to their nearest neighbor by dipole-dipole interaction and exchange interaction. Thus, the spins form a grind, in which spin waves are able to propagate. An elementary excitation of such a spin wave is called magnon. Magnons are also described by the method of quasi particles. In our case, we only consider magnons inside a ferrimagnet. The exact magnon dispersion is dependent on an external magnetic field and the local magnetization, see Eq. (7.9) on page 181 in Ref. [43].

$$\epsilon_{\vec{k}} = \sqrt{(\omega_\mathrm{H} + D_\mathrm{ex}k^2)(\omega_\mathrm{H} + D_\mathrm{ex}k^2 + \omega_\mathrm{M}\sin^2(\vartheta_k))}\,. \tag{2.5}$$

The parameter ϑ_k denotes the angle between the direction of the magnetization $\vec{M}$ and the vector $\vec{k}$. In our case, the dispersion of ferrimagnetic magnons will approximated by an quadratic term plus an offset ω_off. It is

$$\epsilon_{\vec{k}} \approx \omega_\mathrm{off} + D_\mathrm{ex}k^2 \qquad\qquad \omega_\mathrm{off} = \sqrt{\omega_\mathrm{H}(\omega_\mathrm{H} + \omega_\mathrm{M}\sin^2(\vartheta_k))}\,. \tag{2.6}$$

This equation is valid if $\omega_\mathrm{off} \ll D_\mathrm{ex}k^2$ and when $\omega_\mathrm{off} \gg D_\mathrm{ex}k^2$. If one sets $k = 0$ into Eq. (2.5) and into Eq. (2.6), one will find the same result. Additionally, if one assumes $\omega_\mathrm{off} \ll D_\mathrm{ex}k^2$ or $\omega_\mathrm{H}, \omega_\mathrm{M} \ll D_\mathrm{ex}k^2$, both expressions in Eq. (2.5) and in Eq. (2.6) can be approximated to $\epsilon_{\vec{k}} \approx D_\mathrm{ex}k^2$. Later, when we set in numbers into this expression, we will see good accordance for all wave numbers k between the exact result and the approximation. The other parameters in the dispersion relation are [43, p. 12 and 15]

$$\omega_\mathrm{H} = \gamma H_0 \qquad\qquad \omega_\mathrm{M} = 4\pi\gamma M_0\,. \tag{2.7}$$

The parameter H_0 denotes the field strength of an external magnetic field. M_0 denotes the field strength of the local magnetization of the ferrimagnet. Beyond, γ denotes the gyromagnetic ratio for the electron. Since magnons will be treated as bosons, the equilibrium magnon density is Bose-Einstein distributed. It is [43, p. 203]

$$f_{\vec{k}}^{(0)} = \frac{1}{e^{\epsilon_{\vec{k}}/(k_\mathrm{B}T_0)} - 1}\,, \tag{2.8}$$

while $f_{\vec{k}}^{(0)}$ denotes the magnon equilibrium particle density and T_0 the average temperature for the magnons. For a deeper study of magnons, we refer to the book by A. G. Gurevich and G. A. Melkov [43].

2.2 Boltzmann equation

The Boltzmann equation was developed by Ludwig Boltzmann in 1872 [44]. In quantum mechanics, position and momentum cannot be determined exactly, which is known as Heisenberg's uncertainty relation. Since the Boltzmann equation uses position and momentum

as well, the position and momentum must be that large, that the uncertainty from the Heisenberg's uncertainty relation becomes small. This is expressed in a formula [45]

$$p \gg \Delta p \geq \frac{\hbar}{\Delta r} \gg \frac{\hbar}{l}\,, \tag{2.9}$$

while p denotes the momentum of a (quasi-)particle, Δp the uncertainty of the momentum, $\hbar$ the Planck constant, l the length between two scattering events of a particle and Δr its uncertainty in the position. As introduced in the subsection 2.1, we assume that there is a (quasi-)particle distribution $n_{\vec{k}}$ dependent of the position, momentum and time. The Boltzmann equation describes the development of this distribution function. The distribution function can change by three different mechanisms: diffusion, external fields and scattering [46, p. 264 f]. One can evaluate the total time derivative of the distribution function

$$\frac{dn}{dt} = \frac{\partial n}{\partial t} + \frac{\partial \vec{r}}{\partial t} \cdot \vec{\nabla}_{\vec{r}}\, n + \frac{\partial \vec{k}}{\partial t} \cdot \vec{\nabla}_{\vec{k}}\, n = \left.\frac{\partial n}{\partial t}\right|_{\text{scattering}}\,, \tag{2.10}$$

while $\vec{\nabla}_{\vec{r}}$ denotes the gradient in $\vec{r}$-space and $\vec{\nabla}_{\vec{k}}$ the gradient in $\vec{k}$-space. In the stationary case, the partial derivative of the time vanishes $\partial n/\partial t = 0$. Additionally, we use $\partial \vec{r}/\partial t = \vec{v}_{\vec{k}}$. Thus, the equation reads

$$\vec{v}_{\vec{k}} \cdot \vec{\nabla}_{\vec{r}}\, n + \frac{\partial \vec{k}}{\partial t} \cdot \vec{\nabla}_{\vec{k}}\, n = \left.\frac{\partial n}{\partial t}\right|_{\text{scattering}}\,, \tag{2.11}$$

which is the standard form of the Boltzmann equation. The term on the right hand side of the Boltzmann equation is the collision term. This term describes the changing of the particle distribution due to scattering events. The first summand of this equation is the diffusion-term, where a local imbalance of the particle distribution tends to equalize itself. The second summand of this equations is the external field term. In [46, p. 97 and p. 264], one finds the expression for $\partial \vec{k}/\partial t$. It reads

$$\frac{\partial \vec{k}}{\partial t} = \frac{1}{\hbar}\frac{\partial \vec{p}}{\partial t} = \frac{1}{\hbar}\vec{F} \qquad\qquad \frac{\partial \vec{k}}{\partial t} = \frac{e}{\hbar}\left(\vec{E} + \frac{1}{c}\vec{v}_{\vec{k}} \times \vec{H}\right)\,, \tag{2.12}$$

while e denotes the elementary charge, $\hbar$ the Planck constant, $\vec{E}$ the strength of an external electrical field, c the velocity of light, $\vec{v}_{\vec{k}}$ the $\vec{k}$-dependent velocity of the particle and $\vec{H}$ the strength of an external magnetic field. The equation is valid for positive charge carriers. In case of electrons, one has to replace e by $-e$. The diffusion term can further be expressed by an external temperature gradient. It is

$$\vec{\nabla}_{\vec{r}}\, n = \frac{\partial n}{\partial T}\,\vec{\nabla}_{\vec{r}} T = -\frac{\epsilon_{\vec{k}}}{T}\frac{\partial n}{\partial \epsilon_{\vec{k}}}\,\vec{\nabla}_{\vec{r}} T\,, \tag{2.13}$$

which is valid for bosons as well as for fermions. Thus, an external temperature gradient can also cause an deviation in the particle density. Later, we will take the temperature as an open parameter, which will be determined in a resulting differential equation.

Now, we have to write down the collision term. This term is strongly dependent on the predominant interaction processes. There exists an recipe to set up the collision term for any interaction processes, which is a first order approximation in the interaction strength. We will exemplify this recipe in case of electron-phonon interaction. At the beginning, one has

to write down all the transition probabilities of the certain interaction. The collision term will be set up for a certain particle state $f_{\vec{k}}$. All interaction processes, which increase the particle distribution $f_{\vec{k}}$ arise with a positive sign inside the collision term. Consequentially, all interaction processes, which decrease the particle distribution $f_{\vec{k}}$ arise with a negative sign. The collision term for electron-phonon interaction reads [47, p. 19]

$$\left.\frac{\partial f_{\vec{k}}}{\partial t}\right|_{\text{scattering}} = \sum_{\vec{p}} \Big\{ W(e_{\vec{k}+\vec{p}} \to e_{\vec{k}} + \text{Ph}_{\vec{p}}) + W(e_{\vec{k}+\vec{p}} + \text{Ph}_{-\vec{p}} \to e_{\vec{k}}) \\ - W(e_{\vec{k}} + \text{Ph}_{\vec{p}} \to e_{\vec{k}+\vec{p}}) - W(e_{\vec{k}} \to e_{\vec{k}+\vec{p}} + \text{Ph}_{-\vec{p}}) \Big\} , \tag{2.14}$$

while $f_{\vec{k}}$ denotes the electron distribution function and $W(e_{\vec{k}+\vec{p}} \to e_{\vec{k}} + \text{Ph}_{\vec{p}})$ denotes the transition rate for the scattering process, where an incoming electron with momentum $\vec{k}+\vec{p}$ is converted into one electron with momentum $\vec{k}$ by emitting a phonon with momentum $\vec{p}$. Since this interaction increases the number of electrons with momentum $\vec{k}$, it arises with a plus sign. Analogously, we are able to write down the collision term for phonons. Thus, we find [47, p. 19]

$$\left.\frac{\partial n_{\vec{p}}}{\partial t}\right|_{\text{scattering}} = \sum_{\vec{k}} \Big\{ W(e_{\vec{k}+\vec{p}} \to e_{\vec{k}} + \text{Ph}_{\vec{p}}) - W(e_{\vec{k}} + \text{Ph}_{\vec{p}} \to e_{\vec{k}+\vec{p}}) \Big\} , \tag{2.15}$$

while $n_{\vec{p}}$ denotes the phonon distribution function. For writing out the transition probability, there also exists an recipe. The electron-phonon Hamilton operator in second quantization reads [47, p. 6]

$$H_{\text{el-ph}} = \sum_{\sigma,\vec{k},\vec{p}} M_{\vec{k},\vec{p}} (a^\dagger_{-\vec{p}} + a_{\vec{p}}) c^\dagger_{\vec{k}+\vec{p},\sigma} c_{\vec{k},\sigma} , \tag{2.16}$$

where $M_{\vec{k},\vec{p}}$ denotes the strength of the electron-phonon-coupling, $a_{\vec{p}}$ is an operator annihilating a phonon with momentum $\vec{p}$, $a^\dagger_{-\vec{p}}$ is an operator creating a phonon with momentum $-\vec{p}$, $c_{\vec{k},\sigma}$ is an operator annihilating an electron with momentum $\vec{k}$ and spin σ and $c^\dagger_{\vec{k}+\vec{p},\sigma}$ is an operator creating an electron with momentum $\vec{k}+\vec{p}$ and spin σ. The transition probability then follows Fermi's golden rule [47, p. 7]

$$W = \frac{2\pi}{\hbar} \left| \langle \text{f} | H_{\text{el-ph}} | \text{i} \rangle \right|^2 \delta(E_\text{f} - E_\text{i}) , \tag{2.17}$$

while $\langle \text{f}|$ denotes the final state with its energy E_f and $|\text{i}\rangle$ denotes the initial state with its energy E_i.

For writing down the matrix element with particle densities, there exist a recipe. We will explain this recipe by means of the electron phonon interaction in Eq. (2.18). Let $f_{\vec{k}}$ denote the electron distribution function for wave vector $\vec{k}$ and $n_{\vec{p}}$ denote the phonon distribution function for wave vector $\vec{p}$. In Eq. (2.18), the transition from one incoming electron with wave vector $\vec{k}+\vec{p}$ to one outgoing electron with wave vector $\vec{k}$ and one outgoing phonon with wave vector $\vec{p}$ is described. In general, for the incoming particle, its particle distribution occurs. The larger one state is occupied, the larger will be the transition probability. If there are two types of particle states involved in the incoming state, the product of both particle densities will arise. This is attended by the principle, that the interaction tends to equilibrate the states. In our example Eq. (2.18), the electron density $f_{\vec{k}+\vec{p}}$ with wave vector $\vec{k}+\vec{p}$ occurs. For the outgoing state, it will be the same rule unless the particle

densities arise with $(1 - f_{\vec{k}})$ for fermions and with $(1 + n_{\vec{p}})$ for bosons. Because of the Pauli principle for fermions, a state can be occupied maximal one time and the density $(1 - f_{\vec{k}})$ is always positive. Thus, for fermions, the larger the state is occupied, the lower will be the transition probability. This is similarly attended by the principle, that the interaction tends to equilibrate the states. In our example Eq. (2.18), for the outgoing electron, we write $(1 - f_{\vec{k}})$ and for the outgoing phonon we write $(1 + n_{\vec{p}})$. The recipe tells us, that both terms have to occur as factors. Now, we are able to write down, the transition probabilities out of Eq. (2.14) and find

$$W(e_{\vec{k}+\vec{p}} \to e_{\vec{k}} + \mathrm{Ph}_{\vec{p}}) = \frac{2\pi}{\hbar} \left| M_{\vec{k},\vec{p}} \right|^2 f_{\vec{k}+\vec{p}}(1 - f_{\vec{k}})(1 + n_{\vec{p}})\delta(\epsilon_{\vec{k}+\vec{p}} - \epsilon_{\vec{k}} - \omega_{\vec{p}}) \tag{2.18}$$

$$W(e_{\vec{k}+\vec{p}} + \mathrm{Ph}_{-\vec{p}} \to e_{\vec{k}}) = \frac{2\pi}{\hbar} \left| M_{\vec{k},\vec{p}} \right|^2 f_{\vec{k}+\vec{p}} n_{-\vec{p}}(1 - f_{\vec{k}})\delta(\epsilon_{\vec{k}+\vec{p}} + \omega_{-\vec{p}} - \epsilon_{\vec{k}}) \tag{2.19}$$

$$W(e_{\vec{k}} + \mathrm{Ph}_{\vec{p}} \to e_{\vec{k}+\vec{p}}) = \frac{2\pi}{\hbar} \left| M_{\vec{k},\vec{p}} \right|^2 f_{\vec{k}} n_{\vec{p}}(1 - f_{\vec{k}+\vec{p}})\delta(\epsilon_{\vec{k}} + \omega_{\vec{p}} - \epsilon_{\vec{k}+\vec{p}}) \tag{2.20}$$

$$W(e_{\vec{k}} \to e_{\vec{k}+\vec{p}} + \mathrm{Ph}_{-\vec{p}}) = \frac{2\pi}{\hbar} \left| M_{\vec{k},\vec{p}} \right|^2 f_{\vec{k}}(1 - f_{\vec{k}+\vec{p}})(1 + n_{-\vec{p}})\delta(\epsilon_{\vec{k}} - \epsilon_{\vec{k}+\vec{p}} - \omega_{-\vec{p}})\,. \tag{2.21}$$

Thus, we are able to write down the collision term for the electrons. We set Eq. (2.18) until Eq. (2.21) into Eq. (2.14) and find

$$\begin{aligned} \left.\frac{\partial f_{\vec{k}}}{\partial t}\right|_{\text{scattering}} = \frac{2\pi}{\hbar} \sum_{\vec{p}} \left| M_{\vec{k},\vec{p}} \right|^2 \Big[&\left\{ f_{\vec{k}+\vec{p}} + f_{\vec{k}+\vec{p}} n_{\vec{p}} - f_{\vec{k}+\vec{p}} f_{\vec{k}} - f_{\vec{k}} n_{\vec{p}} \right\} \delta(\epsilon_{\vec{k}+\vec{p}} - \epsilon_{\vec{k}} - \omega_{\vec{p}}) \\ &+ \left\{ f_{\vec{k}+\vec{p}} n_{-\vec{p}} + f_{\vec{k}} f_{\vec{k}+\vec{p}} - f_{\vec{k}} - f_{\vec{k}} n_{-\vec{p}} \right\} \delta(\epsilon_{\vec{k}+\vec{p}} + \omega_{-\vec{p}} - \epsilon_{\vec{k}}) \Big]\,. \end{aligned} \tag{2.22}$$

Additionally, we are able to write down the collision term for phonons. We set Eq. (2.18) and Eq. (2.20) into Eq. (2.15) and find

$$\left.\frac{\partial n_{\vec{p}}}{\partial t}\right|_{\text{scattering}} = \frac{2\pi}{\hbar} \sum_{\vec{k}} \left| M_{\vec{k},\vec{p}} \right|^2 \left[f_{\vec{k}+\vec{p}} + f_{\vec{k}+\vec{p}} n_{\vec{p}} - f_{\vec{k}+\vec{p}} f_{\vec{k}} - f_{\vec{k}} n_{\vec{p}} \right] \delta(\epsilon_{\vec{k}+\vec{p}} - \epsilon_{\vec{k}} - \omega_{\vec{p}})\,. \tag{2.23}$$

2.3 Relaxation time approximation

Often, there does not exist an exact analytic solution to the Boltzmann equation out of the upper section. We are able to write down the Boltzmann equation in a short way, called relaxation time approximation. It is

$$\frac{\partial f_{\vec{k}}}{\partial t} = -\frac{\delta f_{\vec{k}}}{\tau_{\vec{k}}} = -\frac{f_{\vec{k}} - f_{\vec{k}}^{(0)}}{\tau_{\vec{k}}}\,, \tag{2.24}$$

where $f_{\vec{k}}^{(0)}$ is the equilibrium density functions for the considered particles with wave vector $\vec{k}$. Additionally, $\tau_{\vec{k}}$ denotes the relaxation time. In principle, one can write down a relaxation time approximation for many interaction processes. Often, this can be done by linearizing the collision integral. Here, one divides the distribution function in the sum of one equilibrium part and one deviation part. In Ref. [47, p. 20 ff], the relaxation time is calculated for the electron-phonon interaction in a solid. The Boltzmann equation (2.24) is now solvable analytically. One finds

$$f_{\vec{k}} = f_{\vec{k}}^{(0)} + C \cdot e^{-t/\tau_{\vec{k}}}\,, \tag{2.25}$$

while C is an open parameter, which needs to be fixed by boundary conditions.

2.3.1 Electrical conductivity

Using the relaxation time approximation, we are able to solve simple transport applications. We will apply an electric field to a metal and calculate the electrical current and the electrical conductivity. We are taking Eq. (2.10), Eq. (2.12) and Eq. (2.24) by using $f_{\vec{k}}$ for the electron density distribution. Since Eq. (2.12) is composed for positive charge carriers, one has to replace e by $-e$ for electrons. Thus, the Boltzmann equation for electrons reads

$$-\frac{e}{\hbar}\vec{E}\cdot\vec{\nabla}_{\vec{k}}\,f_{\vec{k}}^{(0)} = -\frac{\delta f_{\vec{k}}}{\tau_{\vec{k}}}\,. \tag{2.26}$$

It is

$$\vec{\nabla}_{\vec{k}}\,f_{\vec{k}}^{(0)} = \frac{\partial f_{\vec{k}}^{(0)}}{\partial\epsilon_{\vec{k}}}\vec{\nabla}_{\vec{k}}\,\epsilon_{\vec{k}} = \frac{\partial f_{\vec{k}}^{(0)}}{\partial\epsilon_{\vec{k}}}\hbar\vec{v}_{\vec{k}}\,, \tag{2.27}$$

while this uses the expression for the quasi particle velocity [46, p. 92]

$$\vec{v}_{\vec{k}} = \frac{1}{\hbar}\vec{\nabla}_{\vec{k}}\,\epsilon_{\vec{k}}\,. \tag{2.28}$$

Thus, one finds for the Boltzmann equation

$$-e\frac{\partial f_{\vec{k}}^{(0)}}{\partial\epsilon_{\vec{k}}}\left(\vec{E}\cdot\vec{v}_{\vec{k}}\right) = -\frac{\delta f_{\vec{k}}}{\tau_{\vec{k}}}\,. \tag{2.29}$$

Since the equilibrium electron distribution function $f_{\vec{k}}^{(0)}$ does not depend on the direction of $\vec{k}$ and only depend on the absolute value, the following relation is true

$$\sum_{\vec{k}}^{\text{B.Z.}} e\,\vec{v}_{\vec{k}}\,f_{\vec{k}}^{(0)} = 0\,. \tag{2.30}$$

The charge current $\vec{j}_{\text{el}}$ will be measured for positive charge carriers, that is in technical current direction. Electrons will flow into the opposite direction. The charge current will then be calculated by

$$\vec{j}_{\text{el}} = \sum_{\vec{k}}^{\text{B.Z.}} e\,\vec{v}_{\vec{k}}\,f_{\vec{k}} = \sum_{\vec{k}}^{\text{B.Z.}} e\,\vec{v}_{\vec{k}}\,\delta f_{\vec{k}} = e^2\sum_{\vec{k}}^{\text{B.Z.}}\tau_{\vec{k}}\,\vec{v}_{\vec{k}}\left(\vec{E}\cdot\vec{v}_{\vec{k}}\right)\frac{\partial f_{\vec{k}}^{(0)}}{\partial\epsilon_{\vec{k}}}\,. \tag{2.31}$$

Remember, the term $(\partial f_{\vec{k}}^{(0)})/(\partial\epsilon_{\vec{k}})$ is always negative. Ohm's law is

$$\vec{j}_{\text{el}} = \overleftrightarrow{\sigma}\cdot\vec{E}\,. \tag{2.32}$$

Thus, we can write down the expression for the electrical conductivity

$$\overleftrightarrow{\sigma} = e^2\sum_{\vec{k}}^{\text{B.Z.}}\tau_{\vec{k}}\,\vec{v}_{\vec{k}}\otimes\vec{v}_{\vec{k}}\frac{\partial f_{\vec{k}}^{(0)}}{\partial\epsilon_{\vec{k}}}\,, \tag{2.33}$$

while the operator $\otimes$ denotes the outer product. The final electron distribution function consists of two summands, first the equilibrium density $f_{\vec{k}}^{(0)}$ (cf. Eq. (2.2)), and second the deviation $\delta f_{\vec{k}}$ (cf. Eq. (2.29)). The second summand is linear dependent on the electric field. It is $f_{\vec{k}} = f_{\vec{k}}^{(0)} + \delta f_{\vec{k}}$. In figure 8, the influence of an electric field on the band structure for the electrons is shown.

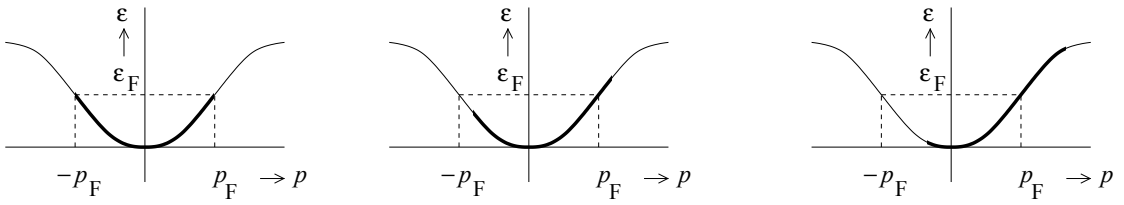

Figure 8: This figure is taken from [45], showing a band structure for an electronic system and demonstrating the impact of an applied electrical field on the occupation of electrons. The distribution function $f_{\vec{k}} = f_{\vec{k}}^{(0)} + \delta f_{\vec{k}}$ denotes, which state is occupied and which is not occupied. The thick line marks occupied states as well as the thin line marks unoccupied states. On the left picture, no electric field is applied. Thus, $\delta f_{\vec{k}} = 0$ and the electrons are filled symmetrically up to the Fermi energy. The velocity of the electrons is $v = p/m$. Since for every electron there is always a partner with opposite momentum, the net momentum and net velocity are zero. On the middle picture, a small electric field is applied, which is directed to the left. Thus, there is a momentum shift $\delta f_{\vec{k}}$ like described in Eq. (2.29). In that equation, the scalar product of electric field and velocity occurs. The term $(\partial f_{\vec{k}}^{(0)})/(\partial \epsilon_{\vec{k}})$ is always negative. Hence, when both vectors are parallel, the electron distribution is decreased and when both vectors are antiparallel, the electron distribution is increased. There are electrons, which do not have a partner with opposite momentum. Thus, for the electrons, there is a net momentum and a net velocity to the right. Since electrons carry negative charge, the positive net charge current is directed to the left. On the right picture, the electric field is increased again. Thus, the deviation from equilibrium becomes larger and the net current becomes larger too.

2.3.2 Thermal conductivity

Now, we want to consider a system, which is heated on the left side at temperature T_L and cooled on the right side at temperature T_R. In chapter 3, we consider a material, where only phonons are able to propagate. Hence we assume, that only phonons contribute to the heat transport. Thus, there will be a temperature gradient, which affects the phonon distribution function. The easiest description would be a one-dimensional Boltzmann approach on the thermodynamic level. The 1D-Boltzmann equation in relaxation time approximation form reads for phonons

$$\frac{\partial n_p^{(0)}}{\partial t} = \frac{\partial n_p^{(0)}}{\partial T}\frac{\partial T}{\partial x}\frac{\partial x}{\partial t} = -\frac{\omega_p}{T_0}\frac{\partial n_p^{(0)}}{\partial \omega_p} v_p \frac{\partial T}{\partial x} = -\frac{\delta n_p}{\tau_p}\,, \tag{2.34}$$

while ω_p denotes the phonon dispersion energy, v_p the phonon velocity, τ_p the phonon relaxation time, T the phonon temperature, $T_0 = (T_L + T_R)/2$ the room temperature and $n_p^{(0)}$ the unperturbed phonon distribution, which is of Bose-Einstein form like in Eq. (2.4). δn_p denotes the deviation from the Bose-Einstein distribution. One has to mention, that derivatives of this deviation are assumed to be small in the upper formula. The heat current can be calculated by

$$j_{tot} = \sum_p^{\text{B.Z.}} \omega_p v_p n_p = \sum_p^{\text{B.Z.}} \omega_p v_p (n_p^{(0)} + \delta n_p) = \sum_p^{\text{B.Z.}} \omega_p v_p (\delta n_p) = \sum_p^{\text{B.Z.}} v_p^2 \tau_p \frac{\omega_p^2}{T_0}\frac{\partial n_p^{(0)}}{\partial \omega_p}\frac{\partial T}{\partial x} = -\kappa \frac{\partial T}{\partial x}\,, \tag{2.35}$$

with

$$\kappa = -\sum_{p}^{\text{B.Z.}} v_p^2 \tau_p \frac{\omega_p^2}{T_0} \frac{\partial n_p^{(0)}}{\partial \omega_p} \,. \tag{2.36}$$

Remember, the term $(\partial n_p^{(0)})/(\partial \omega_p)$ is always negative. Here, v_p denotes the absolute value for the sound velocity. The sum over $\omega_p v_p n_p^{(0)}$ vanishes, because $n_p^{(0)}$, v_p are even and ω_p is odd in momentum p. By current conservation, the current derivative has to vanish

$$\frac{\partial j_{tot}}{\partial x} = 0 \,. \tag{2.37}$$

Thus, there is only a constant or linear solution to the differential equation for the temperature. Including the two boundary conditions $T(-L/2) = T_L = T_0 + \Delta T$ and analogously $T(L/2) = T_R = T_0 - \Delta T$, one finds for the temperature

$$T(x) = T_0 - \frac{2\Delta T}{L} x \,. \tag{2.38}$$

The current can then be calculated out of Eq. (2.35).

$$j_{tot} = \frac{2\Delta T}{L} \kappa \,. \tag{2.39}$$

In this simple model, there will be no perpendicular net current of phonons. Besides, in this calculation the temperature is uniform and not wave vector dependent. And there is no mechanism, which causes the sign change in the measured spin current.

2.3.3 Thermal conductivity in three dimensions

Now, we consider a three-dimensional Boltzmann approach on the level of temperatures. Here, we consider the temperature to be independent on the wave vector. But, the temperature will be space dependent. If one assumes the walls of the substrate to be perfect reflectors, they work as mirrors for the system. The mirrors are located opposite to each other. Furthermore, the mirrors at $y = 0$ and $y = B$ are modeled as perfect reflecting walls. This corresponds to the Eqs. (3.23) and (3.24). Analogously, one finds equations for the mirrors at $z = 0$ and $z = D$. Because of these mirror-walls, the system becomes periodic in $2B$ and $2D$. Since the boundary conditions at the heat reservoir is independent in y and z, the system becomes translation invariant in y and z. Thus, the system can be described effectively as infinite system in y- and z-direction with a periodicity and period length $2D$ and $2B$. At $x = -L/2$, there is one contact area to the ideal thermal heat bath at temperature T_L. Respectively, at $x = L/2$, theta is another contact area to the ideal thermal heat bath at temperature T_R. The 3D-Boltzmann equation with the relaxation time approximation reads

$$\frac{\partial n_{\vec{p}}}{\partial t} = \frac{\partial n_{\vec{p}}^{(0)}}{\partial T} \left[\frac{\partial T}{\partial x}\frac{\partial x}{\partial t} + \frac{\partial T}{\partial y}\frac{\partial y}{\partial t} + \frac{\partial T}{\partial z}\frac{\partial z}{\partial t} \right] = -\frac{\omega_{\vec{p}}}{T_0} \frac{\partial n_{\vec{p}}^{(0)}}{\partial \omega_{\vec{p}}} \vec{v}_{\vec{p}} \cdot \vec{\nabla} T = -\frac{\delta n_{\vec{p}}(\vec{r})}{\tau_{\vec{p}}} \,, \tag{2.40}$$

while $\omega_{\vec{p}}$ denotes the phonon dispersion energy, $\vec{v}_{\vec{p}}$ the phonon velocity, $\tau_{\vec{p}}$ the phonon relaxation time, T the phonon temperature, $T_0 = (T_L + T_R)/2$ the room temperature and $n_{\vec{p}}^{(0)}$ the unperturbed phonon distribution, which is of Bose-Einstein form (cf. Eq. (2.4)). The function $\delta n_{\vec{p}}$ denotes the deviation of the Bose-Einstein distribution, so

$$n_{\vec{p}} = n_{\vec{p}}^{(0)} + \delta n_{\vec{p}} \,. \tag{2.41}$$

One has to mention, that derivatives of this deviation $\delta n_{\vec{p}}$ are assumed to be small in Eq. (2.40). Now, we assume delta scatterers as the main and only scattering process in the bulk material. This implies

$$\tau_{\vec{p}} = \tau_p \,. \tag{2.42}$$

Because $\omega_{\vec{p}}$ and $n^{(0)}_{\vec{p}}$ are only dependent on the absolute value of $\vec{p}$, the following relation holds

$$\sum_{\vec{p}}^{\text{B.Z.}} \omega_{\vec{p}} \vec{v}_{\vec{p}} n^{(0)}_{\vec{p}} = \sum_{\vec{p}}^{\text{B.Z.}} \omega_p n^{(0)}_p \vec{v}_{\vec{p}} = \sum_{\vec{p}}^{\text{B.Z.}} \omega_p n^{(0)}_p v_p \cdot \hat{e}_r = 0 \,, \tag{2.43}$$

while $\hat{e}_r$ denotes the unit vector in $\vec{p}$ direction in spherical coordinates. For the last transformation we transformed the sum into spherical coordinates and used

$$\int_0^{2\pi} \int_0^{\pi} \sin(\vartheta)\, \hat{e}_r \, d\vartheta \, d\phi = 0 \,. \tag{2.44}$$

Now, v_0 denotes the sound velocity of the phonons. By writing $\vec{v}_{\vec{p}} = v_0 \, \hat{e}_{\vec{p}} = v_0 \, \vec{p}/p$ and using Eq. (2.40), the heat current can be calculated by

$$\begin{aligned}
\vec{j}_{tot} &= \sum_{\vec{p}}^{\text{B.Z.}} \omega_{\vec{p}} \vec{v}_{\vec{p}} n_{\vec{p}} = \sum_{\vec{p}}^{\text{B.Z.}} \omega_{\vec{p}} \vec{v}_{\vec{p}} (n^{(0)}_{\vec{p}} + \delta n_{\vec{p}}) = \sum_{\vec{p}}^{\text{B.Z.}} \omega_{\vec{p}} v_{\vec{p}} (\delta n_{\vec{p}}) \\
&= \sum_{\vec{p}}^{\text{B.Z.}} \tau_p \frac{\omega^2_{\vec{p}}}{T_0} \frac{\partial n^{(0)}_{\vec{p}}}{\partial \omega_{\vec{p}}} \vec{v}_{\vec{p}} \left(\vec{v}_{\vec{p}} \cdot \vec{\nabla} T \right) \\
&= \sum_{\vec{p}}^{\text{B.Z.}} \tau_p \frac{\omega^2_{\vec{p}}}{T_0} \frac{\partial n^{(0)}_{\vec{p}}}{\partial \omega_{\vec{p}}} \vec{v}_{\vec{p}} \frac{1}{p} \left[\frac{\partial T}{\partial x} v_0 p_x + \frac{\partial T}{\partial y} v_0 p_y + \frac{\partial T}{\partial z} v_0 p_z \right] .
\end{aligned} \tag{2.45}$$

If one now investigates the terms of being even or odd under inversion of p_x, p_y and p_z, one may cancel odd terms. Then, one finds

$$j_{tot,i} = \sum_{\vec{p}}^{\text{B.Z.}} \tau_p \frac{\omega^2_{\vec{p}}}{T_0} \frac{\partial n^{(0)}_{\vec{p}}}{\partial \omega_{\vec{p}}} \frac{v_0^2 p_i^2}{p^2} \frac{\partial T}{\partial x_i} = -\kappa_{3D} \frac{\partial T}{\partial x_i} \,, \tag{2.46}$$

with

$$\kappa_{3D} = -\sum_{\vec{p}}^{\text{B.Z.}} \tau_p \frac{\omega^2_{\vec{p}}}{T_0} \frac{\partial n^{(0)}_{\vec{p}}}{\partial \omega_{\vec{p}}} v_0^2 \frac{p_i^2}{p^2} = -\frac{1}{3} \sum_{\vec{p}}^{\text{B.Z.}} \tau_p \frac{\omega^2_{\vec{p}}}{T_0} \frac{\partial n^{(0)}_{\vec{p}}}{\partial \omega_{\vec{p}}} v_0^2 \,. \tag{2.47}$$

At the heat reservoirs, one finds the following property because of translational invariance of the system

$$\frac{\partial T(-L/2)}{\partial y} = \frac{\partial T(-L/2)}{\partial z} = 0 \qquad \frac{\partial T(L/2)}{\partial y} = \frac{\partial T(L/2)}{\partial z} = 0 \,. \tag{2.48}$$

This property must be conserved and the translation symmetry makes

$$\frac{\partial j_{tot}}{\partial y} = 0 \qquad \frac{\partial j_{tot}}{\partial z} = 0 \,. \tag{2.49}$$

Thus, the solution becomes the same as in one dimension, which was calculated in section 2.3.2. Including the two boundary conditions $T(-L/2) = T_L = T_0 + \Delta T$ and analogously $T(L/2) = T_R = T_0 - \Delta T$, one finds for the temperature

$$T(x) = T_0 - \frac{2\Delta T}{L} x \,. \tag{2.50}$$

The current can then be calculated out of Eq. (2.46).

$$j_{tot,x} = \frac{2\Delta T}{L} \kappa_{3D} \,. \tag{2.51}$$

In this simple model, there will be no perpendicular net current of phonons. The system is translational invariant. Thus, if there is a perpendicular net current. This current would also be translational invariant. Thus, the origin of this current must placed at infinity, which we exclude in our calculation. If one now has a closer look at the phonon-distribution-function at the boundaries, one finds that the resulting function is not of Bose-Einstein form for incoming and outgoing particles. The function reads

$$\begin{aligned} n_{\vec{p}} =& n_{\vec{p}}^{(0)} + \delta n_{\vec{p}} \\ =& \frac{1}{e^{\omega_{\vec{p}}/(k_B T)} - 1} + \tau_p \frac{\omega_{\vec{p}}}{T_0} \frac{\partial n_{\vec{p}}^{(0)}}{\partial \omega_{\vec{p}}} \left(\vec{v}_{\vec{p}} \cdot \vec{\nabla} T \right) \\ =& \frac{1}{e^{\omega_{\vec{p}}/(k_B T)} - 1} - \tau_p \frac{\omega_{\vec{p}}}{T_0} \frac{\partial n_{\vec{p}}^{(0)}}{\partial \omega_{\vec{p}}} v_{\vec{p},x} \cdot \frac{2\Delta T}{L} \,. \end{aligned} \tag{2.52}$$

For a fixed absolute momentum $|\vec{p}|$, the Bose-Einstein-term is independent of the orientation. If one tries to find an effective temperature for the whole phonon-distribution function, both terms have to have this feature. Since the absolute value for the velocity $v_{\vec{p}}$ is constant and equal to the sound velocity, its x-component depends on the orientation of the momentum vector.

$$v_{\vec{p},x} = v_0 \cdot \sin(\vartheta) \cdot \cos(\varphi) \,. \tag{2.53}$$

Thus, the phonon-distribution-function is not Bose-Einstein like. But, if one assumes ideal reservoirs, the distribution function for the outgoing particles out of the two reservoirs has to be Bose-Einstein like. Because of that, we need a more detailed investigation of the effect.

2.4 Summary

In this section, we have introduced the methods, which will be used in the entire thesis. At the beginning, the concept of quasi particles is introduced. Phonons, which are elementary excitations of a wave in the lattice structure of the solid, will be treated in the concept of quasi particles. Similarly, magnons will be treated in the concept of quasi particles. Every atom of the lattice of the solid carries a spin, which can be oriented in a different direction. Magnons are elementary excitations of a spin wave inside the solid. Furthermore, we introduced the Boltzmann equation, which is appropriate to consider transport phenomena. By way of example, we set the collision term, which is part of the Boltzmann equation, for the electron-phonon interaction and explained the exact rules to write down the collision term in general. Electrons will be described with the theory of free electron gas. After that, we introduced the relaxation time approximation. This approximation can be used, when the deviation of the particle distribution from equilibrium is small. Then, the collision term can be linearized

and one finds a quotient between the deviation function from equilibrium and a short written relaxation time. With this relaxation time approximation, we calculated in a simple model the electrical conductivity for a metal and a phonon-mediated thermal conductivity.

3 Phonon-temperature in a cuboid

In this chapter, we investigate the phonon propagation in a cuboid (a $Gd_3Ga_5O_{12}$ crystal), where only phonons are able to propagate. This cuboid is positioned between two heat baths at different temperatures. By making use of the Boltzmann equation, we will calculate the wave number dependent phonon density and temperature profiles.

We start with a motivation to this calculation in section 3.1. In this motivation, we first introduce the full problem of the transverse spin Seebeck effect and than argue, why we need to solve the phonon only problem, first.

The cuboid is enclosed between two ideal heat reservoirs. The left reservoir is a bit warmer and the right reservoir is a bit colder than the average temperature, respectively. The difference in temperature (ΔT) is much smaller than the average temperature T_0. This treatment of the cuboid is needed for the understanding of the transversal Spin-Seebeck effect, which will be treated in later chapters. The setup for the full transversal Spin-Seebeck effect is shown in figure 9. On top of the GGG ($Gd_3Ga_5O_{12}$) there is an insulating ferrimagnet, here YIG ($Y_3Fe_5O_{12}$), where phonons and magnons are able to propagate as well. Electrons are not able to propagate in the YIG film and in the GGG substrate. Above that, there is a small stripe of platinum and a voltmeter at the ends of the stripe. Here, electrons and phonons are able to propagate. This can be seen in figure 4.

Since the thickness of the YIG is much smaller than the thickness of the GGG crystal, phonons are propagating in the GGG substrate most of the time. There, magnons do not exist. Additionally, the heat reservoirs are non-magnetic reservoirs, where only phonons are able to propagate. Hence, the influence from the magnons on the distribution function of the phonons can assumed to be small. Only phonon-phonon interaction as well as impurity scattering takes place in the GGG substrate. Based on these phonon-only interactions, we first calculate the phonon density and temperature profiles in this chapter.

Figure 9: Schematical setup for measuring the transverse spin Seebeck effect. Two thermal heat reservoirs are attached to the gallium gadolinium garnet crystal ($Gd_3Ga_5O_{12}$). On top of the GGG crystal, there is an evaporated YIG-film, whose thickness is much smaller than the thickness of the GGG. Beyond that, there is a platinum stripe on top of the YIG-crystal. The voltage is measured on the platinum stripe perpendicular to the plane of projection. The magnons in the YIG-stripe are thermally not connected to the heat reservoirs.

This will be done by treating the phonon distribution to be wave vector dependent. We will perform an approximation, where we assume that the angle averaged phonon distribution (proportional to the temperature deviation) to have a linear structure. We call this approximation half-analytic method. With the above approximation we will calculate the wave vector dependent phonon temperature in section 3.2 to use it in later chapters for calculating the magnon temperature. In section 3.3 we will find out, that a simple calculation is not enough. After that, we will justify the half-analytic approximation in section 3.4. There, we will calculate the problem without the approximation but by separating the distribution

functions into moments and using Chebyshev polynomials. Additionally we consider the full phonon problem iteratively and numerically. By comparison of the three methods, we will see, that the deviation in the temperature (or in the angle averaged phonon distribution) is small.

3.1 Motivation - Complete treatment of the transverse spin Seebeck effect

In this thesis, we investigate the transversal spin Seebeck effect. The schematical setup of this experiment is depicted in figure 9. In the middle, there is a GGG crystal, where only phonons and no magnons as well as no electrons are able to propagate. For our calculation, we take the sample size out of Ref. [21]. Here, the length of the GGG crystal is at $L_{\mathrm{GGG}} = 8$ mm, the width is at $w_{\mathrm{GGG}} = 4$ mm and the thickness is at $d_{\mathrm{GGG}} = 0.5$ mm. On the left side on the long end of the crystal, there is an ideal heat reservoir at temperature $T_0+\Delta T$ attached to the GGG crystal. Analogously, on the right side on the long end of the crystal, there is an ideal heat reservoir at temperature $T_0 - \Delta T$ attached to the GGG crystal. Since the heat reservoirs are non-magnetic, magnons are not able to enter or leave the heat reservoirs. One has to mention, that only phonons are able to propagate into and out of the ideal heat reservoirs. As we set $\Delta T > 0$, the left heat reservoir is warmer than average temperature (as depicted by red color) and the right reservoir is colder than average temperature (as depicted by blue color). Both heat reservoirs are modeled as perfect phonon heat reservoirs, i.e. every incoming phonon relaxes immediately to the equilibrium distribution. Besides, the outgoing phonons are distributed by the equilibrium Bose-Einstein distribution (cf. Eq. (2.4)).

For a better visualization, we introduce the concept of a Bose sphere. This view is comparable to the concept of the Fermi sphere. Therefore, we pick out a certain absolute value of $\vec{k}$. For a certain direction, we read out the quasi-particle density and draw a line from the origin in that direction, which length is proportional to the density of quasiparticles in this direction with absolute value of $\vec{k}$. In general, the Bose-Einstein distribution is independent of the direction of the particle, which is called isotropic. Thus, this would give us a sphere, which we call Bose sphere. The two black semi circles in figure 9 demonstrate a magnitude of outgoing phonon density in a certain direction.

On top of the GGG crystal, there is an evaporated YIG-film, where magnons and phonons but no electrons are able to propagate. The thickness of the YIG-film is much smaller than the thickness of the GGG crystal. In the GGG substrate, only phonons are able to propagate, while in the YIG-film, phonons and magnons are able to propagate. Electrons are not able to propagate in the GGG as well as in the YIG-film. We assume, that magnons are not able to leave or enter the YIG-film. The quasi-particle density distributions are composed as follows

$$f_{\vec{k}} = f^{(0)}_{\vec{k}} + \tilde{f}_{\vec{k}} = f^{(0)}_{\vec{k}} + f_{0,k} + \delta f_{\vec{k}} \tag{3.1}$$

$$n_{\vec{p}} = n^{(0)}_{\vec{p}} + \tilde{n}_{\vec{p}} = n^{(0)}_{\vec{p}} + n_{0,p} + \delta n_{\vec{p}}. \tag{3.2}$$

The first summand in both equations which has a zero in superscript denotes the equilibrium density distribution $f^{(0)}_{\vec{k}}$ for magnons and $n^{(0)}_{\vec{p}}$ for phonons at temperature T_0, respectively. When there is an index or a parenthesis with p, the quantity is dependent on the wave vector. For them, we take Eq. (2.8) for magnons and Eq. (2.4) for phonons, respectively. The summand in both equations which has a zero in subscript denotes the zeroth moment of the distribution function. This zeroth moment is independent on the direction of the wave vector and only dependent on its absolute value. The functions $\delta f_{\vec{k}}$ and $\delta n_{\vec{p}}$ include

all higher moments. The n-th moments in three dimensions by using spherical coordinates are in general defined as

$$f_{n,k} = \frac{1}{2}\int_0^\pi \sin(\vartheta)\cos(n\vartheta)\tilde{f}_{\vec{k}}\, d\vartheta \tag{3.3}$$

$$n_{n,p} = \frac{1}{2}\int_0^\pi \sin(\vartheta)\cos(n\vartheta)\tilde{n}_{\vec{p}}\, d\vartheta\,. \tag{3.4}$$

We assume, that the density functions $\tilde{f}_{\vec{k}}$ and $\tilde{n}_{\vec{p}}$ are not dependent on ϕ. With that, we can write down the coupled phonon and magnon Boltzmann equations. These equations are valid in the ferrimagnetic YIG-film. In the GGG substrate, only the pure phonon terms of the equation are valid. It is for the magnons with wave vector $\vec{k}$ and phonons with wave vector $\vec{p}$

$$-\frac{\epsilon_{\vec{k}}}{T_0}\frac{\partial f^{(0)}_{\vec{k}}}{\partial\epsilon}(\vec{v}_{\vec{k}}\cdot\vec{\nabla}T_\mathrm{M}) + \vec{v}_{\vec{k}}\cdot\vec{\nabla}\delta f_{\vec{k}} = \left.\frac{\partial f_{\vec{k}}}{\partial t}\right|_{\mathrm{St,mag\text{-}pho}} + \left.\frac{\partial f_{\vec{k}}}{\partial t}\right|_{\mathrm{St,mag\text{-}mag}} \tag{3.5}$$

$$-\frac{\omega_{\vec{p}}}{T_0}\frac{\partial n^{(0)}_{\vec{p}}}{\partial\omega}(\vec{u}_{\vec{p}}\cdot\vec{\nabla}T_\mathrm{Ph}) + \vec{u}_{\vec{p}}\cdot\vec{\nabla}\delta n_{\vec{p}} = \left.\frac{\partial n_{\vec{p}}}{\partial t}\right|_{\mathrm{St,pho\text{-}mag}} + \left.\frac{\partial n_{\vec{p}}}{\partial t}\right|_{\mathrm{St,pho\text{-}pho}}, \tag{3.6}$$

with

$$T_\mathrm{M} = T_\mathrm{M}(x,\vec{k}) \qquad f_{\vec{k}} = f_{\vec{k}}(x,\vec{k}) \qquad \delta f_{\vec{k}} = \delta f_{\vec{k}}(x,\vec{k}) \tag{3.7}$$

$$T_\mathrm{Ph} = T_\mathrm{Ph}(x,\vec{p}) \qquad n_{\vec{p}} = n_{\vec{p}}(x,\vec{p}) \qquad \delta n_{\vec{p}} = \delta n_{\vec{p}}(x,\vec{p})\,, \tag{3.8}$$

while T_M denotes the spatial and wave vector dependent magnon temperature and T_Ph the spatial and wave vector dependent phonon temperature. T_0 is the average temperature. The wave vector dependent magnon energy dispersion is denoted by $\epsilon_{\vec{k}}$ (cf. Eq. (2.6)). Alike, the wave vector dependent phonon energy dispersion is denoted by $\omega_{\vec{p}}$ (cf. Eq. (2.3)). The parameter $\vec{v}_{\vec{k}}$ denotes the wave vector dependent magnon velocity and analogously the parameter $\vec{u}_{\vec{p}}$ denotes the wave vector dependent phonon velocity. In general one finds their absolute value, by taking the wave vector derivative of the energy dispersion. One has to mention, that the quasi particle temperature is coupled to the zeroth moment in the following way

$$f_{0,k}(x) = -\frac{\epsilon_{\vec{k}}}{T_0}\frac{\partial f^{(0)}_{\vec{k}}}{\partial\epsilon}(T_\mathrm{M}(x) - T_0) \tag{3.9}$$

$$n_{0,p}(x) = -\frac{\omega_{\vec{p}}}{T_0}\frac{\partial n^{(0)}_{\vec{p}}}{\partial\omega}(T_\mathrm{Ph}(x) - T_0)\,. \tag{3.10}$$

Later, we will suppress the spatial dependence. This correspondence is only valid, because the temperature differences are much smaller than the average temperature

$$|T_\mathrm{M} - T_0| \ll T_0 \qquad |T_\mathrm{Ph} - T_0| \ll T_0\,. \tag{3.11}$$

Additionally, one has to mention, that $(\partial k^{(0)}_{\vec{k}})/(\partial\epsilon) < 0$ and $(\partial n^{(0)}_{\vec{p}})/(\partial\omega) < 0$. The geometry of the setup can be found in figure 10.

Figure 10: This is the geometry for the cuboid. The angle ϕ is the angle between the x-axis (dashed line) and the projection of the wave-vector on the x-y-plane (plane of projection). The angle ϑ is the angle between the wave-vector and its projection on the x-y-plane.

The first summand on the right hand side of the Eq. (3.5) determines the collision integral of the magnon-phonon-interaction. It will be derived in section 4.3 and reads

$$\left.\frac{\partial f_{\vec{k}}}{\partial t}\right|_{\text{St,mag-pho}} = \sum_{\vec{p}}^{B.Z.} \left\{ \frac{1}{\tau_{pk}^{mp}} \frac{T_{\text{Ph}}(p) - T_{\text{M}}(k)}{T_0} - \frac{1}{\tilde{\tau}_{pk}^{mp}} \frac{T_{\text{Ph}}(p) - T_{\text{M}}(|\vec{k} - \vec{p}|)}{T_0} \right\}, \tag{3.12}$$

while the abbreviations are given in Eqs. (4.56) and (4.57). In the same way, the collision term for the magnon-magnon interaction will be derived in section 5. The result can be found in Eqs. (5.11) and (5.63) and reads as follows

$$\begin{aligned}\left.\frac{\partial f_{\vec{k}}}{\partial t}\right|_{\text{St,mag-mag}} = &\sum_{\vec{k}'}^{B.Z.} \left(\frac{|V|^2}{\tau_A^{mm}} \frac{T_{\text{M}}(\vec{k})}{T_0} + \frac{|V|^2}{\tau_B^{mm}} \frac{T_{\text{M}}(\vec{k}')}{T_0} + \frac{|V|^2}{\tau_C^{mm}} \frac{T_{\text{M}}(\vec{k} \pm \vec{k}')}{T_0} \right) \\ &+ \sum_{\vec{q}\vec{k}'}^{B.Z.} \left\{ \frac{|V|^2}{\tau_{M1}} \frac{T_{\text{M}}(\vec{k})}{T_0} + \frac{|V|^2}{\tau_{M2}} \frac{T_{\text{M}}(\vec{k}')}{T_0} + \frac{|V|^2}{\tau_{M3}} \frac{T_{\text{M}}(\vec{k} - \vec{q})}{T_0} + \frac{|V|^2}{\tau_{M4}} \frac{T_{\text{M}}(\vec{k}' + \vec{q})}{T_0} \right\},\end{aligned} \tag{3.13}$$

while the abbreviations are given in Eqs. (5.12), (5.16), (5.20), (5.64), (5.65), (5.66) and (5.67). The scattering amplitude $|V|$ will be calculated in section 5. The results can be found in Eqs. (5.29) and (5.72). The abbreviations for the phonon Boltzmann equation (3.6) read

$$\left.\frac{\partial n_{\vec{p}}}{\partial t}\right|_{\text{St,pho-pho}} \approx -\frac{\delta n_{\vec{p}}}{\tau_p}, \tag{3.14}$$

and

$$\left.\frac{\partial n_{\vec{p}}}{\partial t}\right|_{\text{St,pho-mag}} = \sum_{\vec{k}}^{B.Z.} \left\{ \frac{1}{\tau_{pk}^{mp}} \frac{T_{\text{Ph}}(p) - T_{\text{M}}(k)}{T_0} - \frac{1}{\tilde{\tau}_{pk}^{mp}} \frac{T_{\text{Ph}}(p) - T_{\text{M}}(|\vec{k} - \vec{p}|)}{T_0} \right\}. \tag{3.15}$$

Again, the abbreviations can be found in Eqs. (4.56) and (4.57). The thickness of the YIG-film is much smaller than the thickness of the GGG crystal (i.e. $d_{\text{YIG}} \ll d_{\text{GGG}}$). Typically, the thickness of the YIG-film is at the order of micrometers. For our calculations, only the order of magnitude of the YIG-thickness is important, the exact value must not be specified. Phonons are propagating in the GGG substrate most of the time, where magnons are not able to propagate. Because of that, the influence from the magnons onto the phonons is assumed to be small. Thus, the term (3.15) can be approximated to be zero, when one is calculating the phonon-temperature.

3.2 Calculation with translational symmetry in three dimensions

We consider a three-dimensional model of the GGG substrate. At the beginning, we have a look at one single GGG ($Gd_3Ga_5O_{12}$) substrate without any installation on it. The x-axis

is put parallel to the temperature gradient out of figure 10 (marked by dashed line) and is placed (as above) at $-L/2 < x < L/2$. The GGG substrate is of finite size and placed at $0 < y < B$ and $0 < z < D$.

Now, we assume the left and right boundary to be perfect thermal reservoirs at different temperatures. A thermal reservoir features the fact, that every incoming phonon will be thermalized. Outcoming phonons are distributed by the Bose-Einstein-distribution function for the certain temperature of the thermal reservoir. Thus, we know half of the phonon distribution function at the thermal reservoir

$$n\left(x = -\frac{L}{2}\right)\Theta\left(|\pi - \phi| - \frac{\pi}{2}\right) = (n_{0,p}(T_0) + (\Delta N)_p)\ \Theta\left(|\pi - \phi| - \frac{\pi}{2}\right) \tag{3.16}$$

$$n\left(x = \frac{L}{2}\right)\Theta\left(\frac{\pi}{2} - |\pi - \phi|\right) = (n_{0,p}(T_0) - (\Delta N)_p)\ \Theta\left(\frac{\pi}{2} - |\pi - \phi|\right)\,, \tag{3.17}$$

with $0 < \phi \leq 2\pi$. The choice of the coordinate system is different to Eqs. (3.3) and (3.4) but will end up in the same results. The constant $(\Delta N)_p$ features the increase or decrease of the temperature at the left and right reservoir, respectively. Outgoing particles are Bose-Einstein distributed with temperature $T + \Delta T$ at the left hand side and temperature $T - \Delta T$ at the right hand side. By making use of Eq. (3.10), one can convert the temperature difference into a particle density difference $(\Delta N)_p$ in the following way

$$(\Delta N)_p = -\frac{\omega_{\vec{p}}}{T_0}\frac{\partial n^{(0)}_{\vec{p}}}{\partial \omega}\Delta T\,. \tag{3.18}$$

One has to mention, that ΔT is independent of the wave vector, but $(\Delta N)_p$ is dependent on the absolute value of the wave vector. This implies for $0 \leq \phi \leq \pi/2$ and for $3\pi/2 \leq \phi \leq 2\pi$ i.e. for right moving particles

$$n_{p,\phi,\mathrm{right}}(x = -L/2) = \frac{1}{e^{\omega_p/(k_B T_L)} - 1} \approx \frac{1}{e^{\omega_p/(k_B T_0)} - 1} + (\Delta N)_p = N_{0,p} + (\Delta N)_p\,, \tag{3.19}$$

with T_L as fixed temperature for the left thermal reservoir at $x = -L/2$. Similarly, one writes for the other reservoir for $\pi/2 \leq \phi \leq 3\pi/2$ i.e. for left moving particles

$$n_{p,\phi,\mathrm{left}}(x = L/2) = \frac{1}{e^{\omega_p/(k_B T_R)} - 1} \approx \frac{1}{e^{\omega_p/(k_B T_0)} - 1} - (\Delta N)_p = N_{0,p} - (\Delta N)_p\,, \tag{3.20}$$

with T_R as fixed temperature for the right thermal reservoir at $x = L/2$. Thus, we find

$$\tilde{n}_{p,\phi,\mathrm{right}}(x = -L/2) = (\Delta N)_p \tag{3.21}$$

$$\tilde{n}_{p,\phi,\mathrm{left}}(x = L/2) = -(\Delta N)_p\,. \tag{3.22}$$

In this thesis, we will consider two different cases. First, the boundaries at $y = 0$, $y = B = w_{\mathrm{GGG}}$, $z = 0$ and $z = D = d_{\mathrm{GGG}}$ are modeled as perfectly reflecting walls. Second, they are modeled as rough walls.

In case of perfectly reflecting walls, every incident particle will be completely reflected in the same angle measured to the plummet. The parallel component of the incident direction of propagation will be conserved, while the perpendicular component of the incident direction will be turned to the opposite direction.

$$\tilde{n}_{p,\phi}(y = 0) = \tilde{n}_{p,2\pi-\phi}(y = 0)\,. \tag{3.23}$$

Similarly, the other wall is reflecting too

$$\tilde{n}_{p,\phi}(y = B) = \tilde{n}_{p,2\pi-\phi}(y = B)\,. \tag{3.24}$$

A similar equation holds for the boundaries at $z = 0$ and $z = D$. Because of these mirror-walls, the system becomes periodic in $2B$ and $2D$. Since the boundary conditions at the heat reservoirs are independent in y and z, the system becomes translation invariant in y and z. Thus, the model is qualitatively congruent with an infinite GGG substrate in the y- and z-direction with translation symmetry in the y- and z-direction. Of course, this only works if also the boundary conditions fulfill this translational symmetry, which is the case. This brings us to an effective one dimensional calculation, which features different angles for particle propagation. There will be three different ways of treating the problem. The first method, which we perform now and denote as half-analytic, uses an approximation, where the zeroth moment of the phonon density is assumed to have linear structure. The second method splits the distribution function in several moments of propagation direction and makes use of the Chebyshev polynomials. The resulting integrals and infinite sums need to be solved numerically. The third method uses an iterative and converging ansatz to the original Boltzmann equation.

When we include boundary scattering, we assume roughly reflecting walls at $y = 0$, $y = B$, $z = 0$ and $z = D$. This will be modeled by introducing an effective relaxation length which is the geometric mean of the sizes of the GGG substrate

$$L_{\text{eff}} = \sqrt[3]{L_{\text{GGG}} \cdot w_{\text{GGG}} \cdot d_{\text{GGG}}} = \sqrt[3]{8\,\text{mm} \cdot 4\,\text{mm} \cdot 0.5\,\text{mm}} \approx 2.51984\,\text{mm}\,, \tag{3.25}$$

while we took the numbers out of Ref. [21]. In this thesis, we will consider the case with and without boundary scattering.

3.2.1 Half-analytic method

At the beginning, we write down the Boltzmann equation in three dimensions for the phonon-only problem. We take Eq. (3.6) and replace the phonon-temperature by the zeroth moment via Eq. (3.10). Additionally, we exclude the phonon-magnon interaction because the ferrimagnetic YIG-stripe is assumed to be much smaller than the GGG substrate, as already discussed above. One finds

$$\cos(\vartheta)\frac{\partial \tilde{n}_{\vec{p}}}{\partial z} + \sin(\vartheta)\sin(\phi)\frac{\partial \tilde{n}_{\vec{p}}}{\partial y} + \sin(\vartheta)\cos(\phi)\frac{\partial \tilde{n}_{\vec{p}}}{\partial x} = -\frac{\tilde{n}_{\vec{p}} - n_{0,p}}{l_p}\,. \tag{3.26}$$

It is for the relaxation length $l_p = \tau_p \cdot v_p$. We model the left and right reservoirs to be ideal heat reservoirs. Here, we us Eqs. (3.21) and (3.22) for the boundary conditions at the heat reservoirs. Phonons with $0 < \phi \leq \pi/2$ and $3\pi/2 < \phi \leq 2\pi$ are propagating to the right and phonons with $\pi/2 < \phi \leq 3\pi/2$ are propagating to the left. Since the system is effectively invariant in y- and z-direction, the corresponding derivatives in Eq. (3.26) vanish. We make an ansatz containing a linear term for the average density

$$n_{0,p} = (\Delta N)_p \beta x\,. \tag{3.27}$$

In subsections 3.4.1 and 3.4.2 we will see why this approximation is appropriate, when we compare the results with the methods of Chebyshev polynomials and the iterative method. One finds for the Boltzmann equation

$$\sin(\vartheta)\cos(\phi)\frac{\partial \tilde{n}_{\vec{p}}}{\partial x} = -\frac{\tilde{n}_{\vec{p}} - n_{0,p}}{l_p} \approx -\frac{\tilde{n}_{\vec{p}} - (\Delta N)_p \beta x}{l_p}\,, \tag{3.28}$$

while β still has to be found. This differential equation can be solved analytically. One finds

$$\tilde{n}_{\vec{p}} = De^{-\frac{x}{r_p \cos(\phi)\sin(\vartheta)}} + (\Delta N)_p \beta x - (\Delta N)_p \beta\, l_p \cos(\phi)\sin(\vartheta)\,. \tag{3.29}$$

The variable D is still open and will be determined by the boundary conditions at the heat reservoirs (cf. Eq. (3.21) and (3.22)). Calculate the boundary conditions at the reservoir and setting them back into the phonon density function results in

$$\begin{aligned}\tilde{n}_{\vec{p},\text{right}} =&(\Delta N)_p \beta x - (\Delta N)_p l_p \beta \cos(\phi)\sin(\vartheta) \\ &+ \frac{1}{2}(\Delta N)_p (\beta L + 2\beta\, l_p \cos(\phi)\sin(\vartheta) + 2) e^{-\frac{(L+2x)\sec(\phi)}{2 l_p \sin(\vartheta)}}\,,\end{aligned} \tag{3.30}$$

and

$$\begin{aligned}\tilde{n}_{\vec{p},\text{left}} =&(\Delta N)_p \beta x - (\Delta N)_p l_p \beta \cos(\phi)\sin(\vartheta) \\ &- \frac{1}{2}(\Delta N)_p (\beta L - 2\beta\, l_p \cos(\phi)\sin(\vartheta) + 2) e^{\frac{(L-2x)\sec(\phi)}{2 l_p \sin(\vartheta)}}\,.\end{aligned} \tag{3.31}$$

The parameter β still has to be found. Additionally, we need

$$n_{0,p} = \frac{1}{4\pi}\int_0^{2\pi}\int_0^{\pi} \sin(\vartheta)\tilde{n}_{\vec{p}}\, d\vartheta\, d\phi\,, \tag{3.32}$$

which is similar to Eq. (3.4) for $n = 0$. We have performed the iterative solution by using above equation and Eqs. (3.30) and (3.31) and starting with some random parameters. Another option, we have done, is to perform a single-point approximation, which is sketched in the next subsection. At the end, we will see that both methods will converge in good agreement.

3.2.2 Single-Point approximation

By now, we perform a single-point approximation. The name for this approximation originates from the procedure to evaluate the zeroth moment calculation at one single point in the GGG substrate. In the following, we evaluate both sides of the Eq. (3.32) on a single point at $x = -L/2$. Additionally, we take Eqs. (3.30) and (3.31). With that equation, we are able to determine the open parameter β. This approximation is still in good agreement. we find

$$\begin{aligned}-(\Delta N)_p \beta \frac{L}{2} =& n_{0,p}(-L/2) \\ =& \frac{1}{4\pi}\int_0^{2\pi}\int_0^{\pi} \sin(\vartheta)\tilde{n}_{\vec{p}}(-L/2)\, d\vartheta\, d\phi \\ =& \frac{1}{2\pi}\int_0^{\pi/2}\int_0^{\pi} \sin(\vartheta)\tilde{n}_{\vec{p},\text{right,approx}}(-L/2)\, d\vartheta\, d\phi \\ &+ \frac{1}{2\pi}\int_{\pi/2}^{\pi}\int_0^{\pi} \sin(\vartheta)\tilde{n}_{\vec{p},\text{left,approx}}(-L/2)\, d\vartheta\, d\phi\,.\end{aligned} \tag{3.33}$$

This is

$$
\begin{aligned}
-(\Delta N)_p\beta\frac{L}{2} =& \frac{1}{2\pi}\int_0^{\pi/2}\int_0^{\pi}\sin(\vartheta)(-(\Delta N)_p\beta\frac{L}{2}-(\Delta N)_p\, l_p\beta\cos(\phi)\sin(\vartheta))\,d\vartheta\,d\phi \\
&+\frac{1}{2\pi}\int_0^{\pi/2}\int_0^{\pi}\sin(\vartheta)(+\frac{1}{2}(\Delta N)_p(\beta L+2\beta\, l_p\cos(\phi)\sin(\vartheta)+2)e^{-\frac{(L-L)\sec(\phi)}{2l_p\sin(\vartheta)}})\,d\vartheta\,d\phi \\
&+\frac{1}{2\pi}\int_{\pi/2}^{\pi}\int_0^{\pi}\sin(\vartheta)(-(\Delta N)_p\beta\frac{L}{2}-(\Delta N)_p l_p\beta\cos(\phi)\sin(\vartheta))\,d\vartheta\,d\phi \\
&+\frac{1}{2\pi}\int_{\pi/2}^{\pi}\int_0^{\pi}\sin(\vartheta)(-\frac{1}{2}(\Delta N)_p(\beta L-2\beta l_p\cos(\phi)\sin(\vartheta)+2)e^{\frac{(L+L)\sec(\phi)}{2l_p\sin(\vartheta)}})\,d\vartheta\,d\phi \\
=&\frac{1}{2\pi}\int_0^{\pi}\int_0^{\pi}\sin(\vartheta)(-(\Delta N)_p\beta\frac{L}{2}-(\Delta N)_p l_p\beta\cos(\phi)\sin(\vartheta))\,d\vartheta\,d\phi \\
&+\frac{1}{2\pi}\int_0^{\pi/2}\int_0^{\pi}\sin(\vartheta)\frac{1}{2}(\Delta N)_p(\beta L+2\beta\, l_p\cos(\phi)\sin(\vartheta)+2)\,d\vartheta\,d\phi \\
&-\frac{1}{2\pi}\beta\frac{(\Delta N)_p}{2}\int_{\pi/2}^{\pi}\int_0^{\pi}\sin(\vartheta)(L-2l_p\cos(\phi)\sin(\vartheta))e^{\frac{L\sec(\phi)}{l_p\sin(\vartheta)}}\,d\vartheta\,d\phi \\
&-\frac{1}{2\pi}(\Delta N)_p\int_{\pi/2}^{\pi}\int_0^{\pi}\sin(\vartheta)e^{\frac{L\sec(\phi)}{l_p\sin(\vartheta)}}\,d\vartheta\,d\phi \\
=&-(\Delta N)_p\frac{\beta L}{2}+(\Delta N)_p\frac{\beta L}{4}+(\Delta N)_p\frac{\beta\, l_p}{4}+(\Delta N)_p\frac{1}{2}-\beta(\Delta N)_pI_1-(\Delta N)_pI_2\,,
\end{aligned}
\tag{3.34}
$$

with

$$
I_1 = \frac{1}{2\pi}\int_{\pi/2}^{\pi}\int_0^{\pi}\sin(\vartheta)\left(\frac{L}{2}-l_p\cos(\phi)\sin(\vartheta)\right)e^{\frac{L\sec(\phi)}{l_p\sin(\vartheta)}}\,d\vartheta\,d\phi \tag{3.35}
$$

$$
I_2 = \frac{1}{2\pi}\int_{\pi/2}^{\pi}\int_0^{\pi}\sin(\vartheta)e^{\frac{L\sec(\phi)}{l_p\sin(\vartheta)}}\,d\vartheta\,d\phi\,. \tag{3.36}
$$

The integrals in I_1 and I_2 will be determined numerically. The upper equation can be transformed and one finds

$$
\beta = -\frac{2-4I_2}{L+l_p-4I_1}\,. \tag{3.37}
$$

The same result would be obtained by evaluating Eq. (3.32) with Eqs. (3.30) and (3.31) for $x = +L/2$ instead for $x = -L/2$. If one takes a point between $x = -L/2$ and $x = L/2$, the result would be a little different. The results for n_0, the difference of the angle averaged phonon density with respect to equilibrium, is plotted in figure 11. As suspected, if the relaxation length l_p is larger than the system length L, the slope is very small, because the phonons propagate nearly hitchless through the GGG crystal. Left and right moving phonons average to the equilibrium density. There is also a large density / temperature jump at the edges. If the relaxation length is smaller than the system length, the slope is very large, because these phonons scatter only with neighboring phonons and thus, the jump at the edges becomes small.

3.2.3 Diffusive regime approximation

If the relaxation length is much smaller than the system length (i.e. $l_p \ll L$), one can perform an approximation for the phonon density. Inside the Eqs. (3.35) and (3.36), the exponent in

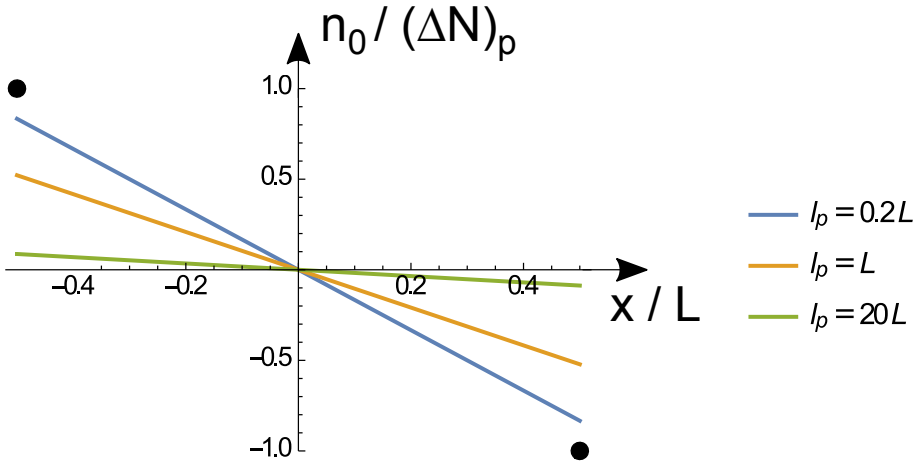

Figure 11: Difference of the angle averaged phonon density with respect to equilibrium n_0 is plotted dependent on the position inside the cuboid for different relaxation length l_p. The phonon density for the phonons inside the heat reservoir are denoted as black circles. They are at $n_0 = (\Delta N)_p$ for $x = -L/2$ and at $n_0 = -(\Delta N)_p$ for $x = +L/2$. Thus, there is a density jump (or temperature jump) at the edges of the heat reservoirs.

the exponential function becomes close to zero, because $\sec(\phi) < 0$. Thus, I_1 and I_2 become close to zero. The result reads

$$\beta \approx -\frac{2}{L + l_p}\,. \tag{3.38}$$

The phonon density n_0 at the left end of the substrate (i.e. $x = -L/2$) is plotted in figures 12 and 13 for different methods. For the "half-analytic" method, we have done this iteratively by using first Eq. (3.30) and (3.31) and second Eq. (3.32) and starting with some random parameters. For performing the single point approximation and the diffusive regime approximation, we used Eq. (3.27) and Eq. (3.37) for the single point approximation or Eq. (3.38) for the diffusive regime approximation. Here, we plot the calculated ratio $n_0/(\Delta N)_p$. Since Eq. (3.10) and (3.18) hold, we find the same ratio to be

$$\frac{n_{0,p}}{(\Delta N)_p} = \frac{T_{\mathrm{Ph}}(p) - T_0}{\Delta T}\,. \tag{3.39}$$

When there is an index or a parenthesis with p, the quantity is dependent on the wave vector.

Generally, particles are only influenced by the particle density in the proximity of length l_p. Here, we consider phonons. For large relaxation length (i.e. $l_p \gtrsim L$), out coming phonons from the left lead are able to propagate to the right end nearly without any scattering and thus keep their particle density as well as the temperature. Phonons coming out of the right lead are also propagating to the left lead and keep their particle density as well as temperature. The average particle density and temperature for those phonons is nearly the same in the whole substrate. The average temperature is the mean value T_0 of the left and right thermal baths. For phonons with a short relaxation length (if the relaxation length is smaller than the sample length) it is the opposite. Because they scatter very often, out coming particles from the right lead relax before they reach the left end. Because of that, those particles are only influenced by the phonon density in the proximity.

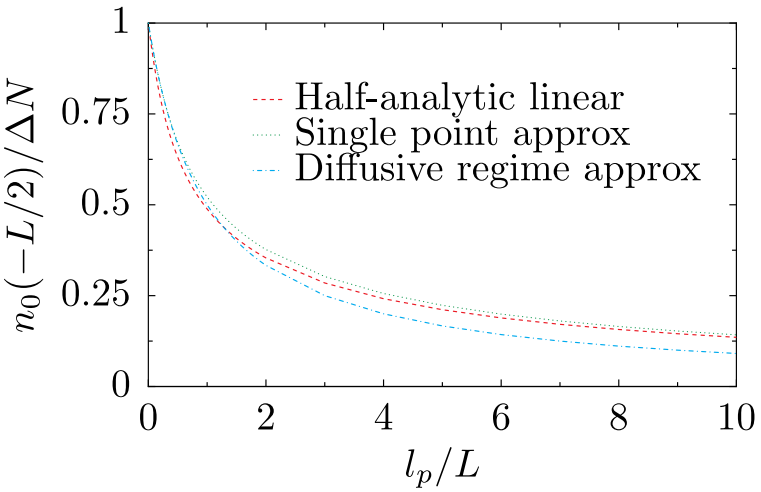

Figure 12: Deviation of phonon density from equilibrium at $x = -L/2$ for different methods and relaxation length l_p in three dimensions at 300 Kelvin without boundary scattering.

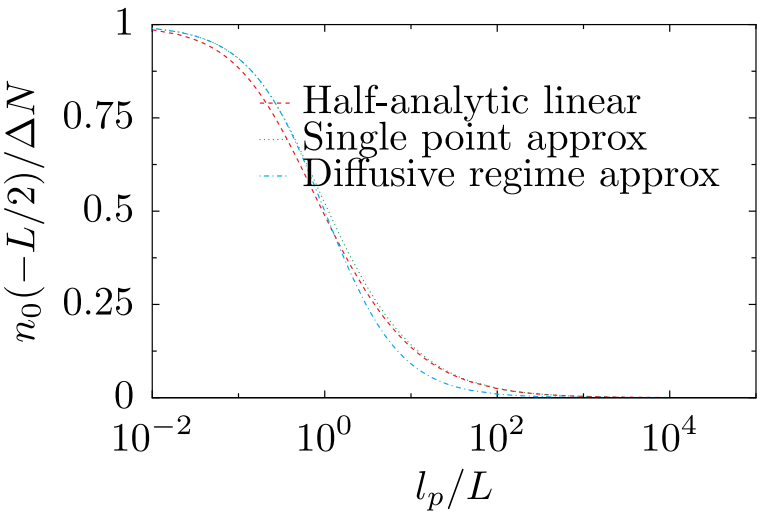

Figure 13: Deviation of phonon density from equilibrium at $x = -L/2$ for different methods and relaxation length l_p in three dimensions at 300 Kelvin without boundary scattering.

Now, we want to calculate the relaxation length l_p dependent on the wave vector. Neelmani *et al.* [48] made temperature dependent phonon conductivity calculations for GGG. They used Callaway's model [49] for their calculations. The formula for the relaxation length reads

$$l_p = v\tau_p = \frac{v}{\tau_{\mathrm{bd}}^{-1} + \tau_{\mathrm{pt}}^{-1} + \tau_{\mathrm{um}}^{-1}} = \frac{v}{E_{\mathrm{bd}} + E_{\mathrm{pt}}\xi^4 T^4 + E_{\mathrm{um}}\xi^2 T^3 e^{-T_C/(bT)}}\,, \tag{3.40}$$

with

$$\xi = \frac{\hbar\omega}{k_B T} = \frac{\hbar v p}{k_B T}\,. \tag{3.41}$$

In this thesis, we will perform the calculation with and without boundary scattering. The boundary scattering describes the scattering process of phonons at the boundary of the

system (or the cuboid). When one phonon reaches the boundary, it relaxes and gets the local temperature of the diffusive phonons. Diffusive phonons are phonons with a small relaxation length and as we will see with a large wave number. In the case without boundary scattering, we use perfectly reflecting walls. Thus, we set the boundary scattering relaxation length $E_{\mathrm{bd}} = v/L_{\mathrm{eff}}$ to zero. For including boundary scattering, the boundaries of the GGG substrate are rough and we set the effective relaxation length to the geometric mean of the sizes of the GGG substrate. This is Eq. (3.25). In all cases $E_{\mathrm{pt}} = 5.0\,\mathrm{s}^{-1}\mathrm{K}^{-4}$ denotes the point-defect scattering rate, $E_{\mathrm{um}} = 1.577 \cdot 10^{4}\mathrm{s}^{-1}\mathrm{K}^{-3}$ denotes the prefactor to the Umklapp relaxation rate of the phonons. The critical temperature is denoted by $T_{\mathrm{C}} = 125.7$ K. The parameters $b = 2.0$ and sound velocity $v = 5.07 \cdot 10^{5}\,\mathrm{cm/s}$ are given. These numbers are taken from Ref. [48].

The Normal scattering relaxation length cannot be taken from Neelmani *et al.* [48]. For that, we performed an estimation, which can be found in the appendix A.

In figures 14 and 15, the phonon relaxation length out of Eq. (3.40) and the Normal scattering relaxation length dependent on the absolute value of the wave vector are plotted at 300 K and 3 K, respectively. The phonon relaxation length's are separated by their origin. A short relaxation length corresponds to a dominant scattering process. For 3 K, the impurity scattering and the boundary scattering are dominant.

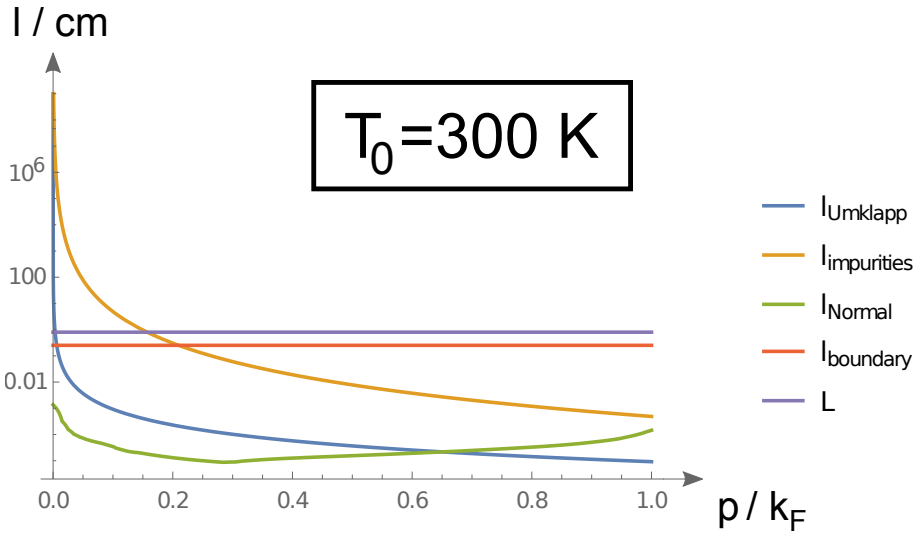

Figure 14: The relaxation length dependent on the absolute value of the wave vector is plotted at 300 K. The phonon relaxation length's are separated by their origin. It is $l_\alpha = v \cdot \tau_\alpha$ with $\alpha \in \{\mathsf{bd}, \mathsf{pt}, \mathsf{um}, \mathsf{no}\}$.

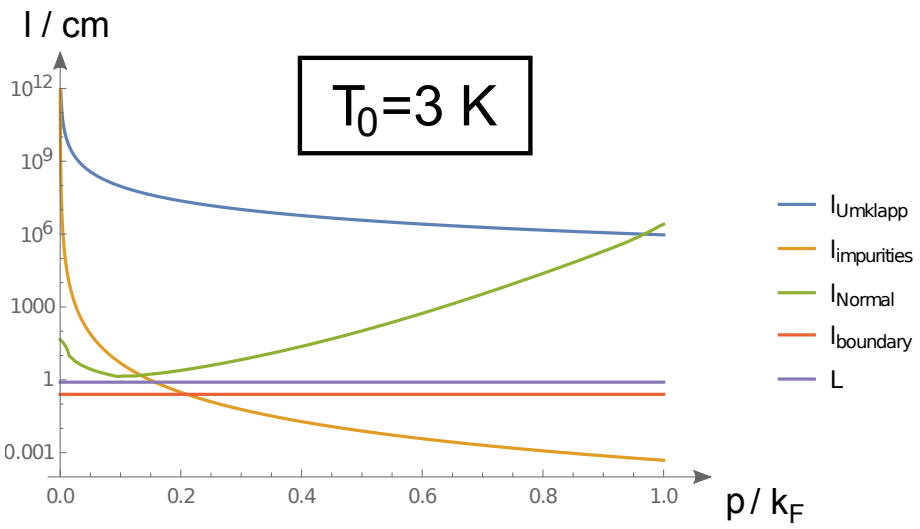

Figure 15: The relaxation length dependent on the absolute value of the wave vector is plotted at 3 K. The phonon relaxation length's are separated by their origin. It is $l_\alpha = v \cdot \tau_\alpha$ with $\alpha \in \{\mathsf{bd}, \mathsf{pt}, \mathsf{um}, \mathsf{no}\}$.

With that, we will calculate the phonon density depending on the absolute value of the wave vector. With Eq. (3.40) we are able to convert the absolute value of the wave vector p into the relaxation length l_p. In figures 16 and 17 the particle density at the left end of the substrate (i.e. $x = -L/2$) is plotted dependent on the absolute value of the p-vector of the phonons. Phonons with a large wave vector have a short relaxation length (cf. figure 14 and 15) and thus their density is influenced only by neighboring phonons in a range of the relaxation length. Since the deviation from the equilibrium density of the emitting particles on the left lead is fixed to $(\Delta N)_p$, those phonons have nearly this temperature of the reservoir and a density with a value close to 1 in the two plots. Phonons with a short wave vector have a long relaxation length (cf. figure 14 and 15). Thus, they propagate nearly without scattering through the substrate and thus have the average phonon density, because we consider left and right moving phonons together.

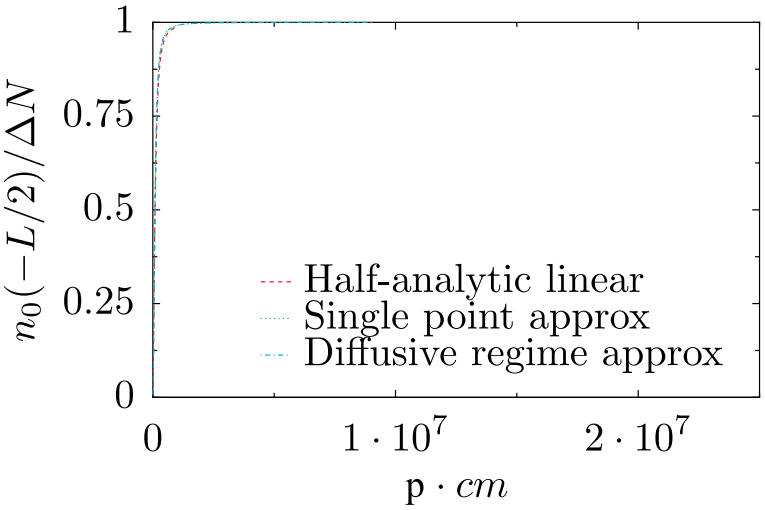

Figure 16: Deviation of phonon density from equilibrium at $x = -L/2$ for different methods and wave numbers k in three dimensions at 300 Kelvin without boundary scattering. The Fermi wave number is $k_\mathsf{F} = 3.10175 \cdot 10^7\,\mathrm{cm}^{-1}$.

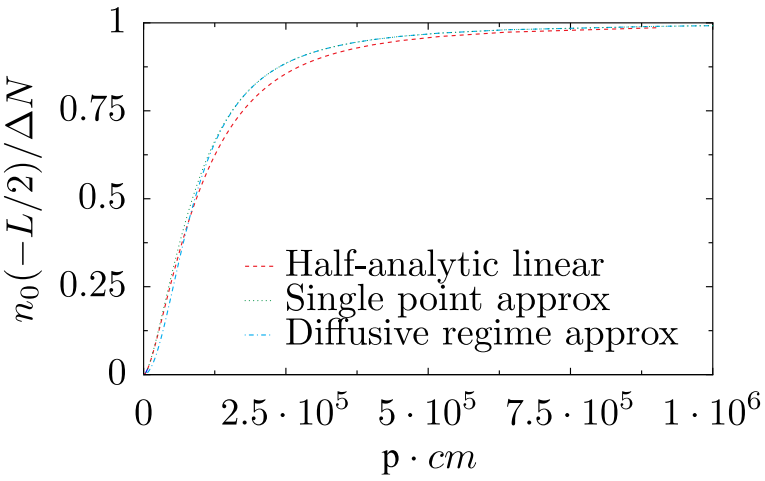

Figure 17: Zoom of figure 16: Deviation of phonon density from equilibrium at $x = -L/2$ for different methods and wave numbers k in three dimensions at 300 Kelvin without boundary scattering. The Fermi wave number is $k_\mathsf{F} = 3.10175 \cdot 10^7\,\mathrm{cm}^{-1}$.

The wave vector dependent phonon temperature at the left lead (i.e. $x = -L/2$) is plotted in figures 18 and 19 for different average temperatures T_0. In figure 18 boundary scattering is excluded, while in figure 19 boundary scattering is included. Here, we do not neglect the relaxation length from Eq. (3.25).

In figures 18 and 19, the phonon temperature decreases for small wave numbers (or large wave lengths). The smaller the average temperature T_0 is, the greater the decrease of temperature for the small wave number phonons is. When we include boundary scattering, the phonon temperature does not decrease that much as by excluding boundary scattering. The reason for this is, that small wavenumber phonons can no longer propagate hitchless in the GGG substrate and relax to the diffusive temperature when they scatter at the boundary. If one wants to construct the spatial temperature profile for one certain wave number, one

has to take the value out of the figures 18 or 19 as one point of the profile at $x = -L/2$. All temperature profiles are linear and crossing the value T_0 at position $x = 0$. With these two points, one is able to construct the linear temperature profile (cf. figure 11).

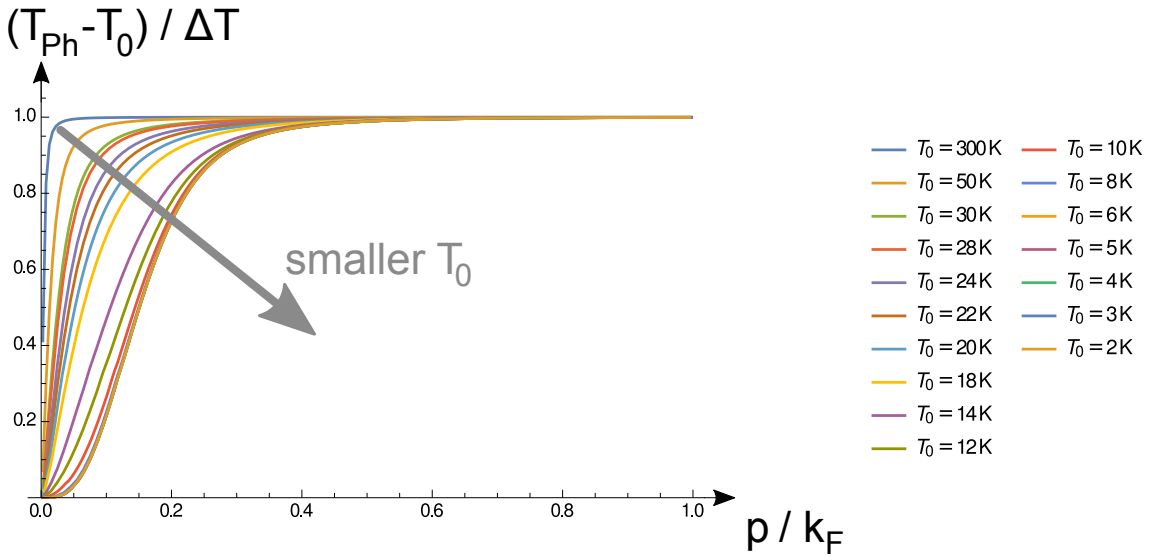

Figure 18: Here, the p-dependent phonon temperature at position $x = -L/2$ is plotted for different average temperatures T_0. Boundary scattering is not included in this figure.

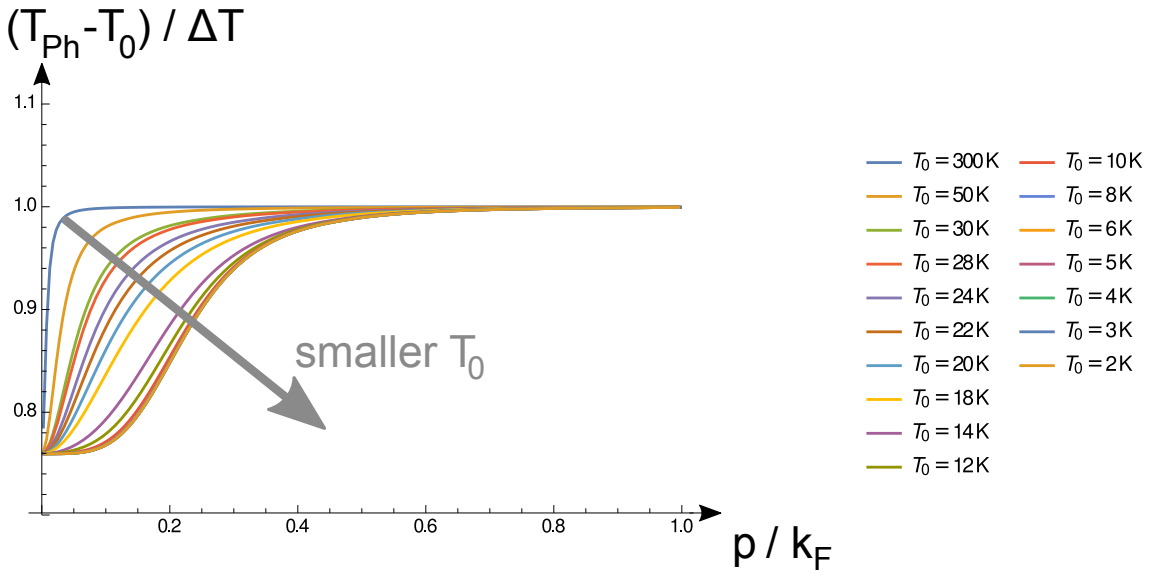

Figure 19: Here, the p-dependent phonon temperature at position $x = -L/2$ is plotted for different average temperatures T_0. Boundary scattering is included in this figure.

In figures 20, 21 and 22, one can find polar plots of the angle φ of the phonon density distribution out of Eqs. (3.30), (3.31) and (3.37) in units of $(\Delta N)_p$ at different positions in the substrate and for different relaxation length. These plots are performed with a fixed angle ϑ and with an offset of 2. For large relaxation length (cf. figure 22), the phonons propagate nearly ballistic. Thus, the distribution function nearly does not change by propagating

through the substrate. In contrast, phonons with a small relaxation length (cf. figure 20) propagate diffusive. Thus, the distribution function changes a lot by propagating through the substrate.

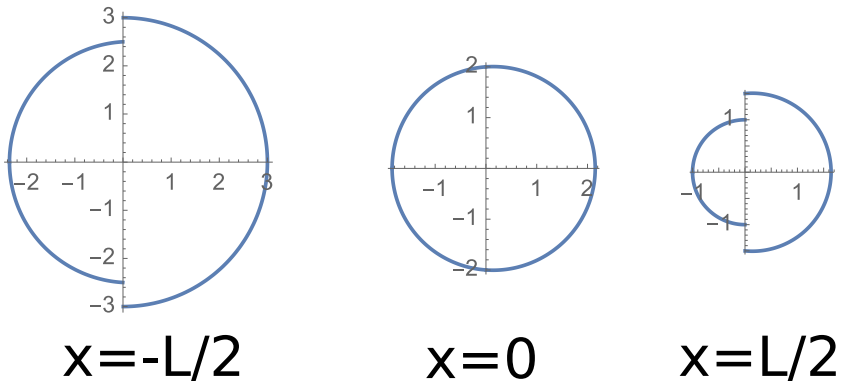

Figure 20: Polar plot of the angle φ of the phonon density distribution in units of $(\Delta N)_p$ at different positions in the substrate. Here, the relaxation length is $l_p = \frac{1}{5}L$.

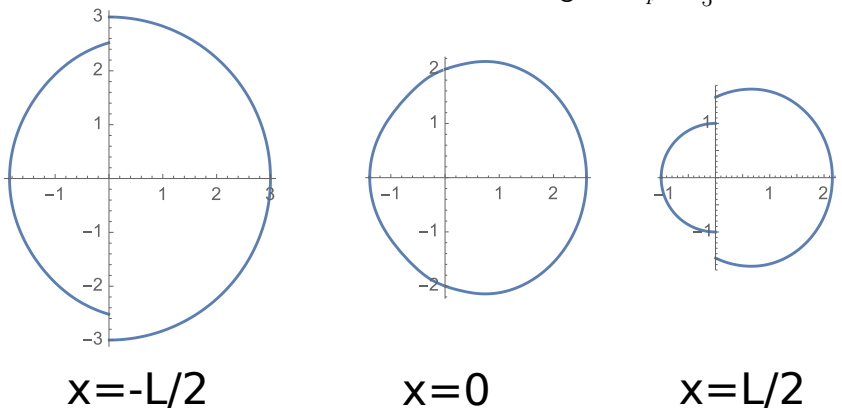

Figure 21: Polar plot of the angle φ of the phonon density distribution in units of $(\Delta N)_p$ at different positions in the substrate. Here, the relaxation length is $l_p = L$.

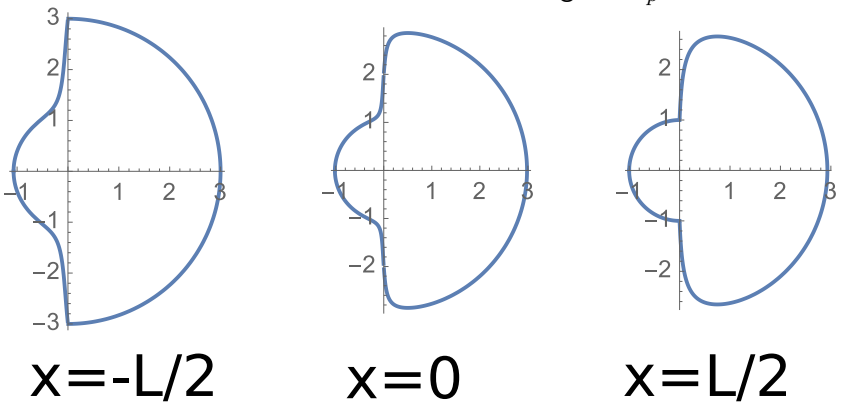

Figure 22: Polar plot of the angle φ of the phonon density distribution in units of $(\Delta N)_p$ at different positions in the substrate. Here, the relaxation length is $l_p = 20L$.

3.3 Justification for the method

Now, we want to setup a simpler model than discussed above and show, why this simple model is not appropriate to explain the investigated effects. We will use a strictly one dimensional calculation, but with a wave vector dependent phonon density. At the end, we will see, that we need a wave vector dependent temperature and a three dimensional consideration.

3.3.1 Microscopic calculation in one dimension

Now, we take a closer look on the phonon distribution function and the role of the two heat baths. The feature of a heat bath is, that it emits particles in a well defined and Bose-Einstein distributed temperature and density distribution. The temperature, which will be used in the Bose-Einstein distribution is the bath temperature and not the average temperature. This distribution is unaffected by incoming particles, which are thermalized immediately (very fast, for realistic setups). Thus, the boundary conditions can only be written down for one half of the particle distribution, for the outgoing particles at the boundary. Thus, we consider a one dimensional lead including impurity scattering. We investigate a one dimensional lead of length L including impurity-interaction, but no phonon-phonon-interaction. The heat reservoirs are located at the left side $x = -L/2$ and at the right side $x = L/2$ of the substrate. The distribution function can be separated into left movers n_L and right movers n_R. For the right movers, the distribution function is known at the left end of the lead $n_R(-L/2) = N_R$ and for the left movers analogous $n_L(L/2) = N_L$. The possibility to change the direction by elastic scattering is denoted as $W = 1/(2\tau_p)$. The distribution function can be separated into left movers n_L and right movers n_R. The Boltzmann equation reads

$$-v_p \frac{\partial n_L}{\partial x} = \int (W(R \to L) - W(L \to R))\delta(p_L - p_R)dp = W(n_R(n_L + 1) - n_L(n_R + 1)) \tag{3.42}$$

$$v_p \frac{\partial n_R}{\partial x} = \int (W(L \to R) - W(R \to L))\delta(p_L - p_R)dp = W(n_L(n_R + 1) - n_R(n_L + 1))\,, \tag{3.43}$$

while $W(R \to L)$ denotes the possibility for a scattering event from a right moving into a left moving particle. $W(L \to R)$ denotes the possibility for the opposite scattering event. It is $W(R \to L) = W(L \to R) = W$. At the end, we find

$$-v_p \frac{\partial n_L}{\partial x} = W(n_R - n_L) \tag{3.44}$$

$$v_p \frac{\partial n_R}{\partial x} = W(n_L - n_R)\,. \tag{3.45}$$

This system of differential equations has the following solution

$$n_L(x) = \frac{Wx}{v_p}(C_1 - C_2) + C_1 \tag{3.46}$$

$$n_R(x) = \frac{Wx}{v_p}(C_1 - C_2) + C_2\,. \tag{3.47}$$

There are two open parameters C_1 and C_2, which can be fixed by the following boundary conditions

$$n_R(-L/2) = N_R \qquad n_L(L/2) = N_L\,. \tag{3.48}$$

The solution including these boundary condition reads

$$n_L(x) = N_L + \frac{(N_R - N_L)W(L - 2x)}{2(v_p + LW)} \tag{3.49}$$

$$n_R(x) = N_R - \frac{(N_R - N_L)W(L + 2x)}{2(v_p + LW)}\,. \tag{3.50}$$

Now, temperature (or better particle distribution) can be calculated

$$n_0(x) = \frac{n_R(x) + n_L(x)}{2} = \frac{N_R + N_L}{2} - \frac{(N_R - N_L)W}{(v_p + LW)}x\,, \tag{3.51}$$

and the particle current

$$n_1(x) = \frac{n_R(x) - n_L(x)}{2} = \frac{(N_R - N_L)v_p}{2(v_p + LW)}\,. \tag{3.52}$$

It is $W = 1/(2\tau_p)$. Now, it is interesting, that if $N_R > N_L$, left moving phonons are less populated than right moving phonons, or vice versa. In this simple model, there are no particles propagating in a certain angle to the x-axis. These particles have a different x-component for the relaxation length. For our treatment of the full problem, we also need phonons, which do not propagate directly in the x-direction. Then, we find different temperature or particle density profiles. This more exact calculation, we have done in section 3.2.

3.4 Justification for the approximation in two dimensions

By now, we want to justify the approximations, we performed in section 3.2. Thus, we consider a two-dimensional model of the GGG substrate. In two dimensions, the effort for the comparison is less than in three dimensions, especially for the iterative method.

The first method splits the distribution function in several moments of propagation direction and makes use of the Chebyshev polynomials. The resulting integrals and infinite sums need to be solved numerically. The second method uses an iterative and converging ansatz to the original Boltzmann equation. And third, we will perform a calculation by using the "half-analytic" method out of section 3.2. These three methods will be compared in this section.

The x-axis is put parallel to the temperature gradient out of figure 9 and 10 and is placed (as above) at $-L/2 < x < L/2$. The GGG substrate is of finite size and placed at $0 < y < B$. The boundaries at $y = 0$ and $y = B$ are modeled as perfectly reflecting walls.

3.4.1 Chebyshev polynomials

Again, we consider an effective one dimensional lead with two thermal baths with fixed different temperatures on both sides. Only phonons are able to propagate. The system is invariant in y-direction. Higher temperature will be translated into a higher density of phonons via Bose-Einstein-distribution (see Eqs. (2.4) and (3.10)). The composition of the phonon density function is given in Eq. (3.2). Thus, the Boltzmann equation reads

$$v_p \cos(\phi)\frac{\partial n_{0,p}}{\partial x} + v_p \cos(\phi)\frac{\partial \delta n_{\vec{p}}}{\partial x} = -\frac{\delta n_{\vec{p}}}{\tau_{\vec{p}}}\,, \tag{3.53}$$

with $\vec{p} = p\cos(\phi)\hat{e}_x + p\sin(\phi)\hat{e}_y$. Now, we assume delta scatterers as the main and only scattering process in the bulk material. This implies

$$\tau_{\vec{p}} = \tau_p \,. \tag{3.54}$$

We perform an expansion of the deviating part of the distribution function

$$\delta n_{\vec{p}} = n_{1,p}\cos(\phi) + n_{2,p}\cos(2\phi) + n_{3,p}\cos(3\phi) + \dots \,. \tag{3.55}$$

If we set this expansion into our Boltzmann equation, we arrive at

$$v_p\cos(\phi)\frac{\partial n_{0,p}}{\partial x} + v_p\cos(\phi)\sum_{i=1}^{\infty}\frac{\partial n_{i,p}}{\partial x}\cos(i\phi) = -\sum_{i=1}^{\infty}\frac{n_{i,p}\cos(i\phi)}{\tau_p} \,. \tag{3.56}$$

This differential equation can be separated by integration on both sides by $\frac{1}{2\pi}\int_{-\pi}^{\pi} d\phi\cos(n\phi)$ for every non-negative integer n. This leads us to

$$\frac{1}{2}v_p\frac{\partial n_{1,p}}{\partial x} = 0 \tag{3.57}$$

$$\frac{1}{2}v_p\frac{\partial n_{0,p}}{\partial x} + \frac{1}{4}v_p\frac{\partial n_{2,p}}{\partial x} = -\frac{1}{2}\frac{n_{1,p}}{\tau_p} \tag{3.58}$$

$$\frac{1}{4}v_p\frac{\partial n_{i-1,p}}{\partial x} + \frac{1}{4}v_p\frac{\partial n_{i+1,p}}{\partial x} = -\frac{1}{2}\frac{n_{i,p}}{\tau_p} \qquad \forall\, i \geq 2 \,. \tag{3.59}$$

For solving this system of equations, first we perform the following ansatz

$$n_{0,p}(x) = -\frac{n_1}{l_p}x + c \tag{3.60}$$

$$n_{1,p}(x) = n_1 \tag{3.61}$$

$$n_{i,p}(x) = 0 \qquad \forall\, i \geq 2 \,, \tag{3.62}$$

with $l_p = v_p\tau_p$. This ansatz fulfills the system of differential equations (3.57), (3.58) and (3.59) with the open parameters n_1 and c. Since $n_{0,p}$ is proportional to the temperature, this expression corresponds to a linear temperature profile. Another solution can be set up by the following ansatz

$$n_{0,p}(x) = A_0 e^{-\frac{x}{rl_p}} \tag{3.63}$$

$$n_{1,p}(x) = 0 \tag{3.64}$$

$$n_{i,p}(x) = A_i e^{-\frac{x}{rl_p}} \qquad \forall\, i \geq 2 \,. \tag{3.65}$$

If we set in this ansatz into Eqs. (3.57), (3.58) and (3.59), we obtain the following system of equations for A_i with $i \in \mathbb{N}_0\backslash\{1\}$

$$0 = 0 \tag{3.66}$$

$$-\frac{1}{2}v_p\frac{A_0}{rl_p} - \frac{1}{4}v_p\frac{A_2}{rl_p} = 0 \tag{3.67}$$

$$-\frac{1}{4}v_p\frac{A_3}{rl_p} = -\frac{1}{2}\frac{A_2}{\tau_p} \tag{3.68}$$

$$-\frac{1}{4}v_p\frac{A_{i-1}}{rl_p} - \frac{1}{4}v_p\frac{A_{i+1}}{rl_p} = -\frac{1}{2}\frac{A_i}{\tau_p} \qquad \forall\, i \geq 3 \,. \tag{3.69}$$

Eq. (3.69) is analogue to the well known recursive definition for the Chebyshev polynomials of the second kind [50, p. 771 ff]. The prefactor of the solution can be different for a different parameter r. Thus, we introduce a prefactor $B(r)$, which is dependent on the choice of r in the solution. $B(r)$ is a common prefactor for all A_i with $i \in \mathbb{N}_0 \backslash \{1\}$. Thus, the solution can be written down in the following way

$$A_0 = -\frac{1}{2} B(r) U_0(r) \tag{3.70}$$

$$A_i = B(r) U_{i-2}(r) \qquad \forall\, i \geq 2\,, \tag{3.71}$$

while $U_i(r)$ denotes the i-th Chebyshev polynomial of the second kind with argument r. At the end, we have to sum all possible solutions. Hence, the complete solution reads

$$n_{0,p}(x) = -\frac{1}{2} \int_{-1}^{1} B(r) e^{-\frac{x}{r l_p}}\, dr - \frac{n_1}{l_p} x + c \tag{3.72}$$

$$n_{1,p}(x) = n_1 \tag{3.73}$$

$$n_{i,p}(x) = \int_{-1}^{1} B(r) U_{i-2}(r) e^{-\frac{x}{r l_p}}\, dr \qquad \forall\, i \geq 2\,, \tag{3.74}$$

with the open parameter $B(r)$, n_1, c and

$$n(x) = \sum_{i=0}^{\infty} n_{i,p}(x) \cos(i\phi)\,. \tag{3.75}$$

Now, we assume the left and right boundary to be perfect thermal reservoirs at different temperatures. A thermal reservoir features the fact, that every incoming phonon will be thermalized. Outcoming phonons are distributed by the Bose-Einstein-distribution function for the certain temperature of the thermal reservoir. Thus, we know half of the phonon distribution function at the thermal reservoir. Here, we use Eqs. (3.16) and (3.17). Now, we insert Eq. (3.75) into Eqs. (3.16). After that, we divide the equations by the following integral $\frac{1}{2\pi} \int_{-\pi/2}^{\pi/2} d\phi \cos(n\phi)$ for every non-negative integer n. If one would insert Eq. (3.75) into Eq. (3.17) instead of Eq. (3.16), one finds the same system of equations, if the following property is fulfilled

$$B(-r) = -B(r)\,. \tag{3.76}$$

Using this identity, we perform the following transformation for all $i \geq 2$ (and the integral inside of $n_{0,p}$)

$$n_{i,p}(x) = \int_{-1}^{1} B(r) U_{i-2}(r) e^{-\frac{x}{r l_p}}\, dr \tag{3.77}$$

$$= \int_{0}^{1} B(r) U_{i-2}(r) e^{-\frac{x}{r l_p}}\, dr + \int_{-1}^{0} B(r) U_{i-2}(r) e^{-\frac{x}{r l_p}}\, dr \tag{3.78}$$

$$= \int_{0}^{1} B(r) U_{i-2}(r) \left(e^{-\frac{x}{r l_p}} \mp e^{\frac{x}{r l_p}} \right) dr \tag{3.79}$$

$$= \int_{0}^{1} C(r) U_{i-2}(r) \left(e^{-\frac{x}{r l_p} - \frac{L}{2 r l_p}} \mp e^{\frac{x}{r l_p} - \frac{L}{2 r l_p}} \right) dr\,, \tag{3.80}$$

while the upper sign is for even i and the lower sign for odd i. It is

$$C(r) = B(r) e^{\frac{L}{2 r l_p}}\,. \tag{3.81}$$

To find $C(r)$, we perform a discretization of the integral in the following way for all $i \geq 2$ (and the integral inside of $n_{0,p}$)

$$n_{i,p}(x) = \int_0^1 C(r) U_{i-2}(r) \left(e^{-\frac{x}{rl_p} - \frac{L}{2rl_p}} \mp e^{\frac{x}{rl_p} - \frac{L}{2rl_p}} \right) dr \tag{3.82}$$

$$= \sum_{j=1}^{N} C(r_j) U_{i-2}(r_j) \left(e^{-\frac{x}{r_j l_p} - \frac{L}{2r_j l_p}} \mp e^{\frac{x}{r_j l_p} - \frac{L}{2r_j l_p}} \right) , \tag{3.83}$$

with $r_j = (2j-1)/(2N)$. Now, we insert Eq. (3.75) into Eq. (3.16) by making use of Eqs. (3.72), (3.73). For $n_{i,p}$ with $i \leq 2$ and for the integral inside of $n_{0,p}$, we use Eq. (3.83). Then, we take the integral $\frac{1}{2\pi} \int_{-\pi/2}^{\pi/2} d\phi \cos(n\phi)$ for the non-negative integer n. Every non-negative integer n stays for one equation in the system of equations. Herein, the coefficients $C(r_j)$ and n_1 are the unknown parameters. We find the following system of equations

$$\begin{aligned}(\Delta N)_p \, H(n,0) = &\left(-\frac{1}{2} H(n,0) + H(n,2) \right) \sum_{j=1}^{N} C(r_j) \left(1 - e^{-\frac{L}{r_j l_p}} \right) \\ &+ \left(\frac{L}{2l_p} H(n,0) + H(n,1) \right) n_1 \\ &+ \sum_{i=3}^{N_{\max}} \sum_{j=1}^{N} H(n,i) \, C(r_j) \, U_{i-2}(r_j) \left(1 - (-1)^i e^{-\frac{L}{r_j l_p}} \right) ,\end{aligned} \tag{3.84}$$

including the following integral

$$\begin{aligned}H(n,m) &= \frac{1}{2\pi} \int_{-\pi}^{\pi} \cos(n\phi) \, \cos(m\phi) \, \Theta\left(\frac{\pi}{2} - |\phi| \right) d\phi \\ &= \begin{cases} \frac{m \sin\left(\frac{\pi m}{2}\right) \cos\left(\frac{\pi n}{2}\right)}{\pi(m^2 - n^2)} - \frac{n \cos\left(\frac{\pi m}{2}\right) \sin\left(\frac{\pi n}{2}\right)}{\pi(m^2 - n^2)} & m \neq n \\ 1/4 & m = n \neq 0 \\ 1/2 & m = n = 0 \end{cases} .\end{aligned} \tag{3.85}$$

In the system of equations, we have $N+1$ open parameters. To have a quadratic system of equations, we need to take the same number of equations (which is denoted by n). Thus n must be an integer and $0 \leq n \leq N$. Additionally, we have to find a number for $N_{\max}$. The most exact result, one would get by taking $N_{\max} \to \infty$, but in reality we need to break down the summation at a certain value. The numerical error converges very slowly to zero, so that we need to calculate until $N_{\max} \approx 5000$ or larger and have to take a geometric average over different solutions for different $N_{\max}$.

3.4.2 Iterative method

Now, we want to solve the Boltzmann equation iteratively without making any approximation out of the upper sections. We start with a similar Boltzmann equation as in the upper section in Eq. (3.53). It is

$$v_p \sin(\phi) \frac{\partial n_{0,p}}{\partial y} + v_p \sin(\phi) \frac{\partial \delta n_{\vec{p}}}{\partial y} + v_p \cos(\phi) \frac{\partial n_{0,p}}{\partial x} + v_p \cos(\phi) \frac{\partial \delta n_{\vec{p}}}{\partial x} = -\frac{\delta n_{\vec{p}}}{\tau_{\vec{p}}} , \tag{3.86}$$

with $\vec{p} = p\cos(\phi)\hat{e}_x + p\sin(\phi)\hat{e}_y$. Again, we assume delta scatterers to be the main and only scattering process in the bulk material. This implies

$$\tau_{\vec{p}} = \tau_p . \tag{3.87}$$

However, we perform a transformation and write (cf. Eq. (3.2))

$$n_{\vec{p}} = n_{\vec{p}}^{(0)} + \tilde{n}_{\vec{p}} = n_{\vec{p}}^{(0)} + n_{0,p} + \delta n_{\vec{p}}\,, \tag{3.88}$$

with

$$n_{\vec{p}}^{(0)} = \frac{1}{e^{\omega_p/(k_B T_0)} - 1}\,, \tag{3.89}$$

which is independent of x. The temperature T_0 is here free to choose and will be fixed later to be the average temperature of the system. Therewith, the new equation reads

$$\sin(\phi)\frac{\partial \tilde{n}_{\vec{p}}}{\partial y} + \cos(\phi)\frac{\partial \tilde{n}_{\vec{p}}}{\partial x} = -\frac{\tilde{n}_{\vec{p}} - n_{0,p}}{r_p}\,, \tag{3.90}$$

with $l_p = v_p \tau_p$. Additionally, the following condition must be fulfilled

$$n_{0,p} = \frac{1}{2\pi}\int_0^{2\pi} \tilde{n}_{\vec{p}}\, d\phi\,. \tag{3.91}$$

The solution of (3.90) can directly be written down

$$\tilde{n}_{\vec{p}}(x,y) = e^{-\frac{x\sec(\phi)}{l_p}}\left(\int_1^x \frac{\sec(\phi)e^{\frac{\sec(\phi)s}{l_p}} n_{0,p}(s, \tan(\phi)(s-x)+y)}{l_p}\, ds + c_1(y - x\tan(\phi))\right). \tag{3.92}$$

By labeling a particle trajectory with the label m, the trajectory will be $y = (m-(1/2))\sec(\phi) + x\tan(\phi)$. Thus, the upper expression can be rewritten

$$\tilde{n}_{\vec{p}}(x,m) = e^{-\frac{x\sec(\phi)}{l_p}}\left(\int_1^x \frac{\sec(\phi)e^{\frac{\sec(\phi)s}{l_p}} n_{0,p}(s, \tan(\phi)s + \left(m-\frac{1}{2}\right)\sec(\phi))}{l_p}\, ds + D(m,k)\right). \tag{3.93}$$

The open constant $D(m,k)$ will be matched by the boundary conditions. By now, Eqs. (3.91) and (3.93) form a system of integral equations. The strategy of finding the correct solution for the upper system of integral equations contains a starting function for $n_{0,p}$. Here, we take the result out of section 3.3.1. As usual in numeric calculations, we discretize the functions $n_{0,p}$ and $\tilde{n}_{\vec{p}}$. After that, we alternately use Eqs. (3.91) and (3.93) as long as the result converges. Additionally, the fixed temperatures have to fulfill the following inequalities

$$T_0 = \frac{T_L + T_R}{2} \qquad |T_L - T_0| \ll T_0 \qquad |T_R - T_0| \ll T_0\,. \tag{3.94}$$

Perfectly reflecting walls

Now, the walls at $y = 0$ and $y = B$ are modeled as perfect reflecting walls. This corresponds to Eqs. (3.23) and (3.24). Because of these mirror-walls, the system becomes periodic in $2B$. Additionally, Eqs. (3.19) (3.20) (3.21) and (3.22) hold. Then Eq. (3.21) becomes

$$(\Delta N)_p = e^{\frac{L\sec(\phi)}{2l_p}}\left(\int_1^{-L/2} \frac{\sec(\phi)e^{\frac{\sec(\phi)s}{l_p}} n_{0,p}(s, \tan(\phi)s + \left(m-\frac{1}{2}\right)\sec(\phi))}{l_p}\, ds + D(m,k)\right). \tag{3.95}$$

Converted to

$$D(m,k) = -\int_{1}^{-L/2} \frac{\sec(\phi) e^{\frac{\sec(\phi)s}{l_p}} n_{0,p}(s, \tan(\phi)s + \left(m - \frac{1}{2}\right)\sec(\phi))}{l_p}\, ds + (\Delta N)_p e^{\frac{-L\sec(\phi)}{2l_p}}\,. \tag{3.96}$$

Setting this term into Eq. (3.93) brings us to

$$\begin{aligned}\tilde{n}_{\vec{p},\phi,\text{right}}(x,m) =& (\Delta N)_p\, e^{-\frac{(L+2x)\sec(\phi)}{2l_p}} \\ &+ e^{-\frac{x\sec(\phi)}{l_p}} \int_{-L/2}^{x} \frac{\sec(\phi) e^{\frac{\sec(\phi)s}{l_p}} n_{0,p}(s, \tan(\phi)s + \left(m - \frac{1}{2}\right)\sec(\phi))}{l_p}\, ds\,.\end{aligned} \tag{3.97}$$

Similarly Eq. (3.22), becomes

$$-(\Delta N)_p = e^{-\frac{L\sec(\phi)}{2l_p}} \left(\int_{1}^{L/2} \frac{\sec(\phi) e^{\frac{\sec(\phi)s}{l_p}} n_{0,p}(s, \tan(\phi)s + \left(m - \frac{1}{2}\right)\sec(\phi))}{l_p}\, ds + D(m,k) \right). \tag{3.98}$$

Converted to

$$D(m,k) = -\int_{1}^{L/2} \frac{\sec(\phi) e^{\frac{\sec(\phi)s}{l_p}} n_{0,p}(s, \tan(\phi)s + \left(m - \frac{1}{2}\right)\sec(\phi))}{l_p}\, ds - (\Delta N)_p e^{\frac{L\sec(\phi)}{2l_p}}\,. \tag{3.99}$$

Setting this term into Eq. (3.93) brings us to

$$\begin{aligned}\tilde{n}_{\vec{p},\phi,\text{left}}(x,m) =& -(\Delta N)_p\, e^{-\frac{(2x-L)\sec(\phi)}{2l_p}} \\ &- e^{-\frac{x\sec(\phi)}{l_p}} \int_{x}^{L/2} \frac{\sec(\phi) e^{\frac{\sec(\phi)s}{l_p}} n_{0,p}(s, \tan(\phi)s + \left(m - \frac{1}{2}\right)\sec(\phi))}{l_p}\, ds\,.\end{aligned} \tag{3.100}$$

Here, one has to consider $\sec(\phi) < 0$ for left moving particles. By now, Eqs. (3.97) and (3.100) as well as Eq. (3.91) form the system of integral equations which can be solved iteratively. For numerical calculation, we discretize the system. We sub-divide the GGG crystal into a lattice of small squares. For faster calculation, we first set up a four dimensional tensor, which fulfills the following identity

$$n_{0,p}(x_0, y_0) = \sum_{x,y} A(x_0, y_0, x, y)\, n_{0,p}(x, y) + A_{\text{offset}}(x_0, y_0)\,. \tag{3.101}$$

The tensor A will be found by taking Eq. (3.91) and insert Eqs. (3.97) and (3.100) and then read out the prefactors. The equations (3.97) and (3.100) are composed in a specific way. The first summand describes the distribution of particles coming out of the thermal reservoir and relaxed over the distance $(x+L/2)$ or $(L/2-x)$, respectively. The second summand contains particles, which have been scattered by impurities in the bulk GGG crystal at position $(s, \tan(\phi)s + \left(m - \frac{1}{2}\right)\sec(\phi))$ and then propagating to the position (x, y) with relaxation length l_p. As a test for consistency, one may take a uniform additional particle density $(\Delta N)_p$ on both sides of the boundaries ($x = \pm L/2$). One would expect a uniform and overall additional particle density $(\Delta N)_p$. If one applies these boundary conditions, one has to change the minus sign in front of $(\Delta N)_p$ in Eq. (3.22). This corresponds to change the minus

sign of $(\Delta N)_p$ in Eq. (3.100). If one takes a uniform particle density as a starting function for the convergence process, i.e. one takes $n_{0,p}(s, \tan(\phi)s + \left(m - \frac{1}{2}\right)\sec(\phi)) = +(\Delta N)_p$, then Eqs. (3.97) and (3.100) reduce to $(\Delta N)_p$.

By now, we compare the phonon distribution iterative numeric results for different thicknesses B. Because translation symmetry is present, the result should not change by increasing or decreasing the thickness. This expectation will be found in figure 23. There, the particle density along the GGG substrate is plotted for different thicknesses B.

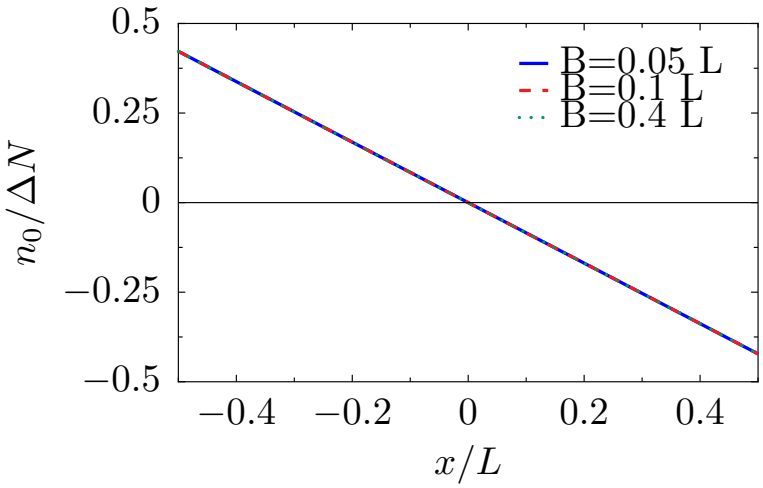

Figure 23: Phonon density for different thicknesses B by using Boltzmann iterative method. Because the system is translational invariant, the results are identical for different B. For our numerical simulation, we used a grid with site length of 1 and a length of $L = 100$. The relaxation length is $l_p = 100$.

The accordance of the particle density with different thicknesses B also holds, when the relaxation time is smaller or larger than here.

3.4.3 Comparison of Chebyshev polynomials with iterative method

Furthermore, one may compare the iterative method out of section 3.4.2 with results from Chebyshev-method out of section 3.4.1. The comparison can be found in figure 24. The accordance is also given at other relaxation lengths.

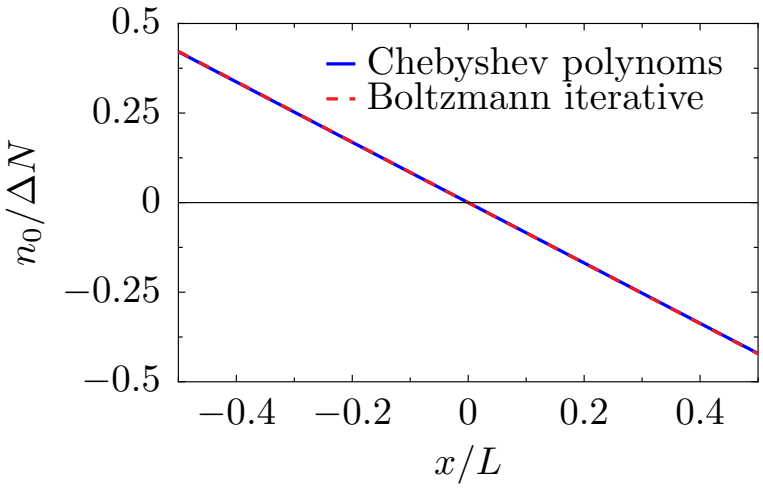

Figure 24: Phonon density by using Chebyshev polynomials and Boltzmann iterative method. For our numerical simulation, we used a grid with site length of 1 and a length of $L = 100$. The relaxation length is $l_p = 100$.

Just as well, we calculate the phonon net current by making use of Chebyshev polynomials and the iterative method. The result can be found in figure 25. We see, that the results are the same for Chebyshev polynomials and iterative method. Also, the current conservation law is fulfilled. Later, we will see that the phonon net current does not coincide with the phonon net current out of the half-analytic method.

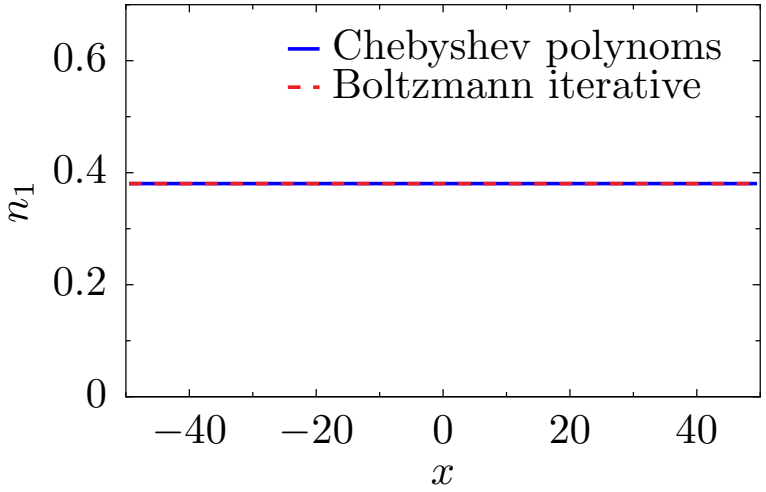

Figure 25: Phonon net current with relaxation length $l_p = 100$ and length of the system $L = 100$ by using Chebyshev polynomials method and Boltzmann iterative method.

Additionally, we analyze the phonon distribution dependent on the relaxation length l_p, which is plotted in figure 26. For ballistic particles, i.e. $l_p \gg L$, we find a line with a

small slope and a large particle density jump (or temperature jump) at the edges. At the reservoir edges ($x = \pm L/2$), half of the phonon distribution is given (cf. Eqs. (3.21) and (3.22)). Ballistic particles scatter rarely by propagating through the GGG substrate. Thus, the phonon distribution does change marginal. If one would have fully ballistic particles, the given distribution would not change in the field of the GGG substrate. The phonon density n_0 is always a mixture between left moving and right moving particles (cf. Eq. (3.91)) and averages to zero for fully ballistic particles. If the phonon relaxation length decreases, the slope of the phonon density n_0 enlarges and the temperature jump at the edges reduces. Diffusive particles (i.e. $l_p \ll L$) scatter often by propagating through the substrate. Thus, the phonon distribution does not change marginal and we can find a large slope for the particle density (or temperature).

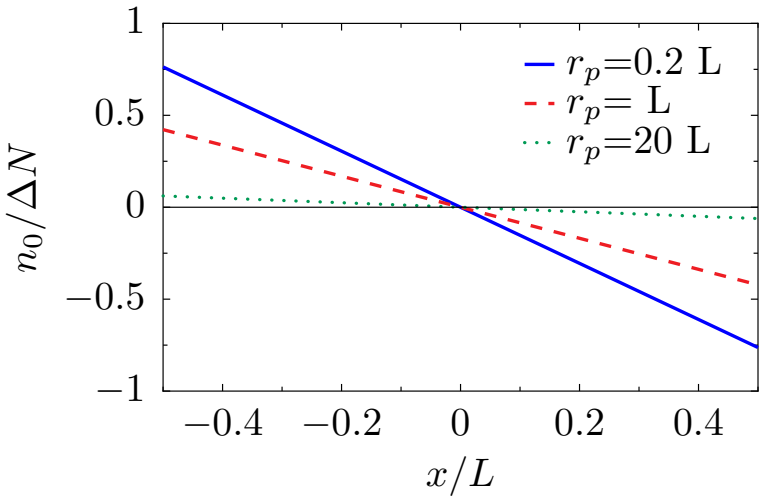

Figure 26: Phonon density for different relaxation length $r_p = l_p$ by using Boltzmann iterative method.

3.4.4 Half-analytic method

By now, we want to develop the half-analytic method in two dimensions to compare the results with the Chebyshev polynomial method and with the iterative method. Here, we will proceed as already done for three dimensions in section 3.2.1. We start with Eq. (3.90) and perform an approximation of the function $n_{0,p}$. We make the same ansatz as already done in Eq. (3.27). It is

$$n_{0,p} = (\Delta N)_p \beta x \,. \tag{3.102}$$

It is $r_p = l_p$ and we set in the upper ansatz into Eq. (3.90). We find for the Boltzmann equation

$$\sin(\phi)\frac{\partial \tilde{n}_{\vec{p}}}{\partial y} + \cos(\phi)\frac{\partial \tilde{n}_{\vec{p}}}{\partial x} = -\frac{\tilde{n}_{\vec{p}} - n_{0,p}}{r_p} \approx -\frac{\tilde{n}_{\vec{p}} - (\Delta N)_p \beta x}{r_p} \,, \tag{3.103}$$

while β still has to be found. Again, the walls at $y = 0$ and $y = B$ are modeled as perfect reflecting walls (cf. Eq. (3.23) and (3.24)). Thus, the system is effectively translational invariant in y-direction. Because of that, the y-derivative vanishes. The upper differential equation can be solved analytically. One finds

$$\tilde{n}_{\vec{p}} = D e^{-\frac{x}{l_p \cos(\phi)}} + \beta (\Delta N)_p x - \beta (\Delta N)_p l_p \cos(\phi) \,. \tag{3.104}$$

Again, the variable D will be determined by the boundary conditions at the heat reservoirs. At the reservoir edges ($x = \pm L/2$), the phonon distribution is given (cf. Eqs. (3.21) and (3.22)).

$$\tilde{n}_{p,\phi,\text{right}}(x = -L/2) = (\Delta N)_p \tag{3.105}$$

$$\tilde{n}_{p,\phi,\text{left}}(x = L/2) = -(\Delta N)_p\,. \tag{3.106}$$

Calculate the boundary conditions at the reservoir, rearrange them for the parameter D and setting them back into the phonon density function (Eq. (3.104)) results in

$$\begin{aligned}\tilde{n}_{\vec{p},\text{right}} =&(\Delta N)_p \beta x - (\Delta N)_p l_p \beta \cos(\phi) \\ &+ \frac{1}{2}(\Delta N)_p(\beta L + 2\beta\, l_p \cos(\phi) + 2) e^{-\frac{(L+2x)\sec(\phi)}{2l_p}}\,,\end{aligned} \tag{3.107}$$

and

$$\begin{aligned}\tilde{n}_{\vec{p},\text{left}} =&(\Delta N)_p \beta x - (\Delta N)_p l_p \beta \cos(\phi) \\ &- \frac{1}{2}(\Delta N)_p(\beta L - 2\beta\, l_p \cos(\phi) + 2) e^{\frac{(L-2x)\sec(\phi)}{2l_p}}\,.\end{aligned} \tag{3.108}$$

The parameter β still has to be found. We have done this iteratively by alternately using above equations and Eq. (3.91) and starting with some random parameters. The half-analytic method is compared to numerical calculations out of section 3.4.2. In figures 27, 28 and 29 the phonon distribution is plotted. Here we will find accordance between the iterative method and the half-analytic method. If one would compare the phonon net current, there will be no accordance in the results. For later chapters, we only need the phonon density distribution. Because of that, we will use the results out of the half-analytic method out of section 3.2 for further calculations.

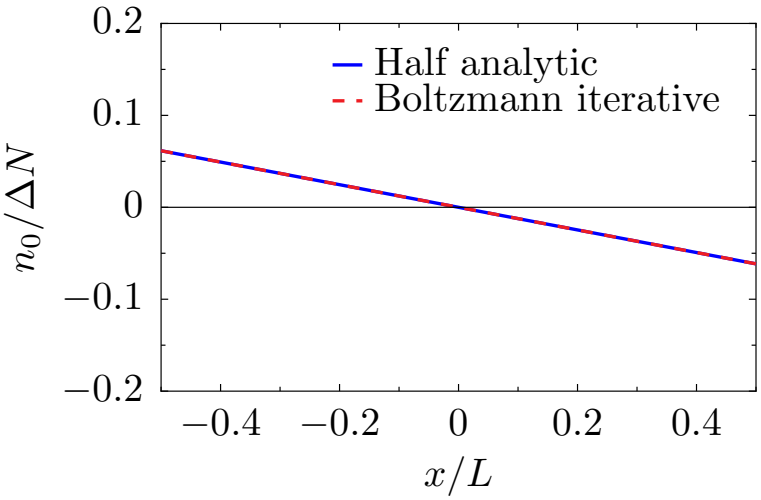

Figure 27: Phonon density for $l_p = 20L$ by using Boltzmann iterative method and half-analytic method.

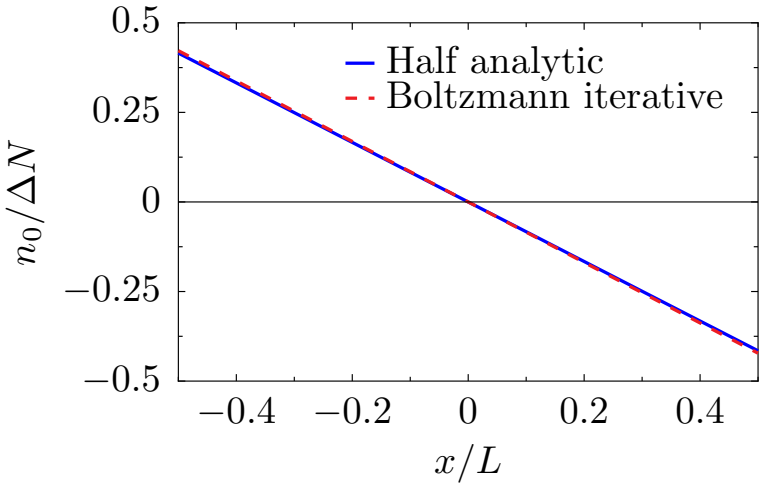

Figure 28: Phonon density for $l_p = L$ by using Boltzmann iterative method and half-analytic method.

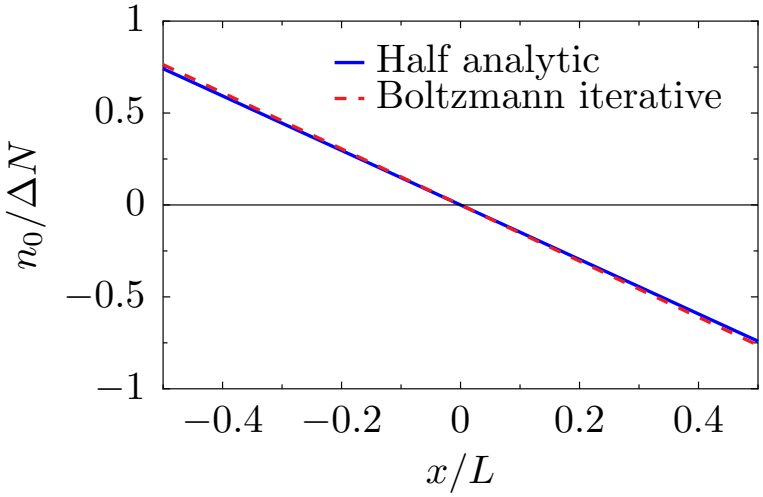

Figure 29: Phonon density for $l_p = 0.2L$ by using Boltzmann iterative method and half-analytic method.

3.4.5 Single-Point approximation

Now, we perform a single-point approximation as already done in section 3.2.2. We approximate the average phonon density $n_{0,p}$ to be linear and evaluate both sides of Eq. (3.91) on a single point at $x = -L/2$. If one performs the diffusive approximation, we take Eqs. (3.107) and (3.108) and set in $x = -L/2$. We evaluate this equation and find

$$\begin{aligned}
-(\Delta N)_p \beta \frac{L}{2} =& n_{0,p}(-L/2) \\
=& \frac{1}{2\pi} \int_0^{2\pi} \tilde{n}_{\vec{p}}(-L/2)\, d\phi \\
=& \frac{1}{\pi} \int_0^{\pi/2} \tilde{n}_{\vec{p},\text{right,diffusive}}(-L/2)\, d\phi + \frac{1}{\pi} \int_{\pi/2}^{\pi} \tilde{n}_{\vec{p},\text{left,diffusive}}(-L/2)\, d\phi
\end{aligned} \tag{3.109}$$

This is

$$\begin{aligned}
-(\Delta N)_p\beta\frac{L}{2} =& \frac{1}{\pi}\int_0^{\pi/2}(-(\Delta N)_p\beta\frac{L}{2} - (\Delta N)_p l_p\beta\cos(\phi) \\
&+ \frac{1}{2}(\Delta N)_p(\beta L + 2\beta\, l_p\cos(\phi) + 2)e^{-\frac{(L-L)\sec(\phi)}{2l_p}})\, d\phi \\
&+ \frac{1}{\pi}\int_{\pi/2}^{\pi}(-(\Delta N)_p\beta\frac{L}{2} - (\Delta N)_p l_p\beta\cos(\phi) \\
&- \frac{1}{2}(\Delta N)_p(\beta L - 2\beta\, l_p\cos(\phi) + 2)e^{\frac{(L+L)\sec(\phi)}{2l_p}})\, d\phi \\
=& -(\Delta N)_p\frac{\beta L}{2} + (\Delta N)_p\frac{\beta L}{4} + (\Delta N)_p\frac{\beta\, l_p}{\pi} + (\Delta N)_p\frac{1}{2} \\
&- \beta(\Delta N)_p I_1 - (\Delta N)_p I_2\,, \qquad (3.110)
\end{aligned}$$

with

$$I_1 = \frac{1}{\pi}\int_{\pi/2}^{\pi}\left(\frac{L}{2} - l_p\cos(\phi)\right)e^{\frac{L\sec(\phi)}{l_p}}\, d\phi \qquad (3.111)$$

$$I_2 = \frac{1}{\pi}\int_{\pi/2}^{\pi}e^{\frac{L\sec(\phi)}{l_p}}\, d\phi\,. \qquad (3.112)$$

The upper equation can be transformed and one finds

$$\beta = -\frac{2\pi - 4\pi I_2}{\pi L + 4l_p - 4\pi I_1}\,. \qquad (3.113)$$

The same result would be obtained by evaluating Eq. (3.91) for $x = +L/2$.

3.4.6 Diffusive regime approximation

If the relaxation length is much smaller than the system length (i.e. $l_p \ll L$), one can perform an approximation for the phonon density. This is already done in section 3.2.3. Inside the Eqs. (3.111) and (3.112), the exponent in the exponential function becomes close to zero, because $\sec(\phi) < 0$. Thus I_1 and I_2 become close to zero. The result reads

$$\beta \approx -\frac{2\pi}{\pi L + 4l_p}\,. \qquad (3.114)$$

The phonon density at the left end of the substrate (i.e. $x = -L/2$) is plotted in figures 30 and 31. Generally, particles are only influenced by the phonon density in the proximity of length l_p.

For large relaxation length (i.e. $l_p \gtrsim L$), the average particle density and temperature for those phonons is nearly the same in the whole substrate, i.e. they have a small slope. The average temperature is the mean value T_0 of the left and right thermal baths. If the relaxation length is smaller than the sample length, out coming particles from the right lead relax before they reach the left end. Then, those particles are only influenced by the phonon density in the proximity, i.e. they have a large slope.

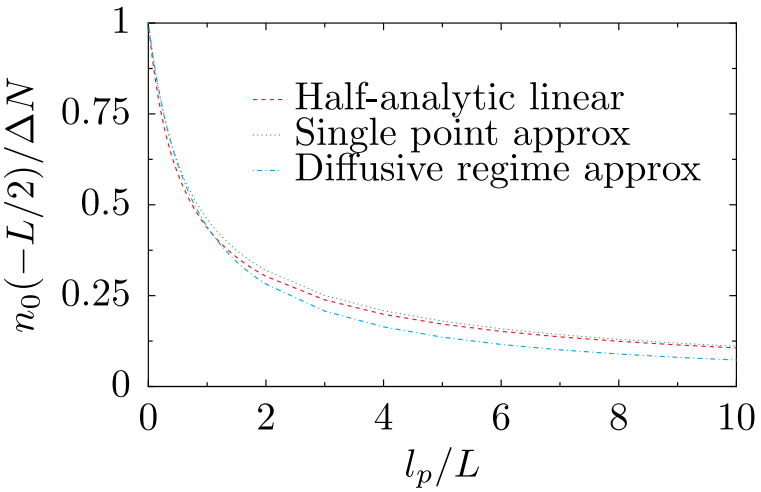

Figure 30: Phonon density at $x = -L/2$ for different methods and relaxation length l_p.

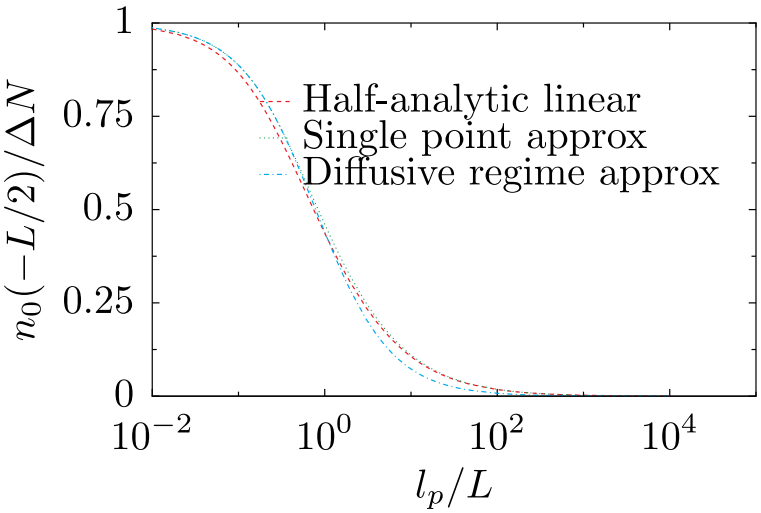

Figure 31: Phonon density at $x = -L/2$ for different methods and relaxation length l_p.

Now, we want to calculate the relaxation length l_p dependent on the phonon wave number. In section 3.2.3, we already set up the relations between wave number and the relaxation length. The formula for relaxation length are in Eqs. (3.40) and (3.41). We take the same parameters as in section 3.2.3. In figures 32 and 33 the particle density in two dimensions at the left end of the substrate (i.e. $x = -L/2$) is plotted dependent on the absolute value of the k-vector of the phonons.

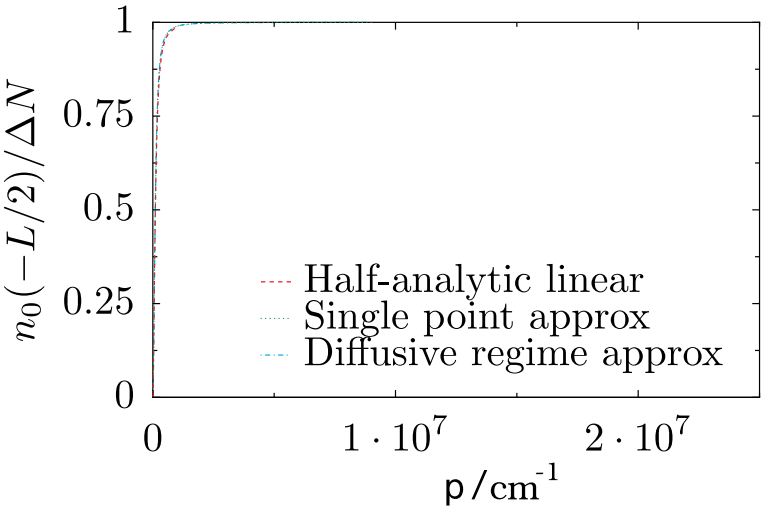

Figure 32: Phonon density at $x = -L/2$ for different methods and wave numbers k at 300 Kelvin. The Fermi wave number is $k_\mathrm{F} = 3.10 \cdot 10^7 \cdot \mathrm{cm}^{-1}$.

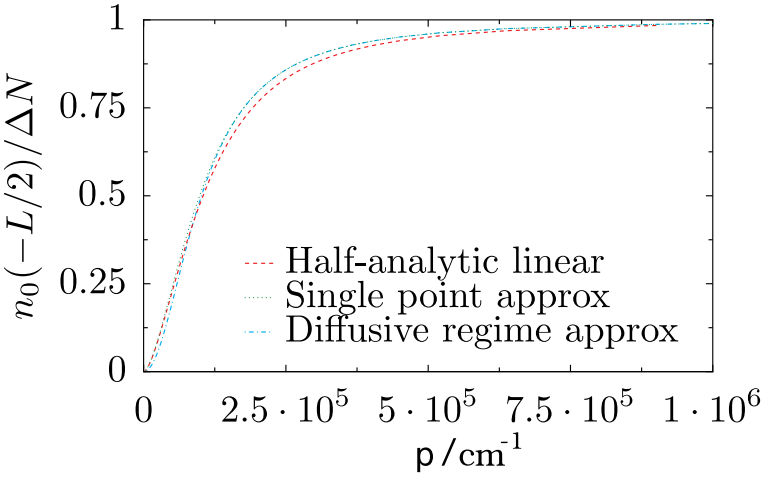

Figure 33: Zoom of figure 32: Phonon density at $x = -L/2$ for different methods and wave numbers k at 300 Kelvin. The Fermi wave number is $k_\mathrm{F} = 3.10 \cdot 10^7 \cdot \mathrm{cm}^{-1}$.

In Eq. (3.40), we introduced the boundary scattering as a fixed relaxation time in the relaxation time approximation. Now, we want to compare this relaxation time approximation in the half-analytic approximation with a full numeric calculation of the phonon problem in two dimensions. We consider a system of length L and width $W = 0.2 \cdot L$. With that, we have an effective relaxation length of $L_\mathrm{eff} = \sqrt{L \cdot W}$. For the numerical calculation, we take the method out of subsection 3.4.2. Instead of perfectly reflecting walls, we will use rough walls in our simulation. In figure 34, we compared the numerical calculation with the relaxation time approximation for the boundary scattering.

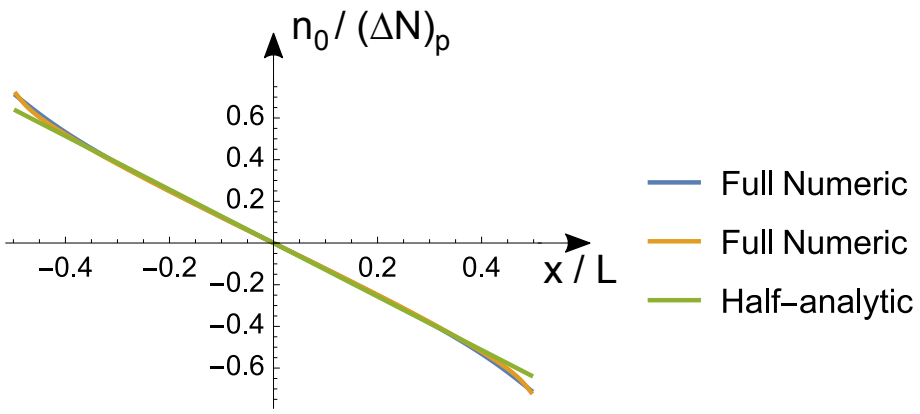

Figure 34: Comparison of numeric calculation (method from subsection 3.4.2 with rough walls) and half-analytic relaxation time approximation for boundary scattering. Here the spatial phonon density distribution is plotted.

3.5 Summary

In this chapter, we considered the phonon propagation in a cuboid when a temperature difference is applied and for different average temperatures T_0. The material is chosen to be GGG ($Gd_3Ga_5O_{12}$). On the left side, the cuboid is connected to an ideal heat reservoir at temperature $T_0 + \Delta T$. Alike, on the right side, the cuboid is connected to an ideal heat reservoir at temperature $T_0 - \Delta T$. Thus, there will be a net current of phonons flowing to the right side and current conservation is fulfilled. Since the heat reservoirs are modeled to be perfect heat reservoirs, outcoming phonons are Bose-Einstein distributed with temperature $T_0 + \Delta T$ for the left and $T_0 - \Delta T$ for the right reservoir, respectively. Here, we calculated the resulting spatial phonon density dependent on the relaxation length and later dependent on the wave number.

At the end, we calculate the slope of the temperature profile for different phonons. Phonons with a large wave number have a small relaxation length and thus are diffusive phonons. We will find a large slope of the phonon density / temperature for these diffusive phonons. Diffusive phonons only scatter with phonons which are in the proximity in a range of the relaxation length. Ballistic phonons have a large relaxation length. Typically, phonons with a small wave number have a large relaxation length and thus are ballistic phonons. These phonons have a small slope in the phonon density / temperature. Ballistic phonons propagate nearly hitchless through the substrate and thus keep their phonon density / temperature. This means, that right moving phonons have the temperature $T_0 + \Delta T$ and left moving particles have temperature $T_0 - \Delta T$. For calculating the density, one takes the average, which is at T_0 with the correspondent phonon density. If one decreases the temperature T_0, the ratio of ballistic phonons increases.

The calculation will be done by using the Boltzmann equation in relaxation time approximation in three dimensions. At the beginning, we performed a half-analytic approximation. That is, we approximate the angle averaged phonon density to have a linear structure. With that, we are able to solve the Boltzmann equation analytically. The result is dependent on the phonon relaxation length. For calculating the slope of the angle averaged phonon density, we perform a single-point approximation. That is, we evaluate the function for the angle average at a certain point, here at the border to the left heat reservoir. The result can also be simplified for phonons with a shorter relaxation length l_p compared to the cuboid length

L. For calculating the connection between relaxation length and phonon wave number, we use calculations from Neelmani *et al.* [48]. They made temperature dependent phonon conductivity calculations for GGG and used Callaway's model [49] for their calculations.

Furthermore, we performed a microscopic calculation in one dimension. We have shown, that these simpler calculations are not appropriate to describe the phonon density distribution / temperature.

It is also possible to leave out the half-analytic approximation, but then one has to use numeric methods to calculate the resulting phonon density / temperature. We developed a method by making use of Chebyshev polynomials and another method with an iterative algorithm. We compared these two methods in two dimensions with the half-analytic approximation in two dimensions. We found a good matching in the results by comparing the phonon density for different phonon wave numbers.

4 Coupled phonon-magnon system

In this chapter, we consider a thin film out of a magnetic insulator on top of the GGG ($Gd_3Ga_5O_{12}$) substrate. This magnetic insulator is chosen to be YIG (Yttrium iron garnet, $Y_3Fe_5O_{12}$). This is a typical setup for the transverse spin Seebeck effect. We will analyze the influence of the phonons onto the magnons inside the magnetic insulator by making use of the Boltzmann equation. Since the thickness of the GGG substrate is much thicker than the thickness of the YIG film, the phonons are rarely influenced by the magnons. Thus, the phonon temperature profile out of chapter 3 will be used as an input parameter. The spatial temperature profile of the magnons will be calculated.

For calculating the influence of the phonons onto the magnons, we will derive the Hamilton operator in section 4.1 for dipolar magnons as well as for exchange magnons. In section 4.2, we will derive the Boltzmann equation of the coupled phonon-magnon system. The collision integral to this Boltzmann equation will be calculated in section 4.3. Here, we will make use of the prefactors in front of the creation and annihilation operators in the Hamilton operator, which was derived in section 4.1. With that, we want to develop an integral equation for the wave vector dependent magnon temperature, which can be solved numerically. The wave vector dependent phonon temperature will be treated as an input parameter and cannot be changed. The magnon-magnon interaction will be included in section 5.

For our calculation, we take the sample size out of Ref. [21]. The GGG substrate is $d_{\mathrm{GGG}} = 0.5$ mm thick, $L_{\mathrm{GGG}} = 8$ mm long and $w_{\mathrm{GGG}} = 4$ mm wide. On top of it, there is a YIG-film, which is $d_{\mathrm{YIG}} = 3.9$ µm thick, $L_{\mathrm{YIG}} = 8$ mm long and $w_{\mathrm{YIG}} = 4$ mm wide. One has to mention, that the length and the width of the GGG substrate are the same as for the YIG-film. At the end, there will be a small Pt-stripe on top of the YIG-film. This is $d_{\mathrm{Pt}} = 15$ nm thick, $L_{\mathrm{Pt}} = 0.1$ mm long and $w_{\mathrm{Pt}} = 4$ mm wide. One has to mention, that the width of the Pt stripe is the same as for the YIG-film and the GGG substrate. The length of the Pt-stripe is smaller than of the YIG film. The schematical setup can be found in figure 4 in chapter 1 or figure 9 in chapter 3.

The thickness of the GGG substrate is much thicker than the thickness of the YIG film ($d_{\mathrm{YIG}} \ll d_{\mathrm{GGG}}$). Because of that, propagating phonons are mostly propagating in an area, where no magnons are present. Phonons with a large relaxation length, coming out of the YIG-stripe will propagate nearly hitchless until they reach the thermal reservoir and relax there. Only particles coming out of the YIG-stripe in a very small angular range, which is close to perpendicular to the surface will be reflected at the opposite wall and then come back into the stripe. Thus, the phonons are not much influenced by magnons and we can neglect the influence from the magnons onto the phonons. In section 3, we calculated the phonon density distribution. Based on this calculation, we will calculate the influence from the phonons onto the magnons. This will be done in this chapter. Magnons are only able to propagate in the YIG-film. In the whole YIG-film phonons are also able to propagate. Thus, one has to write down the full Boltzmann equation for magnons and has to include phonon-magnon interaction as well as magnon-magnon interaction. The phonon density distribution here is treated as an input parameter and cannot be changed. We write down the Boltzmann equation for the magnons as already done in Eq. (3.5). It is

$$-\frac{\epsilon_{\vec{k}}}{T_0}\frac{\partial f^{(0)}_{\vec{k}}}{\partial \epsilon}(\vec{v}_{\vec{k}}\cdot\vec{\nabla}T_{\mathrm{M}}) + \vec{v}_{\vec{k}}\cdot\vec{\nabla}\delta f_{\vec{k}} = \left.\frac{\partial f_{\vec{k}}}{\partial t}\right|_{\mathrm{St,mag\text{-}pho}} + \left.\frac{\partial f_{\vec{k}}}{\partial t}\right|_{\mathrm{St,mag\text{-}mag}}, \tag{4.1}$$

while T_{M} denotes the spatial and wave vector dependent magnon temperature. T_0 is the average temperature. The wave vector dependent magnon energy dispersion is denoted by

$\epsilon_{\vec{k}}$, while we use Eq. (2.6). The parameter $\vec{v}_{\vec{k}}$ denotes the wave vector dependent magnon velocity. In general one finds their absolute value, by taking the wave vector derivative of the energy dispersion. The magnon density distribution $f_{\vec{k}}$ is composed as in Eq. (3.1). Additionally Eqs. (3.9) and (3.10) are valid. The first summand on the right hand side of Eq. (4.1) determines the collision integral of the magnon-phonon-interaction. It will be derived in section 4.3 and reads

$$\left.\frac{\partial f_{\vec{k}}}{\partial t}\right|_{\text{St,mag-pho}} = \sum_{\vec{p}} \left\{ \frac{1}{\tau_{pk}^{mp}} \frac{T_{\text{Ph}}(p) - T_{\text{M}}(k)}{T_0} - \frac{1}{\tilde{\tau}_{pk}^{mp}} \frac{T_{\text{Ph}}(p) - T_{\text{M}}(|\vec{k}-\vec{p}|)}{T_0} \right\}, \tag{4.2}$$

while the abbreviations are given in Eqs. (4.56) and (4.57). T_{Ph} denotes the spatial and wave vector dependent phonon temperature. In the same way, the collision term for the magnon-magnon interaction will be derived in section 5. The result is the sum of the two Eqs. (5.11) and (5.63).

4.1 Hamilton operators for magnon-phonon-interaction

The goal of this chapter is to calculate the collision integral for the magnon-phonon interaction in the transverse spin Seebeck effect. To reach this goal, we start by writing down the Hamilton operator for the magnon-phonon coupling. At first, we will consider dipole dipole magnons and after that exchange magnons. The prefactor of the Hamilton operator will be used for writing down the collision integral in the Boltzmann equation. In this section, we will present a short calculation of the Hamilton operator. The detailed calculation can be found in the appendix (chapter B).

4.1.1 Dipole-dipole interaction

Here, we want to calculate the Hamilton operator and read out its prefactors. We start with the magnetoelastic energy for the magnon-phonon interaction with dipolar magnons [43, p. 315].

$$U_{\text{mel}} = \frac{B_1}{M_0^2} \sum_{p=1}^{3} M_p^2 e_{pp} + \frac{B_2}{M_0^2} \sum_{p,q=1,q\neq p}^{3} M_p M_q e_{pq}\,, \tag{4.3}$$

while M_p denotes the local magnetization in spatial direction p and e_{pq} denotes the symmetric strain tensor. The indices are $p, q \in \{x, y, z\}$. We follow the calculation of Kaganov *et al.* [51]. In our calculation, the YIG lattice structure will be modeled by a 3-dimensional cubic lattice with identical unit cell volume (lattice constant $a = 1.25$ nm [52, 53]). The spin inside one single unit cell will be modeled as one single spin with strength $S = 14.2$ [53]. In the following we use the transformations

$$M_i = -\gamma \hbar S_i \tag{4.4}$$

$$e_{pq} = \frac{1}{2}\left(\frac{\partial u_p}{\partial x_q} + \frac{\partial u_q}{\partial x_p}\right) \tag{4.5}$$

$$\vec{u}(\vec{r}) = \sum_{\vec{p}} e^{-i\vec{p}\vec{r}} u_{\vec{p}}\, \hat{e}_{\vec{p}} = \sum_{\vec{p}} \sqrt{\frac{\hbar}{2mN\omega_p}} (b_{\vec{p}} + b_{-\vec{p}}^{\dagger}) e^{-i\vec{p}\vec{r}}\, \hat{e}_{\vec{p}}, \tag{4.6}$$

while ω_p denotes the angular frequency for phonons with wave number p (cf. Eq. (2.3)). Additionally, $\vec{S}$ denotes the net spin and its orientation of all atoms in one YIG unit cell and

S denotes its absolute value. m denotes the mass of one unit cell and N denotes the number of lattice points in the whole solid. $\vec{u}$ denotes the spatial dependent displacement vector of the lattice atom. The operators $b_{\vec{q},i}$ and $b^\dagger_{\vec{q},i}$ denote the annihilation and the creation of one phonon with wave vector $\vec{q}$ and mode i, respectively. The gyromagnetic ratio is denoted by γ and the Planck constant by $\hbar$. We insert Eq. (4.4) into the magnetoelastic energy. The spin operators S_x and S_y can be rewritten in the following way

$$S^+ = S_x + iS_y \qquad S^- = S_x - iS_y\,. \tag{4.7}$$

On the other hand, we replace the spin operators with creation and annihilation operators. This we do by using the Holstein-Primakoff transformation [54, p. 78]. To lowest order approximation, we find

$$S^+ \approx \sqrt{2S}\,a \qquad S^- \approx \sqrt{2S}\,a^\dagger \qquad S_z \approx S - a^\dagger a\,. \tag{4.8}$$

The operators a and $a^\dagger$ denote the annihilation and the creation of one magnon at position $\vec{r}$, respectively. The operators are still dependent on position $\vec{r}$. Thus, we need to Fourier transform

$$a = \frac{1}{\sqrt{N}}\sum_{\vec{k}} a_{\vec{k}} e^{-i\vec{k}\vec{r}} \qquad a^\dagger = \frac{1}{\sqrt{N}}\sum_{\vec{k}'} a^\dagger_{\vec{k}'} e^{i\vec{k}'\vec{r}}\,, \tag{4.9}$$

while N denotes the number of lattice points in three dimensions [54, p. 79]. The operators $a_{\vec{k}}$ and $a^\dagger_{\vec{k}}$ denote the annihilation and the creation of one magnon with wave vector $\vec{k}$, respectively. The Hamilton operator is the summation of the energy in the whole solid. One finds

$$H = \int_V d^3\vec{x}\, U_{\text{mel}}\,. \tag{4.10}$$

We rearrange the terms by assuming $b_2 = b_1$ for an isotropic ferromagnet [43, p. 315]. Energy conservation needs to be fulfilled. Terms with only annihilation- or creation-operators vanish, because energy conservation is never fulfilled in these cases. After a long calculation, we find

$$\begin{aligned}
H =& H_{\text{const}} + \frac{6a^3}{\pi}\sqrt{N}\sum_{\vec{p}} \frac{b_1\sqrt{2S}S}{2i}\sqrt{\frac{\hbar}{2mN\omega_p}}(p_z(a^\dagger_{\vec{p}}(b_{\vec{p}}\,e_{\vec{p},x} - ib_{\vec{p}}\,e_{\vec{p},y}) + a_{-\vec{p}}(b^\dagger_{-\vec{p}}\,e_{\vec{p},x} + ib^\dagger_{-\vec{p}}\,e_{\vec{p},y})) \\
&\quad + (p_x + ip_y)a^\dagger_{\vec{p}}b_{\vec{p}}\,e_{\vec{p},z} + (p_x - ip_y)a_{-\vec{p}}b^\dagger_{-\vec{p}}\,e_{\vec{p},z}) \\
&+ \frac{6a^3}{\pi}\sum_{\vec{k}\vec{p}} \frac{b_1 S}{2i}\sqrt{\frac{\hbar}{2mN\omega_p}}(a_{\vec{k}}a_{-\vec{k}-\vec{p}}(p_x - ip_y)(b^\dagger_{-\vec{p}}\,e_{\vec{p},x} - ib^\dagger_{-\vec{p}}\,e_{\vec{p},y}) \\
&\quad + a^\dagger_{\vec{k}}a^\dagger_{-\vec{k}+\vec{p}}(p_x + ip_y)(b_{\vec{p}}\,e_{\vec{p},x} + ib_{\vec{p}}\,e_{\vec{p},y})) \\
&+ \frac{6a^3}{\pi}\sum_{\vec{k}\vec{p}} \frac{b_1 S}{2i}\sqrt{\frac{\hbar}{2mN\omega_p}}a_{\vec{k}}a^\dagger_{\vec{k}+\vec{p}}((p_x + ip_y)(b_{\vec{p}}\,e_{\vec{p},x} + b^\dagger_{-\vec{p}}\,e_{\vec{p},x} - ib_{\vec{p}}\,e_{\vec{p},y} - ib^\dagger_{-\vec{p}}\,e_{\vec{p},y}) \\
&\quad + (p_x - ip_y)(b_{\vec{p}}\,e_{\vec{p},x} + b^\dagger_{-\vec{p}}\,e_{\vec{p},x} + ib_{\vec{p}}\,e_{\vec{p},y} + ib^\dagger_{-\vec{p}}\,e_{\vec{p},y})) \\
&- \frac{6a^3}{\pi}\sum_{\vec{k}\vec{p}} \frac{b_1 S}{2i}\sqrt{\frac{\hbar}{2mN\omega_p}}a_{\vec{k}}a^\dagger_{\vec{k}+\vec{p}}(4p_z(b_{\vec{p}} + b^\dagger_{-\vec{p}})\,e_{\vec{p},z})\,.
\end{aligned} \tag{4.11}$$

Now, we need to identify the prefactors of the different Hamilton operators. The first summand contains the conversion from one magnon into one phonon and vice versa. Energy

and momentum conservation needs to be fulfilled. This is only the case, when the dispersion relation for magnons and phonons intersect (cf. figure 39). Since this is true only for two points of the dispersion relation, the first summand will be neglected in the upper expression for the Hamilton operator. The second summand contains the transformation of one phonon into two magnons and vice versa. Furthermore, the scattering from one magnon into one magnon and one phonon and vice versa is contained in the third as well as in the fourth summand. Now, we read out the prefactor to the second summand. Thus we have to identify the prefactor to the phonon and magnon operators times the unit vector. Since $e_{\vec{p},x} - i\, e_{\vec{p},y}$ is not a unit vector, we need to take out a prefactor $\sqrt{2}$, that makes this vector to a unit vector. We find

$$V_{2\mathrm{M}} = \frac{6a^3}{\pi}\frac{\sqrt{2}b_1 S}{2i}\sqrt{\frac{\hbar}{2mN\omega_p}}(p_x - ip_y) = \frac{6a^3}{\pi}\frac{B_1}{\sqrt{2}iS}\sqrt{\frac{\hbar}{2mN\omega_p}}(p_x - ip_y)\,. \tag{4.12}$$

Thus

$$|V_{2\mathrm{M}}|^2 = \frac{36a^6}{\pi^2}\frac{B_1^2}{2S^2}\frac{\hbar}{2mN\omega_p}(p_x^2 + p_y^2) = \frac{36a^6}{\pi^2}\frac{\hbar B_1^2}{4mNc_{\mathrm{Ph}}S^2}p\sin^2(\vartheta)\,. \tag{4.13}$$

The scattering amplitude, which is the prefactor to the third and fourth summand, reads

$$V_{\mathrm{Sc}} = \frac{6a^3}{\pi}\frac{b_1 S}{2i}\sqrt{\frac{\hbar}{2mN\omega_p}}((p_x + ip_y)\sqrt{2} + (p_x - ip_y)\sqrt{2} - 4p_z)\,. \tag{4.14}$$

Thus

$$|V_{\mathrm{Sc}}|^2 = \frac{36a^6}{\pi^2}\frac{\hbar B_1^2}{4S^2mN\omega_p}\frac{1}{2}(8p^2\sin^2(\vartheta)\cos^2(\varphi) - 16\sqrt{2}\sin(\vartheta)\cos(\varphi)\cos(\vartheta) + 16\cos^2(\vartheta))\,. \tag{4.15}$$

We perform an approximation, where we average over the angles ϑ and φ of the orientation of the magnon magnetic moment. We get

$$|V_{\mathrm{Sc,av}}|^2 = \frac{1}{4\pi}\int_0^{2\pi}\int_0^{\pi}\sin(\vartheta)\,|V_{\mathrm{Sc}}|^2 d\vartheta d\varphi = \frac{36a^6}{\pi^2}\frac{\hbar B_1^2}{4S^2mNc_{\mathrm{Ph}}}\frac{1}{2}p\left(\frac{8}{3} + 0 + \frac{16}{3}\right)\,, \tag{4.16}$$

where ϑ denotes the angle between the magnetization direction and the vector $\vec{p}$. It is $m = \rho \cdot V_{\mathrm{EZ}} = \rho \cdot a^3$ and $B_{\mathrm{ges}} = B_1 \cdot a^3$. To calculate the prefactor, we take

$$\hbar = 1.05457266 \cdot 10^{-34}\,\mathrm{Js} \tag{4.17}$$

$$B_1 = 3.48 \cdot 10^6\,\mathrm{erg/cm^3} = 0.348\,\mathrm{J/cm^3}\,[43, p.\ 315] \tag{4.18}$$

$$\rho = 5170\,\mathrm{kg/m^3}\,[52,\ 55] \tag{4.19}$$

$$a = 1.2376\,\mathrm{nm}\,[52,\ 53] \tag{4.20}$$

$$c_{\mathrm{Ph}} = 3843\,\mathrm{m/s}\,[55] \tag{4.21}$$

$$S = 14.2\,[53]\,. \tag{4.22}$$

In the end, we find

$$|V_{2\mathrm{M}}|^2 = V_{\mathrm{mel}}^2 p\sin^2(\vartheta) \tag{4.23}$$

$$|V_{\mathrm{Sc}}|^2 = V_{\mathrm{mel}}^2\frac{1}{2}(8p^2\sin^2(\vartheta)\cos^2(\varphi) - 16\sqrt{2}\sin(\vartheta)\cos(\varphi)\cos(\vartheta) + 16\cos^2(\vartheta))\,, \tag{4.24}$$

with

$$V_{\mathrm{mel}}^2 = \frac{36a^6}{\pi^2}\frac{\hbar B_1^2}{4mNc_{\mathrm{Ph}}S^2} = \frac{1}{N}\cdot 4.95482\cdot 10^{-8}\mathrm{GHz}^2\mathrm{cm}\,. \tag{4.25}$$

The averages read

$$|V_{\mathrm{2M,av}}|^2 = \frac{1}{4\pi}\int_0^{2\pi}\int_0^{\pi}\sin(\vartheta)\,|V_{\mathrm{2M}}|^2 d\vartheta d\varphi = \frac{2}{3}\cdot\frac{p}{N}\cdot 4.95482\cdot 10^{-8}\,\mathrm{GHz}^2\,\mathrm{cm} \tag{4.26}$$

$$|V_{\mathrm{Sc,av}}|^2 = \frac{1}{4\pi}\int_0^{2\pi}\int_0^{\pi}\sin(\vartheta)\,|V_{\mathrm{Sc}}|^2 d\vartheta d\varphi = 4\cdot\frac{p}{N}\cdot 4.95482\cdot 10^{-8}\,\mathrm{GHz}^2\,\mathrm{cm}\,. \tag{4.27}$$

4.1.2 Exchange interaction

Now, we have a look at the coupling of phonons with exchange magnons. Again, we want to calculate the Hamilton operator and read out its prefactors. The magnetoelastic energy reads [43, p. 315] [51]

$$U_{\mathrm{mel}} = \frac{A_1}{M_0^2}\sum_{p,q,l=1,l\neq q}^{3}\frac{\partial M_p}{\partial x_q}\frac{\partial M_p}{\partial x_l}e_{ql} + \frac{A_2}{M_0^2}\sum_{p,q=1}^{3}\left(\frac{\partial M_p}{\partial x_q}\right)^2 e_{qq} + \frac{A_3}{M_0^2}\sum_{p,q,l=1,l\neq q}^{3}\left(\frac{\partial M_p}{\partial x_q}\right)^2 e_{ll}\,, \tag{4.28}$$

while M_p denotes the local magnetization in spatial direction p and e_{pq} denotes the symmetric strain tensor. Again, we follow the calculation of Kaganov *et al.* [51]. The long calculation can be found in the appendix (chapter B.2). We perform the transformations out of Eqs. (4.4), (4.5) and (4.6). We insert (4.4) into the magnetoelastic energy. The spin operators S_x and S_y can be rewritten. This we do by using Eqs. (4.7), (4.8) and (4.9). Additionally, we calculate the Hamilton operator via Eq. (4.10). Now, we neglect higher order terms with more than two annihilation or creation operators. If one assumes $a_2 = a_1$ (cf. Eq. (2) of Ref. [51]), then one finds

$$\begin{aligned} H =& \frac{6a^3}{\pi}\frac{a_1 S}{i}\sum_{p=1}^{3}\sum_{\vec{k}\vec{p}}\sqrt{\frac{\hbar}{2mN\omega_p}}a_{\vec{k}}a^{\dagger}_{\vec{k}+\vec{p}}\left(k_p((\vec{k}+\vec{p})\cdot\vec{p}) + (\vec{k}\cdot\vec{p})(k_p+p_p)\right)\left(b_{\vec{p}} + b^{\dagger}_{-\vec{p}}\right)e_{\vec{p},p} \\ &+ \frac{6a^3}{\pi}\frac{2a_3 S}{i}\sum_{p=1}^{3}\sum_{\vec{k}\vec{p}}\sqrt{\frac{\hbar}{2mN\omega_p}}a_{\vec{k}}a^{\dagger}_{\vec{k}+\vec{p}}p_p((\vec{k}+\vec{p})\cdot\vec{k})(b_{\vec{p}} + b^{\dagger}_{-\vec{p}})\,e_{\vec{p},p}\,. \end{aligned} \tag{4.29}$$

Let us assume $a_3 = a_1$ for simplicity. We have three phonon modes (one for each spatial dimension). Thus, we find three coupling parameters

$$V_{\mathrm{ex,x}} = \frac{6a^3}{\pi}\frac{a_1 S}{i}\sqrt{\frac{\hbar}{2mN\omega_p}}\left(k_x((\vec{k}+\vec{p})\cdot\vec{p}) + (\vec{k}\cdot\vec{p})(k_x+p_x) + 2p_x((\vec{k}+\vec{p})\cdot\vec{k})\right) \tag{4.30}$$

$$V_{\mathrm{ex,y}} = \frac{6a^3}{\pi}\frac{a_1 S}{i}\sqrt{\frac{\hbar}{2mN\omega_p}}\left(k_y((\vec{k}+\vec{p})\cdot\vec{p}) + (\vec{k}\cdot\vec{p})(k_y+p_y) + 2p_y((\vec{k}+\vec{p})\cdot\vec{k})\right) \tag{4.31}$$

$$V_{\mathrm{ex,z}} = \frac{6a^3}{\pi}\frac{a_1 S}{i}\sqrt{\frac{\hbar}{2mN\omega_p}}\left(k_z((\vec{k}+\vec{p})\cdot\vec{p}) + (\vec{k}\cdot\vec{p})(k_z+p_z) + 2p_z((\vec{k}+\vec{p})\cdot\vec{k})\right)\,. \tag{4.32}$$

Because these three interactions are different, the squares of absolute value are added in the collision integral

$$\begin{aligned}|V_{\mathrm{ex,ges}}|^2 =&|V_{\mathrm{ex,x}}|^2 + |V_{\mathrm{ex,y}}|^2 + |V_{\mathrm{ex,z}}|^2 \\ =&\frac{36a^6}{\pi^2}\frac{\hbar A_1^2}{2mNS^2\omega_p}\left((\vec{k}\cdot\vec{k})((\vec{k}+\vec{p})\cdot\vec{p})^2 + (\vec{k}\cdot\vec{p})^2(\vec{k}+\vec{p})^2 + 4(\vec{p}\cdot\vec{p})((\vec{k}+\vec{p})\cdot\vec{k})^2\right) \\ &+ \frac{36a^6}{\pi^2}\frac{\hbar A_1^2}{2mNS^2\omega_p}\left(10(\vec{k}\cdot(\vec{k}+\vec{p}))((\vec{k}+\vec{p})\cdot\vec{p})(\vec{k}\cdot\vec{p})\right) . \end{aligned} \tag{4.33}$$

The average can be calculated in the following way. Let $k' = |\vec{k}+\vec{p}|$, $\vartheta_1 = \measuredangle(\vec{p}, \vec{k}+\vec{p})$, and $\vartheta_2 = \measuredangle(\vec{k}, \vec{k}+\vec{p})$. Then

$$\begin{aligned}|V_{\mathrm{ex,ges}}|^2 =&\frac{36a^6}{\pi^2}\frac{\hbar A_1^2}{2mNS^2\omega_p}\left(kk(k'p\cos(\vartheta_1))^2 + (kp\cos(\vartheta_1+\vartheta_2))^2k'k' + 4pp(k'k\cos(\vartheta_2))^2\right. \\ &\left. + 10(kk'\cos(\vartheta_2))(k'p\cos(\vartheta_1))(kp\cos(\vartheta_1+\vartheta_2))\right) . \end{aligned} \tag{4.34}$$

The average coupling parameter read

$$\begin{aligned}|V_{\mathrm{ex,ges,av}}|^2 &= \frac{1}{(4\pi)^2}\int_0^{2\pi}\int_0^{2\pi}\int_0^{\pi}\int_0^{\pi} sin(\vartheta_1)sin(\vartheta_2)|V_{\mathrm{ex,ges}}|^2\, d\vartheta_1\, d\vartheta_2\, d\varphi_1\, d\varphi_2 \\ &= \frac{36a^6}{\pi^2}\frac{\hbar A_1^2}{2mNS^2\omega_p}\frac{10}{3}k^2k'^2p^2 \\ &= \frac{A}{N}k^2k'^2p\,. \end{aligned} \tag{4.35}$$

For calculating the numeric parameters, we use an identity out of [43, p. 333]. This is

$$\left|\frac{V_{\mathrm{ex,ges,av}}}{V_{\mathrm{Sc,av}}}\right| \propto \frac{M_0Dk^2}{B} \propto 1\,, \tag{4.36}$$

for $k = k' \approx 10^6\mathrm{cm}^{-1}$. We make use of Eq. (4.27). From there, we get for $k = k'$

$$\frac{|V_{\mathrm{ex,ges,av}}|^2}{|V_{\mathrm{Sc,av}}|^2} = \frac{(A/N)k^2k'^2p}{4\cdot(1/N)\cdot 4.95482\cdot 10^{-8}\,\mathrm{GHz}^2\,\mathrm{cm}\,p} = \frac{Ak^4}{4\cdot 4.95482\cdot 10^{-8}\,\mathrm{GHz}^2\,\mathrm{cm}} = 1\,, \tag{4.37}$$

for $k \approx 10^6\mathrm{cm}^{-1}$. Thus, we get

$$A = \frac{4\cdot 4.95482\cdot 10^{-8}\,\mathrm{GHz}^2\,\mathrm{cm}}{(10^6\mathrm{cm}^{-1})^4} = 1.98197\cdot 10^{-31}\,\mathrm{GHz}^2\,\mathrm{cm}^5\,. \tag{4.38}$$

For further calculations, we will take Eqs. (4.35) and (4.38).

4.2 Boltzmann equation of phonon-magnon coupled system

For the calculation of the magnon temperature contribution, we write down the Boltzmann equation for magnons including magnon-phonon interaction. We take Eq. (4.1) and neglect the magnon-magnon collision term. The magnon-magnon interaction will be treated in section 5. Furthermore, we use the effective translation symmetry in y- and z-direction. Thus the derivatives in y- and z-direction vanish. Then, the Boltzmann equation reads

$$-\frac{\epsilon_{\vec{k}}}{T_0}\frac{\partial f^{(0)}_{\vec{k}}}{\partial\epsilon}v_{\vec{k},x}\frac{\partial T_{\mathrm{M}}}{\partial x} + v_{\vec{k},x}\frac{\partial\delta f_{\vec{k}}}{\partial x} = \left.\frac{\partial f_{\vec{k}}}{\partial t}\right|_{\mathrm{St}}\,, \tag{4.39}$$

while T_M denotes the spatial dependent magnon temperature, $f_{\vec{k}}$ denotes the momentum dependent magnon distribution function, $\epsilon_{\vec{k}}$ the magnon-energy (cf. Eq. (2.6)), T_0 the average magnon-temperature, and $\vec{v}_{\vec{k}}$ the magnon velocity. The magnon density distribution $f_{\vec{k}}$ is composed as in Eq. (3.1). Additionally Eqs. (3.9) and (3.10) are valid.

First of all, Sanders and Walton [24] performed a calculation on a coupled magnon-phonon system and calculated the space dependent magnon temperature. They considered a ferromagnetic or ferrimagnetic stripe, where phonons and magnons are able to propagate. At the endings of the stripe, only phonons are coupled to heat reservoirs with fixed temperatures. Later, Xiao *et al.* [23] rarefied the calculation. They assumed weak coupling of the magnons to the heat reservoirs. Because magnons cannot propagate into the heat reservoirs (or are only weakly coupled), there will be a magnon accumulation at the one end and a lack of magnons at the other end. Since the magnon temperature T_M depends on the magnon particle distribution via Bose-Einstein-distribution (c.f. Eq. (2.8))

$$f_{\vec{k}}^{(0)} = \frac{1}{e^{\frac{\epsilon_{\vec{k}}}{k_\mathrm{B} T_\mathrm{M}}} - 1}\,, \tag{4.40}$$

the temperature will be increased at the one end and decreased at the other end. Here k_B denotes the Boltzmann constant. Both authors found a length scale λ on which the deviation of temperatures takes place. Xiao *et al.* claimed λ to be in the magnitude of millimeters [23]. Later, Agrawal *et al.* [31] performed direct measurements of the magnon temperature in a comparable system. They found a very small difference between the magnon temperature and the phonon temperature. Thus, the characteristic length λ achieves to be much smaller than stated by Xiao *et al.*. Nevertheless Agrawal *et al.* themselves said, that their method is only able to measure high wave vector (small wavelength) magnons. The density of small wave vector (long wavelength) magnons cannot be measured and their temperature may still deviate from the phonon temperature and affect the transverse spin Seebeck effect. This is the case, as we will see later.

In our calculation we do not consider the effect described by Sanders and Walton. Beyond, we approximate the deviation in magnon- and phonon-temperatures (T_M and T_Ph) to be small in comparison to the average temperature T_0. That is

$$|T_\mathrm{M} - T_0| \ll T_0 \qquad\qquad |T_\mathrm{Ph} - T_0| \ll T_0\,. \tag{4.41}$$

Now, we separate the Boltzmann equation (4.39) into moments of $\cos(0\vartheta)$ and $\cos(1\vartheta)$. Here, we use spherical coordinates in a modified way. The angle ϑ is the angle between the x-axis and the vector $\vec{k}$. We want to emphasize, that the density functions and the collision integral do not depend on the angle φ because of the rotational invariance of the system, which we consider here. We assume

$$f_{\vec{k}}(x) = f_{\vec{k}}^{(0)} + \delta f_{\vec{k}}(x) = f_{\vec{k}}^{(0)} + \delta f_k(x)\cos(\vartheta)\,. \tag{4.42}$$

We rewrite the Boltzmann equation

$$-\frac{\epsilon_{\vec{k}}}{T_0}\frac{\partial f_{\vec{k}}^{(0)}}{\partial \epsilon}\frac{\partial T_M}{\partial x} v_k\,\cos(\vartheta) + \frac{\partial \delta f_k}{\partial x}\,\cos(\vartheta)\,v_k\,\cos(\vartheta) = \left.\frac{\partial f_{\vec{k}}}{\partial t}\right|_\mathrm{St}\,. \tag{4.43}$$

The separation, we perform by integration over $\frac{1}{2}\int_0^\pi \sin(\vartheta)\cos(n\vartheta)d\vartheta$ with $n \in \mathbb{N}_0$ (cf. Eq.

(3.3)). We use Eq. (4.42) and find

$$\frac{1}{3}\frac{\partial \delta f_k}{\partial x} v_k = \frac{1}{2}\int_0^\pi \sin(\vartheta) d\vartheta \left.\frac{\partial f_{\vec{k}}}{\partial t}\right|_{\mathrm{St}} \tag{4.44}$$

$$-\frac{1}{3}\frac{\epsilon_{\vec{k}}}{T_0}\frac{\partial f_{\vec{k}}^{(0)}}{\partial \epsilon}\frac{\partial T_M}{\partial x} v_k = \frac{1}{2}\int_0^\pi \sin(\vartheta) d\vartheta \cos(\vartheta) \left.\frac{\partial f_{\vec{k}}}{\partial t}\right|_{\mathrm{St}} \approx -\frac{\delta f_k}{3\tau_k}\,. \tag{4.45}$$

If one takes Eq. (4.45) and put it in Eq. (4.44), one finds

$$\frac{1}{3}\frac{\epsilon_{\vec{k}}}{T_0}\frac{\partial f_{\vec{k}}^{(0)}}{\partial \epsilon}\frac{\partial^2 T_M}{\partial x^2} v_k^2 \tau_k = \frac{1}{2}\int_0^\pi \sin(\vartheta) d\vartheta \left.\frac{\partial f_{\vec{k}}}{\partial t}\right|_{\mathrm{St}}\,. \tag{4.46}$$

Xiao *et al.* [23] as well as Sanders and Walton [24] calculated a magnon temperature profile, which has a structure of an hyperbolic sine with the decay parameter λ. They assumed this parameter to be at the order of the system length (centimeters). Agrawal *et al.* [31] performed measurements and claimed the parameter λ to be much smaller than the system length for large wave number phonons. Also other experiments found a linear behavior.

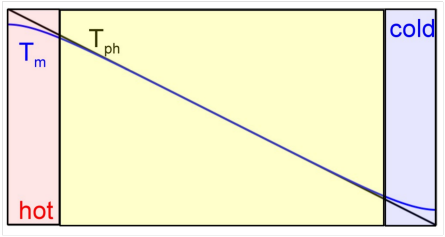

Figure 35: This is a sketch of the estimated spatial temperature profile for magnon and phonon temperature. The Sanders and Walton effect takes place at the boundaries in a proximity of length λ. In the middle region, we can estimate that $(\partial^2 T_M)/(\partial x^2) = 0$.

Thus, we approximate the magnon-temperature to be linear and the second derivative vanishes. This simplifies the collision integral

$$0 = \frac{1}{2}\int_0^\pi \sin(\vartheta) d\vartheta \left.\frac{\partial f_{\vec{k}}}{\partial t}\right|_{\mathrm{St}}\,. \tag{4.47}$$

In figure 18 and 19, one finds the phonon density at $x = -L/2$ for different wave numbers p. The long wavevector (short wavelength) phonons, follow the major density (or phonon temperature). Thus, the relaxation of them can be neglected, because they are already at equilibrium. The short wavevector (long wavelength) phonons have a long relaxation length (up to millimeters). The thickness of the YIG-stripe is at the order of micrometers. Thus, nearly all of those phonons propagate through without any phonon-phonon collisions in the YIG-stripe and will be reflected back into the substrate.

4.3 Collision integral

Now, we will write down the collision integral for the magnon-phonon interaction. With that and with Eq. (4.47), we want to derive an integral equation for the wave vector dependent magnon temperature. The wave vector dependent phonon temperature will be treated as

an input parameter and cannot be changed, as already discussed above. We perform some analytic transformations to solve the resulting integral equation numerically.

If the phonon- and magnon-distribution do not depend on the orientation (or angle) of the wave vector, one can write the distribution as Bose-Einstein distribution

$$f_{\vec{k}} = \frac{1}{e^{\epsilon_{\vec{k}}/(k_\mathrm{B}T_\mathrm{M}(\vec{k}))} - 1} \qquad n_{\vec{p}} = \frac{1}{e^{\omega_{\vec{p}}/(k_\mathrm{B}T_\mathrm{Ph}(\vec{p}))} - 1}\,. \tag{4.48}$$

Here $T_\mathrm{M}(\vec{k})$ denotes the momentum dependent magnon temperature and $T_\mathrm{Ph}(\vec{p})$ denotes the momentum dependent phonon temperature. If one compares the upper distributions with Eqs. (3.1) and (3.2), they are comparable with $\delta f_{\vec{k}} = 0$ and $\delta n_{\vec{p}} = 0$. Thus, the upper distributions can be separated in two summands, in the ground state plus the zeroth moment of Eqs. (3.3) and (3.4). In the ground state, the distribution functions are Bose-Einstein distributions with temperature T_0 (cf. Eqs. (2.4) and (2.8))

$$f^{(0)}_{\vec{k}} = \frac{1}{e^{\epsilon_{\vec{k}}/(k_\mathrm{B}T_0)} - 1} \qquad n^{(0)}_{\vec{p}} = \frac{1}{e^{\omega_{\vec{p}}/(k_\mathrm{B}T_0)} - 1}\,, \tag{4.49}$$

for magnons and phonons, respectively. Here T_0 denotes the overall average temperature. The wave vector dependent magnon energy dispersion is denoted by $\epsilon_{\vec{k}}$, while we use Eq. (2.6). Alike, the wave vector dependent phonon energy dispersion is denoted by $\hbar\omega_{\vec{p}}$, while we use Eq. (2.3). From now on, we will leave out the prefactor $\hbar$ in the phonon energy dispersion.

First, we have the scattering interaction. One phonon and one magnon are scattering into one magnon ore vice versa by respecting energy and momentum conservation. The collision integral for exchange and for dipole-dipole scattering reads

$$\begin{aligned}\left.\frac{\partial f_{\vec{k}}}{\partial t}\right|_{\mathrm{St,mag\text{-}pho,1}} =& \sum_{\vec{p}}^{\mathrm{B.Z.}} \Big\{ W(\mathrm{M}_{\vec{k}-\vec{p}} + \mathrm{Ph}_{\vec{p}} \to \mathrm{M}_{\vec{k}}) + W(\mathrm{M}_{\vec{k}-\vec{p}} \to \mathrm{Ph}_{-\vec{p}} + \mathrm{M}_{\vec{k}}) \\ & - W(\mathrm{M}_{\vec{k}} + \mathrm{Ph}_{-\vec{p}} \to \mathrm{M}_{\vec{k}-\vec{p}}) - W(\mathrm{M}_{\vec{k}} \to \mathrm{Ph}_{\vec{p}} + \mathrm{M}_{\vec{k}-\vec{p}}) \Big\}\,,\end{aligned} \tag{4.50}$$

while $W(\mathrm{M}_{\vec{k}-\vec{p}} + \mathrm{Ph}_{\vec{p}} \to \mathrm{M}_{\vec{k}})$ denotes the probability for the scattering of one magnon with wave vector $\vec{k}-\vec{p}$ and one phonon with wave vector $\vec{p}$ into one magnon with wave vector $\vec{k}$. In chapter 2.2 we introduced the procedure, how one has to set up the collision integral for a given interaction. We will apply this procedure on the Hamilton operators with the magnon-phonon interactions, which we have derived above. These are Eq. (4.11) for dipolar magnons and Eq. (4.29) for exchange-magnons. Thus, we find

$$\begin{aligned}\left.\frac{\partial f_{\vec{k}}}{\partial t}\right|_{\mathrm{St,mag\text{-}pho,1}} =& \frac{2\pi}{\hbar} \sum_{\vec{p}}^{\mathrm{B.Z.}} |V|^2 \delta(\epsilon_{\vec{k}} - \epsilon_{\vec{k}-\vec{p}} - \omega_{\vec{p}}) \left[f_{\vec{k}-\vec{p}} n_{\vec{p}} (1 + f_{\vec{k}}) - f_{\vec{k}} (1 + f_{\vec{k}-\vec{p}})(1 + n_{\vec{p}}) \right] \\ & + \frac{2\pi}{\hbar} \sum_{\vec{p}}^{\mathrm{B.Z.}} |V|^2 \delta(\epsilon_{\vec{k}} - \epsilon_{\vec{k}-\vec{p}} + \omega_{\vec{p}}) \left[f_{\vec{k}-\vec{p}} (1 + n_{\vec{p}})(1 + f_{\vec{k}}) - f_{\vec{k}} (1 + f_{\vec{k}-\vec{p}}) n_{\vec{p}} \right]\,,\end{aligned} \tag{4.51}$$

while $|V|^2$ denotes the scattering amplitude. This will be Eq. (4.27) and Eq. (4.35). For the density functions, we take Eq. (4.48). There, the magnon and phonon temperature arises. Since Eq. (4.41) holds, we perform a first order Taylor expansion in the magnon

temperature T_{M} as well as in the phonon temperature temperature T_{Ph} around the overall average temperature T_0. Thus we find

$$\begin{aligned}\left.\frac{\partial f_{\vec{k}}}{\partial t}\right|_{\text{St,mag-pho,1}} \approx & \frac{2\pi}{\hbar}\sum_{\vec{p}}^{\text{B.Z.}} |V|^2 \delta(\epsilon_{\vec{k}} - \epsilon_{\vec{k}-\vec{p}} - \omega_{\vec{p}})(1+f^0_{\vec{k}}) f^0_{\vec{k}-\vec{p}} n^0_{\vec{p}} \frac{1}{k_{\mathrm{B}} T_0^2} \\ & \times \left[\epsilon_{\vec{k}}(T_{\mathrm{Ph}}(p) - T_{\mathrm{M}}(k)) - (\epsilon_{\vec{k}} - \omega_{\vec{p}})(T_{\mathrm{Ph}}(p) - T_{\mathrm{M}}(|\vec{k}-\vec{p}|))\right] \\ & + \frac{2\pi}{\hbar}\sum_{\vec{p}}^{\text{B.Z.}} |V|^2 \delta(\epsilon_{\vec{k}} - \epsilon_{\vec{k}-\vec{p}} + \omega_{\vec{p}}) f^0_{\vec{k}} (1+f^0_{\vec{k}-\vec{p}}) n^0_{\vec{p}} \frac{1}{k_{\mathrm{B}} T_0^2} \\ & \times \left[\epsilon_{\vec{k}}(T_{\mathrm{Ph}}(p) - T_{\mathrm{M}}(k)) - (\epsilon_{\vec{k}} + \omega_{\vec{p}})(T_{\mathrm{Ph}}(p) - T_{\mathrm{M}}(|\vec{k}-\vec{p}|))\right] . \end{aligned} \tag{4.52}$$

The same procedure will be done for the conversion scattering from one phonon into two magnons. Here only the dipole-dipole interaction occurs. The Hamilton operator is in Eq. (4.11). The deduced collision integral reads

$$\begin{aligned}\left.\frac{\partial f_{\vec{k}}}{\partial t}\right|_{\text{St,mag-pho,2}} = & \sum_{\vec{p}}^{\text{B.Z.}} \Big\{ W(\mathrm{Ph}_{\vec{p}} \to \mathrm{M}_{\vec{k}} + \mathrm{M}_{-\vec{k}+\vec{p}}) + W(\mathrm{Ph}_{\vec{p}} \to \mathrm{M}_{-\vec{k}+\vec{p}} + \mathrm{M}_{\vec{k}}) \\ & - W(\mathrm{M}_{\vec{k}} + \mathrm{M}_{-\vec{k}+\vec{p}} \to \mathrm{Ph}_{\vec{p}}) - W(\mathrm{M}_{-\vec{k}+\vec{p}} + \mathrm{M}_{\vec{k}} \to \mathrm{Ph}_{\vec{p}}) \Big\} \\ = & \frac{2\pi}{\hbar}\sum_{\vec{p}}^{\text{B.Z.}} |V|^2 \delta(\epsilon_{\vec{k}} + \epsilon_{-\vec{k}+\vec{p}} - \omega_{\vec{p}}) \left[n_{\vec{p}}(1+f_{\vec{k}})(1+f_{-\vec{k}+\vec{p}}) - f_{\vec{k}} f_{-\vec{k}+\vec{p}}(1+n_{\vec{p}}) \right] \\ \approx & \frac{2\pi}{\hbar}\sum_{\vec{p}}^{\text{B.Z.}} |V|^2 \delta(\epsilon_{\vec{k}} + \epsilon_{-\vec{k}+\vec{p}} - \omega_{\vec{p}}) f_{\vec{k}} f_{-\vec{k}+\vec{p}}(1+n_{\vec{p}}) \frac{1}{k_{\mathrm{B}} T_0^2} \\ & \times \left[\epsilon_{\vec{k}}(T_{\mathrm{Ph}}(p) - T_{\mathrm{M}}(k)) - (\epsilon_{\vec{k}} - \omega_{\vec{p}})(T_{\mathrm{Ph}}(p) - T_{\mathrm{M}}(|\vec{k}-\vec{p}|))\right] . \end{aligned} \tag{4.53}$$

while the scattering amplitude $|V|^2$ is given by Eq. (4.26). Since Eqs. (3.9) and (3.10) hold and the quasi-particle energy is only dependent on the absolute value of the wave vector, the temperature is dependent on the momentum, but independent on the orientation of the momentum. At the end, the collision integral can be written down in relaxation time notation

$$\begin{aligned} 0 = \left.\frac{\partial f_{\vec{k}}}{\partial t}\right|_{\text{St,mag-pho}} &= \left.\frac{\partial f_{\vec{k}}}{\partial t}\right|_{\text{St,mag-pho,1}} + \left.\frac{\partial f_{\vec{k}}}{\partial t}\right|_{\text{St,mag-pho,2}} \\ &= \sum_{\vec{p}}^{\text{B.Z.}} \left\{ \frac{1}{\tau^{mp}_{pk}} \frac{T_{\mathrm{Ph}}(p) - T_{\mathrm{M}}(k)}{T_0} - \frac{1}{\tilde{\tau}^{mp}_{pk}} \frac{T_{\mathrm{Ph}}(p) - T_{\mathrm{M}}(|\vec{k}-\vec{p}|)}{T_0} \right\} , \end{aligned} \tag{4.54}$$

or transposed

$$0 = \left.\frac{\partial f_{\vec{k}}}{\partial t}\right|_{\text{St,mag-pho}} = \sum_{\vec{p}}^{\text{B.Z.}} \frac{T_{\mathrm{Ph}}(p)}{T_0} \left(\frac{1}{\tau^{mp}_{pk}} - \frac{1}{\tilde{\tau}^{mp}_{pk}} \right) - \frac{T_{\mathrm{M}}(k)}{T_0} \sum_{\vec{p}}^{\text{B.Z.}} \frac{1}{\tau^{mp}_{pk}} + \sum_{\vec{p}}^{\text{B.Z.}} \frac{1}{\tilde{\tau}^{mp}_{pk}} \frac{T_{\mathrm{M}}(|\vec{k}-\vec{p}|)}{T_0} , \tag{4.55}$$

with

$$\begin{aligned}\frac{1}{\tau_{pk}^{mp}} =& \frac{2\pi}{\hbar}\left(|V_{\mathrm{Sc,av}}|^2 + |V_{\mathrm{ex,ges,av}}|^2\right)\delta(\epsilon_{\vec{k}} - \epsilon_{\vec{k}-\vec{p}} - \omega_{\vec{p}})(1+f^0_{\vec{k}})f^0_{\vec{k}-\vec{p}}n^0_{\vec{p}}\frac{\epsilon_{\vec{k}}}{k_{\mathrm{B}}T_0} \\ &+ \frac{2\pi}{\hbar}\left(|V_{\mathrm{Sc,av}}|^2 + |V_{\mathrm{ex,ges,av}}|^2\right)\delta(\epsilon_{\vec{k}} - \epsilon_{\vec{k}-\vec{p}} + \omega_{\vec{p}})f^0_{\vec{k}}(1+f^0_{\vec{k}-\vec{p}})n^0_{\vec{p}}\frac{\epsilon_{\vec{k}}}{k_{\mathrm{B}}T_0} \\ &+ \frac{2\pi}{\hbar}|V_{\mathrm{2M,av}}|^2\delta(\epsilon_{\vec{k}} + \epsilon_{-\vec{k}+\vec{p}} - \omega_{\vec{p}})f_{\vec{k}}f_{-\vec{k}+\vec{p}}(1+n_{\vec{p}})\frac{\epsilon_{\vec{k}}}{k_{\mathrm{B}}T_0}\,, \end{aligned} \tag{4.56}$$

and

$$\begin{aligned}\frac{1}{\tilde{\tau}_{pk}^{mp}} =& \frac{2\pi}{\hbar}\left(|V_{\mathrm{Sc,av}}|^2 + |V_{\mathrm{ex,ges,av}}|^2\right)\delta(\epsilon_{\vec{k}} - \epsilon_{\vec{k}-\vec{p}} - \omega_{\vec{p}})(1+f^0_{\vec{k}})f^0_{\vec{k}-\vec{p}}n^0_{\vec{p}}\frac{\epsilon_{\vec{k}}-\omega_{\vec{p}}}{k_{\mathrm{B}}T_0} \\ &+ \frac{2\pi}{\hbar}\left(|V_{\mathrm{Sc,av}}|^2 + |V_{\mathrm{ex,ges,av}}|^2\right)\delta(\epsilon_{\vec{k}} - \epsilon_{\vec{k}-\vec{p}} + \omega_{\vec{p}})f^0_{\vec{k}}(1+f^0_{\vec{k}-\vec{p}})n^0_{\vec{p}}\frac{\epsilon_{\vec{k}}+\omega_{\vec{p}}}{k_{\mathrm{B}}T_0} \\ &+ \frac{2\pi}{\hbar}|V_{\mathrm{2M,av}}|^2\delta(\epsilon_{\vec{k}} + \epsilon_{-\vec{k}+\vec{p}} - \omega_{\vec{p}})f_{\vec{k}}f_{-\vec{k}+\vec{p}}(1+n_{\vec{p}})\frac{\epsilon_{\vec{k}}-\omega_{\vec{p}}}{k_{\mathrm{B}}T_0}\,. \end{aligned} \tag{4.57}$$

Here, we have taken Eqs. (4.26), (4.27), (4.35) and (4.38) for the scattering amplitudes. To evaluate the expression numerically, we need to perform analytic transformations. Especially, evaluating the delta-distribution would be difficult numerically.

4.3.1 Numerical treatment

For avoiding numerical difficulties, we perform a transformation of the integration procedure. We start with introducing some abbreviations

$$|V_{\mathrm{Sc,av}}|^2 = \frac{1}{N}|V_{\mathrm{Sc,av,N}}|^2 \tag{4.58}$$

$$|V_{\mathrm{ex,ges,av}}|^2 = \frac{1}{N}|V_{\mathrm{ex,av,N}}|^2 \tag{4.59}$$

$$|V_{\mathrm{2M,av}}|^2 = \frac{1}{N}|V_{\mathrm{2M,av,N}}|^2\,, \tag{4.60}$$

and

$$\frac{1}{\tau_{pk}^{mp}} = \frac{1}{N}\left(\frac{1}{\tau^A_{pk}}\delta(\epsilon_{\vec{k}} - \epsilon_{\vec{k}-\vec{p}} - \omega_{\vec{p}}) + \frac{1}{\tau^B_{pk}}\delta(\epsilon_{\vec{k}} - \epsilon_{\vec{k}-\vec{p}} + \omega_{\vec{p}}) + \frac{1}{\tau^C_{pk}}\delta(\epsilon_{\vec{k}} + \epsilon_{-\vec{k}+\vec{p}} - \omega_{\vec{p}})\right) \tag{4.61}$$

$$\frac{1}{\tau^A_{pk}} = \frac{2\pi}{\hbar}\left(|V_{\mathrm{Sc,av,N}}|^2 + |V_{\mathrm{ex,av,N}}|^2\right)(1+f^0_{\vec{k}})f^0_{\vec{k}-\vec{p}}n^0_{\vec{p}}\frac{\epsilon_{\vec{k}}}{k_{\mathrm{B}}T_0} \tag{4.62}$$

$$\frac{1}{\tau^B_{pk}} = \frac{2\pi}{\hbar}\left(|V_{\mathrm{Sc,av,N}}|^2 + |V_{\mathrm{ex,av,N}}|^2\right)f^0_{\vec{k}}(1+f^0_{\vec{k}-\vec{p}})n^0_{\vec{p}}\frac{\epsilon_{\vec{k}}}{k_{\mathrm{B}}T_0} \tag{4.63}$$

$$\frac{1}{\tau^C_{pk}} = \frac{2\pi}{\hbar}|V_{\mathrm{2M,av,N}}|^2 f_{\vec{k}}f_{-\vec{k}+\vec{p}}(1+n_{\vec{p}})\frac{\epsilon_{\vec{k}}}{k_{\mathrm{B}}T_0}\,, \tag{4.64}$$

and

$$\frac{1}{\tilde{\tau}_{pk}^{mp}} = \frac{1}{N}\left(\frac{1}{\tilde{\tau}_{pk}^{A}}\delta(\epsilon_{\vec{k}} - \epsilon_{\vec{k}-\vec{p}} - \omega_{\vec{p}}) + \frac{1}{\tilde{\tau}_{pk}^{B}}\delta(\epsilon_{\vec{k}} - \epsilon_{\vec{k}-\vec{p}} + \omega_{\vec{p}}) + \frac{1}{\tilde{\tau}_{pk}^{C}}\delta(\epsilon_{\vec{k}} + \epsilon_{-\vec{k}+\vec{p}} - \omega_{\vec{p}})\right) \tag{4.65}$$

$$\frac{1}{\tilde{\tau}_{pk}^{A}} = \frac{2\pi}{\hbar}\left(|V_{\mathrm{Sc,av,N}}|^2 + |V_{\mathrm{ex,av,N}}|^2\right)(1 + f_{\vec{k}}^0) f_{\vec{k}-\vec{p}}^0 n_{\vec{p}}^0 \frac{\epsilon_{\vec{k}} - \omega_{\vec{p}}}{k_{\mathrm{B}}T_0} \tag{4.66}$$

$$\frac{1}{\tilde{\tau}_{pk}^{B}} = \frac{2\pi}{\hbar}\left(|V_{\mathrm{Sc,av,N}}|^2 + |V_{\mathrm{ex,av,N}}|^2\right) f_{\vec{k}}^0 (1 + f_{\vec{k}-\vec{p}}^0) n_{\vec{p}}^0 \frac{\epsilon_{\vec{k}} + \omega_{\vec{p}}}{k_{\mathrm{B}}T_0} \tag{4.67}$$

$$\frac{1}{\tilde{\tau}_{pk}^{C}} = \frac{2\pi}{\hbar}|V_{\mathrm{2M,av,N}}|^2 f_{\vec{k}} f_{-\vec{k}+\vec{p}}(1 + n_{\vec{p}}) \frac{\epsilon_{\vec{k}} - \omega_{\vec{p}}}{k_{\mathrm{B}}T_0}\,, \tag{4.68}$$

and

$$T_1(k,p,|\vec{k}-\vec{p}|) = \frac{T_{\mathrm{Ph}}(p)}{T_0}\left(\frac{1}{\tau_{pk}^{A}} - \frac{1}{\tilde{\tau}_{pk}^{A}}\right) - \frac{T_{\mathrm{M}}(k)}{T_0}\frac{1}{\tau_{pk}^{A}} + \frac{1}{\tilde{\tau}_{pk}^{A}}\frac{T_{\mathrm{M}}(|\vec{k}-\vec{p}|)}{T_0} \tag{4.69}$$

$$T_2(k,p,|\vec{k}-\vec{p}|) = \frac{T_{\mathrm{Ph}}(p)}{T_0}\left(\frac{1}{\tau_{pk}^{B}} - \frac{1}{\tilde{\tau}_{pk}^{B}}\right) - \frac{T_{\mathrm{M}}(k)}{T_0}\frac{1}{\tau_{pk}^{B}} + \frac{1}{\tilde{\tau}_{pk}^{B}}\frac{T_{\mathrm{M}}(|\vec{k}-\vec{p}|)}{T_0} \tag{4.70}$$

$$T_3(k,p,|\vec{k}-\vec{p}|) = \frac{T_{\mathrm{Ph}}(p)}{T_0}\left(\frac{1}{\tau_{pk}^{C}} - \frac{1}{\tilde{\tau}_{pk}^{C}}\right) - \frac{T_{\mathrm{M}}(k)}{T_0}\frac{1}{\tau_{pk}^{C}} + \frac{1}{\tilde{\tau}_{pk}^{C}}\frac{T_{\mathrm{M}}(|\vec{k}-\vec{p}|)}{T_0}\,. \tag{4.71}$$

These abbreviations, we insert in Eq. (4.55). Thus, we find

$$\begin{aligned} 0 = &\sum_{\vec{p}}^{\mathrm{B.Z.}} \frac{1}{N} T_1(k,p,|\vec{k}-\vec{p}|)\,\delta(\epsilon_{\vec{k}} - \epsilon_{\vec{k}-\vec{p}} - \omega_{\vec{p}}) \\ &+ \sum_{\vec{p}}^{\mathrm{B.Z.}} \frac{1}{N} T_2(k,p,|\vec{k}-\vec{p}|)\,\delta(\epsilon_{\vec{k}} - \epsilon_{\vec{k}-\vec{p}} + \omega_{\vec{p}}) \\ &+ \sum_{\vec{p}}^{\mathrm{B.Z.}} \frac{1}{N} T_3(k,p,|\vec{k}-\vec{p}|)\,\delta(\epsilon_{\vec{k}} + \epsilon_{-\vec{k}+\vec{p}} - \omega_{\vec{p}}))\,. \end{aligned} \tag{4.72}$$

Since the functions T_1, T_2 and T_3 only depend on absolute values, we can write the p-integration in spherical coordinates. The z-direction of the p-integration will be fixed along the $\vec{k}$-direction. We rewrite the sum into an integral and introduce an integration over

$$k_m = |\vec{k}-\vec{p}| = \sqrt{k^2 + p^2 - 2kp\cos(\vartheta)}\,. \tag{4.73}$$

It is

$$\begin{aligned} 0 = &\frac{3a^3N}{4\pi^4}\frac{1}{N}\int d^3\vec{p}\int_0^{2k_{\mathrm{F}}} dk_m \delta(k_m - |\vec{k}-\vec{p}|)\,T_1(k,p,|\vec{k}-\vec{p}|)\,\delta(\epsilon_{\vec{k}} - \epsilon_{\vec{k}-\vec{p}} - \omega_{\vec{p}}) \\ &+ \frac{3a^3N}{4\pi^4}\frac{1}{N}\int d^3\vec{p}\int_0^{2k_{\mathrm{F}}} dk_m \delta(k_m - |\vec{k}-\vec{p}|)\,T_2(k,p,|\vec{k}-\vec{p}|)\,\delta(\epsilon_{\vec{k}} - \epsilon_{\vec{k}-\vec{p}} + \omega_{\vec{p}}) \\ &+ \frac{3a^3N}{4\pi^4}\frac{1}{N}\int d^3\vec{p}\int_0^{2k_{\mathrm{F}}} dk_m \delta(k_m - |\vec{k}-\vec{p}|)\,T_3(k,p,|\vec{k}-\vec{p}|)\,\delta(\epsilon_{\vec{k}} + \epsilon_{-\vec{k}+\vec{p}} - \omega_{\vec{p}}))\,, \end{aligned} \tag{4.74}$$

with the Fermi wave number $k_\mathrm{F} = 3.10 \cdot 10^7 \cdot \mathrm{cm}^{-1}$. For the p-integration, we us spherical coordinates. We find

$$\begin{aligned}
=&\frac{3a^3}{4\pi^4} 2\pi \int_0^{k_\mathrm{F}} dp\, p^2 \int_0^{\pi} d\cos(\vartheta) \int_0^{2k_\mathrm{F}} dk_m \delta(k_m - |\vec{k} - \vec{p}|)\, T_1(k,p,k_m)\, \delta(\epsilon_{\vec{k}} - \epsilon_{\vec{k}-\vec{p}} - \omega_{\vec{p}}) \\
&+ \frac{3a^3}{4\pi^4} 2\pi \int_0^{k_\mathrm{F}} dp\, p^2 \int_0^{\pi} d\cos(\vartheta) \int_0^{2k_\mathrm{F}} dk_m \delta(k_m - |\vec{k} - \vec{p}|)\, T_2(k,p,k_m)\, \delta(\epsilon_{\vec{k}} - \epsilon_{\vec{k}-\vec{p}} + \omega_{\vec{p}}) \\
&+ \frac{3a^3}{4\pi^4} 2\pi \int_0^{k_\mathrm{F}} dp\, p^2 \int_0^{\pi} d\cos(\vartheta) \int_0^{2k_\mathrm{F}} dk_m \delta(k_m - |\vec{k} - \vec{p}|)\, T_3(k,p,k_m)\, \delta(\epsilon_{\vec{k}} + \epsilon_{-\vec{k}+\vec{p}} - \omega_{\vec{p}}))\,.
\end{aligned} \tag{4.75}$$

We rearrange the delta-distribution to solve the angular integration by taking Eq. (4.73). For the phonon energy dispersion, we use Eq. (2.3) and find

$$\begin{aligned}
=&\frac{3a^3}{2\pi^3} \int_0^{k_\mathrm{F}} dp\, p^2 \int_0^{\pi} d\cos(\vartheta) \int_0^{2k_\mathrm{F}} dk_m \left|\frac{k_m}{kp}\right| \delta\left(\cos(\vartheta) - \frac{k^2+p^2-k_m^2}{2pk}\right) \\
&\qquad \times T_1(k,p,k_m)\, \delta(\epsilon_k - \epsilon_{k_m} - c_\mathrm{ph} p) \\
&+ \frac{3a^3}{2\pi^3} \int_0^{k_\mathrm{F}} dp\, p^2 \int_0^{\pi} d\cos(\vartheta) \int_0^{2k_\mathrm{F}} dk_m \left|\frac{k_m}{kp}\right| \delta\left(\cos(\vartheta) - \frac{k^2+p^2-k_m^2}{2pk}\right) \\
&\qquad \times T_2(k,p,k_m)\, \delta(\epsilon_k - \epsilon_{k_m} + c_\mathrm{ph} p) \\
&+ \frac{3a^3}{2\pi^3} \int_0^{k_\mathrm{F}} dp\, p^2 \int_0^{\pi} d\cos(\vartheta) \int_0^{2k_\mathrm{F}} dk_m \left|\frac{k_m}{kp}\right| \delta\left(\cos(\vartheta) - \frac{k^2+p^2-k_m^2}{2pk}\right) \\
&\qquad \times T_3(k,p,k_m)\, \delta(\epsilon_k + \epsilon_{k_m} - c_\mathrm{ph} p)\,.
\end{aligned} \tag{4.76}$$

Here, c_ph denotes the phonon sound velocity. Since k_m is no longer dependent on p, it is now very simple to solve the energy-delta-distribution for the p-integration. One still has to consider, that the p-integration only takes place in the first Brillouin zone.

$$\begin{aligned}
=&\frac{3a^3}{2\pi^3} \frac{1}{c_\mathrm{ph}} \int_0^{2k_\mathrm{F}} dk_m\, \frac{k_m\, p}{k}\, \Theta\left(1 - \left|\frac{k^2+p^2-k_m^2}{2pk}\right|\right)\, \Theta(k_\mathrm{F} - p)\, \Theta(p)\, T_1(k,p,k_m)\Big|_{p=\frac{\epsilon_k - \epsilon_{k_m}}{c_\mathrm{ph}}} \\
&+ \frac{3a^3}{2\pi^3} \frac{1}{c_\mathrm{ph}} \int_0^{2k_\mathrm{F}} dk_m\, \frac{k_m\, p}{k}\, \Theta\left(1 - \left|\frac{k^2+p^2-k_m^2}{2pk}\right|\right)\, \Theta(k_\mathrm{F} - p)\, \Theta(p)\, T_2(k,p,k_m)\Big|_{p=-\frac{\epsilon_k - \epsilon_{k_m}}{c_\mathrm{ph}}} \\
&+ \frac{3a^3}{2\pi^3} \frac{1}{c_\mathrm{ph}} \int_0^{2k_\mathrm{F}} dk_m\, \frac{k_m\, p}{k}\, \Theta\left(1 - \left|\frac{k^2+p^2-k_m^2}{2pk}\right|\right)\, \Theta(k_\mathrm{F} - p)\, \Theta(p)\, T_3(k,p,k_m)\Big|_{p=\frac{\epsilon_k + \epsilon_{k_m}}{c_\mathrm{ph}}}\,.
\end{aligned} \tag{4.77}$$

With this expression, we are able to set up a system of linear equations for the magnon temperature $T_M(k)$. The magnon temperature is linearly included in the functions $T_1(k,p,k_m)$, $T_2(k,p,k_m)$ and $T_3(k,p,k_m)$. Their expressions are given in Eqs. (4.69), (4.70) and (4.71). The phonon temperature $T_\mathrm{Ph}(p)$ will be treated as an input parameter.

The magnon temperature $T_M(k)$ is dependent on the wave number k. The wave number is limited to the Brillouin zone (i.e. $0 \leq k \leq k_\mathrm{F}$). For solving the system of integral equations, we discretize the wave number k to 100 or 200 numbers in the given range. This is accompanied by a discretization of the integral over k_m in the same way as for k. Now, one can read out the prefactors of the different $T_M(k)$ and set up a matrix with them. The functions $T_1(k,p,k_m)$, $T_2(k,p,k_m)$ and $T_3(k,p,k_m)$ also contain summands, where no magnon

temperature occurs. Instead, the phonon temperature occurs there. Since the phonon temperature is fixed and cannot be changed, these terms will be treated as an inhomogeneity of the system of linear equations.

Before we solve the system of linear equations, we need to add the magnon-magnon interaction to our calculation. This will be done in section 5. There, we will proceed in the same way as in this section and set up a system of linear equations for the magnon temperature. Because the collision integrals will be added (as one can see in Eq. (4.1)), both systems of linear equations also need to be added. After that, we will present solutions to the combined system of equations in section 7. Here, we will calculate the magnon temperature in the YIG-film. The result for the magnon temperature can be found in figures 43 and 44. Later, we calculate the transverse spin Seebeck voltage, which is shown in figure 49.

4.4 Summary

In this chapter, we considered a magnon-phonon coupled system and calculated the collision integral to this system. The substrate consists of a cuboid out of GGG ($Gd_3Ga_5O_{12}$), where only phonons are able to propagate. On top of it, there is a thin film out of ferrimagnetic YIG ($Y_3Fe_5O_{12}$). In this film, magnons and phonons are able to propagate. This YIG-film will be the magnon-phonon coupled system. The thickness of the ferrimagnetic YIG ($d_{\mathrm{YIG}} = 3.9$ µm) is much smaller than the thickness of the GGG substrate ($d_{\mathrm{GGG}} = 0.5$ mm). Thus, phonons propagate in the GGG substrate most of the time. Hence, they are rarely influenced by the magnons via magnon-phonon interaction. For calculating the phonon temperature, only phonon-phonon interaction is important, which was already calculated in section 3. On the opposite, magnons are only propagating in the ferrimagnetic YIG film, where phonons are able to propagate as well. Thus, magnons are strongly influenced by the phonons via magnon-phonon interaction. The phonon temperature we used as an input parameter in this chapter and calculated the wave number dependent magnon temperature.

In the beginning, we wrote down the Hamilton operator for the magnon-phonon coupled system. Here, we considered dipolar magnons as well as exchange magnons. The Hamilton operator was expressed in terms of annihilation and creation operators for phonons and magnons. Also the prefactors were calculated, because we needed them for writing down the collision integral. After calculating the Hamilton operator, we derived the Boltzmann equation for our system. The effect, calculated by Xiao *et al.* [23] as well as by Sanders and Walton [24] was neglected in our calculation, because measurements from Agrawal *et al.* [31] claimed the effect to be small. Thus, we found the equation, that the collision integral of the magnon-phonon interaction has to be zero (see Eq. (4.47)).

After that, we set up the collision integral of the magnon-phonon interaction. Here, we included dipolar magnons as well as exchange magnons. Since the temperature deviations from the equilibrium temperatures are small, we performed a Taylor expansion of the collision integral. In the result, the magnon and phonon temperatures occurred as linear terms in the resulting expression. The resulting equation is an integral equation. To solve the integral equation, we performed some analytical transformations, which can be better evaluated numerically. Since the wave number for the magnon and the phonon temperatures is limited to the Brillouin zone, we discretized the wave number dependent magnon and phonon temperatures. The summation is discretized as well. In the end we got a system of linear equations of the magnon temperature.

In chapter 5 we will add magnon-magnon interaction to our calculation. The resulting system of linear equations is a sum of both interactions. It will be solved in section 7.

5 Magnon-magnon interaction

In this chapter, we add the magnon-magnon interaction to our calculations. The goal of this chapter is to prepare the calculation of the wave number dependent magnon temperature in the setup of the transverse spin Seebeck effect. In chapter 3, we already calculated the phonon temperature in the GGG substrate. Since the thickness of the YIG-film on top of the GGG substrate is much smaller, we calculated the influence from the phonons onto the magnons in chapter 4. The influence from the magnons onto the phonons was neglected. Finally in this chapter, we will prepare the analysis of the influence of the magnon-magnon interaction onto the wave number dependent magnon temperature.

For our calculation, we take the sample size out of Ref. [21]. The GGG substrate is $d_{\mathrm{GGG}} = 0.5$ mm thick, $L_{\mathrm{GGG}} = 8$ mm long and $w_{\mathrm{GGG}} = 4$ mm wide. On top of it, there is a YIG-film, which is $d_{\mathrm{YIG}} = 3.9$ µm thick, $L_{\mathrm{YIG}} = 8$ mm long and $w_{\mathrm{YIG}} = 4$ mm wide. One has to mention, that the length and the width of the GGG substrate are the same as for the YIG-film. At the end, there will be a small Pt-stripe on top of the YIG-film. This is $d_{\mathrm{Pt}} = 15$ nm thick, $L_{\mathrm{Pt}} = 0.1$ mm long and $w_{\mathrm{Pt}} = 4$ mm wide. One has to mention, that the width of the Pt stripe is the same as for the YIG-film and the GGG substrate. The length of the Pt-stripe is smaller than of the YIG film. The schematical setup can be found in figure 9 in chapter 3.

The magnon-magnon interaction consists of the three particle interaction based on dipole-dipole interaction, where one incoming magnon is scattered into two magnons or vice versa. Additionally, there is the four particle interaction based on exchange interaction, where two incoming magnons are scattered into two outgoing magnons, at which energy and momentum are transfered between the magnons. In section 5.1, we will calculate the collision integral for the three particle interaction. After that, we will perform analytic transformations to better evaluate the resulting terms numerically. With that, we want do develop an integral equation for the wave number dependent magnon temperature. The same procedure will be done for the four particle interaction in section 5.2. At the end, one has to sum up the contributions from magnon-phonon interaction and from magnon-magnon interactions. The resulting integral equation is transformed into a system of linear equations for the wave number dependent magnon temperature. In section 7, we will present and discuss the solutions to the system of linear equations.

In Eq. (4.1), we already set up the Boltzmann equation, which has to be solved. The collision integral consists of two summands, one for the magnon-phonon interaction and one for the magnon-magnon interaction. This is

$$-\frac{\epsilon_{\vec{k}}}{T_0}\frac{\partial f_{\vec{k}}^{(0)}}{\partial \epsilon}(\vec{v}_{\vec{k}}\cdot\vec{\nabla}T_{\mathrm{M}})+\vec{v}_{\vec{k}}\cdot\vec{\nabla}\delta f_{\vec{k}}=\left.\frac{\partial f_{\vec{k}}}{\partial t}\right|_{\mathrm{St}}=\left.\frac{\partial f_{\vec{k}}}{\partial t}\right|_{\mathrm{St,mag\text{-}pho}}+\left.\frac{\partial f_{\vec{k}}}{\partial t}\right|_{\mathrm{St,mag\text{-}mag}}, \tag{5.1}$$

while T_{M} denotes the spatial and wave vector dependent magnon temperature. T_0 is the average temperature. The wave vector dependent magnon energy dispersion is denoted by $\epsilon_{\vec{k}}$, while we use Eq. (2.6). The parameter $\vec{v}_{\vec{k}}$ denotes the wave vector dependent magnon velocity. The magnon density distribution $f_{\vec{k}}$ is composed as in Eq. (3.1). Additionally Eqs. (3.9) and (3.10) hold. The boundary areas of the GGG substrate and of the YIG film, which are perpendicular to the unit vector in y- and z-direction are modeled as perfect reflecting walls. Later, we will introduce boundary scattering by an effective relaxation length. The results will be separated by including and excluding boundary scattering. Thus, the system becomes qualitatively invariant in y- and z-direction. Because of that, the derivatives in y- and z-direction in the Boltzmann equation (5.1) vanish. The first summand on the right

hand side of the Eq. (5.1) determines the collision integral of the magnon-phonon-interaction. In section 4.2, we performed some transformations with the upper Boltzmann equation and used experimental findings. We ended up with Eq. (4.47). It is

$$0 = \frac{1}{2}\int_0^\pi d\vartheta\, \sin(\vartheta)\, \left.\frac{\partial f_{\vec{k}}}{\partial t}\right|_{\mathrm{St}}\,, \tag{5.2}$$

while the collision integral is independent on φ. The summand of the collision integral for the magnon-phonon interaction reads

$$\left.\frac{\partial f_{\vec{k}}}{\partial t}\right|_{\mathrm{St,mag\text{-}pho}} = \sum_{\vec{p}} \left\{ \frac{1}{\tau_{pk}^{mp}} \frac{T_{\mathrm{Ph}}(p) - T_{\mathrm{M}}(k)}{T_0} - \frac{1}{\tilde{\tau}_{pk}^{mp}} \frac{T_{\mathrm{Ph}}(p) - T_{\mathrm{M}}(|\vec{k}-\vec{p}|)}{T_0} \right\}, \tag{5.3}$$

while the abbreviations are given in Eqs. (4.56) and (4.57). T_{Ph} denotes the spatial and wave vector dependent phonon temperature. In the same way, the collision integral for the magnon-magnon interaction will be derived in this section. The result can be found in Eqs. (5.11) and (5.63) and reads as follows

$$\left.\frac{\partial f_{\vec{k}}}{\partial t}\right|_{\mathrm{St,mag\text{-}mag}} = \left.\frac{\partial f_{\vec{k}}}{\partial t}\right|_{\mathrm{St,mag\text{-}mag,3}} + \left.\frac{\partial f_{\vec{k}}}{\partial t}\right|_{\mathrm{St,mag\text{-}mag,4}} \tag{5.4}$$

$$\left.\frac{\partial f_{\vec{k}}}{\partial t}\right|_{\mathrm{St,mag\text{-}mag,3}} = \sum_{\vec{k}'} \left(\frac{|V|^2}{\tau_A^{mm}} \frac{T_{\mathrm{M}}(\vec{k})}{T_0} + \frac{|V|^2}{\tau_B^{mm}} \frac{T_{\mathrm{M}}(\vec{k}')}{T_0} + \frac{|V|^2}{\tau_C^{mm}} \frac{T_{\mathrm{M}}(\vec{k}\pm\vec{k}')}{T_0} \right) \tag{5.5}$$

$$\left.\frac{\partial f_{\vec{k}}}{\partial t}\right|_{\mathrm{St,mag\text{-}mag,4}} = \sum_{\vec{q}\vec{k}'} \left\{ \frac{|V|^2}{\tau_{M1}} \frac{T_{\mathrm{M}}(\vec{k})}{T_0} + \frac{|V|^2}{\tau_{M2}} \frac{T_{\mathrm{M}}(\vec{k}')}{T_0} + \frac{|V|^2}{\tau_{M3}} \frac{T_{\mathrm{M}}(\vec{k}-\vec{q})}{T_0} + \frac{|V|^2}{\tau_{M4}} \frac{T_{\mathrm{M}}(\vec{k}'+\vec{q})}{T_0} \right\}, \tag{5.6}$$

The term with index 3 denotes the collision integral for the three particle magnon-magnon interaction via dipole-dipole interaction. Additionally, the four particle magnon-magnon interaction via exchange energy is included in the term with index 4. The abbreviations are given in Eqs. (5.12), (5.16), (5.20), (5.64), (5.65), (5.66) and (5.67). The scattering amplitude $|V|$ will be calculated in this section. The results can be found in Eqs. (5.29) and (5.72).

5.1 Three particle interaction - dipole-dipole-interaction

The goal of this chapter is to prepare the calculation of the magnon-temperature of the phonon-magnon coupled system by including magnon-magnon interaction. Since there is a three particle magnon-magnon interaction via dipole-dipole interaction and a four particle magnon-magnon interaction via exchange interaction, we start with the three particle magnon-magnon interaction in this section. The corresponding collision integral will be calculated now. After that, we perform analytic transformations to better evaluate the resulting expression numerically. The resulting terms must be added to the expression for the phonon-magnon interaction in Eq. (4.77). In this chapter, we describe the calculation. The detailed calculation can be found in the appendix C.1.

5.1.1 Collision integral

We set up the collision integral for three particle magnon-magnon interaction. The corresponding third order collision integral reads (see Eq. (11.9) on page 289 in Ref. [43])

$$\begin{aligned}\left.\frac{\partial f_{\vec{k}}}{\partial t}\right|_{\text{St,mag-mag,3}} =& \sum_{\vec{k}'}\Bigg\{\frac{1}{2}W(\mathrm{M}_{\vec{k}+\vec{k}'}\to\mathrm{M}_{\vec{k}}+\mathrm{M}_{\vec{k}'})+\frac{1}{2}W(\mathrm{M}_{\vec{k}'}\to\mathrm{M}_{\vec{k}'-\vec{k}}+\mathrm{M}_{\vec{k}})\\ &+\frac{1}{2}W(\mathrm{M}_{\vec{k}'}+\mathrm{M}_{\vec{k}-\vec{k}'}\to\mathrm{M}_{\vec{k}})-\frac{1}{2}W(\mathrm{M}_{\vec{k}}+\mathrm{M}_{\vec{k}'}\to\mathrm{M}_{\vec{k}+\vec{k}'})\\ &-\frac{1}{2}W(\mathrm{M}_{\vec{k}'-\vec{k}}+\mathrm{M}_{\vec{k}}\to\mathrm{M}_{\vec{k}'})-\frac{1}{2}W(\mathrm{M}_{\vec{k}}\to\mathrm{M}_{\vec{k}'}+\mathrm{M}_{\vec{k}-\vec{k}'})\Bigg\}\end{aligned}$$

$$\begin{aligned}=&\frac{1}{2}\frac{2\pi}{\hbar}\sum_{\vec{k}'}|V|^2\delta(\epsilon_{\vec{k}+\vec{k}'}-\epsilon_{\vec{k}}-\epsilon_{\vec{k}'})\cdot 4\cdot\left[f_{\vec{k}+\vec{k}'}(1+f_{\vec{k}})(1+f_{\vec{k}'})-f_{\vec{k}}f_{\vec{k}'}(1+f_{\vec{k}+\vec{k}'})\right]\\ &+\frac{1}{2}\frac{2\pi}{\hbar}\sum_{\vec{k}'}|V|^2\delta(\epsilon_{\vec{k}'}-\epsilon_{\vec{k}'-\vec{k}}-\epsilon_{\vec{k}})\cdot 4\cdot\left[f_{\vec{k}'}(1+f_{\vec{k}'-\vec{k}})(1+f_{\vec{k}})-f_{\vec{k}}f_{\vec{k}'-\vec{k}}(1+f_{\vec{k}'})\right]\\ &+\frac{1}{2}\frac{2\pi}{\hbar}\sum_{\vec{k}'}|V|^2\delta(\epsilon_{\vec{k}-\vec{k}'}+\epsilon_{\vec{k}'}-\epsilon_{\vec{k}})\cdot 4\cdot\left[f_{\vec{k}-\vec{k}'}f_{\vec{k}'}(1+f_{\vec{k}})-f_{\vec{k}}(1+f_{\vec{k}-\vec{k}'})(1+f_{\vec{k}'})\right]. \quad (5.7)\end{aligned}$$

The term $W(\mathrm{M}_{\vec{k}+\vec{k}'}\to\mathrm{M}_{\vec{k}}+\mathrm{M}_{\vec{k}'})$ denotes the probability for the transformation of one magnon with wave vector $\vec{k}+\vec{k}'$ into one magnon with wave vector $\vec{k}$ and one magnon with wave vector $\vec{k}'$. Again, $f_{\vec{k}}$ denotes the magnon density with wave vector $\vec{k}$ and $\epsilon_{\vec{k}}$ denotes the magnon energy for magnons with wave vector $\vec{k}$. The term $|V|^2$ denotes the matrix-element of the transition and will be determined later. The result can be found in Eq. (5.29). The factor $1/2$ occurs, because scattering processes are double counted. The equivalences read

$$W(\mathrm{M}_{\vec{k}+\vec{k}'}\to\mathrm{M}_{\vec{k}}+\mathrm{M}_{\vec{k}'})\mathrel{\hat{=}}W(\mathrm{M}_{\vec{k}+\vec{k}'}\to\mathrm{M}_{\vec{k}'}+\mathrm{M}_{\vec{k}}) \quad (5.8)$$

$$W(\mathrm{M}_{\vec{k}'}\to\mathrm{M}_{\vec{k}'-\vec{k}}+\mathrm{M}_{\vec{k}})\mathrel{\hat{=}}W(\mathrm{M}_{\vec{k}'}\to\mathrm{M}_{\vec{k}}+\mathrm{M}_{\vec{k}'-\vec{k}}) \quad (5.9)$$

$$W(\mathrm{M}_{\vec{k}'}+\mathrm{M}_{\vec{k}-\vec{k}'}\to\mathrm{M}_{\vec{k}})\mathrel{\hat{=}}W(\mathrm{M}_{\vec{k}-\vec{k}'}+\mathrm{M}_{\vec{k}'}\to\mathrm{M}_{\vec{k}})\,. \quad (5.10)$$

Now, we perform a first order Taylor expansion for the temperatures in the same way as in section 4.3 and find

$$0=\left.\frac{\partial f_{\vec{k}}}{\partial t}\right|_{\text{St,mag-mag,3}}=\sum_{\vec{k}'}\left(\frac{|V|^2}{\tau_A^{mm}}\frac{T_{\mathrm{M}}(\vec{k})}{T_0}+\frac{|V|^2}{\tau_B^{mm}}\frac{T_{\mathrm{M}}(\vec{k}')}{T_0}+\frac{|V|^2}{\tau_C^{mm}}\frac{T_{\mathrm{M}}(\vec{k}\pm\vec{k}')}{T_0}\right). \quad (5.11)$$

In this expression, the magnon temperature occurs as a linear parameter. Later, we will discretize the magnon temperature and the summation. Thus, we will get a system of linear equations for the magnon temperature. The abbreviations read

$$\frac{1}{\tau_A^{mm}}=\frac{1}{\tau_{A1}^{mm}}\delta(\epsilon_{\vec{k}+\vec{k}'}-\epsilon_{\vec{k}}-\epsilon_{\vec{k}'})+\frac{1}{\tau_{A2}^{mm}}\delta(\epsilon_{\vec{k}'}-\epsilon_{\vec{k}'-\vec{k}}-\epsilon_{\vec{k}})+\frac{1}{\tau_{A3}^{mm}}\delta(\epsilon_{\vec{k}-\vec{k}'}+\epsilon_{\vec{k}'}-\epsilon_{\vec{k}}) \quad (5.12)$$

$$\frac{1}{\tau_{A1}^{mm}}=\frac{4\pi}{\hbar}f^0_{\vec{k}+\vec{k}'}(1+f^0_{\vec{k}})(1+f^0_{\vec{k}'})\frac{-\epsilon_{\vec{k}}}{k_{\mathrm{B}}T_0} \quad (5.13)$$

$$\frac{1}{\tau_{A2}^{mm}}=\frac{4\pi}{\hbar}f^0_{\vec{k}'}(1+f^0_{\vec{k}'-\vec{k}})(1+f^0_{\vec{k}})\frac{-\epsilon_{\vec{k}}}{k_{\mathrm{B}}T_0} \quad (5.14)$$

$$\frac{1}{\tau_{A3}^{mm}}=\frac{4\pi}{\hbar}f^0_{\vec{k}-\vec{k}'}f^0_{\vec{k}'}(1+f^0_{\vec{k}})\frac{-\epsilon_{\vec{k}}}{k_{\mathrm{B}}T_0}\,, \quad (5.15)$$

and

$$\frac{1}{\tau_B^{mm}} = \frac{1}{\tau_{B1}^{mm}}\delta(\epsilon_{\vec{k}+\vec{k}'} - \epsilon_{\vec{k}} - \epsilon_{\vec{k}'}) + \frac{1}{\tau_{B2}^{mm}}\delta(\epsilon_{\vec{k}'} - \epsilon_{\vec{k}'-\vec{k}} - \epsilon_{\vec{k}}) + \frac{1}{\tau_{B3}^{mm}}\delta(\epsilon_{\vec{k}-\vec{k}'} + \epsilon_{\vec{k}'} - \epsilon_{\vec{k}}) \quad (5.16)$$

$$\frac{1}{\tau_{B1}^{mm}} = \frac{4\pi}{\hbar} f^0_{\vec{k}+\vec{k}'}(1+f^0_{\vec{k}})(1+f^0_{\vec{k}'})\frac{-\epsilon_{\vec{k}'}}{k_\mathrm{B}T_0} \quad (5.17)$$

$$\frac{1}{\tau_{B2}^{mm}} = \frac{4\pi}{\hbar} f^0_{\vec{k}'}(1+f^0_{\vec{k}'-\vec{k}})(1+f^0_{\vec{k}})\frac{+\epsilon_{\vec{k}'}}{k_\mathrm{B}T_0} \quad (5.18)$$

$$\frac{1}{\tau_{B3}^{mm}} = \frac{4\pi}{\hbar} f^0_{\vec{k}-\vec{k}'} f^0_{\vec{k}'}(1+f^0_{\vec{k}})\frac{+\epsilon_{\vec{k}'}}{k_\mathrm{B}T_0}\,, \quad (5.19)$$

and

$$\frac{1}{\tau_C^{mm}} = \frac{1}{\tau_{C1}^{mm}}\delta(\epsilon_{\vec{k}+\vec{k}'} - \epsilon_{\vec{k}} - \epsilon_{\vec{k}'}) + \frac{1}{\tau_{C2}^{mm}}\delta(\epsilon_{\vec{k}'} - \epsilon_{\vec{k}'-\vec{k}} - \epsilon_{\vec{k}}) + \frac{1}{\tau_{C3}^{mm}}\delta(\epsilon_{\vec{k}-\vec{k}'} + \epsilon_{\vec{k}'} - \epsilon_{\vec{k}}) \quad (5.20)$$

$$\frac{1}{\tau_{C1}^{mm}} = \frac{4\pi}{\hbar} f^0_{\vec{k}+\vec{k}'}(1+f^0_{\vec{k}})(1+f^0_{\vec{k}'})\frac{(\epsilon_{\vec{k}}+\epsilon_{\vec{k}'})}{k_\mathrm{B}T_0} \quad (5.21)$$

$$\frac{1}{\tau_{C2}^{mm}} = \frac{4\pi}{\hbar} f^0_{\vec{k}'}(1+f^0_{\vec{k}'-\vec{k}})(1+f^0_{\vec{k}})\frac{(\epsilon_{\vec{k}}-\epsilon_{\vec{k}'})}{k_\mathrm{B}T_0} \quad (5.22)$$

$$\frac{1}{\tau_{C3}^{mm}} = \frac{4\pi}{\hbar} f^0_{\vec{k}-\vec{k}'} f^0_{\vec{k}'}(1+f^0_{\vec{k}})\frac{(\epsilon_{\vec{k}}-\epsilon_{\vec{k}'})}{k_\mathrm{B}T_0}\,, \quad (5.23)$$

These abbreviations we insert in Eq. (5.11). We rewrite the sum into an integral and introduce an integration over

$$k_m = |\vec{k} \pm \vec{k}'| = \sqrt{k^2 + k'^2 \pm 2kk'(\cos(\vartheta)\cos(\vartheta') + \sin(\vartheta)\sin(\vartheta')\cos(\varphi-\varphi'))}\,. \quad (5.24)$$

In our calculation, we are interested in the equation integrated over ϑ and φ (cf. Eq. (5.2)). It is

$$\begin{aligned}
0 = &\int \frac{d\Omega}{4\pi}\frac{3a^3N}{4\pi^4}\int d^3\vec{k}'\int_0^{2k_\mathrm{F}} dk_m \delta(k_m - |\vec{k}+\vec{k}'|)\,|V|^2\,T_1(k,k',|\vec{k}+\vec{k}'|)\,\delta(\epsilon_{\vec{k}+\vec{k}'} - \epsilon_{\vec{k}} - \epsilon_{\vec{k}'}) \\
&+ \int \frac{d\Omega}{4\pi}\frac{3a^3N}{4\pi^4}\int d^3\vec{k}'\int_0^{2k_\mathrm{F}} dk_m \delta(k_m - |\vec{k}-\vec{k}'|)\,|V|^2\,T_2(k,k',|\vec{k}-\vec{k}'|)\,\delta(\epsilon_{\vec{k}'} - \epsilon_{\vec{k}'-\vec{k}} - \epsilon_{\vec{k}}) \\
&+ \int \frac{d\Omega}{4\pi}\frac{3a^3N}{4\pi^4}\int d^3\vec{k}'\int_0^{2k_\mathrm{F}} dk_m \delta(k_m - |\vec{k}-\vec{k}'|)\,|V|^2\,T_3(k,k',|\vec{k}-\vec{k}'|)\,\delta(\epsilon_{\vec{k}-\vec{k}'} + \epsilon_{\vec{k}'} - \epsilon_{\vec{k}})\,,
\end{aligned} \quad (5.25)$$

with the Fermi wave number $k_\mathrm{F} = k_\mathrm{max} = 3.10 \cdot 10^7 \cdot \mathrm{cm}^{-1}$. We used

$$T_1(\vec{k},\vec{k}',\vec{k}+\vec{k}') = \left(\frac{1}{\tau_{A1}^{mm}}\frac{T_\mathrm{M}(\vec{k})}{T_0} + \frac{1}{\tau_{B1}^{mm}}\frac{T_\mathrm{M}(\vec{k}')}{T_0} + \frac{1}{\tau_{C1}^{mm}}\frac{T_\mathrm{M}(\vec{k}+\vec{k}')}{T_0}\right) \quad (5.26)$$

$$T_2(\vec{k},\vec{k}',\vec{k}-\vec{k}') = \left(\frac{1}{\tau_{A2}^{mm}}\frac{T_\mathrm{M}(\vec{k})}{T_0} + \frac{1}{\tau_{B2}^{mm}}\frac{T_\mathrm{M}(\vec{k}')}{T_0} + \frac{1}{\tau_{C2}^{mm}}\frac{T_\mathrm{M}(\vec{k}-\vec{k}')}{T_0}\right) \quad (5.27)$$

$$T_3(\vec{k},\vec{k}',\vec{k}-\vec{k}') = \left(\frac{1}{\tau_{A3}^{mm}}\frac{T_\mathrm{M}(\vec{k})}{T_0} + \frac{1}{\tau_{B3}^{mm}}\frac{T_\mathrm{M}(\vec{k}')}{T_0} + \frac{1}{\tau_{C3}^{mm}}\frac{T_\mathrm{M}(\vec{k}-\vec{k}')}{T_0}\right)\,. \quad (5.28)$$

Since the magnon temperature only depends on absolute values of the wave vectors, we can write the integration over $d^3\vec{k}'$ in spherical coordinates. Then, we use Eq. (5.24) to solve

the angular integration. We relocate the angular delta function. Kaganov *et al.* [56] made calculations on the Hamilton operator for different magnon-magnon scattering processes. We take Eq. (39) out of Ref. [56]

$$\begin{aligned}|V|^2 =& \frac{1}{N} V_{\text{abs}}^2 \left| \cos(\vartheta)\sin(\vartheta)(\cos(\varphi) + i\sin(\varphi)) + \cos(\vartheta')\sin(\vartheta')(\cos(\varphi') + i\sin(\varphi'))\right|^2 \\ =& \frac{1}{N} V_{\text{abs}}^2 \left(\cos^2(\vartheta)\sin^2(\vartheta) + \cos^2(\vartheta')\sin^2(\vartheta') + 2\cos(\vartheta)\sin(\vartheta)\cos(\vartheta')\sin(\vartheta')\cos(\varphi - \varphi')\right)\end{aligned} \tag{5.29}$$

$$V_{\text{abs}}^2 = \frac{(2\pi\mu_{\text{B}})^2\, 2\mu_0\mu_{\text{B}} M_0}{a^3} = 52.1824 \cdot \text{GHz}^2\,, \tag{5.30}$$

while $\mu_{\text{B}} = 9.2740154 \cdot 10^{-24} J/T$ denotes the Bohr magneton. Additionally, the constant $\mu_0 = 12.566370614 \cdot 10^{-7} T^2 \cdot m^3/J$ denotes the vacuum permeability, and the magnetic saturation $M_0 = 139\,\text{G} = 0.0139\,\text{T}$ [43, p. 182]. The lattice constant of YIG is $a = 1.2376\,\text{nm}$ [52, 53]. The upper expression will be set in into the collision integral term. After that, we substitute $\varphi \to \varphi + \varphi'$. Thus, we are able to perform the integration via φ'. For the φ-integration, the term does only depend on $\cos(\varphi)$. Thus, we can separate the integration into 0 to π and π to 2π. Additionally, we perform a transformation $p = \cos(\varphi)$ of the angular delta-function. Thus, we are able to perform the integration via φ and solve the p-integral. We introduce the following expressions

$$\beta^+ = \frac{\cos(\vartheta)\cos(\vartheta') + \alpha}{\sin(\vartheta)\sin(\vartheta')} \qquad \beta^- = \frac{\cos(\vartheta)\cos(\vartheta') - \alpha}{\sin(\vartheta)\sin(\vartheta')} \qquad \alpha = \frac{k_m^2 - k^2 - k'^2}{2kk'}\,. \tag{5.31}$$

Now, we want to handle the integration via ϑ and ϑ' in Eq. (5.25). Since, it is not possible to solve the resulting integral of ϑ and ϑ', one has to perform it numerically. This we can treat by perform an approximation of the solution to the integral dependent on the parameter α out of Eq. (5.31). Since Eq. (5.24) is true, $0 \le k \le k_{\max}$ and $0 \le k' \le k_{\max}$, the parameter α is limited to $-1 \le \alpha \le 1$. We can write down the integral

$$\begin{aligned}h(\alpha) = & \int d\vartheta \int d\vartheta'\, \Theta(1-\beta^\pm)\,\Theta(1+\beta^\pm)\,\frac{1}{\sqrt{1-(\beta^\pm)^2}} \\ & \times \left(\cos^2(\vartheta)\sin^2(\vartheta) + \cos^2(\vartheta')\sin^2(\vartheta') - 2\cos(\vartheta)\sin(\vartheta)\cos(\vartheta')\sin(\vartheta')\,\beta^\pm\right)\,.\end{aligned} \tag{5.32}$$

At the end, the result can be approximated in the following way

$$h(\alpha) \approx \Theta(1-|\alpha|)\left(c_1 + c_2\,\alpha^2 + c_3\,\alpha^4\right)\,. \tag{5.33}$$

One finds

$$c_1 = 0.838041 \tag{5.34}$$

$$c_2 = 2.49346 \tag{5.35}$$

$$c_3 = 0.0113386\,. \tag{5.36}$$

In figure 36, the accordance of the approximation is shown. This approximation, we include for the collision integral. Since k_m is no longer dependent on k', it is now very simple to solve the energy-delta-distribution for the k'-integration. One still has to consider, that the k'-integration only takes place in the first Brillouin zone. It is $k_{\text{F}} = k_{\max}$. We set the energy dispersion for the magnons [43, p. 181] (or cf. Eq. (2.6)) for $k \le k_F$

$$\epsilon_k = \omega_{\text{off}} + D_{\text{ex}} k^2\,, \tag{5.37}$$

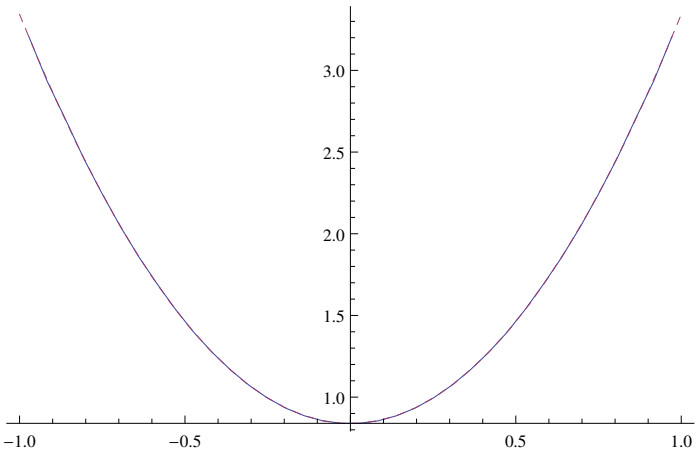

Figure 36: Plot of function $h(\alpha)$. The blue and solid line describes the numeric evaluation of Eq. (5.32). The red and dashed line denotes the approximated function out of Eq. (5.33)

and for $k > k_\mathrm{F} \wedge k \leq 2k_\mathrm{F}$

$$\epsilon_k = \omega_\mathrm{off} + D_\mathrm{ex}(2k_\mathrm{F} - k)^2 \,. \tag{5.38}$$

Now, we separate the calculation into normal processes N_p and Umklapp processes U. Here, we regard the Umklapp processes of k, k' and k_m. It is

$$0 = N_p + U \,. \tag{5.39}$$

At the end, we find

$$\begin{aligned} N_p =& \frac{3a^3}{4\pi^4}\frac{1}{2D_\mathrm{ex}}\int_0^{k_\mathrm{F}} dk_m\, \frac{k_m}{k}\, h\left(\frac{k_m^2 - k^2 - k'^2}{2kk'}\right) V_\mathrm{abs}^2\, \Theta(k_\mathrm{F} - k')\, \Theta(k')\, T_1(k, k', k_m)\Big|_{k'=\sqrt{\frac{\epsilon_{k_m} - \epsilon_k - \epsilon_0}{D_\mathrm{ex}}}} \\ &+ \frac{3a^3}{4\pi^4}\frac{1}{2D_\mathrm{ex}}\int_0^{k_\mathrm{F}} dk_m\, \frac{k_m}{k}\, h\left(\frac{k_m^2 - k^2 - k'^2}{2kk'}\right) V_\mathrm{abs}^2\, \Theta(k_\mathrm{F} - k')\, \Theta(k')\, T_2(k, k', k_m)\Big|_{k'=\sqrt{\frac{\epsilon_{k_m} + \epsilon_k - \epsilon_0}{D_\mathrm{ex}}}} \\ &+ \frac{3a^3}{4\pi^4}\frac{1}{2D_\mathrm{ex}}\int_0^{k_\mathrm{F}} dk_m\, \frac{k_m}{k}\, h\left(\frac{k_m^2 - k^2 - k'^2}{2kk'}\right) V_\mathrm{abs}^2\, \Theta(k_\mathrm{F} - k')\, \Theta(k')\, T_3(k, k', k_m)\Big|_{k'=\sqrt{\frac{\epsilon_k - \epsilon_{k_m} - \epsilon_0}{D_\mathrm{ex}}}} \,. \end{aligned} \tag{5.40}$$

For the Umklapp processes we choose a symmetrized way. It is

$$\begin{aligned} U =& \frac{1}{3}\, N_p\left(k_m \in [k_\mathrm{F}, 2k_\mathrm{F}]\right) + \frac{1}{3}\,\frac{k'}{|2k_\mathrm{F} - k'|}\, N_p\left(k' \in [k_\mathrm{F}, 2k_\mathrm{F}]\right) \\ &+ \frac{1}{3}\, N_p\left(k \in [k_\mathrm{F}, 2k_\mathrm{F}]\right) \,. \end{aligned} \tag{5.41}$$

The extra factor in the second summand arises from a different algebraic term of the energy dispersion $\epsilon_{\vec{k}'} = \omega_H + D_\mathrm{ex}(2k_\mathrm{F} - k')^2$ for $k' \in [k_\mathrm{F}, 2k_\mathrm{F}]$.

5.2 Four particle interaction - exchange interaction

The goal of this chapter is to prepare the calculation of the magnon-temperature of the phonon-magnon coupled system by including magnon-magnon interaction. In this section,

we handle four particle magnon-magnon interaction via exchange interaction. The corresponding collision integral will be calculated now. After that, we perform analytic transformations to better evaluate the resulting expression numerically. The resulting terms must be added to the expression for the phonon-magnon interaction in Eq. (4.77). In this chapter, we describe the calculation. The detailed calculation can be found in the appendix C.2.

5.2.1 Hamilton operator

We write down the following Hamilton operator for the magnons [54, p. 76]

$$\hat{H}_{\text{Heisenberg}} = -J \sum_{\langle mn \rangle} \vec{S}_m \vec{S}_n \,, \tag{5.42}$$

while J denotes the coupling constant or exchange energy and where $\langle mn \rangle$ denotes the summation over the nearest neighbors. We introduce raising and lowering operators

$$S^+_{\vec{m}} = S^x_{\vec{m}} + iS^y_{\vec{m}} \qquad S^-_{\vec{m}} = S^x_{\vec{m}} - iS^y_{\vec{m}} \qquad S^z_{\vec{m}} = S^z_{\vec{m}} \,, \tag{5.43}$$

while $S^\pm_m$ denote the lowering (-) and raising (+) operators. The commutator relations are [54, p. 76]

$$\left[S^i_{\vec{m}}, S^j_{\vec{n}}\right] = i\delta_{\vec{m},\vec{n}} \epsilon^{ijk} S^k_{\vec{m}} \qquad \left[S^z_{\vec{m}}, S^\pm_{\vec{n}}\right] = \pm\delta_{\vec{m},\vec{n}} S^\pm_{\vec{m}} \qquad \left[S^+_{\vec{m}}, S^-_{\vec{n}}\right] = 2\delta_{\vec{m},\vec{n}} S^z_{\vec{m}} \,. \tag{5.44}$$

We perform the Holstein-Primakoff-transformation [43, p. 207] and rewrite the Hamilton operator. The simple case of the calculation can be found in Ref. [54, p. 77 ff]. The Holstein-Primakoff-transformation is performed by introducing the following operators

$$S^-_{\vec{m}} = a^\dagger_{\vec{m}} \sqrt{2S - a^\dagger_{\vec{m}} a_{\vec{m}}} \qquad S^+_m = \sqrt{2S - a^\dagger_{\vec{m}} a_{\vec{m}}}\, a_m \qquad S^z_{\vec{m}} = S - a^\dagger_{\vec{m}} a_{\vec{m}} \,. \tag{5.45}$$

The operators $a_{\vec{m}}$ and $a^\dagger_{\vec{m}}$ denote the annihilation and the creation of one magnon at position $\vec{m}$, respectively. All operators fulfill the common commutation relations.

$$[a_{\vec{m}}, a_{\vec{n}}] = 0 \qquad \left[a^\dagger_{\vec{m}}, a^\dagger_{\vec{n}}\right] = 0 \qquad \left[a_{\vec{m}}, a^\dagger_{\vec{n}}\right] = \delta_{\vec{m},\vec{n}} \,. \tag{5.46}$$

Since $S = 14.2$ (cf. Eq. (4.22)), the above operators may be approximated as

$$S^-_{\vec{m}} \approx \sqrt{2S} a^\dagger_{\vec{m}} - \frac{1}{\sqrt{8S}} a^\dagger_{\vec{m}} a^\dagger_{\vec{m}} a_{\vec{m}} \qquad S^+_{\vec{m}} \approx \sqrt{2S} a_{\vec{m}} - \frac{1}{\sqrt{8S}} a^\dagger_{\vec{m}} a_{\vec{m}} a_{\vec{m}} \,. \tag{5.47}$$

One finds the following expansion of the operator product

$$\begin{aligned}
\hat{H}_{\text{Heisenberg}} =& -J \sum_{\vec{m},i} \vec{S}_{\vec{m}} \vec{S}_{\vec{m}+\vec{e}_i} && (5.48)\\
=& -JNS^2 - JS \sum_{\vec{m},i} \left(-2a^\dagger_{\vec{m}} a_{\vec{m}} + a^\dagger_{\vec{m}} a_{\vec{m}+\vec{e}_i} + a_{\vec{m}} a^\dagger_{\vec{m}+\vec{e}_i} \right) \\
& - \frac{J}{4} \sum_{\vec{m},i} \left(4a^\dagger_{\vec{m}} a^\dagger_{\vec{m}+\vec{e}_i} a_{\vec{m}} a_{\vec{m}+\vec{e}_i} \right) \\
& - \frac{J}{4} \sum_{\vec{m},i} \left(-a^\dagger_{\vec{m}} a^\dagger_{\vec{m}+\vec{e}_i} a_{\vec{m}} a_{\vec{m}} - a^\dagger_{\vec{m}+\vec{e}_i} a^\dagger_{\vec{m}} a_{\vec{m}} a_{\vec{m}} - a^\dagger_{\vec{m}} a^\dagger_{\vec{m}} a_{\vec{m}} a_{\vec{m}+\vec{e}_i} - a^\dagger_{\vec{m}} a^\dagger_{\vec{m}} a_{\vec{m}+\vec{e}_i} a_{\vec{m}} \right) , && (5.49)
\end{aligned}$$

while $\vec{e}_i$ denotes the vector in direction i with length of the lattice constant. Let us now perform a Fourier transformation. We use

$$a_{\vec{k}} = \frac{1}{\sqrt{N}} \sum_{m_1,m_2,m_3=1}^{\sqrt[3]{N}} e^{i\vec{k}\vec{m}} a_{\vec{m}} \qquad a_{\vec{m}} = \frac{1}{\sqrt{N}} \sum_{\vec{k}}^{\text{B.Z.}} e^{-i\vec{k}\vec{m}} a_{\vec{k}}\,. \tag{5.50}$$

The operators $a_{\vec{k}}$ and $a^\dagger_{\vec{k}}$ denote the annihilation and the creation of one magnon with wave vector $\vec{k}$, respectively. The commutator relations are still fulfilled in the reciprocal case. It is

$$\left[a_{\vec{k}}, a_{\vec{k}'}\right] = 0 \qquad \left[a^\dagger_{\vec{k}}, a^\dagger_{\vec{k}'}\right] = 0 \qquad \left[a_{\vec{k}}, a^\dagger_{\vec{k}'}\right] = \delta_{\vec{k},\vec{k}'}\,. \tag{5.51}$$

After set in the transformation, we perform the sum over m which leads to delta-distributions. We introduce the abbreviations $\vec{k}_3 = \vec{k} - \vec{q}$ and $\vec{k}_4 = \vec{k}' + \vec{q}$. For the dispersion, we get a expression including cosine terms. Here we perform an approximation for small wave numbers, i.e. $ak, ak', ak_3, ak_4, aq \ll 1$. A symmetrized version can be written down

$$\begin{aligned}\hat{H}_{\text{Heisenberg}} \approx &- JNS^2 + \sum_{\vec{k},i}^{\text{B.Z.}} D_{\text{ex}} k^2 a^\dagger_{\vec{k}} a_{\vec{k}} \\ &- \frac{J}{4N} \sum_{\vec{k}\vec{k}'\vec{q},i}^{\text{B.Z.}} \frac{a^2}{2} \left(k_i^2 + k_i'^2 + k_{3,i}^2 + k_{4,i}^2 - 4q_i^2\right) a^\dagger_{\vec{k}} a^\dagger_{\vec{k}'} a_{\vec{k}-\vec{q}} a_{\vec{k}'+\vec{q}},\end{aligned} \tag{5.52}$$

with

$$\vec{k}_3 = \vec{k} - \vec{q} \qquad \vec{k}_4 = \vec{k}' + \vec{q}. \tag{5.53}$$

We can read out the interaction prefactor for the exchange-interaction

$$|V_{\text{ex}}| = \frac{Ja^2}{8N}(k^2 + k'^2 + k_3^2 + k_4^2 - 4q^2)\,. \tag{5.54}$$

To calculate the coupling parameter J, we use an identity from [43, p. 210]. If one only includes first nearest neighbor hopping, one finds for a simple cubic lattice

$$J \approx \frac{D_{\text{ex}}}{Sa^2}\,. \tag{5.55}$$

It is

$$\hbar = 1.05457266 \cdot 10^{-34}\,\text{Js} \tag{5.56}$$

$$S = 14.2\,[53] \tag{5.57}$$

$$D_{\text{ex}} = 9.16 \cdot 10^{-11}\,\text{GHz cm}^2 [43, p.\ 182] \tag{5.58}$$

$$a = 1.2376\,\text{nm}\,[52,\ 53]\,. \tag{5.59}$$

Thus, we find

$$J = 421.159\,\text{GHz}\,. \tag{5.60}$$

5.2.2 Collision integral

Now, we set up the collision integral of the Boltzmann equation for the four particle magnon-magnon interaction (see Eq. (11.22) on page 294 in Ref. [43])

$$\begin{aligned}\left.\frac{\partial f_{\vec{k}}}{\partial t}\right|_{\text{St,mag-mag,4}} =&\frac{1}{2}\sum_{\vec{q}\vec{k}'}\Big\{W(\mathrm{M}_{\vec{k}-\vec{q}}+\mathrm{M}_{\vec{k}'+\vec{q}}\to\mathrm{M}_{\vec{k}}+\mathrm{M}_{\vec{k}'})+W(\mathrm{M}_{\vec{k}'+\vec{q}}+\mathrm{M}_{\vec{k}-\vec{q}}\to\mathrm{M}_{\vec{k}}+\mathrm{M}_{\vec{k}'})\\ &-W(\mathrm{M}_{\vec{k}}+\mathrm{M}_{\vec{k}'}\to\mathrm{M}_{\vec{k}-\vec{q}}+\mathrm{M}_{\vec{k}'+\vec{q}})-W(\mathrm{M}_{\vec{k}}+\mathrm{M}_{\vec{k}'}\to\mathrm{M}_{\vec{k}'+\vec{q}}+\mathrm{M}_{\vec{k}-\vec{q}})\Big\} \qquad (5.61)\\ =&\frac{1}{2}\frac{2\pi}{\hbar}\sum_{\vec{q}\vec{k}'}|V|^2\delta(\epsilon_{\vec{k}}+\epsilon_{\vec{k}'}-\epsilon_{\vec{k}-\vec{q}}-\epsilon_{\vec{k}'+\vec{q}})\cdot 16\cdot f_{\vec{k}-\vec{q}}f_{\vec{k}'+\vec{q}}(1+f_{\vec{k}})(1+f_{\vec{k}'})\\ &-\frac{1}{2}\frac{2\pi}{\hbar}\sum_{\vec{q}\vec{k}'}|V|^2\delta(\epsilon_{\vec{k}}+\epsilon_{\vec{k}'}-\epsilon_{\vec{k}-\vec{q}}-\epsilon_{\vec{k}'+\vec{q}})\cdot 16\cdot(1+f_{\vec{k}-\vec{q}})(1+f_{\vec{k}'+\vec{q}})f_{\vec{k}}f_{\vec{k}'}\,. \qquad (5.62)\end{aligned}$$

Now, we perform a first order Taylor expansion for the temperatures in the same way as in section 4.3 and find

$$\left.\frac{\partial f_{\vec{k}}}{\partial t}\right|_{\text{St,mag-mag,4}}\approx\sum_{\vec{q}\vec{k}'}\left\{\frac{|V|^2}{\tau_{M1}}\frac{T_{\mathrm{M}}(|\vec{k}|)}{T_0}+\frac{|V|^2}{\tau_{M2}}\frac{T_{\mathrm{M}}(|\vec{k}'|)}{T_0}+\frac{|V|^2}{\tau_{M3}}\frac{T_{\mathrm{M}}(|\vec{k}-\vec{q}|)}{T_0}+\frac{|V|^2}{\tau_{M4}}\frac{T_{\mathrm{M}}(|\vec{k}'+\vec{q}|)}{T_0}\right\}, \qquad (5.63)$$

with

$$\begin{aligned}\frac{1}{\tau_{M1}}=&\frac{1}{\tilde{\tau}_{M1}}\delta(\epsilon_{\vec{k}}+\epsilon_{\vec{k}'}-\epsilon_{\vec{k}-\vec{q}}-\epsilon_{\vec{k}'+\vec{q}}) &(5.64)\\ \frac{1}{\tau_{M2}}=&\frac{1}{\tilde{\tau}_{M2}}\delta(\epsilon_{\vec{k}}+\epsilon_{\vec{k}'}-\epsilon_{\vec{k}-\vec{q}}-\epsilon_{\vec{k}'+\vec{q}}) &(5.65)\\ \frac{1}{\tau_{M3}}=&\frac{1}{\tilde{\tau}_{M3}}\delta(\epsilon_{\vec{k}}+\epsilon_{\vec{k}'}-\epsilon_{\vec{k}-\vec{q}}-\epsilon_{\vec{k}'+\vec{q}}) &(5.66)\\ \frac{1}{\tau_{M4}}=&\frac{1}{\tilde{\tau}_{M4}}\delta(\epsilon_{\vec{k}}+\epsilon_{\vec{k}'}-\epsilon_{\vec{k}-\vec{q}}-\epsilon_{\vec{k}'+\vec{q}})\,, &(5.67)\end{aligned}$$

and

$$\begin{aligned}\frac{1}{\tilde{\tau}_{M1}}=&\frac{16\pi}{\hbar}\cdot f^0_{\vec{k}-\vec{q}}f^0_{\vec{k}'+\vec{q}}(1+f^0_{\vec{k}})(1+f^0_{\vec{k}'})\frac{1}{k_BT_0}(-\epsilon_{\vec{k}}) &(5.68)\\ \frac{1}{\tilde{\tau}_{M2}}=&\frac{16\pi}{\hbar}\cdot f^0_{\vec{k}-\vec{q}}f^0_{\vec{k}'+\vec{q}}(1+f^0_{\vec{k}})(1+f^0_{\vec{k}'})\frac{1}{k_BT_0}(-\epsilon_{\vec{k}'}) &(5.69)\\ \frac{1}{\tilde{\tau}_{M3}}=&\frac{16\pi}{\hbar}\cdot f^0_{\vec{k}-\vec{q}}f^0_{\vec{k}'+\vec{q}}(1+f^0_{\vec{k}})(1+f^0_{\vec{k}'})\frac{1}{k_BT_0}(+\epsilon_{\vec{k}-\vec{q}}) &(5.70)\\ \frac{1}{\tilde{\tau}_{M4}}=&\frac{16\pi}{\hbar}\cdot f^0_{\vec{k}-\vec{q}}f^0_{\vec{k}'+\vec{q}}(1+f^0_{\vec{k}})(1+f^0_{\vec{k}'})\frac{1}{k_BT_0}(+\epsilon_{\vec{k}'+\vec{q}})\,, &(5.71)\end{aligned}$$

and

$$|V|=|V_{\text{ex}}|=\frac{Ja^2}{8N}(k^2+k'^2+k_3^2+k_4^2-4q^2)\,. \qquad (5.72)$$

For avoiding some difficulties, we perform a transformation of the integration procedure. Since the function magnon temperature only depends on absolute values, we can write the

integration in spherical coordinates. We rewrite the sum into an integral and introduce an integration over

$$k_m = |\vec{k} - \vec{q}| = \sqrt{k^2 + q^2 - 2kq\cos(\sphericalangle(\vec{k}, \vec{q}))} \tag{5.73}$$

$$k_p = |\vec{k}' + \vec{q}| = \sqrt{k'^2 + q^2 + 2k'q\cos(\sphericalangle(\vec{k}', \vec{q}))}\,. \tag{5.74}$$

We are making use of Eq. (B.51). The delta function which contains the energy dispersion relations can be solved in two different ways. One may change the equation for k_m, k_p or k'. Since k_m and k_p are on an equal footing, we change the equation of the energy dispersions for k_m on the one hand and for k' on the other hand. At the end we sum up both contributions with a weighting factor of $1/2$ for both contributions respectively. Additionally, we rotate the $\vec{q}$ coordinate system in that way, that its z-axis is parallel to the vector $\vec{k}$. In the same way, we rotate the $\vec{k}'$ coordinate system in that way, that its z-axis is parallel to the vector $\vec{q}$. Thus, we can set $\sphericalangle(\vec{k}, \vec{q}) = \alpha$ and $\sphericalangle(\vec{k}', \vec{q}) = \vartheta$. Since the resulting integrand does not longer depend on the φ-angle of the $\vec{k}'$ and $\vec{q}$ coordinate system, their integral reduces to 2π. Additionally, we use the identities from Eqs. (C.94), (C.95) and (C.96). We define

$$|V_{\mathrm{ex}}|^2 = |V_{\mathrm{ex,abs}}|^2 \frac{1}{N^2} a^4 (k^2 + k'^2 + k_3^2 + k_4^2 - 4q^2)^2 \tag{5.75}$$

$$|V_{\mathrm{ex,abs}}| = \frac{J}{8} = \frac{D_{\mathrm{ex}}}{8Sa^2}\,, \tag{5.76}$$

and

$$T_1(k, k', |\vec{k} - \vec{q}|, |\vec{k}' + \vec{q}|) = \left\{ \frac{1}{\tilde{\tau}_{M1}} \frac{T_{\mathrm{M}}(|\vec{k}|)}{T_0} + \frac{1}{\tilde{\tau}_{M2}} \frac{T_{\mathrm{M}}(|\vec{k}'|)}{T_0} + \frac{1}{\tilde{\tau}_{M3}} \frac{T_{\mathrm{M}}(|\vec{k} - \vec{q}|)}{T_0} + \frac{1}{\tilde{\tau}_{M4}} \frac{T_{\mathrm{M}}(|\vec{k}' + \vec{q}|)}{T_0} \right\}, \tag{5.77}$$

and

$$\begin{aligned} Q(k, k', k_m, k_p) =& a^4 \cdot (k^2 + k'^2 + k_m^2 + k_p^2)^2 \cdot \big(\min\left[k_{max}, \min\left(k_m + k, k_p + k'\right)\right] \\ & - \min\left[k_{max}, \max\left(|k_m - k|, |k_p - k'|\right), \min\left(k_m + k, k_p + k'\right)\right]\big) \\ & - 8a^4 \cdot (k^2 + k'^2 + k_m^2 + k_p^2) \cdot \Bigg(\frac{(\min\left[k_{max}, \min\left(k_m + k, k_p + k'\right)\right])^3}{3} \\ & - \frac{(\min\left[k_{max}, \max\left(|k_m - k|, |k_p - k'|\right), \min\left(k_m + k, k_p + k'\right)\right])^3}{3} \Bigg) \\ & + 16a^4 \cdot \Bigg(\frac{(\min\left[k_{max}, \min\left(k_m + k, k_p + k'\right)\right])^5}{5} \\ & - \frac{(\min\left[k_{max}, \max\left(|k_m - k|, |k_p - k'|\right), \min\left(k_m + k, k_p + k'\right)\right])^5}{5} \Bigg)\,. \end{aligned} \tag{5.78}$$

We have to divide the calculation into normal processes N_p and Umklapp processes U. In Eq. (5.63), the vectors $\vec{k}$, $\vec{k}'$ and $\vec{q}$ are formally limited to the first Brillouin zone. When we consider Umklapp processes, we consider the case, where the vectors $\vec{k} - \vec{q}$ and $\vec{k}' + \vec{q}$ are outside the first Brillouin zone. For a symmetric calculation, we also consider the case, where the other expressions in the temperature $\vec{k}$ and $\vec{k}'$ are outside the Brillouin zone and weight the contributions. Thus, we find

$$0 = N_p + U\,, \tag{5.79}$$

while N_p denotes the sum for normal processes and U the sum for Umklapp processes. At the end, we get

$$\begin{aligned} N_p =& \frac{1}{2}\frac{9a^6}{4\pi^6}\frac{1}{2D_{ex}}\int_0^{k_{max}} dk' \int_0^{k_{max}} dk_p \, \frac{k'\,k_p}{k}\, T_1(k,k',k_m,k_p)\,\Theta(k_m)\,\Theta(k_{max}-k_m) \\ &\times |V_{\text{ex,abs}}|^2 \cdot Q(k,k',k_m,k_p)\Big|_{k_m=\sqrt{\frac{\epsilon_k+\epsilon_{k'}-\epsilon_{\vec{k}_p}-\epsilon_0}{D_{ex}}}} \\ &+ \frac{1}{2}\frac{9a^6}{4\pi^6}\frac{1}{2D_{ex}}\int_0^{k_{max}} dk_m \int_0^{k_{max}} dk_p \, \frac{k_m\,k_p}{k}\, T_1(k,k',k_m,k_p)\,\Theta(k_m)\,\Theta(k_{max}-k_m) \\ &\times |V_{\text{ex,abs}}|^2 \cdot Q(k,k',k_m,k_p)\Big|_{k'=\sqrt{\frac{\epsilon_{k_p}+\epsilon_{k_m}-\epsilon_{\vec{k}}-\epsilon_0}{D_{ex}}}} . \end{aligned} \tag{5.80}$$

This expression will be evaluated numerically. For the Umklapp processes we choose a symmetrized way. It is

$$\begin{aligned} U =& \frac{1}{2}\,N_p\left(k_p \in [k_{max}, 2k_{max}]\right) + \frac{1}{2}\,\frac{k_m}{|2k_{max}-k_m|}\,N_p\left(k_m \in [k_{max}, 2k_{max}]\right) \\ &+ \frac{1}{2}\,\frac{k_m}{|2k_{max}-k_m|}\,N_p\left(k_p \in [k_{max}, 2k_{max}] \wedge k_m \in [k_{max}, 2k_{max}]\right) \\ &+ \frac{1}{2}\,N_p\left(k' \in [k_{max}, 2k_{max}]\right) + \frac{1}{2}\,N_p\left(k \in [k_{max}, 2k_{max}]\right) \\ &+ \frac{1}{2}\,N_p\left(k \in [k_{max}, 2k_{max}] \wedge k' \in [k_{max}, 2k_{max}]\right) . \end{aligned} \tag{5.81}$$

The extra factor in the second and third summand arises from a different algebraic term of the energy dispersion $\epsilon_{\vec{k}_m} = \omega_H + D_{ex}(2k_{max} - k_m)^2$ for $k_m \in [k_{max}, 2k_{max}]$.

With these terms and the terms for the phonon-magnon interaction out of chapter 4, we will calculate the magnon temperature in the YIG-film in chapter 7. Here, the phonon temperature was used as an input parameter. The result for the magnon temperature can be found in figures 43 and 44. Later, we calculate the transverse spin Seebeck voltage, which is shown in figure 49.

5.3 Summary

In this chapter, we included the magnon-magnon interaction in the phonon-magnon coupled YIG-stripe in our calculation.

The setup of the transverse spin Seebeck effect consists of a GGG substrate, while the edge length are in the order of millimeters. On top of the thick GGG substrate, there is a thin YIG-stripe with the same surface area attached. Furthermore on top of the YIG-stripe, there are smaller stripes of platinum. The setup can be found in figures 4 and 9. Since the thickness of the GGG substrate is much thicker than of the YIG-film, the phonons are rarely influenced by the magnons. In contrast, the magnons are strongly influenced by the phonons. Out of the Boltzmann equation, we derived an equation, where the scattering integral needs to be zero by including all relevant interactions. Thus, we calculated the phonon-temperature in chapter 3 by using the Boltzmann equation and including phonon-phonon interaction only. In chapter 4, we calculated the collision integral in the Boltzmann equation for the magnon-phonon interaction and took the phonon temperature as an input parameter. In this chapter, we calculated the collision integral in the Boltzmann equation for the magnon-magnon interaction. Here, we considered exchange magnons and dipolar magnons as well.

For the dipole-dipole interaction, we considered a three particle interaction, while for the exchange interaction, we considered a four particle interaction as well. To evaluate the resulting expressions numerically, we performed analytic transformations. We derived a system of linear equations for the wave number dependent magnon temperature including magnon-phonon and magnon-magnon interaction as well. The phonon temperature was used as an input parameter.

6 Ferromagnet normal-metal junction

In this chapter, we consider a junction between a non-conducting ferromagnet and a normal metal. A temperature difference between the magnons in the ferromagnet and the electrons in the normal metal will induce a spin current in the normal metal, which is called spin pumping. The ferromagnet could be a model for the ferrimagnetic YIG ($Y_3Fe_5O_{12}$) and the normal metal could be platinum. Here, we will describe this effect by using the Boltzmann equation. In 2010, Xiao *et al.* [23] formulated a first theory for the spin pumping mechanism of this setup by using the Landau-Lifshitz-Gilbert equation. Additionally, Schmidt *et al.* [57] developed a theory for this effect. In all three cases, the spin current is proportional to the difference between magnon temperature and electron temperature.

The spin pumping mechanism is important for the understanding of the spin Seebeck effect. There, a thin and ferrimagnetic YIG-film ($Y_3Fe_5O_{12}$) was evaporated on a GGG substrate ($Gd_3Ga_5O_{12}$). Again on top, there are small platinum stripes with a voltmeter attached to measure the inverse spin Hall voltage (cf. figures 4 or 9). In case of the transverse spin Seebeck effect, the applied temperature gradient is parallel to the surface of the YIG-film. In contrast for the longitudinal spin Seebeck effect, the temperature gradient is perpendicular to the surface of the YIG-film. The heat reservoirs, which generate the temperature gradient are assumed to be ideal heat reservoirs. The temperature gradient will induce a deviation of the magnon temperature inside the YIG-film. Since the electrons in the normal metal are strongly coupled to the phonons, there will be a temperature difference between magnons and electrons. Thus, there will be a spin current based on the spin pumping mechanism. The inverse spin Hall effect transfers the spin current into a measurable charge current.

In the ferromagnet, only magnons and phonons are able to propagate, while in the normal metal only electrons and phonons are able to propagate. In our model, there is an intermediate region with thickness L, where all three types of (quasi-)particles can propagate. Here, magnons and electrons are able to interact via sd-interaction. In our calculation, we only consider magnons and electrons. Phonons are able to propagate in all three regions and are assumed to be in equilibrium at temperature T_0. Since the electrons are strongly coupled to the phonons, they are also at temperature T_0, but the chemical potential can deviate. The magnons in the ferromagnet are at temperature $T_{\mathrm{M}0}$ and the electrons are at temperature T_0. For the electrons, we separate between spin up and spin down electrons. We need a finite thickness L of the intermediate region, because then we are able to match the magnon temperature and electron spin chemical potential at the two interfaces. At the end, we will calculate the limes of the thickness L going to zero. The sd-coupling parameter will be inverse proportional to the thickness L of the intermediate region (cf. Eq. (6.64)). A sketch of the setup can be found in figure 37.

Inside the intermediate region based on sd-interaction, the following interactions are possible

$$e_{\vec{k}}^{-\downarrow} \to e_{\vec{k}-\vec{q}}^{-\uparrow} + \mathrm{Mag}_{\vec{q}}^{\downarrow} \tag{6.1}$$

$$\mathrm{Mag}_{\vec{q}}^{\downarrow} + e_{\vec{k}}^{-\uparrow} \to e_{\vec{k}+\vec{q}}^{-\downarrow}, \tag{6.2}$$

while $e_{\vec{k}}^{-\downarrow}$ denotes one electron with the wave vector $\vec{k}$, spin down and negative charge as well as $\mathrm{Mag}_{\vec{q}}^{\downarrow}$ denotes one magnon with the wave vector $\vec{q}$ and spin down. The impurity scattering $e_{\vec{k}}^{-\downarrow} \leftrightarrow e_{\vec{k}}^{-\uparrow}$ will be neglected inside the small intermediate region.

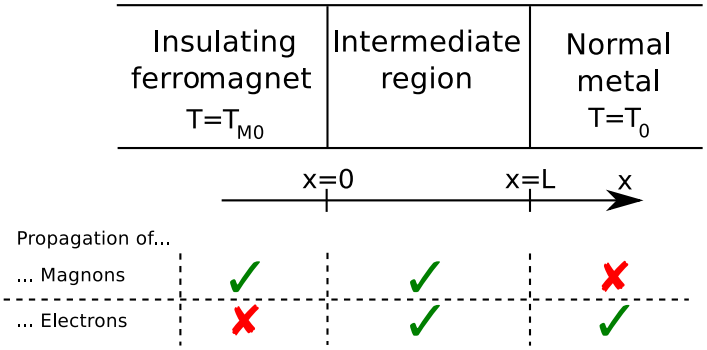

Figure 37: Sketch of the spin pumping setup, which consists of a ferromagnet and a normal metal. In the ferromagnet, only magnons and phonons are able to propagate, while in the normal metal only electrons and phonons are able to propagate. In between, there is an intermediate layer of thickness L, where all three (quasi-)particles can propagate.

6.1 Calculation

For simplicity, we take the system of units in that way, that it is $k_\mathrm{B} = 1$. The collision integral for the magnons reads as follows

$$\left.\frac{\partial f_{\vec{q}}}{\partial t}\right|_\mathrm{St} = \sum_{\vec{k}} \left\{ W(e^{-\downarrow}_{\vec{k}} \to e^{-\uparrow}_{\vec{k}-\vec{q}} + \mathrm{Mag}^{\downarrow}_{\vec{q}}) - W(\mathrm{Mag}^{\downarrow}_{\vec{q}} + e^{-\uparrow}_{\vec{k}} \to e^{-\downarrow}_{\vec{k}+\vec{q}}) \right\} \tag{6.3}$$

$$= \int d^3\vec{k} \left\{ |M_{\vec{k},\vec{k}-\vec{q},\vec{q}}|^2 g_{\downarrow\vec{k}} (1 - g_{\uparrow\vec{k}-\vec{q}})(1 + f_{\vec{q}}) \delta(\epsilon_{\vec{k}} - \epsilon_{\vec{k}-\vec{q}} - \omega_{\vec{q}}) \right.$$
$$\left. - |M_{\vec{k}+\vec{q},\vec{k},\vec{q}}|^2 f_{\vec{q}} g_{\uparrow\vec{k}} (1 - g_{\downarrow\vec{k}+\vec{q}}) \delta(\epsilon_{\vec{k}} - \epsilon_{\vec{k}+\vec{q}} + \omega_{\vec{q}}) \right\} \tag{6.4}$$

$$= \int d^3\vec{k}\, |M_{\vec{k},\vec{k}-\vec{q},\vec{q}}|^2 \left\{ g_{\downarrow\vec{k}} (1 - g_{\uparrow\vec{k}-\vec{q}}) + f_{\vec{q}} (g_{\downarrow\vec{k}} - g_{\uparrow\vec{k}-\vec{q}}) \right\} \delta(\epsilon_{\vec{k}} - \epsilon_{\vec{k}-\vec{q}} - \omega_{\vec{q}}) \,, \tag{6.5}$$

while $W(e^{-\downarrow}_{\vec{k}} \to e^{-\uparrow}_{\vec{k}-\vec{q}} + \mathrm{Mag}^{\downarrow}_{\vec{q}})$ denotes the probability for one electron with spin down and wave vector $\vec{k}$ scatters into one electron with spin up and wave vector $\vec{k}-\vec{q}$ and one magnon with spin down and wave vector $\vec{q}$. The parameter $|M_{\vec{k},\vec{k}-\vec{q},\vec{q}}|^2$ denotes the matrix element for the scattering process. The density functions are (cf. Eqs. (2.2) and (2.8))

$$f_{\vec{q}} = \frac{1}{e^{\frac{\omega_{\vec{q}}}{T_M}} - 1} \qquad g_{\uparrow\vec{k}} = \frac{1}{e^{\frac{\epsilon_{\vec{k}} - \mu_\mathrm{up}}{T_0}} + 1} \qquad g_{\downarrow\vec{k}} = \frac{1}{e^{\frac{\epsilon_{\vec{k}} - \mu_\mathrm{down}}{T_0}} + 1} \,, \tag{6.6}$$

while μ_up denotes the chemical potential for spin up electrons and μ_down denotes the chemical potential for spin down electrons. Approximated the upper collision integral to first order in $(T_0 - T_M)$, in $(\mu_\mathrm{down} - \mu_\mathrm{up})$. We also perform a linearization in the magnon distribution function and in the electron distribution function. This principle of linearization of all density functions was introduced by Gangadharaiah *et al.* [58]. After linearization of the density functions (cf. Eq. (3.1) exemplary) we find

$$\left.\frac{\partial f_{\vec{q}}}{\partial t}\right|_\mathrm{St} \approx \frac{c_{q1}\omega_{\vec{q}}}{\tau_\mathrm{me}}(T_0 - T_M) + \frac{c_{q1}T_0}{\tau_\mathrm{me}}(\mu_\mathrm{down} - \mu_\mathrm{up}) - \frac{\delta f_{\vec{q}}}{\tau_{\vec{q}}} - \sum_{\vec{k}} \left\{ \frac{\delta g_{\downarrow\vec{k}}}{\tau^{e\downarrow\to m}_{\vec{q}\vec{k}}} - \frac{\delta g_{\uparrow\vec{k}}}{\tau^{e\uparrow\to m}_{\vec{q}\vec{k}}} \right\} , \tag{6.7}$$

while we introduce the abbreviations

$$\frac{1}{\tau_q} = -\int d^3\vec{k}\,|M_{\vec{k},\vec{k}-\vec{q},\vec{q}}|^2\left(g^{(0)}_{\vec{k}} - g^{(0)}_{\vec{k}-\vec{q}}\right)\delta(\epsilon_{\vec{k}} - \epsilon_{\vec{k}-\vec{q}} - \omega_{\vec{q}}) \geq 0 \tag{6.8}$$

$$\frac{1}{\tau^{e\downarrow\to m}_{\vec{q}\vec{k}}} = |M_{\vec{k},\vec{k}-\vec{q},\vec{q}}|^2\left(1 + f^{(0)}_{\vec{q}} - g^{(0)}_{\vec{k}-\vec{q}}\right)\delta(\epsilon_{\vec{k}} - \epsilon_{\vec{k}-\vec{q}} - \omega_{\vec{q}}) \geq 0 \tag{6.9}$$

$$\frac{1}{\tau^{e\uparrow\to m}_{\vec{q}\vec{k}}} = |M_{\vec{k}+\vec{q},\vec{k},\vec{q}}|^2\left(f^{(0)}_{\vec{q}} + g^{(0)}_{\vec{k}+\vec{q}}\right)\delta(\epsilon_{\vec{k}} - \epsilon_{\vec{k}+\vec{q}} + \omega_{\vec{q}}) \geq 0\,, \tag{6.10}$$

and

$$\frac{c_{q1}}{\tau_{\mathrm{me}}} = \int d^3\vec{k}\,\delta(\epsilon_{\vec{k}} - \epsilon_{\vec{k}-\vec{q}} - \omega_{\vec{q}})\frac{|M_{\vec{k},\vec{k}-\vec{q},\vec{q}}|^2}{2T_0^2(\sinh(\frac{\epsilon_{\vec{k}}-\mu_0}{T_0}) + \sinh(\frac{\omega_{\vec{q}}}{T_0}) - \sinh(\frac{\epsilon_{\vec{k}}-\omega_{\vec{q}}-\mu_0}{T_0}))} \geq 0\,. \tag{6.11}$$

It is to mention that

$$1 + f^{(0)}_{\vec{q}} - g^{(0)}_{\vec{k}-\vec{q}}\Big|_{\epsilon_{\vec{k}-\vec{q}}=\epsilon_{\vec{k}}-\omega_{\vec{q}}} = f^{(0)}_{\vec{q}} + g^{(0)}_{\vec{k}+\vec{q}}\Big|_{\epsilon_{\vec{k}+\vec{q}}=\epsilon_{\vec{k}}+\omega_{\vec{q}}}\,. \tag{6.12}$$

Now, we write down the electron spin down collision integral

$$\begin{aligned}\left.\frac{\partial g_{\downarrow\vec{k}}}{\partial t}\right|_{\mathrm{St}} =& \sum_{\vec{k}'\vec{q}}\Big\{W(\mathrm{Mag}^{\downarrow}_{\vec{q}} + e^{-\uparrow}_{\vec{k}-\vec{q}} \to e^{-\downarrow}_{\vec{k}}) + W(e^{-\uparrow}_{\vec{k}} \to e^{-\downarrow}_{\vec{k}}) \\ &\quad - W(e^{-\downarrow}_{\vec{k}} \to e^{-\uparrow}_{\vec{k}-\vec{q}} + \mathrm{Mag}^{\downarrow}_{\vec{q}}) - W(e^{-\downarrow}_{\vec{k}} \to e^{-\uparrow}_{\vec{k}})\Big\} \qquad (6.13)\\ =& \int d^3\vec{q}\,\Big\{|M_{\vec{k},\vec{k}-\vec{q},\vec{q}}|^2 f_{\vec{q}} g_{\uparrow\vec{k}-\vec{q}}(1 - g_{\downarrow\vec{k}})\delta(\epsilon_{\vec{k}} - \epsilon_{\vec{k}-\vec{q}} - \omega_{\vec{q}}) \\ &\quad - |M_{\vec{k},\vec{k}-\vec{q},\vec{q}}|^2 g_{\downarrow\vec{k}}(1 - g_{\uparrow\vec{k}-\vec{q}})(1 + f_{\vec{q}})\delta(\epsilon_{\vec{k}} - \epsilon_{\vec{k}-\vec{q}} - \omega_{\vec{q}})\Big\} \\ &\quad + |F_{\vec{k}}|^2 g_{\uparrow\vec{k}}(1 + g_{\downarrow\vec{k}}) - |F_{\vec{k}}|^2 g_{\downarrow\vec{k}}(1 + g_{\uparrow\vec{k}})\,, \qquad (6.14)\end{aligned}$$

while $W(e^{-\uparrow}_{\vec{k}} \to e^{-\downarrow}_{\vec{k}})$ denotes the scattering probability from one electron with spin up into one electron with spin down. The parameter $|F_{\vec{k}}|^2$ denotes the matrix element for this interaction. The collision integral approximated to first order and after linearization reads

$$\begin{aligned}=& -\frac{d_{k1}}{\tau_{\mathrm{me}}}(T_0 - T_M) - \frac{d_{k2}}{\tau_{\mathrm{me}}}(\mu_{\mathrm{down}} - \mu_{\mathrm{up}}) - \frac{\delta g_{\downarrow\vec{k}}}{\tau_{\vec{k}\downarrow}} - \frac{\delta g_{\downarrow\vec{k}} - \delta g_{\uparrow\vec{k}}}{\tau_{s\vec{k}}} \\ &- \frac{\mu_{\mathrm{down}} - \mu_{\mathrm{up}}}{r_{\vec{k}}\tau_{s\vec{k}}} + \sum_{\vec{q}}\left\{\frac{\delta g_{\uparrow\vec{k}-\vec{q}}}{\tau^{e\uparrow\to e\downarrow}_{\vec{q}\vec{k}}} + \frac{\delta f_{\vec{q}}}{\tau^{m\to e\downarrow}_{\vec{q}\vec{k}}}\right\}\,, \qquad (6.15)\end{aligned}$$

with $\tau_{s\vec{k}} = 1/|F_{\vec{k}}|^2$ and with the abbreviations

$$\frac{1}{\tau_{\vec{k}\downarrow}} = \int d^3\vec{q}\,|M_{\vec{k},\vec{k}-\vec{q},\vec{q}}|^2 \left(1 - g^{(0)}_{\vec{k}-\vec{q}} + f^{(0)}_{\vec{q}}\right) \delta(\epsilon_{\vec{k}} - \epsilon_{\vec{k}-\vec{q}} - \omega_{\vec{q}}) \geq 0 \tag{6.16}$$

$$\frac{1}{\tau^{e\uparrow\to e\downarrow}_{\vec{q}\vec{k}}} = |M_{\vec{k},\vec{k}-\vec{q},\vec{q}}|^2 \left(f^{(0)}_{\vec{q}} + g^{(0)}_{\vec{k}}\right) \delta(\epsilon_{\vec{k}} - \epsilon_{\vec{k}-\vec{q}} - \omega_{\vec{q}}) \geq 0 \tag{6.17}$$

$$\frac{1}{\tau^{m\to e\downarrow}_{\vec{q}\vec{k}}} = |M_{\vec{k},\vec{k}-\vec{q},\vec{q}}|^2 \left(g^{(0)}_{\vec{k}-\vec{q}} - g^{(0)}_{\vec{k}}\right) \delta(\epsilon_{\vec{k}} - \epsilon_{\vec{k}-\vec{q}} - \omega_{\vec{q}}) \geq 0 \tag{6.18}$$

$$\frac{d_{k1}}{\tau_{\mathrm{me}}} = \int d^3\vec{q}\,\delta(\epsilon_{\vec{k}} - \epsilon_{\vec{k}-\vec{q}} - \omega_{\vec{q}}) \frac{\omega_{\vec{q}}|M_{\vec{k},\vec{k}-\vec{q},\vec{q}}|^2}{2T_0^2(\sinh(\frac{\epsilon_{\vec{k}}-\mu_0}{T_0}) + \sinh(\frac{\omega_{\vec{q}}}{T_0}) - \sinh(\frac{\epsilon_{\vec{k}}-\omega_{\vec{q}}-\mu_0}{T_0}))} \geq 0 \tag{6.19}$$

$$\frac{d_{k2}}{\tau_{\mathrm{me}}} = \int d^3\vec{q}\,\delta(\epsilon_{\vec{k}} - \epsilon_{\vec{k}-\vec{q}} - \omega_{\vec{q}}) \frac{|M_{\vec{k},\vec{k}-\vec{q},\vec{q}}|^2}{2T_0(\sinh(\frac{\epsilon_{\vec{k}}-\mu_0}{T_0}) + \sinh(\frac{\omega_{\vec{q}}}{T_0}) - \sinh(\frac{\epsilon_{\vec{k}}-\omega_{\vec{q}}-\mu_0}{T_0}))} \geq 0 \tag{6.20}$$

$$r_{\vec{k}}\tau_{s\vec{k}} = 4T_0 \sinh^2(\frac{\epsilon_{\vec{k}} - \mu_0}{T_0}) \geq 0\,. \tag{6.21}$$

Analogously, one obtains for the electron spin up collision integral approximated to first order

$$\begin{aligned}\left.\frac{\partial g_{\uparrow\vec{k}}}{\partial t}\right|_{\mathrm{St}} =& \frac{d_{k3}}{\tau_{\mathrm{me}}}(T_0 - T_M) + \frac{d_{k4}}{\tau_{\mathrm{me}}}(\mu_{\mathrm{down}} - \mu_{\mathrm{up}}) - \frac{\delta g_{\uparrow\vec{k}}}{\tau_{\vec{k}\uparrow}} + \frac{\delta g_{\downarrow\vec{k}} - \delta g_{\uparrow\vec{k}}}{\tau_{s\vec{k}}} \\ &+ \frac{\mu_{\mathrm{down}} - \mu_{\mathrm{up}}}{r_{\vec{k}}\tau_{s\vec{k}}} + \sum_{\vec{q}} \left\{ \frac{\delta g_{\downarrow\vec{k}+\vec{q}}}{\tau^{e\downarrow\to e\uparrow}_{\vec{q}\vec{k}}} - \frac{\delta f_{\vec{q}}}{\tau^{m\to e\uparrow}_{\vec{q}\vec{k}}} \right\},\end{aligned} \tag{6.22}$$

with the abbreviations

$$\frac{1}{\tau_{\vec{k}\uparrow}} = \int d^3\vec{q}\,|M_{\vec{k}+\vec{q},\vec{k},\vec{q}}|^2 \left(g^{(0)}_{\vec{k}+\vec{q}} + f^{(0)}_{\vec{q}}\right) \delta(\epsilon_{\vec{k}} - \epsilon_{\vec{k}+\vec{q}} + \omega_{\vec{q}}) \geq 0 \tag{6.23}$$

$$\frac{1}{\tau^{e\downarrow\to e\uparrow}_{\vec{q}\vec{k}}} = |M_{\vec{k}+\vec{q},\vec{k},\vec{q}}|^2 \left(1 + f^{(0)}_{\vec{q}} - g^{(0)}_{\vec{k}}\right) \delta(\epsilon_{\vec{k}} - \epsilon_{\vec{k}+\vec{q}} + \omega_{\vec{q}}) \geq 0 \tag{6.24}$$

$$\frac{1}{\tau^{m\to e\uparrow}_{\vec{q}\vec{k}}} = |M_{\vec{k}+\vec{q},\vec{k},\vec{q}}|^2 \left(g^{(0)}_{\vec{k}} - g^{(0)}_{\vec{k}+\vec{q}}\right) \delta(\epsilon_{\vec{k}} - \epsilon_{\vec{k}+\vec{q}} + \omega_{\vec{q}}) \geq 0 \tag{6.25}$$

$$\frac{d_{k3}}{\tau_{\mathrm{me}}} = -\int d^3\vec{q}\,\delta(\epsilon_{\vec{k}} - \epsilon_{\vec{k}+\vec{q}} + \omega_{\vec{q}}) \frac{\omega_{\vec{q}}|M_{\vec{k}+\vec{q},\vec{k},\vec{q}}|^2}{2T_0^2(\sinh(\frac{\epsilon_{\vec{k}}-\mu_0}{T_0}) - \sinh(\frac{\omega_{\vec{q}}}{T_0}) - \sinh(\frac{\epsilon_{\vec{k}}+\omega_{\vec{q}}-\mu_0}{T_0}))} \geq 0 \tag{6.26}$$

$$\frac{d_{k4}}{\tau_{\mathrm{me}}} = -\int d^3\vec{q}\,\delta(\epsilon_{\vec{k}} - \epsilon_{\vec{k}+\vec{q}} + \omega_{\vec{q}}) \frac{|M_{\vec{k}+\vec{q},\vec{k},\vec{q}}|^2}{2T_0(\sinh(\frac{\epsilon_{\vec{k}}-\mu_0}{T_0}) - \sinh(\frac{\omega_{\vec{q}}}{T_0}) - \sinh(\frac{\epsilon_{\vec{k}}+\omega_{\vec{q}}-\mu_0}{T_0}))} \geq 0 \tag{6.27}$$

$$r_{\vec{k}}\tau_{s\vec{k}} = 4T_0 \sinh^2(\frac{\epsilon_{\vec{k}} - \mu_0}{T_0}) \geq 0\,. \tag{6.28}$$

Thus, we are able to write down the coupled Boltzmann equations

$$-\frac{\omega_{\vec{q}}}{T_0}\frac{\partial f^{(0)}_{\vec{q}}}{\partial\omega}v_{\vec{q},x}\frac{\partial T_M}{\partial x}+v_{\vec{q},x}\frac{\partial\delta f_{\vec{q}}}{\partial x}=\frac{c_{q1}\omega_{\vec{q}}}{\tau_{\mathrm{me}}}(T_0-T_M)+\frac{c_{q1}T_0}{\tau_{\mathrm{me}}}(\mu_{\mathrm{down}}-\mu_{\mathrm{up}})-\frac{\delta f_{\vec{q}}}{\tau_{\vec{q}}}$$
$$-\sum_{\vec{k}}\left\{\frac{\delta g_{\downarrow\vec{k}}}{\tau^{e\downarrow\to m}_{\vec{q}\vec{k}}}-\frac{\delta g_{\uparrow\vec{k}}}{\tau^{e\uparrow\to m}_{\vec{q}\vec{k}}}\right\} \tag{6.29}$$

$$-\frac{\partial g^{(0)}_{\vec{k}}}{\partial\epsilon}u_{\vec{k},x}\frac{\partial\mu_{\mathrm{down}}}{\partial x}+u_{\vec{k},x}\frac{\partial\delta g_{\downarrow\vec{k}}}{\partial x}=-\frac{d_{k1}}{\tau_{\mathrm{me}}}(T_0-T_M)-\frac{d_{k2}}{\tau_{\mathrm{me}}}(\mu_{\mathrm{down}}-\mu_{\mathrm{up}})-\frac{\delta g_{\downarrow\vec{k}}}{\tau^{(0)}_k}-\frac{\delta g_{\downarrow\vec{k}}}{\tau_{\vec{k}\downarrow}}$$
$$-\frac{\delta g_{\downarrow\vec{k}}-\delta g_{\uparrow\vec{k}}}{\tau_{s\vec{k}}}-\frac{\mu_{\mathrm{down}}-\mu_{\mathrm{up}}}{r_{\vec{k}}\tau_{s\vec{k}}}+\sum_{\vec{q}}\left\{\frac{\delta g_{\uparrow\vec{k}-\vec{q}}}{\tau^{e\uparrow\to e\downarrow}_{\vec{q}\vec{k}}}+\frac{\delta f_{\vec{q}}}{\tau^{m\to e\downarrow}_{\vec{q}\vec{k}}}\right\} \tag{6.30}$$

$$-\frac{\partial g^{(0)}_{\vec{k}}}{\partial\epsilon}u_{\vec{k},x}\frac{\partial\mu_{\mathrm{up}}}{\partial x}+u_{\vec{k},x}\frac{\partial\delta g_{\uparrow\vec{k}}}{\partial x}=\frac{d_{k3}}{\tau_{\mathrm{me}}}(T_0-T_M)+\frac{d_{k4}}{\tau_{\mathrm{me}}}(\mu_{\mathrm{down}}-\mu_{\mathrm{up}})-\frac{\delta g_{\uparrow\vec{k}}}{\tau^{(0)}_k}-\frac{\delta g_{\uparrow\vec{k}}}{\tau_{\vec{k}\uparrow}}$$
$$+\frac{\delta g_{\downarrow\vec{k}}-\delta g_{\uparrow\vec{k}}}{\tau_{s\vec{k}}}+\frac{\mu_{\mathrm{down}}-\mu_{\mathrm{up}}}{r_{\vec{k}}\tau_{s\vec{k}}}+\sum_{\vec{q}}\left\{\frac{\delta g_{\downarrow\vec{k}+\vec{q}}}{\tau^{e\downarrow\to e\uparrow}_{\vec{q}\vec{k}}}-\frac{\delta f_{\vec{q}}}{\tau^{m\to e\uparrow}_{\vec{q}\vec{k}}}\right\}, \tag{6.31}$$

while $v_{\vec{q},x}$ denotes the x-component of the magnon velocity with momentum $\vec{q}$ and $u_{\vec{k},x}$ denotes the x-component of the electron velocity with momentum $\vec{k}$. Thus, it is

$$v_{\vec{q},x}=v_{\vec{q}}\cdot\cos(\vartheta)\qquad\qquad u_{\vec{k},x}=u_{\vec{k}}\cdot\cos(\vartheta)\,, \tag{6.32}$$

while ϑ is the angle between $\vec{u}_{\vec{k}}$ or $\vec{v}_{\vec{q}}$ and the x-axis. The terms are independent of φ. The relaxation time $\tau^{(0)}_k$ belongs to inelastic impurity scattering as well as phonon scattering. We assume $\tau^{(0)}_k \ll \tau_{\vec{k}\updownarrow}$. We are able to divide the differential equations by integration over $\int d\vartheta\sin(\vartheta)/2$, $\int d\vartheta\sin(\vartheta)\cos(\vartheta)/2$ and $\int d\vartheta\sin(\vartheta)\cos(2\vartheta)/2$. So, we get nine different equations. From now on, we also neglect the spin flip scattering processes. Thus, the summands including $\tau_{s\vec{k}}$ vanish in Eqs. (6.30) and (6.31). Now, we take equations from the $\int d\vartheta\sin(\vartheta)\cos(\vartheta)/2$-integral and neglect the crossing terms. After solving these three equations for the deviation functions, we set them back into the expressions in curly brackets.

We will now derive a system of differential equations, which only includes the magnon temperature T_M, the spin chemical potential $\mu_{\mathrm{Spin}}=\mu_{\mathrm{up}}-\mu_{\mathrm{down}}$ and the charge chemical potential $\mu_{\mathrm{cha}}=\mu_{\mathrm{up}}+\mu_{\mathrm{down}}$. The deviation functions $\delta f_{\vec{q}}$, $\delta g_{\uparrow\vec{k}}$ and $\delta g_{\downarrow\vec{k}}$ should not longer occur. This, we perform by using the definitions for the magnon current, the spin current and the charge current. The formula for the spin current for magnons reads

$$j_{\mathrm{Mag}}=-\sum_{\vec{q}}v_{\vec{q},x}\,\delta f_{\vec{q}}\,. \tag{6.33}$$

The minus sign arises, because the spin of the magnons is parallel to electron spin down. Now, we continue with the spin current for the electrons. It reads

$$j_{\mathrm{spin}}=\frac{1}{2}\sum_{\vec{k}}u_{\vec{k},x}\,\delta g_{\vec{k}\uparrow}-\frac{1}{2}\sum_{\vec{k}}u_{\vec{k},x}\,\delta g_{\vec{k}\downarrow}\,. \tag{6.34}$$

On the other hand, no charge transport is allowed. This corresponds to

$$0 = j_{\text{charge}} = \sum_{\vec{k}} u_{\vec{k},x}\, \delta g_{\vec{k}\downarrow} + \sum_{\vec{k}} u_{\vec{k},x}\, \delta g_{\vec{k}\uparrow}\,. \tag{6.35}$$

For all three currents, we take the first derivative in coordinate x. On the one hand, we can take the equations out of the $\int d\vartheta \sin(\vartheta)/2$-integration, solve them for the derivative in coordinate x of the deviation functions. After that, we set them into the derivative in coordinate x of the current definitions. On the other hand, we can take the equations out of the $\int d\vartheta \sin(\vartheta)\cos(\vartheta)/2$-integration, solve them for the deviation functions an set them into the derivative in coordinate x of the current definitions. Thus, we get three differential equations, which only include the magnon temperature T_M, the spin chemical potential μ_{Spin} and the charge chemical potential μ_{cha}. This three differential equations, we can set into each other and find the following system of differential equations

$$\Sigma_{Mnew} \frac{\partial^2 T_M}{\partial x^2} = - C_1(T_0 - T_M) + C_2 \mu_{\text{Spin}} \tag{6.36}$$

$$-\Sigma_{Enew} \frac{\partial^2 \mu_{\text{Spin}}}{\partial x^2} = C_1(T_0 - T_M) - C_2 \mu_{\text{Spin}}\,, \tag{6.37}$$

with

$$\Sigma_{Mnew} = - \frac{2\Sigma_1}{\Sigma_{DM}(\Sigma_E + \Sigma_{UD}) + \Sigma_E(-2\Sigma_E + \Sigma_{UM}) + \Sigma_{DU}(2\Sigma_{UD} + \Sigma_{UM})} \tag{6.38}$$

$$\Sigma_{Enew} = \frac{2\Sigma_1}{\Sigma_2} \tag{6.39}$$

$$\begin{aligned}\Sigma_2 =& \Sigma_{DM}\Sigma_{MD} + \Sigma_{DU}(\Sigma_M + 2\Sigma_{MD}) - \Sigma_{DM}\Sigma_{MU} + 2\Sigma_E(\Sigma_M + \Sigma_{MD} + \Sigma_{MU}) \\ &+ \Sigma_M\Sigma_{UD} + 2\Sigma_{MU}\Sigma_{UD} - \Sigma_{MD}\Sigma_{UM} + \Sigma_{MU}\Sigma_{UM}\end{aligned} \tag{6.40}$$

$$\begin{aligned}\Sigma_1 =& \Sigma_E^2\Sigma_M + \Sigma_{DM}\Sigma_E\Sigma_{MD} - \Sigma_{DU}\Sigma_M\Sigma_{UD} + \Sigma_{DM}\Sigma_{MU}\Sigma_{UD} \\ &+ \Sigma_{DU}\Sigma_{MD}\Sigma_{UM} + \Sigma_E\Sigma_{MU}\Sigma_{UM}\,.\end{aligned} \tag{6.41}$$

We use the following short-writing notation

$$\Sigma_{DM} := \frac{\Sigma_{ed\to m}}{2} \qquad \Sigma_{UM} := \frac{\Sigma_{eu\to m}}{2} \qquad \Sigma_{UD} := \frac{\Sigma_{eu\to ed}}{2} \tag{6.42}$$

$$\Sigma_{DU} := \frac{\Sigma_{ed\to eu}}{2} \qquad \Sigma_{MD} := \frac{\Sigma_{m\to ed}}{2} \qquad \Sigma_{MU} := \frac{\Sigma_{m\to eu}}{2}\,, \tag{6.43}$$

and

$$\Sigma_E = \Sigma_{ed}/2 = \Sigma_{eu}/2\,. \tag{6.44}$$

We use as an approximation

$$\Sigma_{ed} = \Sigma_{eu} = -\sum_{\vec{k}} u_{\vec{k},x}\tau_k^{(0)} \frac{\partial g_k^{(0)}}{\partial \epsilon} u_{\vec{k},x} \tag{6.45}$$

$$\Sigma_{eu\to ed} = -\sum_{\vec{k}\vec{q}} u_{\vec{k},x}\tau_k^{(0)} \frac{\tau^{(0)}_{\vec{k}-\vec{q}}}{\tau^{e\uparrow\to e\downarrow}_{\vec{q}\vec{k}}} \frac{\partial g_k^{(0)}}{\partial \epsilon} u_{\vec{k}-\vec{q},x} \qquad \Sigma_{ed\to eu} = -\sum_{\vec{k}\vec{q}} u_{\vec{k},x}\tau_k^{(0)} \frac{\tau^{(0)}_{\vec{k}+\vec{q}}}{\tau^{e\downarrow\to e\uparrow}_{\vec{q}\vec{k}}} \frac{\partial g_k^{(0)}}{\partial \epsilon} u_{\vec{k}+\vec{q},x} \tag{6.46}$$

$$\Sigma_{m\to ed} = -\sum_{\vec{k}\vec{q}} u_{\vec{k},x}\tau_k^{(0)} \frac{\tau_{\vec{q}}}{\tau^{m\to e\downarrow}_{\vec{q}\vec{k}}} \frac{\omega_{\vec{p}}}{T_0} \frac{\partial f_q^{(0)}}{\partial \omega} v_{\vec{q},x} \qquad \Sigma_{m\to eu} = -\sum_{\vec{k}\vec{q}} u_{\vec{k},x}\tau_k^{(0)} \frac{\tau_{\vec{q}}}{\tau^{m\to e\uparrow}_{\vec{q}\vec{k}}} \frac{\omega_{\vec{p}}}{T_0} \frac{\partial f_q^{(0)}}{\partial \omega} v_{\vec{q},x}\,. \tag{6.47}$$

One has to remember that it is $v_{\vec{q},x} = v_{\vec{q}} \cdot \cos(\vartheta)$ and $u_{\vec{k},x} = u_{\vec{k}} \cdot \cos(\vartheta)$. Additionally, we abbreviated

$$\Sigma_M = -\sum_{\vec{q}} v_{\vec{q},x}\tau_q \frac{\omega_{\vec{p}}}{T_0}\frac{\partial f_q^{(0)}}{\partial \omega} v_{\vec{q},x} \tag{6.48}$$

$$\Sigma_{ed\to m} = -\sum_{\vec{q}\vec{k}} \frac{v_{\vec{q},x}\tau_{\vec{q}}\tau_k^{(0)}}{\tau_{\vec{q}\vec{k}}^{e\downarrow\to m}}\frac{\partial g_k^{(0)}}{\partial \epsilon} u_{\vec{k},x} \tag{6.49}$$

$$\Sigma_{eu\to m} = -\sum_{\vec{q}\vec{k}} \frac{v_{\vec{q},x}\tau_{\vec{q}}\tau_k^{(0)}}{\tau_{\vec{q}\vec{k}}^{e\uparrow\to m}}\frac{\partial g_k^{(0)}}{\partial \epsilon} u_{\vec{k},x}\,, \tag{6.50}$$

and introduced the coefficients

$$C_1 = \sum_{\vec{q}} 2\cos^2(\vartheta)\frac{c_{q1}\omega_q}{\tau_{\mathrm{me}}} \qquad C_2 = \sum_{\vec{q}} 2\cos^2(\vartheta)\frac{c_{q1}T_0}{\tau_{\mathrm{me}}}\,. \tag{6.51}$$

By neglecting the crossing terms in the collision integral, we would have

$$\Sigma_{eu\to ed} = \Sigma_{ed\to eu} = \Sigma_{m\to ed} = \Sigma_{m\to eu} = \Sigma_{ed\to m} = \Sigma_{eu\to m} = 0\,. \tag{6.52}$$

Then, we would find for the system of differential equations

$$\Sigma_M \frac{\partial^2 T_M}{\partial x^2} = -C_1(T_0 - T_M) + C_2\mu_{\mathrm{Spin}} \tag{6.53}$$

$$-\Sigma_E \frac{\partial^2 \mu_{\mathrm{Spin}}}{\partial x^2} = C_1(T_0 - T_M) - C_2\mu_{\mathrm{Spin}}\,. \tag{6.54}$$

These two equations for the intermediate layer and the Eq. (6.55) for the normal metal will form the key system of differential equations, which will be solved further down. In the same way, as described above, we are able to derive a Boltzmann differential equation for the electrons in the region of the normal metal ($x \geq L$), where only electrons and phonons are able to propagate. Magnons are not able to propagate in this region. In this region, we include the spin relaxation. Here, we start with Eqs. (6.30) and (6.31) and do not neglect the spin flip scattering. But, we neglect the scattering with magnons. Phonons are equilibrated at temperature T_0 and strongly coupled to the electrons. Thus, the electron temperature is fixed at T_0, but the chemical potential may deviate. As already done above, we perform a separation by the integration over $\int d\vartheta \sin(\vartheta)/2$ and $\int d\vartheta \sin(\vartheta)\cos(\vartheta)/2$. Then, we take Eq. (6.34), which is the definition of the spin current and take the first derivative in coordinate x. Again, we solve the two equations from the $\int d\vartheta \sin(\vartheta)/2$-integration for the first derivative in coordinate x of the deviation density functions and set them into Eq. (6.34). Additionally, we take the two equations from the $\int d\vartheta \sin(\vartheta)\cos(\vartheta)/2$-integration and solve them for the deviation density distribution. Then, we also set these equations into Eq. (6.34). Finally, we find

$$-\Sigma_{E,\mathrm{right}} \frac{\partial^2 \mu_{\mathrm{Spin,right}}}{\partial x^2} = -C_5\mu_{\mathrm{Spin,right}}\,, \tag{6.55}$$

while $\mu_{\mathrm{Spin,right}}$ denotes the spin chemical potential in the normal metal, where only electrons and phonons can propagate ($x \geq L$). It is $\mu_{\mathrm{Spin,right}} = \mu_{\mathrm{up,right}} - \mu_{\mathrm{down,right}}$. The parameter

$\Sigma_{E,\mathrm{right}}$ now becomes renormalized because of the spin relaxation term in Eqs. (6.30) and (6.31). The abbreviations read

$$\Sigma_{E,\mathrm{right}} = -\sum_{\vec{k}} \frac{\tau_k^{(0)}\tau_{sk}}{2\tau_k^{(0)}+\tau_{sk}} u_{\vec{k}}^2 \frac{\partial g_k^{(0)}}{\partial \epsilon}\,, \tag{6.56}$$

and

$$C_5 = \sum_{\vec{k}} 2\cos^2(\varphi)\frac{1}{r_k \tau_{sk}}\,. \tag{6.57}$$

Now, we want to solve the resulting system of differential equations consisting of the three differential equations with three unknown functions T_M, μ_{Spin} and $\mu_{\mathrm{Spin,right}}$. For the intermediate region at $0 \leq x < L$, the differential equations (6.36) and (6.37) hold. However, the differential equation (6.55) holds in the normal metal, where only electrons and phonons are able to propagate ($x \geq L$). The boundary conditions read

$$j_{\mathrm{Mag}}(L) = 0 \qquad T_M(0) = T_{\mathrm{M0}} \tag{6.58}$$

$$j_{\mathrm{Spin}}(0) = 0 \qquad \mu_{\mathrm{Spin}}(L) = \mu_{\mathrm{Spin,right}}(L) \tag{6.59}$$

$$j_{\mathrm{Spin}}(L) = j_{\mathrm{Spin,right}}(L) \qquad \lim_{x\to\infty} \mu_{\mathrm{Spin,right}}(x) = 0\,, \tag{6.60}$$

while T_{M0} denotes the magnon temperature at position $x = 0$. For writing down the boundary conditions, we need the expressions for the magnon current and the spin current. The expressions for the magnon current, the spin current and the charge current read

$$j_{\mathrm{Mag}} = \Sigma_M \frac{\partial T_M}{\partial x} + \left(\frac{\Sigma_{UM}}{2} + \frac{\Sigma_{DM}}{2}\right)\frac{\partial \mu_{\mathrm{Spin}}}{\partial x} - \left(\frac{\Sigma_{DM}}{2} - \frac{\Sigma_{UM}}{2}\right)\frac{\partial \mu_{\mathrm{cha}}}{\partial x} \tag{6.61}$$

$$j_{\mathrm{Spin}} = -\Sigma_E \frac{\partial \mu_{\mathrm{Spin}}}{\partial x} + \frac{\Sigma_{UD}+\Sigma_{DU}}{2}\frac{\partial \mu_{\mathrm{Spin}}}{\partial x} + \frac{\Sigma_{UD}-\Sigma_{DU}}{2}\frac{\partial \mu_{\mathrm{cha}}}{\partial x} + (\Sigma_{MD}+\Sigma_{MU})\frac{\partial T_M}{\partial x} \tag{6.62}$$

$$j_{\mathrm{cha}} = -\Sigma_E \frac{\partial \mu_{\mathrm{cha}}}{\partial x} - \frac{\Sigma_{UD}-\Sigma_{DU}}{2}\frac{\partial \mu_{\mathrm{Spin}}}{\partial x} - \frac{\Sigma_{UD}+\Sigma_{DU}}{2}\frac{\partial \mu_{\mathrm{cha}}}{\partial x} + (-\Sigma_{MD}+\Sigma_{MU})\frac{\partial T_M}{\partial x} = 0\,. \tag{6.63}$$

For writing down the boundary conditions, one needs to eliminate $\partial\mu_{\mathrm{cha}}/\partial x$. By solving Eq. (6.63) for $\partial\mu_{\mathrm{cha}}/\partial x$ and setting it into the other two Eqs. (6.61) and (6.62), we eliminate the dependence of the charge chemical potential in the boundary conditions.

The explicit spatially dependent solutions to the problem is to complicated to write down. We are interested in small interface length L. Thus, the interaction needs to scale with this interface length in the following way

$$|M_{\vec{k},\vec{k}-\vec{q},\vec{q}}|^2 \propto \frac{1}{L}\,. \tag{6.64}$$

In addition to that, we assume lattice mismatching at the interface between the insulating ferromagnet and the conducting normal metal. This leads to a boosted impurity relaxation time for magnons and electrons, which is assumed to scale in the following way

$$\tau_k^{(0)} \propto L \qquad \tau_q^{(0)} \propto L\,. \tag{6.65}$$

Because of that, the coefficients $C_1 = C_1(L)$ and $C_2 = C_2(L)$ as well as the spin conductivities also depend on the interface length and we can identify the following dependencies of the arising coefficients

$$C_1(L) = \frac{c_1}{L} \qquad C_2(L) = \frac{c_2}{L} \qquad \Sigma_E(L) = \sigma_E L \qquad \Sigma_M(L) = \sigma_M L \qquad \Sigma_{ab}(L) = \sigma_{ab} L\,. \tag{6.66}$$

For a, b one sets the letters D, U or M. Including these definitions, the result becomes independent of the interface length L. Since it is also to lengthy to write down, we perform an approximation in the magnon-electron interaction strength (influencing c_1, c_2 and σ_{ab}). The total current can be calculated by Eq. (6.62) and one finds for the total spin current exactly behind the interface

$$\begin{aligned} j_{\mathrm{Spin}}(L) \approx &- c_1(T_{\mathrm{M0}} - T_0) + \frac{c_1(c_1\sigma_E\sqrt{C_5\Sigma_{E,\mathrm{right}}} + c_2(3\sigma_E + \sqrt{C_5\Sigma_{E,\mathrm{right}}})\sigma_M)(T_{\mathrm{M0}} - T_0)}{3\sigma_E\sqrt{C_5\Sigma_{E,\mathrm{right}}}\sigma_M} \\ &- \frac{c_1(8c_1^2C_5\sigma_E^2\Sigma_{E,\mathrm{right}} + 4c_2^2\sigma_M^2(15\sigma_E^2 + 2C_5\Sigma_{E,\mathrm{right}} + 10\sigma_E\sqrt{C_5\Sigma_{E,\mathrm{right}}}))(T_{\mathrm{M0}} - T_0)}{60C_5\Sigma_{E,\mathrm{right}}\sigma_E^2\sigma_M^2} \\ &- \frac{c_1(10c_2\sigma_M C_5\Sigma_{E,\mathrm{right}}(\sigma_E(\sigma_{MD} + \sigma_{MU}) - \sigma_M(\sigma_{DU} + \sigma_{UD})))(T_{M0} - T_0)}{60C_5\Sigma_{E,\mathrm{right}}\sigma_E^2\sigma_M^2} \\ &- \frac{c_1(c_1\sigma_E\sigma_M(c_2(11C_5\Sigma_{E,\mathrm{right}} + 40\sigma_E\sqrt{C_5\Sigma_{E,\mathrm{right}}}) - 5C_5\Sigma_{E,\mathrm{right}}(\sigma_{DM} + \sigma_{UM})))}{60C_5\Sigma_{E,\mathrm{right}}\sigma_E^2\sigma_M^2} \\ &\times (T_{\mathrm{M0}} - T_0)\,. \end{aligned} \tag{6.67}$$

We want to point out, that this resulting term does not depend on the thickness L of the intermediate region. Hence, this term does not change, when we perform the limes of $L \to 0$. Of course, the zero order term in temperature difference vanishes, because the interaction is needed to transfer the magnons into electron spin excitations. The leading contribution is just c_1 times the temperature difference, since this term results from the first order collision integral for the temperature variation. Behind the interface ($x > L$), the current decays exponentially.

If one compares the expression for the spin current in Eq. (6.67), one finds that the spin current is proportional to c_1 and $(T_{\mathrm{M0}} - T_0)$ in leading order of the sd-coupling strength. Also, Schmidt *et al.* [57] performed a calculation on a related setup. Their expression is similar to our result.

In order to describe the spin pumping on an YIG-Pt interface, where the intermediate region is small, i.e. on an atomic scale, we take the two dimensional limit of our calculation. One has to consider, that the parameter c_1 is an $\vec{k}$-integrated coefficient. For considering wave vector dependent magnon temperatures, we have to take out the $\vec{k}$-integration and integrate after multiplying the wave vector dependent temperature. Taking into account, that for a two dimensional interface, the three dimensional momentum conservation reduces to a two dimensional momentum conservation and recovering the k-dependent form of c_1, in order to allow the treatment of the k-dependent temperatures, we arrive at the following

expression for the spin pumping

$$j_s = \sum_{\vec{k}} G_{m,k} \left(T_{\mathrm{M}}(k) - T_0 \right) \tag{6.68}$$

$$\begin{aligned} G_{m,k}^{(\mathrm{clean})} =& \frac{L\, m_{\mathrm{eff}}\, N_{\mathrm{s}}^2\, k_{\mathrm{B}}}{\pi\, \hbar^2} \left(\frac{4\pi^4}{3a^3} \right) \omega_{\vec{k}} \frac{\partial b_{\vec{k}}^0}{\partial T} \\ & \times \int_0^{p_{\max}} dp\, p^2 \left(-\frac{\partial f_{\vec{p}}^{\,0}}{\partial \epsilon} \right) \int d\Omega_{\vec{k}} \int d\Omega_{\vec{p}}\, |M|^2\, \frac{\theta(p'_\perp) \cdot \theta(p_{\max} - p'_\perp)}{|p'_\perp|}\,, \end{aligned} \tag{6.69}$$

with

$$p'_\perp = \pm \sqrt{p_\perp^2 + \frac{2 m_{\mathrm{eff}} \omega_{\vec{k}}}{\hbar^2} - k_\parallel^2 - 2 p_\parallel k_\parallel \cos(\varphi_{\vec{k}} - \varphi_{\vec{p}})}\,. \tag{6.70}$$

Here, $T_{\mathrm{M}}(k)$ denotes the local and wave vector dependent magnon temperature in the YIG-film. Additionally, it is $p_\parallel = p \cdot \sin(\vartheta_{\vec{p}})$, $p_\perp = p \cdot \cos(\vartheta_{\vec{p}})$ and $k_\parallel = k \cdot \sin(\vartheta_{\vec{k}})$. We have $b_{\vec{k}}^0 = f_{\vec{k}}^{(0)}$ for the equilibrium density for the magnons at wave vector $\vec{k}$ (cf. Eq. (2.8)) and the energy dispersion $\omega_{\vec{k}} = \epsilon_{\vec{k}}$ (cf. Eq. (2.6)). Besides, the equilibrium electron density is denoted by $f_{\vec{p}}^{\,0} = f_{\vec{p}}^{\,(0)}$ (cf. Eq. (2.2)) and the electron energy dispersion is denoted by $\epsilon_{\vec{p}}$ (cf. Eq. (2.1)). The parameter m_{eff} denotes the effective mass for the electrons and N_{s} is the number of valence electrons in a platinum unit cell. The upper expression is equivalent to the spin pumping found by Schmidt *et al.* [57] for a clean interface. For the comparison between the two theories, we have

$$|M|^2 = \frac{1}{L} \left(\frac{3a^3}{4\pi^4} \right) \frac{\pi S}{2A} \left(\frac{J_{\mathrm{sd}}}{N_s} \right)^2 \frac{1}{k_{\mathrm{B}}} \tag{6.71}$$

The numbers are

$$J_{\mathrm{sd}} = 1.48884\,\mathrm{meV} \tag{6.72}$$

$$a_{\mathrm{YIG}} = 12.4\,\mathrm{nm}\ [52,\ 53] \tag{6.73}$$

$$A = a_{\mathrm{YIG}}^2 \tag{6.74}$$

$$m_{\mathrm{e}} = 9.1093897 \cdot 10^{-31}\,\mathrm{kg} \tag{6.75}$$

$$m_{\mathrm{eff}} = 1.38 \cdot m_{\mathrm{e}}\,[57]\,. \tag{6.76}$$

The parameter J_{sd} will be adjusted in chapter 7. It will be adjusted in that way, that the resulting transverse spin Seebeck voltage for $T_0 = 300$ K is the same for the theory from Xiao *et al.* [23], from Schmidt *et al.* [57] and from ourselves as well.

6.2 Summary

In this chapter, we considered the spin pumping mechanism between an insulating ferromagnet and a normal metal by using the Boltzmann equation. We found the spin current to be proportional to the difference between magnon and electron temperature.

In the insulating ferromagnet only magnons and phonons are able to propagate, while in the normal metal only electrons and phonons are able to propagate. In our model, there is an intermediate layer of thickness L, where all three types of (quasi-)particles are able to propagate. The electrons in the normal metal are strongly coupled to the phonons and thus both are at temperature T_0. Only the magnons in the insulating ferromagnet are at a

different temperature $T_{\mathrm{M}0}$. But the chemical potential for the electrons can deviate in the normal metal and in the intermediate region.

Here, we set up the Boltzmann equation for the intermediate region and for the normal metal. In the intermediate region we consider electrons and magnons, while in the normal metal we consider electrons only. The magnon-electron interaction is mediated by a sd-interaction. At the end, we derive a system of differential equations for the problem. After solving the system of differential equations, we calculate the spin current at the contact area between the intermediate layer and the normal metal ($x = L$). The interaction strength is assumed to be proportional to $1/L$ (cf. Eq. (6.64)). Thus, we take the limes of the thickness of the intermediate layer going to zero ($L \to 0$). At the end, the spin current is proportional to the difference of the magnon temperature $T_{\mathrm{M}0}$ and the electron temperature T_0. This dependency on the temperature difference agrees with the theory of Xiao *et al.* [23] and with Schmidt *et al.* [57]. Our detailed expression coincides with the expression of Schmidt *et al.* [57].

The better understanding of the spin pumping mechanism helps us to better understand the spin Seebeck effect. There, a thin and ferromagnetic YIG-film was evaporated on a GGG substrate ($Gd_3Ga_5O_{12}$). Again on top, there are small platinum stripes with a voltmeter attached to measure the inverse spin Hall voltage (cf. figure 4). The heat reservoirs, which generate the temperature gradient are assumed to be ideal heat reservoirs. The temperature gradient will induce a deviation of the magnon temperature inside the YIG-film. Since the electrons in the normal metal are strongly coupled to the phonons, there will be a temperature difference between magnons and electrons. Thus, there will be a spin current based on the spin pumping mechanism. The inverse spin Hall effect transfers the spin current into a measurable charge current.

7 Results

In this section, we discuss the results out of the system of linear equations for the magnon temperature in the transverse spin Seebeck effect, which was derived in chapters 3, 4 and 5. Additionally, we will calculate the transverse spin Seebeck voltage. The setup can be found in figures 4 and 9.

The setup of the transverse spin Seebeck effect consists of a GGG substrate formed as a cuboid, while the edge length are in the order of millimeters. On top of the thick GGG substrate, there is a thin YIG-stripe with the same surface area attached. Furthermore on top of the YIG-stripe, there are smaller stripes of platinum. In the GGG substrate, only phonons are able to propagate. Since the thickness of the GGG substrate is much thicker than of the YIG-film, the phonons are propagating in the GGG substrate most of the time. Thus, they are only rarely influenced by the magnons. We neglect the influence from the magnons onto the phonons. In contrast, the magnons are strongly influenced by the phonons, because they propagate only in the YIG-film, where phonons and magnons are able to propagate as well. Thus, we calculated the phonon-temperature in chapter 3 by using the Boltzmann equation and including phonon-phonon interaction only.

In chapter 4, we calculated the collision integral in the Boltzmann equation for the magnon-phonon interaction and took the phonon temperature as an input parameter. After that, we calculated the collision integral in the Boltzmann equation for the magnon-magnon interaction in chapter 5. In both interactions, we considered exchange magnons and dipolar magnons as well. To evaluate the resulting expressions numerically, we performed analytic transformations and a discretization of the wave vector dependent temperature in 100 or 200 points. We derived a system of linear equations for the wave number dependent magnon temperature including magnon-phonon and magnon-magnon interaction as well. The phonon temperature was used as an input parameter. The solution to the system of linear equations will be presented in this chapter.

The resulting system of equations is composed of contributions from magnon-phonon interaction, dipole-dipole magnon-magnon interaction and exchange magnon-magnon interaction. We have to sum up the three contributions in a system of equations. It is

$$\left.\frac{\partial f_{\vec{k}}}{\partial t}\right|_{\mathrm{St}} = \left.\frac{\partial f_{\vec{k}}}{\partial t}\right|_{\mathrm{St,mag\text{-}pho}} + \left.\frac{\partial f_{\vec{k}}}{\partial t}\right|_{\mathrm{St,mag\text{-}mag,3}} + \left.\frac{\partial f_{\vec{k}}}{\partial t}\right|_{\mathrm{St,mag\text{-}mag,4}} . \tag{7.1}$$

In Eq. (4.47) we motivated the integral identity, which has to be fulfilled

$$0 = \frac{1}{2}\int_0^\pi \sin(\vartheta)\, d\vartheta \left.\frac{\partial f_{\vec{k}}}{\partial t}\right|_{\mathrm{St}} , \tag{7.2}$$

while this equation is assumed to be independent on φ. With these two equations, we set up the system of linear equations for the wave number dependent magnon temperature. For the contribution of the magnon-phonon interaction, we take Eq. (4.77). We take Eq. (5.40) for the contribution of the magnon-magnon interaction which is mediated by dipole-dipole interaction. For the contribution of the magnon-magnon interaction, which is mediated by exchange interaction, we take Eq. (5.80). For magnons in this section, we only consider normal scattering processes. Umklapp scattering processes are neglected for magnons. These three contributions sum up to a system of integral equations, where the wave number dependent magnon temperature occurs only linear. Since there are summands including phonon temperature but no magnon temperature, they are treated as inhomogeneities in the system of linear equations.

For setting up the system of linear equations, we discretize the integration and also discretize the wave number dependent magnon temperature and phonon temperature. For our calculation, we discretize the wave number interval $0 \leq k \leq k_\mathrm{F}$ into $n = 100$ or $n = 200$ small intervals. It turns out, that the result converges with these numbers. Then, we get a system of linear equations with n equations and n unknown magnon temperatures.

In figures 38 and 39, one finds a plot of the dispersion relation for the phonons and for the magnons. Here we use Eq. (2.3) for the linear phonon dispersion. The magnon dispersion relation consists of an offset plus a quadratic term. For this, we take Eqs. (2.6) and (2.7). We take $H_0 = 99.9$ Oe for the external magnetic field and $M_0 = 139$ G [43, p. 182] for the local magnetization (cf. Eq. (2.7)). This is consistent with the parameters used for the magnon-magnon interaction in Eq. (5.30). If we set in the angle $\vartheta_k = \pi/4$ (cf. Eq. (2.6)), we end up with

$$\omega_\mathrm{off} = 5.49\,\mathrm{GHz}\,. \tag{7.3}$$

With these numbers, we compared the exact formula for the magnon dispersion and the approximation. The exact formula is in Eq. (2.5), while the approximation is in Eq. (2.6). The accordance of both formulas is good for the expected numbers. In figure 40, we added an exemplary optical phonon mode.

$$\omega_{\vec{q},\mathrm{optical}} = \omega_\mathrm{gap} - c_\mathrm{ph,2}\,q\,, \tag{7.4}$$

with $\omega_\mathrm{gap} = 19094$ GHz and $c_\mathrm{ph,2} = 768.6$ m/s. The temperature for the optical phonons is set to ΔT at position $x = -L/2$, which is approximately the temperature for diffusive phonons. For our calculation, we use the following numbers

$$\hbar = 1.05457266 \cdot 10^{-34}\,\mathrm{Js} \tag{7.5}$$
$$k_\mathrm{B} = 1.380658 \cdot 10^{-23}\,\mathrm{J/K} \tag{7.6}$$
$$a = 1.2376\,\mathrm{nm}\,[52,\ 53] \tag{7.7}$$
$$c_\mathrm{Ph} = 3843\,\mathrm{m/s}\,[55] \tag{7.8}$$
$$S = 14.2\,[53] \tag{7.9}$$
$$D_\mathrm{ex} = 9.16 \cdot 10^{-11}\,\mathrm{GHz\ cm^2}[43, p.\ 182] \tag{7.10}$$
$$k_\mathrm{F} = k_\mathrm{max} = 3.10 \cdot 10^{7} \cdot \mathrm{cm}^{-1}\,. \tag{7.11}$$

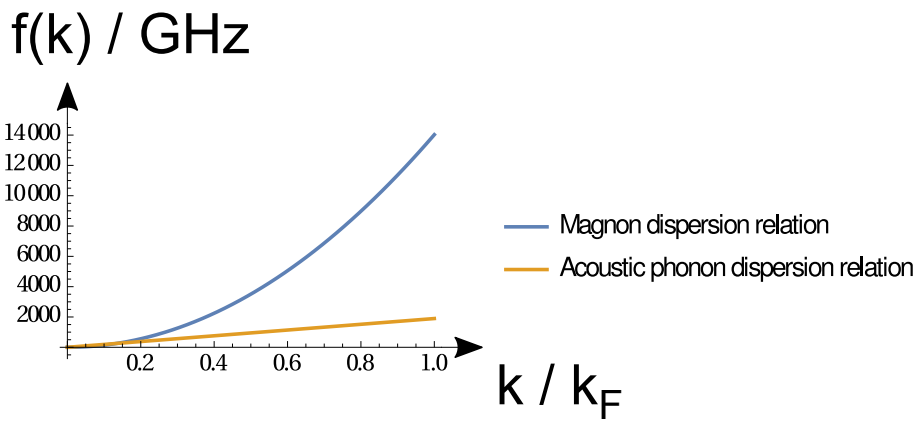

Figure 38: Here, the k-dependent frequency (not angular velocity) of magnons and phonons is plotted. The phonon dispersion relation is linear, while the magnon dispersion relation is quadratic plus an offset. Thus, the dispersion relations intersect twice.

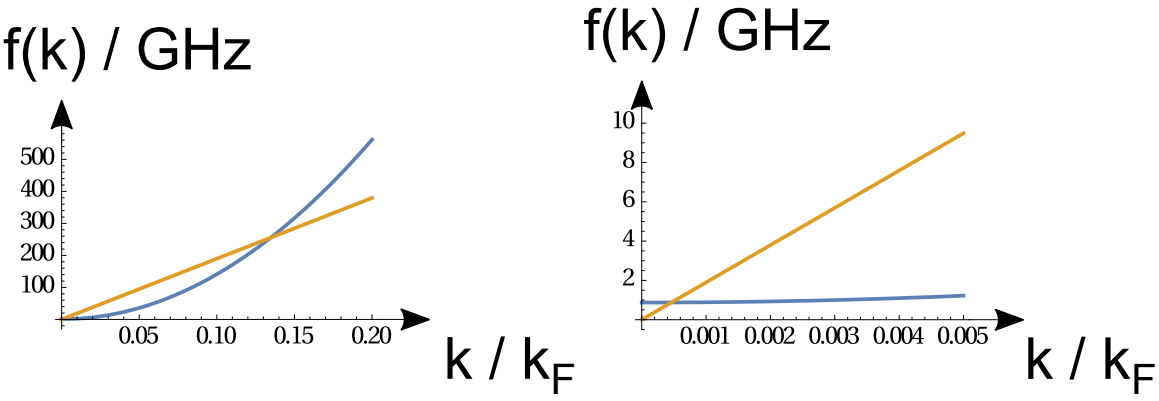

Figure 39: Zoom of the phonon and magnon dispersion relation. The dispersion relations intersect twice.

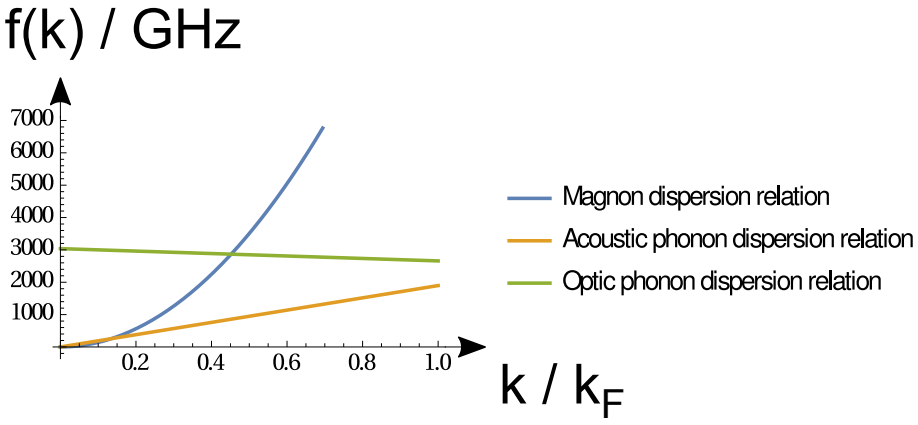

Figure 40: Here, the k-dependent frequency (not angular velocity) of magnons and phonons is plotted. The linear phonon dispersion relation is extended by a linear optical phonon mode. As in figures 38 and 39, the magnon dispersion relation is quadratic plus an offset.

Now, we discuss the results from the system of linear equations, which was derived above. The wave vector dependent phonon temperature was already calculated in chapter 3. We will recapitulate the results. The wave vector dependent phonon temperature for different average temperatures T_0 is plotted. In figure 41 the boundary scattering is not included, while in figure 42 boundary scattering is included. For constructing the spatial temperature profile, one takes the value for $x = -L/2$ out of figure 41 and 42 and places a straight line through this point and zero at $x = 0$. In the absence of boundary scattering, the ballistic phonons propagate nearly hitchless through the GGG substrate. Thus, they keep the temperature of the heat bath where they came from. In average, left and right moving ballistic phonons therefore have the average temperature T_0. When boundary scattering is included, the phonons scatter at the boundary of the substrate and relax to the local temperature of diffusive phonons, as described above. Thus they are only able to keep the temperature for a length in order of the boundary relaxation length.

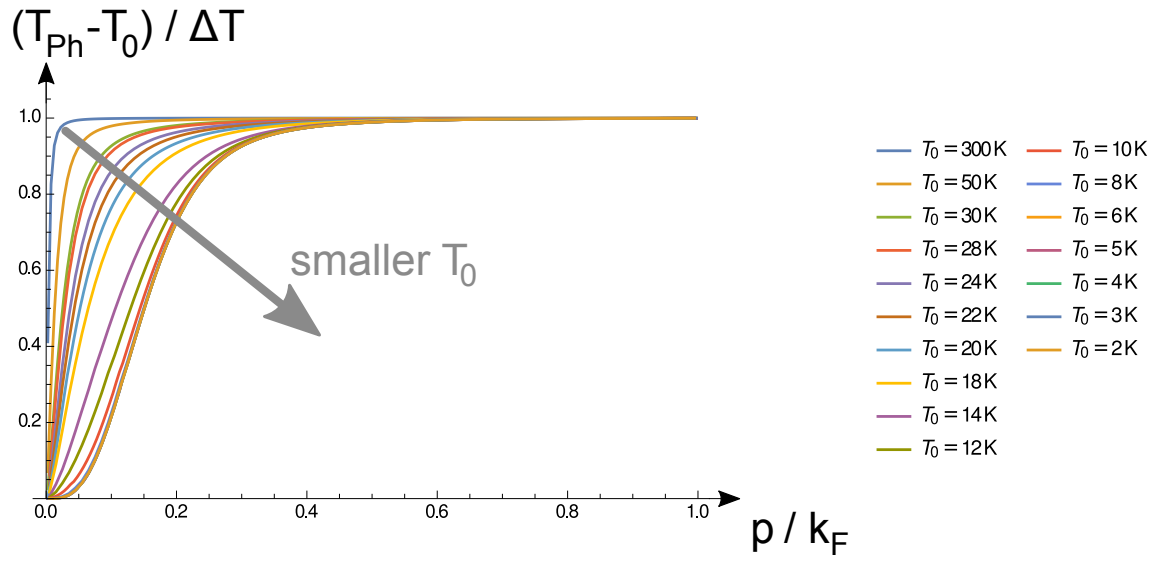

Figure 41: Here, the k-dependent phonon temperature at position $x = -L/2$ is plotted for different average temperatures T_0. Boundary scattering is not included in this figure.

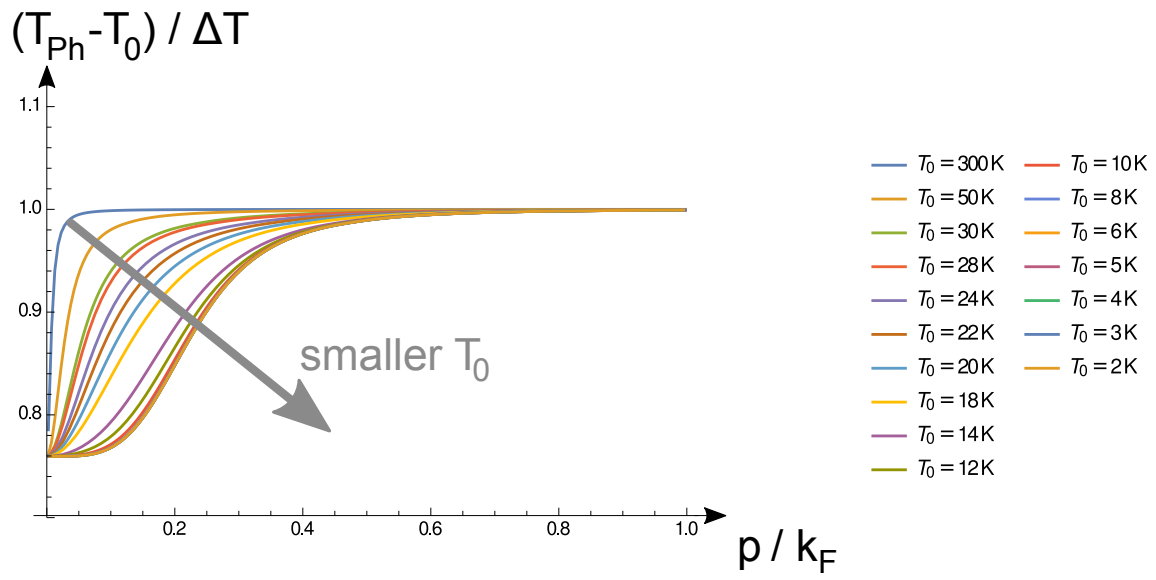

Figure 42: Here, the k-dependent phonon temperature at position $x = -L/2$ is plotted for different average temperatures T_0. Boundary scattering is included in this figure.

Now, we calculate the wave vector dependent magnon temperature. Here, we include magnon-phonon interaction as well as magnon-magnon interaction. For both interactions we consider dipolar magnons and exchange magnons separately. We take Eqs. (7.1) and (7.2) and solve the system of linear equations for the discretized wave vector dependent magnon temperature. In figure 43, the resulting magnon temperature is shown without boundary scattering. Instead in figure 44, the resulting magnon temperature is plotted and the boundary scattering is included. The boundary scattering describes the scattering process of phonons at the boundary of the system (or the cuboid). When one phonon reaches the boundary, it relaxes and gets the local temperature of the diffusive phonons. Diffusive phonons are phonons with a small relaxation length and hence with a large wave number. The boundary scattering is also explained around Eqs. (3.25) and (3.40).

Similar to the wave vector dependent phonon temperature, the magnon temperature decreases for small wave numbers (or large wave lengths). The smaller the average temperature T_0 is, the greater the decrease of temperature for the small wave number magnons is. In contrast to the phonon temperature, the magnon temperature does not decrease to T_0 for small wave numbers even without boundary scattering. When we include boundary scattering, the magnon temperature decreases less for small wave vectors similar to the phonon case. If one wants to construct the spatial temperature profile for one certain wave number, one has to take the value out of the figures 43 or 44 as one point of the profile at $x = -L/2$. All temperature profiles are linear and crossing the value T_0 at position $x = 0$. With these two points, one is able to construct the linear temperature profile.

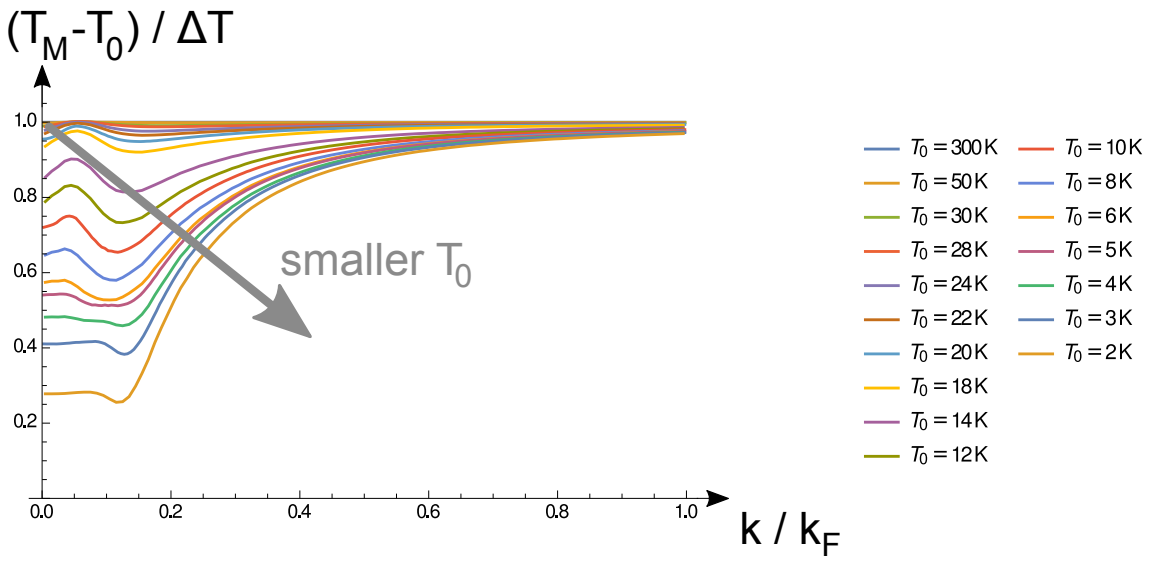

Figure 43: Here, the k-dependent magnon temperature at position $x = -L/2$ is plotted for different average temperatures T_0. Boundary scattering is not included in this figure.

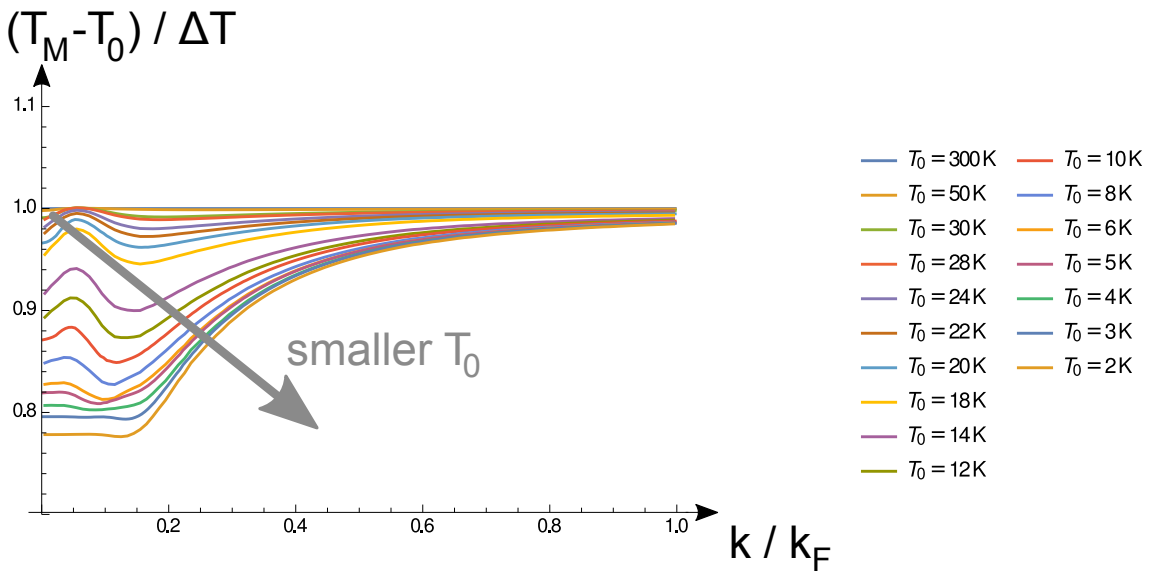

Figure 44: Here, the k-dependent magnon temperature at position $x = -L/2$ is plotted for different average temperatures T_0. Boundary scattering is included in this figure.

Now, we add an optical phonon mode to the phonon dispersion relation. In principle, optical phonon modes are present and we want to analyze their influence on our transverse spin Seebeck voltage. Because of that we consider one representative optical phonon mode. Here, we use Eq. (7.4) and the dispersion relation can be seen in figure 40. The interaction strength between magnons and optical phonons is set to be the same strength as for interaction between magnons and acoustic phonons. At the end, we have the results for the cases with the same interaction strength and with zero interaction strength for magnons with optical phonons. The temperature for the optical phonons is set to ΔT at position $x = -L/2$, which is approximately the temperature for diffusive phonons. The magnon temperature by

including the optical phonon mode and without boundary scattering is shown in figure 45 and with boundary scattering shown in figure 46. If the average temperature T_0 is small, the result does nearly not change by adding an additional optical phonon mode. This we will also see later, when we calculate the spin Seebeck voltage. For higher temperatures T_0, the numeric calculation does not converge within the bounds of computing capacity. But, we can state, that the temperature profile for the magnon temperature including optical phonons deviates from without optical phonons.

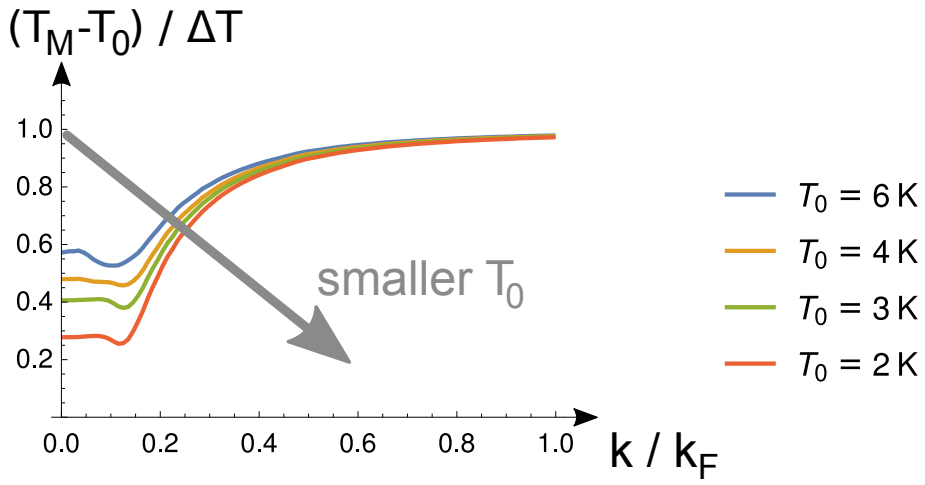

Figure 45: Here, the k-dependent magnon temperature at position $x = -L/2$ is plotted for different average temperatures T_0. In this calculation, we included an optical phonon mode, as shown in figure 40. In this figure, boundary scattering is not included.

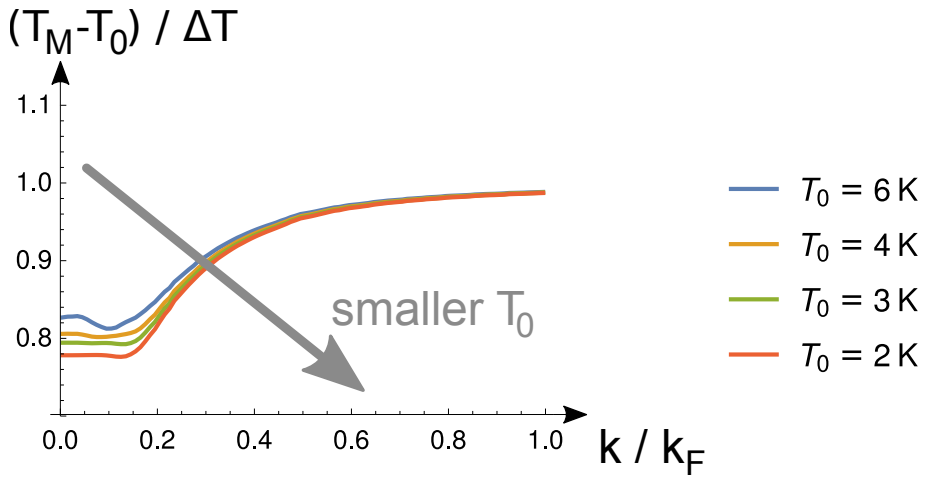

Figure 46: Here, the k-dependent magnon temperature at position $x = -L/2$ is plotted for different average temperatures T_0. In this calculation, we included an optical phonon mode, as shown in figure 40. In this figure, boundary scattering is included.

For calculating the transverse spin Seebeck voltage, we need to calculate the average temperatures for phonons and magnons before. By calculating the phonon temperature average, we weight the summation by the Bose-Einstein distribution. Since the temperature is only dependent on the absolute value of the wave vector, we transform the summation

into spherical coordinates. Thus, the factor p^2 occurs as an additional weighting factor. The formula for the phonon temperature average reads

$$\bar{T}_{\mathrm{Ph}} = \frac{4\pi \sum_p p^2 \cdot n(p, T_0) \cdot T_{\mathrm{Ph}}(p)}{4\pi \sum_p p^2 \cdot n(p, T_0)}\,, \tag{7.12}$$

while the summation goes via the discretized points between 0 and k_{F} of the magnon temperature. Here, the function $n(p, T_0)$ denotes the wave number and temperature dependent phonon distribution, which is a Bose-Einstein distribution (cf. Eq. (2.4)). If optical phonons are included, on also have to consider them in the upper summation with their correct dispersion and Bose-Einstein distribution. The average magnon temperature will be calculated in the same way as for the phonon temperature. The summation is weighted by the Bose-Einstein distribution. In the same way, the factor k^2 occurs because of the transformation into spherical coordinates. The formula for the magnon temperature average reads

$$\bar{T}_{\mathrm{M}} = \frac{4\pi \sum_k k^2 \cdot f(k, T_0) \cdot T_{\mathrm{M}}(k)}{4\pi \sum_k k^2 \cdot f(k, T_0)}\,, \tag{7.13}$$

while the summation goes via the discretized points between 0 and k_{F} of the magnon temperature. Here, the function $f(k, T_0)$ denotes the wave number and temperature dependent magnon distribution, which is a Bose-Einstein distribution (cf. Eq. (2.8)).

The results for the phonon average temperature $\bar{T}_{\mathrm{Ph}}$ and the magnon average temperature $\bar{T}_{\mathrm{M}}$ dependent on the overall average temperature T_0 are shown in figure 47(a) without boundary scattering. The same results by including boundary scattering are shown in figure 47(b). The smaller the overall average temperature T_0 is, the smaller the average temperature for phonons and magnons is. For calculating the wave vector average, the Bose-Einstein distribution times k^2 occurs as a weighting factor. At small overall average temperature T_0, small wave vector phonons and magnons are much higher weighted than large wave vector phonons and magnons. Thus, their influence on the wave vector averaged temperature is large. The consequence is, that here the wave vector averaged phonon and magnon temperatures are close by the temperature for small wave vector phonons and magnons, respectively. For larger overall temperature, the situation is different for phonons and magnons. At room temperature ($T_0 = 300$ K), the phonon weight function is nearly linear and the magnon weight function has a small and negative slope. In that situation, all phonons and magnons contribute to the wave vector average.

As a next step, we consider the difference between the averaged phonon temperature $\bar{T}_{\mathrm{Ph}}$ and the averaged magnon temperature $\bar{T}_{\mathrm{M}}$ for different overall averaged temperature T_0. The difference is shown in figure 48. The sign change in the temperature difference is caused by the crossing of average phonon temperature and average magnon temperature in figure 47. Additionally, the plots are also made by including an extra optical phonon mode (cf. Eq. (7.4)). The optical phonons are expected to have the diffusive temperature. For calculating the phonon average temperature, one also has to respect optical phonons, their temperature and the correct dispersion relation in the Bose-Einstein weighting factor. For small temperatures T_0, the deviation between including and excluding optical phonon modes is small. For larger temperatures, we can state that there is a significant change in the behavior. But, there is no decrease in the absolute value of the temperature difference and the sign change still remains.

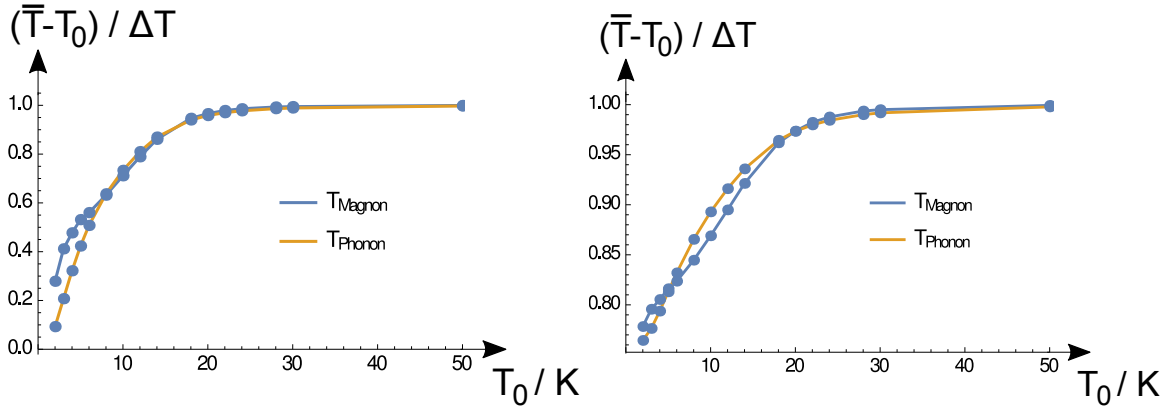

(a) Average phonon and magnon temperature without boundary scattering

(b) Average phonon and magnon temperature with boundary scattering

Figure 47: The wave vector averaged phonon temperature $\bar{T}_{\mathrm{Ph}}$ and magnon temperature $\bar{T}_{\mathrm{M}}$ was calculated dependent on the overall average temperature T_0. These figures do not include optical phonon modes.

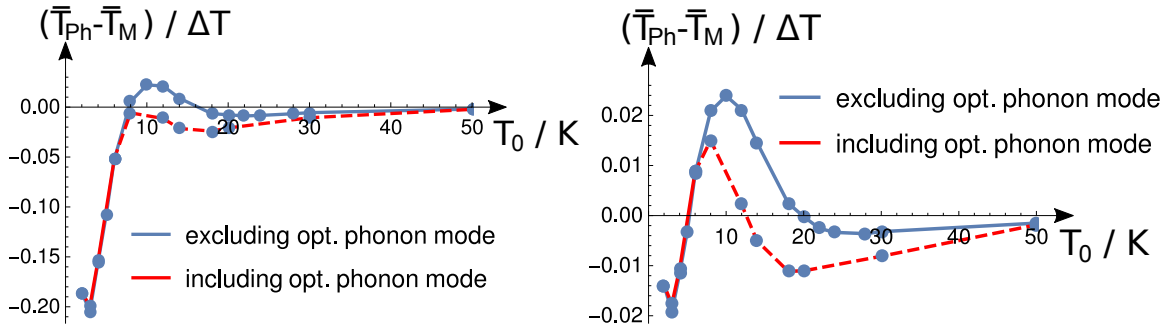

(a) Without boundary scattering

(b) With boundary scattering

Figure 48: The difference of the averaged phonon temperature $\bar{T}_{\mathrm{Ph}}$ and averaged magnon temperature $\bar{T}_{\mathrm{M}}$ is plotted dependent on the overall averaged temperature T_0. Additionally, we performed the same calculation by including an optical phonon mode. The dashed line for larger than 6 K illustrates just the magnitude of the result, because there are significant numerical errors, which are caused by finite size effects.

Now, we want to calculate the transverse spin Seebeck voltage in the platinum stripe. The setup can be found in figures 4 and 9. For the conversion of a temperature difference between magnons and phonons into a transverse spin Seebeck voltage, we take the theory from Xiao *et al.* [23]. As described by them, the temperature of the electrons in the platinum stripe is strongly correlated to the phonon temperature in the YIG ferrimagnet. Thus, we expect the electron temperature to be the same as the averaged phonon temperature. If there is a temperature difference between the magnons in the ferrimagnet and the electrons in the platinum stripe, there will be a net spin current in the platinum stripe, which is proportional to this temperature difference. This proportionality we also find in our theory of chapter 6 and in the theory of Schmidt *et al.* [57]. This mechanism is called spin pumping. The inverse spin Hall effect converts a spin current into a charge current, which is perpendicular to the direction of the spin current and additionally perpendicular to the polarization of the spin

current. The mechanism causes the transverse spin Seebeck voltage and is sketched in figure 4b. For the formula for the transverse spin Seebeck effect, we compare Eqs. (18) and (25) from Ref. [23]. Thus, we find

$$V_{\mathrm{SSE}} = \frac{\theta_H \, \rho \, w_{\mathrm{Pt}} \, g_r \, \gamma \, |e| \, k_{\mathrm{B}}}{\pi \, M_s \, V_a \, A} \cdot (\bar{T}_{\mathrm{Ph}} - \bar{T}_{\mathrm{M}}) \, . \tag{7.14}$$

We take the numbers from Ref. [23]

$$\theta_H = 0.0037 \tag{7.15}$$
$$\rho = 0.91 \, \mu\Omega \, \mathrm{m} \tag{7.16}$$
$$w_{\mathrm{Pt}} = 4 \, \mathrm{mm} \tag{7.17}$$
$$g_r/A = 10^{16} \, \mathrm{m}^{-2} \tag{7.18}$$
$$\gamma = 1.76 \cdot 10^{11} \, \mathrm{T}^{-1}\mathrm{s}^{-1} \tag{7.19}$$
$$e = 1.60217733 \cdot 10^{-19} \, \mathrm{C} \tag{7.20}$$
$$k_{\mathrm{B}} = 1.380658 \cdot 10^{-23} \, \mathrm{J/K} \tag{7.21}$$
$$4\pi M_s = 1.4 \cdot 10^{5} \, \mathrm{A/m} \tag{7.22}$$
$$V_a^{1/3} = 14.1 \, \mathrm{nm} \, . \tag{7.23}$$

Additionally, we have to respect the temperature dependence of the magnetic coherence volume V_a. The upper value is given for $T_0 = 300$ K. Out of Eq. (15) of Ref. [23], we extract the following temperature dependence

$$V_a \propto \frac{1}{\sqrt{\bar{T}_{\mathrm{M}}}} \approx \frac{1}{\sqrt{T_0}} \, . \tag{7.24}$$

With these numbers, we calculate the transverse spin Seebeck voltage. The results can be found in figure 49. The results are separately plotted by including and excluding the boundary scattering. We find, that the transverse spin Seebeck voltage is larger for small temperatures T_0 than for room temperature. Besides for small overall averaged temperatures T_0, the difference in the results between including and excluding the optical phonon mode is very small. For larger overall temperatures T_0 the difference between including and excluding the optical phonon mode becomes larger.

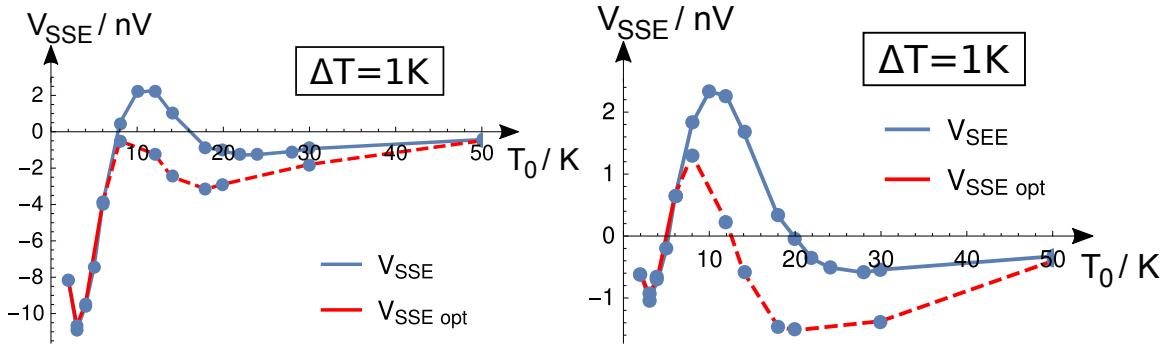

(a) Without boundary scattering (b) With boundary scattering

Figure 49: The transverse spin Seebeck voltage V_{SSE} is plotted dependent on the overall average temperature T_0. Additionally, the transverse spin Seebeck voltage by including an optical phonon mode in the calculation $V_{\mathrm{SSE\ opt}}$ is plotted here. The dashed line for larger than 6 K illustrates just the magnitude of the result, because there are significant numerical errors, which are caused by finite size effects. The temperature difference between the two heat baths is set to $2\Delta T = 2$ K. The results are proportional to this temperature difference.

In figure 14 and 15 of section 3.2, we discussed the several relaxation processes for the phonons. Now, we separate the calculation by including and excluding the phonon normal scattering processes. In figure 50, we plot the transverse spin Seebeck voltage by performing this separation. As one can see for $T_0 = 3$ K in figure 15, the normal scattering relaxation length is length is always larger than the boundary scattering. Thus, there is nearly no difference between including and excluding normal scattering processes when boundary scattering is including. Only by excluding boundary scattering, the result becomes a little different. For higher overall average temperatures T_0 with and without boundary scattering, the normal scattering relaxation length becomes more important (cf. figure 14) and reduces the transverse spin Seebeck voltage significantly. If we combine including normal scattering and optical phonon mode, we suspect the influence of the optical phonons to the spin Seebeck voltage to be small for all T_0.

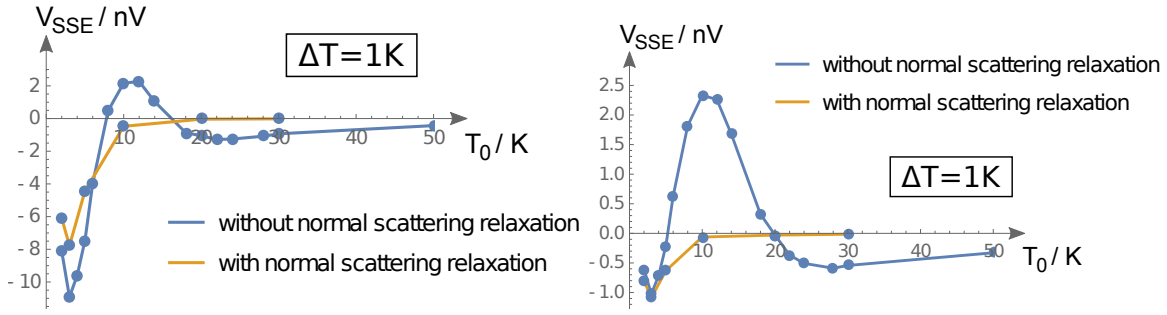

(a) Without boundary scattering (b) With boundary scattering

Figure 50: The transverse spin Seebeck voltage V_{SSE} is plotted dependent on the overall average temperature T_0 with and without boundary scattering. Additionally, the transverse spin Seebeck voltage is separated by including and excluding phonon-phonon normal scattering events in the calculation for the relaxation length.

Now, we will use another theory out of chapter 6 for the spin pumping mechanism. As already discussed at the end of chapter 6, ourselves and Schmidt *et al.* [57] developed a theory for the spin pumping mechanism. The expressions can be found in Eqs. (6.68), (6.69), (6.70) and (6.71).

Schmidt *et al.* [57] developed a more exact equation for the inverse spin Hall effect. They included spin-flip mechanism in the platinum stripe. Thus, the spin current decays by penetrating from the contact area into the platinum stripe. The averaged spin Seebeck voltage reads

$$\overline{V_{\mathrm{SSE}}} = \theta_H \, \rho \, w_{\mathrm{Pt}} \frac{2|e|}{\hbar} \frac{\tanh\left(\frac{L_{\mathrm{N}}}{2\lambda_{\mathrm{sf}}}\right)}{\frac{L_{\mathrm{N}}}{\lambda_{\mathrm{sf}}}} \cdot j_s \, . \tag{7.25}$$

The numbers are

$$L_N = d_{\mathrm{Pt}} = 15\,\mathrm{nm}\ [21,\ 57] \tag{7.26}$$
$$\lambda_{\mathrm{sf}} = 14\,\mathrm{nm}\ [57] \tag{7.27}$$
$$J_{\mathrm{sd}} = 1.48884\,\mathrm{meV} \tag{7.28}$$
$$\theta_H = 0.0037\ [23] \tag{7.29}$$
$$\rho = 0.91\,\mu\Omega\,\mathrm{m}\ [23] \tag{7.30}$$
$$w_{\mathrm{Pt}} = 4\,\mathrm{mm}\ [23]\,. \tag{7.31}$$

The parameter J_{sd} out of Eq. (6.71) was adjusted in that way, that the resulting transverse spin Seebeck voltage for $T_0 = 300$ K is the same for the theory from Xiao *et al.* [23], from ourselves and from Schmidt *et al.* [57] as well. The resulting transverse spin Seebeck voltage out of Eq. (7.25) dependent on the overall average temperature T_0 is plotted in figure 51. If one compares the results with the transverse spin Seebeck voltage in figure 49, one finds, that the result in figure 51 is about one magnitude smaller. This belongs to the fact that the general temperature dependence of the spin pumping mechanism is different.

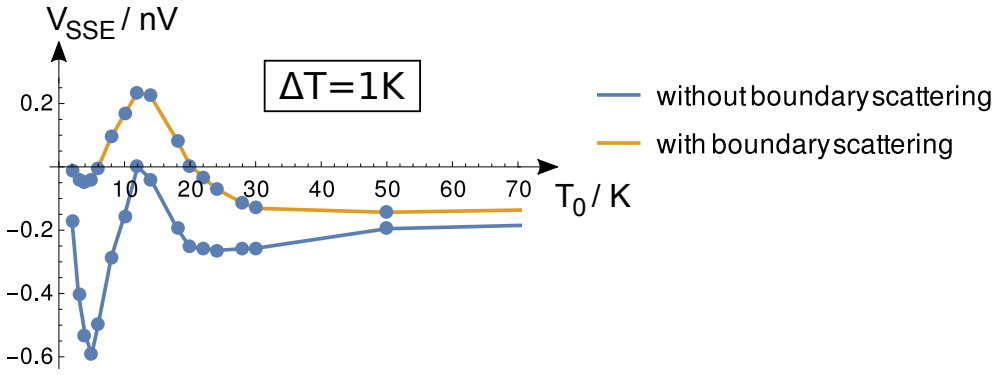

Figure 51: Here, the theory from ourselves and Schmidt *et al.* [57] is used. The transverse spin Seebeck voltage is plotted dependent on the overall average temperature T_0. The plot is separated between excluding and including boundary scattering.

Now, we want to separate the calculation by including and excluding phonon normal scattering processes by using the spin pumping theory from ourselves and Schmidt *et al.* [57]. The transverse spin Seebeck voltage by performing this separation can be found in figure 52. As already found in figure 50, there is nearly no difference between including and excluding normal scattering processes when boundary scattering is including. This is

the case, because the normal scattering relaxation length is length is always larger than the boundary scattering (cf. figure 15 for $T_0 = 3$ K). Only by excluding boundary scattering, the result becomes a little different. For higher overall average temperatures T_0 with and without boundary scattering, the normal scattering relaxation length becomes more important (cf. figure 14) and reduces the transverse spin Seebeck voltage significantly.

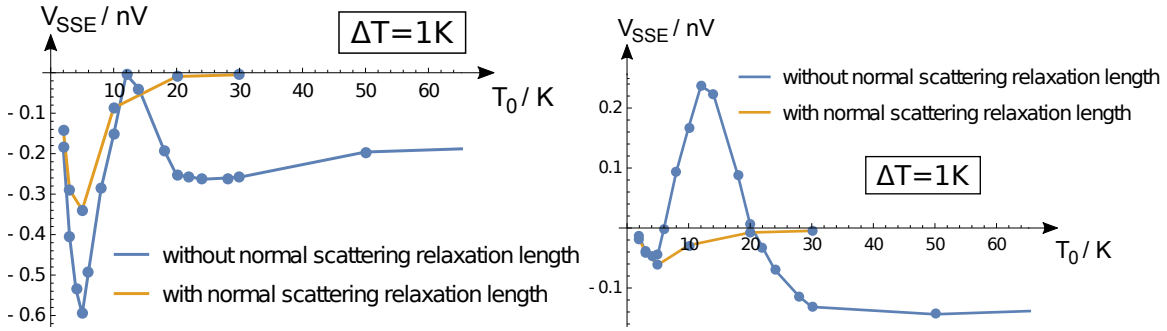

(a) Without boundary scattering

(b) With boundary scattering

Figure 52: Here, the transverse spin Seebeck voltage is separated by including and excluding phonon-phonon normal scattering events in the calculation for the relaxation length. In addition, the theory from ourselves and Schmidt *et al.* [57] is used.

Now, we want to compare the results with experimental measurements. As we found in our calculations, the transverse spin Seebeck voltage is at the order of tenth of nanovolts for room temperature ($T_0 = 300$ K). This result coincides with the measurements of Schmid *et al.* [33], Avery *et al.* [35] and Meier *et al.* [39]. They found, that the transverse spin Seebeck voltage is not larger than nanovolts at $T_0 = 300$ K. Our results do not coincide with Uchida *et al.* [21], they found a transverse spin Seebeck voltage at the order of microvolts. Our calculation of the magnon and phonon temperature coincides with the measurements of the magnon temperature by Agrawal *et al.* [31]. They found a small deviation between the magnon temperature and the phonon temperature, while they are only able to measure the temperature of large wave number magnons. For large wave number magnons, we found a similar result, while the deviation becomes larger for short wave number magnons. For smaller overall average temperatures T_0, the resulting transverse spin Seebeck voltage increases in general. Until now, there has been no experiment performed at this temperature regime.

7.1 Summary

In this chapter, we took the system of linear equations for the magnon-phonon coupled system out of chapters 3, 4 and 5 and solved it for the magnon temperature in the YIG-stripe. After that, we calculated the transverse spin Seebeck voltage by using the phonon and magnon temperature.

The setup of the transverse spin Seebeck effect consists of a GGG substrate, while the edge length are in the order of millimeters. On top of the thick GGG substrate, there is a thin YIG-stripe with the same surface area attached. Furthermore on top of the YIG-stripe, there are smaller stripes of platinum. The setup can be found in figures 4 and 9. Since the thickness of the GGG substrate is much thicker than of the YIG-film, the phonons are rarely influenced by the magnons. In contrast, the magnons are strongly influenced by the phonons. Thus, we calculated the phonon-temperature in chapter 3 by using the Boltzmann

equation and including phonon-phonon interaction only. We calculated the collision integral in the Boltzmann equation for the magnon-phonon interaction and took the phonon temperature as an input parameter in chapter 4. In chapter 5, we calculated the collision integral in the Boltzmann equation for the magnon-magnon interaction. In both interactions, we considered exchange magnons and dipolar magnons as well. We derived a system of linear equations for the wave number dependent magnon temperature including magnon-phonon and magnon-magnon interaction as well. The phonon temperature was used as an input parameter. Finally, we solved the system of equations for the wave number dependent magnon temperature in this chapter.

With these solutions, we calculated the wave number averaged phonon and magnon temperature. This, we did for different overall averaged temperatures T_0. For calculating the transverse spin Seebeck voltage, we needed the temperature difference between the wave number averaged phonon and magnon temperature. Here, we used the theory of Xiao *et al.* [23] to calculate the transverse spin Seebeck voltage. We separately plotted the results by including phonon boundary scattering on the one hand and excluded phonon boundary scattering on the other hand. Our theory out of chapter 6 and the theory of Schmidt *et al.* [57] are similar to each other. Additionally, we used them for calculating the transverse spin Seebeck voltage. The three methods were adjusted, so that they give the same transverse spin Seebeck voltage for room temperature. In both theories we found, that the transverse spin Seebeck voltage is larger for small temperatures than for room temperature. Furthermore, we included an optical phonon mode in our calculation with the theory of Xiao *et al.* [23]. For small overall averaged temperatures T_0, the change in the results is very small, when we include an optical phonon mode. But it becomes larger for larger overall temperatures T_0. Besides, normal phonon scattering decreases the transverse spin Seebeck voltage for large overall averaged temperatures T_0.

8 Conclusions and Outlook

In the present theoretical thesis, we analyzed the influence of quasiballistic phonons to the transverse spin Seebeck effect by making use of the Boltzmann equation.

In one of the experimental setup, where the spin Seebeck effect was observed, a thin, ferrimagnetic, and here insulating YIG-film ($Y_3Fe_5O_{12}$) was evaporated on an insulating and non-magnetic GGG substrate ($Gd_3Ga_5O_{12}$). Again on top, there are small platinum stripes with a voltmeter attached to measure the inverse spin Hall voltage (cf. figures 4 or 9). The sizes are at the order of millimeters, except for the thicknesses of YIG which is at the order of micrometers, and except for the thickness of platinum which is at the order of nanometers. In case of the transverse spin Seebeck effect, the applied temperature gradient is parallel to the surface of the YIG-film. In contrast for the longitudinal spin Seebeck effect, the applied temperature gradient is perpendicular to the surface of the YIG-film. The heat reservoirs, which generate the temperature gradient, are assumed to be ideal heat reservoirs.

In this thesis, we focused on the transverse spin Seebeck effect. The goal was it to calculate the transverse spin Seebeck voltage in the platinum stripes, which is measurable. This transverse spin Seebeck voltage is generated by a spin current which comes out of the YIG-stripe. Via the inverse spin Hall effect, the spin current is converted to a charge current. Xiao *et al.* [23], Schmidt *et al.* [57] and ourselves showed, that the spin current is generated, when there is a temperature difference between the magnons in the YIG-stripe and the electrons in the platinum. This effect is called spin pumping. The phonons are strongly coupled to the electrons in the platinum and thus have the same temperature. Hence, we needed to calculate the magnon temperature and the phonon temperature in the YIG-stripe. Since the thickness of the YIG-stripe is much smaller than the thickness of the GGG-substrate, the phonons are propagating most of the time in the GGG-substrate and are thus rarely influenced by the magnons. In contrast, the magnons are only propagating in the YIG-film and hence interact with the phonons all the time. Because of that, we first calculated the phonon temperature in the GGG-substrate by only including phonon-phonon interaction in chapter 3. After that, we prepared the calculation of the influence of the phonons onto the magnon temperature in chapters 4 and 5. In chapter 7, we presented the results.

The left heat reservoir is at temperature $T_0 + \Delta T$ at position $x = -L/2$, while the right heat reservoir is at temperature $T_0 - \Delta T$ at position $x = L/2$. Xiao *et al.* [23] as well as Sanders and Walton [24] performed calculations on the transverse spin Seebeck effect on the magnon temperature. Since measurements from Agrawal *et al.* [31] claimed their effect to be small for large wave number magnons, we performed a wave vector dependent calculation based on local interactions, where small wave number phonons, which are quasiballistic phonons, play an important role. Additionally, there are contradictory measurements [33, 34, 35], which motivated us to perform the calculation.

In the collision integral of the Boltzmann equation, the relaxation length occurs. Neelmani *et al.* [48] calculated the phonon relaxation length dependent on the wave vector, where Umklapp processes are included. Additionally, we performed an estimation for the Normal process scattering length. These we used and solved the Boltzmann equation for the wave number dependent phonon temperature by performing some approximations. For this calculation, the temperature deviation needs to be much smaller than the overall average temperature T_0. Additionally, we performed this calculation for different overall average temperatures T_0.

The resulting phonon temperature profiles are linear in space and crossing the overall

average temperature T_0 in the middle of the substrate at $x = 0$ (cf. figure 11). The values for $x = -L/2$ dependent on the wave number can be found in figures 18 and 19. The temperature of the phonons is connected to the density of the phonons via the Bose-Einstein distribution function. A large phonon temperature corresponds to a large density of phonons. Phonons with a large wave vector have a small relaxation length. Thus, they scatter very often and adopt the temperature from the proximity. So, there is nearly no temperature jump at the heat reservoir and the slope of the temperature profile is large. Phonons with a small wave vector have a large relaxation length. Hence, these phonons propagate nearly hitchless through the GGG-substrate and keep their density as well as the temperature from the heat bath, where they come from. Thus, right moving phonons with a small wave vector nearly keep the temperature $T_0 + \Delta T$ and left moving phonons with a small wave vector nearly keep the temperature $T_0 - \Delta T$, respectively. In average they have a temperature, which is close to T_0. Thus, their spatial temperature profile has a very small slope and a large temperature jump at the heat reservoir contacts. The slope for the small wave number phonons reaches zero slope for zero wave number. Additionally for a fixed wave number k, the slope of the phonon temperature decreases, when the overall average temperature decreases. When we include boundary scattering in our calculation, the slope does not decrease that much as without boundary scattering.

In chapter 4 and 5, we enlarged our calculation by including phonon-magnon- and magnon-magnon-interaction in the YIG-film. We considered exchange-magnons and dipolar magnons as well, set up a system of linear equations for the wave number dependent magnon temperature and performed some analytical transformations. The wave number dependent phonon temperature was used as an input parameter. Similarly as for the phonons, the resulting magnon temperature profiles are linear in space and crossing the overall average temperature T_0 in the middle of the substrate at $x = 0$. The slope of the magnon temperature profile is dependent on the wave number. The values for $x = -L/2$ can be found in figures 43 and 44. In the same way as for the phonons, we found a large slope of the temperature profile for the long wave number magnons. The slope for the small wave number magnons is small, but does not reach zero slope. Additionally for fixed wave number k, the slope of the magnon temperature decreases, when the overall average temperature decreases. When we include boundary scattering in our calculation, the slope does not decrease that much as without boundary scattering.

If we include optical phonons to our calculations (cf. figures 45 and 46), the result does not change significantly for small overall average temperature T_0. For higher T_0, the existence of the spin Seebeck effect is not affected.

Furthermore, we had a closer look on the spin pumping mechanism in chapter 6. We investigated this spin pumping mechanism between a ferromagnetic insulator and a normal metal (platinum) by making use of the Boltzmann equation. In our theory, we assumed that there is an intermediate region between the ferrimagnetic insulator and the normal metal, where magnons and valence electrons are able to interact via sd-interaction. We assumed the electrons in the normal metal to be strongly coupled to the phonons. We set up a system of differential equations to solve the magnon temperature in the intermediate layer as well as the electron chemical potential in the intermediate layer and the normal metal. At the end, the resulting spin current at $x = L$ is proportional to the temperature difference of the magnons in the ferrimagnetic insulator and the temperature of the electrons in the normal metal. This dependency on the temperature difference agrees with the theory of Xiao *et al.* [23] and with Schmidt *et al.* [57]. Our detailed expression coincides with the expression of Schmidt *et al.* [57].

After that, we calculated the transverse spin Seebeck voltage. This, we did by using the theory for the spin pumping mechanism of Xiao *et al.* [23]. Additionally, we calculate the transverse spin Seebeck voltage by using our results, which coincide with Schmidt *et al.* [57]. The results by using the spin pumping theory of Xiao *et al.* [23] are plotted in figures 49(a) and 49(b). There we found a larger transverse spin Seebeck voltage if one considers temperatures much lower than room temperature. The results are at the order of nanovolts, which should be measurable in experiments. Again, the result does not change significantly by including an optical phonon mode in the calculation for small overall average temperatures T_0. For higher T_0, the existence of the spin Seebeck effect is not affected. We also used the theory of Schmidt *et al.* [57] for the spin pumping mechanism. There, we found a different transverse spin Seebeck voltage at the order of tenth of nanovolts, which also should be measurable in experiments. The results are plotted in figure 51. Again, the voltage increases, when one considers temperatures much lower than room temperature. The two methods are adjusted, so that they give the same transverse spin Seebeck voltage at room temperature.

For further study of the transverse spin Seebeck effect, one may have a closer look on the phonon boundary scattering. We suspect, that the influence of the phonon boundary scattering decreases, if one enlarges the width B or the thickness D of the GGG substrate. This should cause an increase of the transverse spin Seebeck voltage, we suspect.

As discussed at the end of chapter 7, our results coincide with several experimental results for room temperature [31, 33, 35, 39]. Most of them stated, that the transverse spin Seebeck voltage is not larger than nanovolts at room temperature. This is in striking contrast to the first observation of the spin Seebeck effect by Uchida *et al.* [21]. Since there are no experiments made for lower temperature, it would be interesting to perform measurements at lower temperature. We claim that, the transverse spin Seebeck voltage should become larger for small temperatures.

It also would be interesting to perform a calculation on the longitudinal spin Seebeck effect. There, we can transfer our wave vector dependent calculation on the longitudinal spin Seebeck effect.

A Relaxation length for phonon Normal scattering

In this appendix, we will calculate the phonon relaxation length for normal scattering processes. We start from the elastic energy [41, p. 102]

$$V_3 = \frac{1}{6}\int_V d^3\vec{x} \sum_{lmnijk} A_{ijk}^{lmn} \frac{\partial u_l}{\partial r_i}\frac{\partial u_m}{\partial r_j}\frac{\partial u_n}{\partial r_k}\,. \tag{A.1}$$

We use a generalized version of the phonon operators from Eq. (4.6). This is

$$\vec{u}(\vec{r}) = \sum_{\vec{q},\lambda} e^{-i\vec{q}\vec{r}} u_{\vec{q}}\,\hat{e}_{\vec{q}} = \sum_{\vec{q},\lambda} \sqrt{\frac{\hbar}{2mN\omega_{q,\lambda}}}(b_{\vec{q},\lambda} + b^\dagger_{-\vec{q},\lambda})e^{-i\vec{q}\vec{r}}\,\hat{e}_{\vec{q},\lambda}\,. \tag{A.2}$$

After inserting them into the Eq. (A.1), we find

$$\begin{aligned}
V_3 =& \frac{1}{6}\sum_{lmnijk}\sum_{k_1k_2k_3\lambda_1\lambda_2\lambda_3} A_{ijk}^{lmn}\left(\frac{\hbar}{2Nm}\right)^{3/2}\frac{1}{\sqrt{\omega_{k_1,\lambda_1}\omega_{k_2,\lambda_2}\omega_{k_3,\lambda_3}}} e^l_{k_1,\lambda_1} e^m_{k_2,\lambda_2} e^n_{k_3,\lambda_3} \\
&\times k_{1,i}\,k_{2,j}\,k_{3,k}(b_{\vec{k}_1,\lambda_1} + b^\dagger_{-\vec{k}_1,\lambda_1})(b_{\vec{k}_2,\lambda_2} + b^\dagger_{-\vec{k}_2,\lambda_2})(b_{\vec{k}_3,\lambda_3} + b^\dagger_{-\vec{k}_3,\lambda_3})\int_V d^3\vec{x} e^{i(\vec{k}_1+\vec{k}_2+\vec{k}_3)\cdot\vec{r}} \\
=& \frac{1}{6}\left(\frac{\hbar}{2Nm}\right)^{3/2} N \sum_{kq\lambda_1\lambda_2\lambda_3} \frac{k\,q\,|\vec{k}+\vec{q}|}{\sqrt{\omega_{k,\lambda_1}\omega_{q,\lambda_2}\omega_{|\vec{k}+\vec{q}|,\lambda_3}}} \sum_{lmnijk} A_{ijk}^{lmn} e^l_{k,\lambda_1} e^m_{q,\lambda_2} e^n_{|\vec{k}+\vec{q}|,\lambda_3} \\
&\times \tilde{e}^i_{\vec{k}}\,\tilde{e}^j_{\vec{q}}\,\tilde{e}^k_{\vec{k}+\vec{q}}(b_{\vec{k},\lambda_1} + b^\dagger_{-\vec{k},\lambda_1})(b_{\vec{q},\lambda_2} + b^\dagger_{-\vec{q},\lambda_2})(b_{\vec{k}+\vec{q},\lambda_3} + b^\dagger_{-\vec{k}-\vec{q},\lambda_3})\,,
\end{aligned} \tag{A.3}$$

while $\tilde{e}^i_{\vec{k}}$ denotes the component i of the unit vector of vector $\vec{k}$. For simplicity, we assume

$$\tilde{A} = \frac{1}{6}\sum_{lmnijk} A_{ijk}^{lmn} e^l_{k,\lambda_1} e^m_{q,\lambda_2} e^n_{|\vec{k}+\vec{q}|,\lambda_3}\tilde{e}^i_{\vec{k}}\,\tilde{e}^j_{\vec{q}}\,\tilde{e}^k_{\vec{k}+\vec{q}}. \tag{A.4}$$

We take $\omega_{k,\lambda} = c_\lambda \cdot k$. The sound velocity for longitudinal phonons is $c_1 = 6.393 \cdot 10^3$ m/s. For transverse phonons, the sound velocities are $c_2 = 3.629 \cdot 10^3$ m/s and $c_3 = 3.429 \cdot 10^3$ m/s. Wet find

$$V_3 = \tilde{A}\frac{1}{\sqrt{N}}\left(\frac{\hbar}{2m}\right)^{3/2}\sum_{kq\lambda_1\lambda_2\lambda_3}\sqrt{\frac{k\,q\,|\vec{k}+\vec{q}|}{c_{\lambda_1}c_{\lambda_2}c_{\lambda_3}}}(b_{\vec{k},\lambda_1} + b^\dagger_{-\vec{k},\lambda_1})(b_{\vec{q},\lambda_2} + b^\dagger_{-\vec{q},\lambda_2})(b_{\vec{k}+\vec{q},\lambda_3} + b^\dagger_{-\vec{k}-\vec{q},\lambda_3})\,. \tag{A.5}$$

With this, we can write down the collision integral for the Boltzmann equation. For our calculation, the prefactor of the collision integral is irrelevant. Thus, we write

$$\begin{aligned}
\frac{dn_{k,\lambda}}{dt} = \bar{A}\sum_{q\lambda_2\lambda_3}\frac{k\,q\,|\vec{k}+\vec{q}|}{c_\lambda c_{\lambda_2} c_{\lambda_3}}\Big\{ & -n_{k,\lambda}n_{q,\lambda_2}(n_{|\vec{k}+\vec{q}|,\lambda_3}+1)\delta(\omega_{k,\lambda}+\omega_{q,\lambda_2}-\omega_{|\vec{k}+\vec{q}|,\lambda_3}) \\
& -n_{k,\lambda}(n_{-q,\lambda_2}+1)n_{-|\vec{k}+\vec{q}|,\lambda_3}\delta(\omega_{k,\lambda}-\omega_{q,\lambda_2}+\omega_{|\vec{k}+\vec{q}|,\lambda_3}) \\
& -n_{k,\lambda}(n_{-q,\lambda_2}+1)(n_{|\vec{k}+\vec{q}|,\lambda_3}+1)\delta(\omega_{k,\lambda}-\omega_{q,\lambda_2}-\omega_{|\vec{k}+\vec{q}|,\lambda_3}) \\
& +(n_{k,\lambda}+1)n_{-q,\lambda_2}n_{|\vec{k}+\vec{q}|,\lambda_3}\delta(\omega_{k,\lambda}-\omega_{q,\lambda_2}-\omega_{|\vec{k}+\vec{q}|,\lambda_3}) \\
& +(n_{k,\lambda}+1)n_{-q,\lambda_2}(n_{-|\vec{k}+\vec{q}|,\lambda_3}+1)\delta(\omega_{k,\lambda}-\omega_{q,\lambda_2}+\omega_{|\vec{k}+\vec{q}|,\lambda_3}) \\
& +(n_{k,\lambda}+1)(n_{q,\lambda_2}+1)n_{|\vec{k}+\vec{q}|,\lambda_3}\delta(\omega_{k,\lambda}+\omega_{q,\lambda_2}-\omega_{|\vec{k}+\vec{q}|,\lambda_3})\Big\}\,,
\end{aligned} \tag{A.6}$$

while $n_{k,\lambda}$ denotes the Bose-Einstein distribution for wave number k and acoustical phonon mode λ (cf. Eq. (2.4)). We rearrange this term

$$\begin{aligned}\frac{dn_{k,\lambda}}{dt} =&\bar{A}\sum_{q\lambda_2\lambda_3}\frac{k\,q\,|\vec{k}+\vec{q}|}{c_\lambda c_{\lambda_2} c_{\lambda_3}}\\ &\times\Big\{(n_{k,\lambda}n_{|\vec{k}+\vec{q}|,\lambda_3}+n_{q,\lambda_2}n_{|\vec{k}+\vec{q}|,\lambda_3}+n_{|\vec{k}+\vec{q}|,\lambda_3}-n_{k,\lambda}n_{q,\lambda_2})\delta(\omega_{k,\lambda}+\omega_{q,\lambda_2}-\omega_{|\vec{k}+\vec{q}|,\lambda_3})\\ &+(n_{k,\lambda}n_{-q,\lambda_2}+n_{-q,\lambda_2}n_{-|\vec{k}+\vec{q}|,\lambda_3}+n_{-q,\lambda_2}-n_{k,\lambda}n_{-|\vec{k}+\vec{q}|,\lambda_3})\delta(\omega_{k,\lambda}-\omega_{q,\lambda_2}+\omega_{|\vec{k}+\vec{q}|,\lambda_3})\\ &+(n_{-q,\lambda_2}n_{|\vec{k}+\vec{q}|,\lambda_3}-n_{k,\lambda}n_{-q,\lambda_2}-n_{k,\lambda}n_{|\vec{k}+\vec{q}|,\lambda_3}-n_{k,\lambda})\delta(\omega_{k,\lambda}-\omega_{q,\lambda_2}-\omega_{|\vec{k}+\vec{q}|,\lambda_3})\Big\}\,.\end{aligned} \tag{A.7}$$

To calculate the scattering rate for phonons with wave vector $\vec{k}$, we linearize the collision integral. We take $n_{k,\lambda}=n^0_{k,\lambda}+\delta n_{k,\lambda}$. In Eq. (3.40) as well as in figures 14 and 15, we only consider diagonal terms in the relaxation length. To be consistent, we only consider diagonal terms in this calculation. Because of that, we do not consider contributions from $\delta n_{q,\lambda}$ or $\delta n_{|\vec{k}+\vec{q}|,\lambda}$.

Then, we find

$$\begin{aligned}\frac{dn_{k,\lambda}}{dt} = \bar{A}\sum_{q\lambda_2\lambda_3}\frac{k\,q\,|\vec{k}+\vec{q}|}{c_\lambda c_{\lambda_2} c_{\lambda_3}}\delta n_{k,\lambda}\Big\{&(n_{|\vec{k}+\vec{q}|,\lambda_3}-n_{q,\lambda_2})\delta(\omega_{k,\lambda}+\omega_{q,\lambda_2}-\omega_{|\vec{k}+\vec{q}|,\lambda_3})\\ &+(n_{-q,\lambda_2}-n_{-|\vec{k}+\vec{q}|,\lambda_3})\delta(\omega_{k,\lambda}-\omega_{q,\lambda_2}+\omega_{|\vec{k}+\vec{q}|,\lambda_3})\\ &-(1+n_{-q,\lambda_2}+n_{|\vec{k}+\vec{q}|,\lambda_3})\delta(\omega_{k,\lambda}-\omega_{q,\lambda_2}-\omega_{|\vec{k}+\vec{q}|,\lambda_3})\Big\}\,.\end{aligned} \tag{A.8}$$

We perform a relaxation time approximation:

$$\frac{dn_{k,\lambda}}{dt}=\frac{\delta n_{k,\lambda}}{\tau_k}\,. \tag{A.9}$$

The resulting relaxation time reads

$$\begin{aligned}\frac{1}{\tau_k} = \bar{A}\sum_{q\lambda_2\lambda_3}\frac{k\,q\,|\vec{k}+\vec{q}|}{c_\lambda c_{\lambda_2} c_{\lambda_3}}\Big\{&(n_{|\vec{k}+\vec{q}|,\lambda_3}-n_{q,\lambda_2})\delta(\omega_{k,\lambda}+\omega_{q,\lambda_2}-\omega_{|\vec{k}+\vec{q}|,\lambda_3})\\ &+(n_{-q,\lambda_2}-n_{-|\vec{k}+\vec{q}|,\lambda_3})\delta(\omega_{k,\lambda}-\omega_{q,\lambda_2}+\omega_{|\vec{k}+\vec{q}|,\lambda_3})\\ &-(1+n_{-q,\lambda_2}+n_{|\vec{k}+\vec{q}|,\lambda_3})\delta(\omega_{k,\lambda}-\omega_{q,\lambda_2}-\omega_{|\vec{k}+\vec{q}|,\lambda_3})\Big\}\,.\end{aligned} \tag{A.10}$$

Normal processes

For evaluating the upper expressions, we need to transform the delta distributions to solve the angular integrations. We take $\omega_{k,\lambda}=c_\lambda\cdot k$. For the first and second delta distribution, we take

$$0=\omega_{q,\lambda_2}\pm\omega_{k,\lambda}-\omega_{|\vec{k}+\vec{q}|,\lambda_3}=c_{\lambda_2}q\pm c_\lambda k-c_{\lambda_3}\sqrt{k^2+q^2+2kq\cos(\vartheta)}\,, \tag{A.11}$$

while ϑ denotes the angle between $\vec{k}$ and $\vec{q}$. We transform this expression to

$$\cos(\vartheta)=\frac{(c_{\lambda_2}q\pm c_\lambda k)^2-c^2_{\lambda_3}(k^2+q^2)}{2kqc^2_{\lambda_3}}\,. \tag{A.12}$$

In case of the minus sign, we find in the transformation, that the following relation must be fulfilled

$$c_{\lambda_2} q > c_\lambda k \,. \tag{A.13}$$

In both cases, the following relationship must be fulfilled

$$|\cos(\vartheta)| \leq 1 \qquad\qquad |\vec{k}+\vec{q}| \leq p_\mathrm{F} \,. \tag{A.14}$$

In the same way, we transform the third delta distribution. We have

$$0 = \omega_{q,\lambda_2} - \omega_{k,\lambda} + \omega_{|\vec{k}+\vec{q}|,\lambda_3} = c_{\lambda_2} q - c_\lambda k + c_{\lambda_3}\sqrt{k^2+q^2+2kq\cos(\vartheta)} \tag{A.15}$$

$$\Leftrightarrow \quad \cos(\vartheta) = \frac{(c_\lambda k - c_{\lambda_2} q)^2 - c_{\lambda_3}^2 (k^2+q^2)}{2kqc_{\lambda_3}^2} \,. \tag{A.16}$$

In the transformation, we find the following relationships, which must be fulfilled

$$c_{\lambda_2} q < c_\lambda k \qquad\qquad |\cos(\vartheta)| \leq 1 \qquad\qquad |\vec{k}+\vec{q}| \leq p_\mathrm{F} \,. \tag{A.17}$$

Umklapp processes

Umklapp processes denote processes, where $|\vec{k}+\vec{q}| > p_\mathrm{F}$. For those processes, the delta-distribution must be evaluated differently. For the first and second delta distribution, we find

$$0 = \omega_{q,\lambda_2} \pm \omega_{k,\lambda} - \omega_{|\vec{k}+\vec{q}|,\lambda_3} = c_{\lambda_2} q \pm c_\lambda k - c_{\lambda_3}\left(2p_\mathrm{F} - \sqrt{k^2+q^2+2kq\cos(\vartheta)}\right) \,. \tag{A.18}$$

This expression we transform to

$$\cos(\vartheta) = \frac{(c_{\lambda_3} 2p_\mathrm{F} - c_{\lambda_2} q \mp c_\lambda k)^2 - c_{\lambda_3}^2 (k^2+q^2)}{2kqc_{\lambda_3}^2} \,. \tag{A.19}$$

In the transformation, we find the following relationships, which must be fulfilled

$$q \leq 2p_\mathrm{F}\frac{c_{\lambda_3}}{c_{\lambda_2}} \mp \frac{c_\lambda}{c_{\lambda_2}} k \qquad\qquad |\cos(\vartheta)| \leq 1 \qquad\qquad |\vec{k}+\vec{q}| > p_\mathrm{F} \,. \tag{A.20}$$

For the third delta distribution of the Umklapp processes, we find

$$0 = \omega_{q,\lambda_2} - \omega_{k,\lambda} + \omega_{|\vec{k}+\vec{q}|,\lambda_3} = c_{\lambda_2} q - c_\lambda k + c_{\lambda_3}\left(2p_\mathrm{F} - \sqrt{k^2+q^2+2kq\cos(\vartheta)}\right) \tag{A.21}$$

$$\Leftrightarrow \quad \cos(\vartheta) = \frac{(c_{\lambda_2} q - c_\lambda k + c_{\lambda_3} 2p_\mathrm{F})^2 - c_{\lambda_3}^2 (k^2+q^2)}{2kqc_{\lambda_3}^2} \,. \tag{A.22}$$

In the transformation, we find the following relationships, which must be fulfilled

$$q \geq \frac{c_\lambda}{c_{\lambda_2}} k - 2p_\mathrm{F}\frac{c_{\lambda_3}}{c_{\lambda_2}} \qquad\qquad |\cos(\vartheta)| \leq 1 \qquad\qquad |\vec{k}+\vec{q}| > p_\mathrm{F} \,. \tag{A.23}$$

With these expressions for $\cos(\vartheta)$, we can solve the delta distribution in Eq. (A.10). The $\vec{q}$-integration will be transformed into spherical coordinates. The angular integration is canceled by the delta distribution and we end up with a single integral over the absolute value q. It is important to respect the relations, which are derived above for the Normal scattering and for the Umklapp scattering as well. At the end, we are interested in the quotient between Normal scattering and Umklapp scattering relaxation time or relaxation length. Thus, we do not need the value for $\bar{A}$. The Umklapp scattering relaxation length, is obtained from Neelmani *et al.* [48]. Therewith, we calculate the Normal scattering relaxation length. The results are used in figures 14 and 15.

B Hamilton operators for magnon-phonon-interaction

In this appendix, we will calculate the Hamilton operator for the magnon-phonon coupling in detail. First, we will consider dipole dipole magnons in three particle interactions in section B.1 and after that exchange magnons in four particle interaction in section B.2. The prefactor of the Hamilton operator will be used for writing down the collision integral in the Boltzmann equation. In section 4.1 we already presented the short calculation.

Here, we consider a thin film out of a thin magnetic insulator (YIG, $Y_3Fe_5O_{12}$) on top of the GGG substrate ($Gd_3Ga_5O_{12}$). Since the thickness of the GGG substrate is much thicker than the thickness of the YIG film, the phonons are rarely influenced by the magnons. Thus, the phonon temperature profile out of chapter 3 will be used as an input parameter. In chapter 4, we use the Hamilton operator to calculate the collision integral in the Boltzmann equation. With that, the spatial temperature profile of the magnons will be calculated in chapter 5.

B.1 Dipole-dipole interaction

We start with the magnetoelastic energy for the magnon-phonon interaction with dipolar magnons (cf. Eq. (4.3)) [43, p. 315]

$$U_{\text{mel}} = \frac{B_1}{M_0^2} \sum_{p=1}^{3} M_p^2 e_{pp} + \frac{B_2}{M_0^2} \sum_{\substack{p,q=1 \\ q \neq p}}^{3} M_p M_q e_{pq} \,, \tag{B.1}$$

while M_p denotes the local magnetization in spatial direction p and e_{pq} denotes the symmetric strain tensor. We follow the calculation of Kaganov *et al.* [51]. In our calculation, the YIG lattice structure will be modeled by a 3-dimensional cubic lattice with identical unit cell volume (lattice constant $a = 1.25$ nm [52, 53]). The spin inside one single unit cell will be modeled as one single spin with strength $S = 14.2$. In the following, we use the transformations

$$M_i = -\gamma \hbar S_i \tag{B.2}$$

$$e_{pq} = \frac{1}{2} \left(\frac{\partial u_p}{\partial x_q} + \frac{\partial u_q}{\partial x_p} \right) \tag{B.3}$$

$$\vec{u}(\vec{r}) = \sum_{\vec{p}} e^{-i\vec{p}\vec{r}} u_{\vec{p}} \, \hat{e}_{\vec{p}} = \sum_{\vec{p}} \sqrt{\frac{\hbar}{2mN\omega_p}} (b_{\vec{p}} + b^{\dagger}_{-\vec{p}}) e^{-i\vec{p}\vec{r}} \, \hat{e}_{\vec{p}} \,, \tag{B.4}$$

where $\vec{S}$ denotes the net spin and its orientation of all atoms in one YIG unit cell and S denotes its absolute value. m denotes the mass of one unit cell and N denotes the number of unit cells in the whole solid. $\vec{u}$ denotes the spatial dependent displacement vector of the lattice atom. The operators $b_{\vec{p},i}$ and $b^{\dagger}_{\vec{p},i}$ denote the annihilation and the creation of one phonon with wave vector $\vec{p}$ and mode i, respectively. The gyromagnetic ratio is denoted by γ. We insert (B.2) into the magnetoelastic energy and find

$$U_{\text{mel}} = b_1 \sum_{p=1}^{3} S_p^2 e_{pp} + b_2 \sum_{p,q=1, q \neq p}^{3} S_p S_q e_{pq} \,, \tag{B.5}$$

with the abbreviations

$$b_1 = \frac{\gamma^2 \hbar^2 B_1}{M_0^2} = \frac{B_1}{S^2} \qquad b_2 = \frac{\gamma^2 \hbar^2 B_2}{M_0^2} = \frac{B_2}{S^2} \,. \tag{B.6}$$

The spin operators S_x and S_y can be rewritten in the following way

$$S^+ = S_x + iS_y \qquad S^- = S_x - iS_y\,, \tag{B.7}$$

Including these identities, we rewrite the energy

$$\begin{aligned} U_{\text{mel}} =& b_1(S_x^2 e_{xx} + S_y^2 e_{yy} + S_z^2 e_{zz}) + b_2 e_{xy}(S_x S_y + S_y S_x) + b_2 e_{xz}(S_x S_z + S_z S_x) \\ &+ b_2 e_{yz}(S_y S_z + S_z S_y) \\ =& \frac{b_1}{4}(e_{xx} - e_{yy})(S^+S^+ + S^-S^-) + \frac{b_1}{4}(e_{xx} + e_{yy})(S^+S^- + S^-S^+) \\ &+ b_1 e_{zz} S_z S_z + \frac{b_2}{2i} e_{xy}(S^+S^+ - S^-S^-) + \frac{b_2}{2} e_{xz}(S^+S_z + S_zS^+ + S^-S_z + S_zS^-) \\ &+ \frac{b_2}{2i} e_{yz}(S^+S_z + S_zS^+ - S^-S_z - S_zS^-)\,. \end{aligned} \tag{B.8}$$

On the other hand, we replace the spin operators with creation and annihilation operators. This we do by using the Holstein-Primakoff transformation [54, p. 78]. To lowest order approximation, we find

$$S^+ = \sqrt{2S}\, a \qquad S^- = \sqrt{2S}\, a^\dagger \qquad S_z = S - a^\dagger a\,, \tag{B.9}$$

which is still dependent on position $\vec{r}$. The operators a and $a^\dagger$ denote the annihilation and the creation of one magnon at position $\vec{r}$, respectively. Thus, we need to Fourier transform

$$a = \frac{1}{\sqrt{N}} \sum_{\vec{k}} a_{\vec{k}} e^{-i\vec{k}\vec{r}} \qquad a^\dagger = \frac{1}{\sqrt{N}} \sum_{\vec{k}'} a^\dagger_{\vec{k}'} e^{i\vec{k}'\vec{r}}\,. \tag{B.10}$$

The operators $a_{\vec{k}}$ and $a^\dagger_{\vec{k}}$ denote the annihilation and the creation of one magnon with wave vector $\vec{k}$, respectively. The symmetric strain tensor needs to be rewritten in terms of phonon operators

$$e_{ij} = \frac{1}{2}\left(-i \sum_{\vec{p}} p_j \sqrt{\frac{\hbar}{2mN\omega_p}} (b_{\vec{p}} + b^\dagger_{-\vec{p}})\, e_{\vec{p},i}\, e^{-i\vec{p}\vec{r}} - i \sum_{\vec{p}} p_i \sqrt{\frac{\hbar}{2mN\omega_p}} (b_{\vec{p}} + b^\dagger_{-\vec{p}})\, e_{\vec{p},j}\, e^{-i\vec{p}\vec{r}} \right). \tag{B.11}$$

The Hamilton operator is the summation of the energy in the whole solid with volume V. One finds

$$H = \int_V d^3\vec{x}\, U_{\text{mel}}\,. \tag{B.12}$$

It is

$$\begin{aligned}
H =& \frac{1}{N}\int_V d^3\vec{x}\sum_{\vec{k}\vec{k}'\vec{p}}\frac{b_1 S}{2i}\sqrt{\frac{\hbar}{2mN\omega_p}}(a_{\vec{k}}a_{\vec{k}'}e^{-i\vec{k}\vec{r}-i\vec{k}'\vec{r}-i\vec{p}\vec{r}} + a^\dagger_{\vec{k}}a^\dagger_{\vec{k}'}e^{i\vec{k}\vec{r}+i\vec{k}'\vec{r}-i\vec{p}\vec{r}}) \\
&\times (p_x(b_{\vec{p}} + b^\dagger_{-\vec{p}})\, e_{\vec{p},x} \; - p_y(b_{\vec{p}} + b^\dagger_{-\vec{p}})\, e_{\vec{p},y}) \\
&+ \frac{1}{N}\int_V d^3\vec{x}\sum_{\vec{k}\vec{k}'\vec{p}}\frac{b_1 S}{2i}\sqrt{\frac{\hbar}{2mN\omega_p}}(a_{\vec{k}}a^\dagger_{\vec{k}'}e^{-i\vec{k}\vec{r}+i\vec{k}'\vec{r}-i\vec{p}\vec{r}} + a^\dagger_{\vec{k}}a_{\vec{k}'}e^{i\vec{k}\vec{r}-i\vec{k}'\vec{r}-i\vec{p}\vec{r}}) \\
&\times (p_x(b_{\vec{p}} + b^\dagger_{-\vec{p}})\, e_{\vec{p},x} + p_y(b_{\vec{p}} + b^\dagger_{-\vec{p}})\, e_{\vec{p},y}) \\
&+ \frac{1}{N}\int_V d^3\vec{x}\sum_{\vec{k}\vec{k}'\vec{p}}\frac{b_1 S}{i}\sqrt{\frac{\hbar}{2mN\omega_p}}(Se^{-i\vec{p}\vec{r}} - 2a^\dagger_{\vec{k}}a_{\vec{k}'}e^{i\vec{k}\vec{r}-i\vec{k}'\vec{r}-i\vec{p}\vec{r}})(p_z(b_{\vec{p}} + b^\dagger_{-\vec{p}})\, e_{\vec{p},z}) \\
&- \frac{1}{N}\int_V d^3\vec{x}\sum_{\vec{k}\vec{k}'\vec{p}}\frac{b_2 S}{2}\sqrt{\frac{\hbar}{2mN\omega_p}}(a_{\vec{k}}a_{\vec{k}'}e^{-i\vec{k}\vec{r}-i\vec{k}'\vec{r}-i\vec{p}\vec{r}} - a^\dagger_{\vec{k}}a^\dagger_{\vec{k}'}e^{i\vec{k}\vec{r}+i\vec{k}'\vec{r}-i\vec{p}\vec{r}}) \\
&\times (p_y(b_{\vec{p}} + b^\dagger_{-\vec{p}})\, e_{\vec{p},x} + p_x(b_{\vec{p}} + b^\dagger_{-\vec{p}})\, e_{\vec{p},y}) \\
&+ \frac{1}{\sqrt{N}}\int_V d^3\vec{x}\sum_{\vec{k}\vec{p}}\frac{b_2\sqrt{2S}S}{2i}\sqrt{\frac{\hbar}{2mN\omega_p}}(a_{\vec{k}}e^{-i\vec{k}\vec{r}-i\vec{p}\vec{r}} + a^\dagger_{\vec{k}}e^{i\vec{k}\vec{r}-i\vec{p}\vec{r}}) \\
&\times (p_z(b_{\vec{p}} + b^\dagger_{-\vec{p}})\, e_{\vec{p},x} + p_x(b_{\vec{p}} + b^\dagger_{-\vec{p}})\, e_{\vec{p},z}) \\
&- \frac{1}{\sqrt{N}}\int_V d^3\vec{x}\sum_{\vec{k}\vec{p}}\frac{b_2\sqrt{2S}S}{2}\sqrt{\frac{\hbar}{2mN\omega_p}}(a_{\vec{k}}e^{-i\vec{k}\vec{r}-i\vec{p}\vec{r}} - a^\dagger_{\vec{k}}e^{i\vec{k}\vec{r}-i\vec{p}\vec{r}}) \\
&\times (p_z(b_{\vec{p}} + b^\dagger_{-\vec{p}})\, e_{\vec{p},y} + p_y(b_{\vec{p}} + b^\dagger_{-\vec{p}})\, e_{\vec{p},z})\,. \qquad \text{(B.13)}
\end{aligned}$$

The integral reduces the exponential functions to delta distributions by

$$\int_V d^3\vec{x}e^{-i\vec{Q}\vec{r}} = (2\pi)^3\delta(\vec{Q}) \qquad \text{(B.14)}$$

$$\sum_{\vec{k}'} = \frac{3a^3N}{4\pi^4}\int d^3\vec{k}'\,. \qquad \text{(B.15)}$$

This cancels one summation. One finds

$$\begin{aligned}
H =& H_{\text{const}} + \frac{6a^3}{\pi} \sum_{\vec{k}\vec{p}} \frac{b_1 S}{2i} \sqrt{\frac{\hbar}{2mN\omega_p}} (a_{\vec{k}} a_{-\vec{k}-\vec{p}} + a^\dagger_{\vec{k}} a^\dagger_{-\vec{k}+\vec{p}}) (p_x (b_{\vec{p}} + b^\dagger_{-\vec{p}})\, e_{\vec{p},x} - p_y (b_{\vec{p}} + b^\dagger_{-\vec{p}})\, e_{\vec{p},y}) \\
&+ \frac{6a^3}{\pi} \sum_{\vec{k}\vec{p}} \frac{b_1 S}{2i} \sqrt{\frac{\hbar}{2mN\omega_p}} (a_{\vec{k}} a^\dagger_{\vec{k}+\vec{p}} + a^\dagger_{\vec{k}} a_{\vec{k}-\vec{p}}) (p_x (b_{\vec{p}} + b^\dagger_{-\vec{p}})\, e_{\vec{p},x} + p_y (b_{\vec{p}} + b^\dagger_{-\vec{p}})\, e_{\vec{p},y}) \\
&+ \frac{6a^3}{\pi} \sum_{\vec{k}\vec{p}} \frac{b_1 S}{i} \sqrt{\frac{\hbar}{2mN\omega_p}} (-2 a^\dagger_{\vec{k}} a_{\vec{k}-\vec{p}}) (p_z (b_{\vec{p}} + b^\dagger_{-\vec{p}})\, e_{\vec{p},z}) \\
&- \frac{6a^3}{\pi} \sum_{\vec{k}\vec{p}} \frac{b_2 S}{2} \sqrt{\frac{\hbar}{2mN\omega_p}} (a_{\vec{k}} a_{-\vec{k}-\vec{p}} - a^\dagger_{\vec{k}} a^\dagger_{-\vec{k}+\vec{p}}) (p_y (b_{\vec{p}} + b^\dagger_{-\vec{p}})\, e_{\vec{p},x} + p_x (b_{\vec{p}} + b^\dagger_{-\vec{p}})\, e_{\vec{p},y}) \\
&+ \frac{6a^3}{\pi} \sqrt{N} \sum_{\vec{p}} \frac{b_2 \sqrt{2S} S}{2i} \sqrt{\frac{\hbar}{2mN\omega_p}} (a_{-\vec{p}} + a^\dagger_{\vec{p}}) (p_z (b_{\vec{p}} + b^\dagger_{-\vec{p}})\, e_{\vec{p},x} + p_x (b_{\vec{p}} + b^\dagger_{-\vec{p}})\, e_{\vec{p},z}) \\
&- \frac{6a^3}{\pi} \sqrt{N} \sum_{\vec{p}} \frac{b_2 \sqrt{2S} S}{2} \sqrt{\frac{\hbar}{2mN\omega_p}} (a_{-\vec{p}} - a^\dagger_{\vec{p}}) (p_z (b_{\vec{p}} + b^\dagger_{-\vec{p}})\, e_{\vec{p},y} + p_y (b_{\vec{p}} + b^\dagger_{-\vec{p}})\, e_{\vec{p},z})\,.
\end{aligned} \tag{B.16}$$

We rearrange the terms by setting $b_2 = b_1$ for an isotropic ferromagnet [43, p. 315]

$$\begin{aligned}
H =& H_{\text{const}} + \frac{6a^3}{\pi} \sum_{\vec{k}\vec{p}} \frac{b_1 S}{2i} \sqrt{\frac{\hbar}{2mN\omega_p}} (a_{\vec{k}} a_{-\vec{k}-\vec{p}} + a^\dagger_{\vec{k}} a^\dagger_{-\vec{k}+\vec{p}}) (p_x (b_{\vec{p}} + b^\dagger_{-\vec{p}})\, e_{\vec{p},x} - p_y (b_{\vec{p}} + b^\dagger_{-\vec{p}})\, e_{\vec{p},y}) \\
&- \frac{6a^3}{\pi} \sum_{\vec{k}\vec{p}} \frac{b_1 S}{2} \sqrt{\frac{\hbar}{2mN\omega_p}} (a_{\vec{k}} a_{-\vec{k}-\vec{p}} - a^\dagger_{\vec{k}} a^\dagger_{-\vec{k}+\vec{p}}) (p_y (b_{\vec{p}} + b^\dagger_{-\vec{p}})\, e_{\vec{p},x} + p_x (b_{\vec{p}} + b^\dagger_{-\vec{p}})\, e_{\vec{p},y}) \\
&+ \frac{6a^3}{\pi} \sum_{\vec{k}\vec{p}} \frac{b_1 S}{2i} \sqrt{\frac{\hbar}{2mN\omega_p}} \Big[(a_{\vec{k}} a^\dagger_{\vec{k}+\vec{p}} + a^\dagger_{\vec{k}} a_{\vec{k}-\vec{p}}) (p_x (b_{\vec{p}} + b^\dagger_{-\vec{p}})\, e_{\vec{p},x} + p_y (b_{\vec{p}} + b^\dagger_{-\vec{p}})\, e_{\vec{p},y}) \\
&\qquad - (4 a^\dagger_{\vec{k}} a_{\vec{k}-\vec{p}}) (p_z (b_{\vec{p}} + b^\dagger_{-\vec{p}})\, e_{\vec{p},z}) \Big] \\
&+ \frac{6a^3}{\pi} \sqrt{N} \sum_{\vec{p}} \frac{b_1 \sqrt{2S} S}{2i} \sqrt{\frac{\hbar}{2mN\omega_p}} a_{-\vec{p}} (p_z (b_{\vec{p}} + b^\dagger_{-\vec{p}})\, e_{\vec{p},x} + p_x (b_{\vec{p}} + b^\dagger_{-\vec{p}})\, e_{\vec{p},z} \\
&\qquad - i p_z (b_{\vec{p}} + b^\dagger_{-\vec{p}})\, e_{\vec{p},y} - i p_y (b_{\vec{p}} + b^\dagger_{-\vec{p}})\, e_{\vec{p},z}) \\
&+ \frac{6a^3}{\pi} \sqrt{N} \sum_{\vec{p}} \frac{b_1 \sqrt{2S} S}{2i} \sqrt{\frac{\hbar}{2mN\omega_p}} a^\dagger_{\vec{p}} (p_z (b_{\vec{p}} + b^\dagger_{-\vec{p}})\, e_{\vec{p},x} + p_x (b_{\vec{p}} + b^\dagger_{-\vec{p}})\, e_{\vec{p},z} \\
&\qquad + i p_z (b_{\vec{p}} + b^\dagger_{-\vec{p}})\, e_{\vec{p},y} + i p_y (b_{\vec{p}} + b^\dagger_{-\vec{p}})\, e_{\vec{p},z})\,.
\end{aligned} \tag{B.17}$$

Energy conservation needs to be fulfilled. Terms with only annihilation or creation operators

vanish. Thus, we find

$$\begin{aligned}
H =& H_{\text{const}} + \frac{6a^3}{\pi}\sqrt{N}\sum_{\vec{p}} \frac{b_1\sqrt{2S}S}{2i}\sqrt{\frac{\hbar}{2mN\omega_p}}(p_z(a^\dagger_{\vec{p}}(b_{\vec{p}}\,e_{\vec{p},x} - ib_{\vec{p}}\,e_{\vec{p},y}) + a_{-\vec{p}}(b^\dagger_{-\vec{p}}\,e_{\vec{p},x} + ib^\dagger_{-\vec{p}}\,e_{\vec{p},y})) \\
&\quad + (p_x + ip_y)a^\dagger_{\vec{p}}b_{\vec{p}}\,e_{\vec{p},z} + (p_x - ip_y)a_{-\vec{p}}b^\dagger_{-\vec{p}}\,e_{\vec{p},z}) \\
&+ \frac{6a^3}{\pi}\sum_{\vec{k}\vec{p}} \frac{b_1 S}{2i}\sqrt{\frac{\hbar}{2mN\omega_p}}(a_{\vec{k}}a_{-\vec{k}-\vec{p}}(p_x - ip_y)(b^\dagger_{-\vec{p}}\,e_{\vec{p},x} - ib^\dagger_{-\vec{p}}\,e_{\vec{p},y}) \\
&\quad + a^\dagger_{\vec{k}}a^\dagger_{-\vec{k}+\vec{p}}(p_x + ip_y)(b_{\vec{p}}\,e_{\vec{p},x} + ib_{\vec{p}}\,e_{\vec{p},y})) \\
&+ \frac{6a^3}{\pi}\sum_{\vec{k}\vec{p}} \frac{b_1 S}{2i}\sqrt{\frac{\hbar}{2mN\omega_p}}a_{\vec{k}}a^\dagger_{\vec{k}+\vec{p}}((p_x + ip_y)(b_{\vec{p}}\,e_{\vec{p},x} + b^\dagger_{-\vec{p}}\,e_{\vec{p},x} - ib_{\vec{p}}\,e_{\vec{p},y} - ib^\dagger_{-\vec{p}}\,e_{\vec{p},y}) \\
&\quad + (p_x - ip_y)(b_{\vec{p}}\,e_{\vec{p},x} + b^\dagger_{-\vec{p}}\,e_{\vec{p},x} + ib_{\vec{p}}\,e_{\vec{p},y} + ib^\dagger_{-\vec{p}}\,e_{\vec{p},y})) \\
&- \frac{6a^3}{\pi}\sum_{\vec{k}\vec{p}} \frac{b_1 S}{2i}\sqrt{\frac{\hbar}{2mN\omega_p}}a_{\vec{k}}a^\dagger_{\vec{k}+\vec{p}}(4p_z(b_{\vec{p}} + b^\dagger_{-\vec{p}})\,e_{\vec{p},z})\,.
\end{aligned} \tag{B.18}$$

Now, we need to identify the prefactors of the different Hamilton operators. The first term contains the transformation from one magnon into one phonon and vice versa. Energy and momentum conservation need to be fulfilled. This is only the case, when the dispersion relation for magnons and phonons intersect (cf. figure 39). Since this is true only for two points of the dispersion relation, the first term will be neglected in the upper expression for the Hamilton operator. The second term contains the transformation of one phonon into two magnons and vice versa. Furthermore, the scattering from one magnon into one magnon and one phonon and vice versa is contained in the third as well as in the fourth term. The prefactor to the second term reads

$$V_{2\text{M}} = \frac{6a^3}{\pi}\frac{\sqrt{2}b_1 S}{2i}\sqrt{\frac{\hbar}{2mN\omega_p}}(p_x - ip_y) = \frac{6a^3}{\pi}\frac{B_1}{\sqrt{2}iS}\sqrt{\frac{\hbar}{2mN\omega_p}}(p_x - ip_y)\,. \tag{B.19}$$

Thus

$$|V_{2\text{M}}|^2 = \frac{36a^6}{\pi^2}\frac{B_1^2}{2S^2}\frac{\hbar}{2mN\omega_p}(p_x^2 + p_y^2) = \frac{36a^6}{\pi^2}\frac{\hbar B_1^2}{4mNc_{\text{Ph}}S^2}p\sin^2(\vartheta)\,. \tag{B.20}$$

The scattering amplitude, which is the prefactor of the third and fourth term, reads

$$V_{\text{Sc}} = \frac{6a^3}{\pi}\frac{b_1 S}{2i}\sqrt{\frac{\hbar}{2mN\omega_p}}((p_x + ip_y)\sqrt{2} + (p_x - ip_y)\sqrt{2} - 4p_z)\,. \tag{B.21}$$

We perform an approximation, where we average over the angles ϑ and φ of the orientation of the magnon magnetic moment. Thus

$$|V_{\text{Sc}}|^2 = \frac{36a^6}{\pi^2}\frac{\hbar B_1^2}{4S^2mN\omega_p}\frac{1}{2}(8p^2\sin^2(\vartheta)\cos^2(\varphi) - 16\sqrt{2}\sin(\vartheta)\cos(\varphi)\cos(\vartheta) + 16\cos^2(\vartheta)) \tag{B.22}$$

$$|V_{\text{Sc,av}}|^2 = \frac{1}{4\pi}\int_0^{2\pi}\int_0^{\pi}\sin(\vartheta)\,|V_{\text{Sc}}|^2 d\vartheta d\varphi = \frac{36a^6}{\pi^2}\frac{\hbar B_1^2}{4S^2mNc_{\text{Ph}}}\frac{1}{2}p\left(\frac{8}{3} + 0 + \frac{16}{3}\right)\,, \tag{B.23}$$

where ϑ denotes the angle between the magnetization direction and the vector $\vec{p}$. It is $m = \rho \cdot V_{\mathrm{EZ}} = \rho \cdot a^3$ and $B_{\mathrm{ges}} = B_1 \cdot a^3$. To calculate the prefactor, we take

$$B_1 = 3.48 \cdot 10^6\,\mathrm{erg/cm^3} = 0.348\,\mathrm{J/cm^3}\,[43, p.\ 315] \tag{B.24}$$
$$\rho = 5170\,\mathrm{kg/m^3}\,[52,\ 55] \tag{B.25}$$
$$a = 1.2376\,\mathrm{nm}\,[52,\ 53] \tag{B.26}$$
$$c_{\mathrm{Ph}} = 3843\,\mathrm{m/s}\,[55] \tag{B.27}$$
$$S = 14.2\,[53]\,. \tag{B.28}$$

At the end, we find

$$|V_{\mathrm{2M}}|^2 = V_{\mathrm{mel}}^2 p \sin^2(\vartheta) \tag{B.29}$$
$$|V_{\mathrm{Sc}}|^2 = V_{\mathrm{mel}}^2 \frac{1}{2}(8p^2 \sin^2(\vartheta)\cos^2(\varphi) - 16\sqrt{2}\sin(\vartheta)\cos(\varphi)\cos(\vartheta) + 16\cos^2(\vartheta))\,, \tag{B.30}$$

with

$$V_{\mathrm{mel}}^2 = \frac{36a^6}{\pi^2}\frac{\hbar B_1^2}{4mNc_{\mathrm{Ph}}S^2} = \frac{1}{N}\cdot 4.95482 \cdot 10^{-8}\mathrm{GHz^2cm}\,. \tag{B.31}$$

The average reads

$$|V_{\mathrm{2M,av}}|^2 = \frac{1}{4\pi}\int_0^{2\pi}\int_0^{\pi}\sin(\vartheta)\,|V_{\mathrm{2M}}|^2 d\vartheta d\varphi = \frac{2}{3}\cdot\frac{p}{N}\cdot 4.95482\cdot 10^{-8}\,\mathrm{GHz^2\,cm} \tag{B.32}$$
$$|V_{\mathrm{Sc,av}}|^2 = \frac{1}{4\pi}\int_0^{2\pi}\int_0^{\pi}\sin(\vartheta)\,|V_{\mathrm{Sc}}|^2 d\vartheta d\varphi = 4\cdot\frac{p}{N}\cdot 4.95482\cdot 10^{-8}\,\mathrm{GHz^2\,cm}\,. \tag{B.33}$$

B.2 Exchange interaction

Now, we have a look at the coupling of phonons with exchange magnons. The magnetoelastic energy reads [43, p. 315] [51]

$$U_{\mathrm{mel}} = \frac{A_1}{M_0^2}\sum_{p,q,l=1,l\neq q}^{3}\frac{\partial M_p}{\partial x_q}\frac{\partial M_p}{\partial x_l}e_{ql} + \frac{A_2}{M_0^2}\sum_{p,q=1}^{3}\left(\frac{\partial M_p}{\partial x_q}\right)^2 e_{qq} + \frac{A_3}{M_0^2}\sum_{p,q,l=1,l\neq q}^{3}\left(\frac{\partial M_p}{\partial x_q}\right)^2 e_{ll}\,, \tag{B.34}$$

where M_p denotes the local magnetization in spatial direction p and e_{pq} denotes the symmetric strain tensor. Again, we perform the following transformations

$$M_i = -\gamma\hbar S_i \tag{B.35}$$
$$e_{pq} = \frac{1}{2}\left(\frac{\partial u_p}{\partial x_q} + \frac{\partial u_q}{\partial x_p}\right) \tag{B.36}$$
$$\vec{u}(\vec{r}) = \sum_{\vec{p}} e^{-i\vec{p}\vec{r}}u_{\vec{p}}\,\hat{e}_{\vec{p}} = \sum_{\vec{p}}\sqrt{\frac{\hbar}{2mN\omega_p}}(b_{\vec{p}} + b^{\dagger}_{-\vec{p}})e^{-i\vec{p}\vec{r}}\,\hat{e}_{\vec{p}}\,, \tag{B.37}$$

where $\vec{S}$ denotes the net spin and its orientation of all atoms in one YIG unit cell and S denotes its absolute value. m denotes the mass of one unit cell and N denotes the number of unit cells in the whole solid. $\vec{u}$ denotes the spatial dependent displacement vector of the lattice atom. The gyromagnetic ratio is denoted by γ and the Planck constant by $\hbar$. The

operators $b_{\vec{p},i}$ and $b^\dagger_{\vec{p},i}$ denote the annihilation and the creation of one phonon with wave vector $\vec{p}$ and mode i, respectively. We insert (B.35) into the magnetoelastic energy and find

$$U_{\text{mel}} = a_1 \sum_{p,q,l=1,l\neq q}^{3} \frac{\partial S_p}{\partial x_q}\frac{\partial S_p}{\partial x_l} e_{ql} + a_2 \sum_{p,q=1}^{3} \left(\frac{\partial S_p}{\partial x_q}\right)^2 e_{qq} + a_3 \sum_{p,q,l=1,l\neq q}^{3} \left(\frac{\partial S_p}{\partial x_q}\right)^2 e_{ll}\,, \tag{B.38}$$

with the abbreviations

$$a_1 = \frac{\gamma^2\hbar^2 A_1}{M_0^2} = \frac{A_1}{S^2} \qquad a_2 = \frac{\gamma^2\hbar^2 A_2}{M_0^2} = \frac{A_2}{S^2} \qquad a_3 = \frac{\gamma^2\hbar^2 A_3}{M_0^2} = \frac{A_3}{S^2}\,. \tag{B.39}$$

The spin operators S_x and S_y can be rewritten in the following way

$$S^+ = S_x + iS_y \qquad S^- = S_x - iS_y\,, \tag{B.40}$$

Including these identities, we rewrite the energy

$$\begin{aligned} U_{\text{mel}} =& \frac{a_1}{2} \sum_{q,l=1,l\neq q}^{3} e_{ql} \left(\frac{\partial S^+}{\partial x_q}\frac{\partial S^-}{\partial x_l} + \frac{\partial S^-}{\partial x_q}\frac{\partial S^+}{\partial x_l} + 2\frac{\partial S_z}{\partial x_q}\frac{\partial S_z}{\partial x_l}\right) \\ &+ \frac{a_2}{2} \sum_{q=1}^{3} e_{qq} \left(\frac{\partial S^+}{\partial x_q}\frac{\partial S^-}{\partial x_q} + \frac{\partial S^-}{\partial x_q}\frac{\partial S^+}{\partial x_q} + 2\frac{\partial S_z}{\partial x_q}\frac{\partial S_z}{\partial x_q}\right) \\ &+ \frac{a_3}{2} \sum_{q,l=1,l\neq q}^{3} e_{ll} \left(\frac{\partial S^+}{\partial x_q}\frac{\partial S^-}{\partial x_q} + \frac{\partial S^-}{\partial x_q}\frac{\partial S^+}{\partial x_q} + 2\frac{\partial S_z}{\partial x_q}\frac{\partial S_z}{\partial x_q}\right)\,. \end{aligned} \tag{B.41}$$

On the other hand, we replace the spin operators in the following way [54, p. 78]

$$S^+ = \sqrt{2S}\, a \qquad S^- = \sqrt{2S}\, a^+ \qquad S_z = S - a^+ a\,, \tag{B.42}$$

which is still dependent on position $\vec{r}$. The operators a and $a^\dagger$ denote the annihilation and the creation of one magnon at position $\vec{r}$, respectively. Thus, we need to Fourier transform

$$a = \frac{1}{\sqrt{N}} \sum_{\vec{k}} a_{\vec{k}} e^{-i\vec{k}\vec{r}} \qquad a^\dagger = \frac{1}{\sqrt{N}} \sum_{\vec{k}'} a^\dagger_{\vec{k}'} e^{i\vec{k}'\vec{r}}\,. \tag{B.43}$$

The operators $a_{\vec{k}}$ and $a^\dagger_{\vec{k}}$ denote the annihilation and the creation of one magnon with wave vector $\vec{k}$, respectively. Thus, we find

$$\frac{\partial S^+}{\partial x_q} = \sqrt{2S}\frac{\partial a}{\partial x_q} = \frac{\sqrt{2S}}{\sqrt{N}} \sum_{\vec{k}} a_{\vec{k}} \frac{\partial}{\partial x_q} e^{-i\vec{k}\vec{r}} = -i\frac{\sqrt{2S}}{\sqrt{N}} \sum_{\vec{k}} a_{\vec{k}} k_q e^{-i\vec{k}\vec{r}} \tag{B.44}$$

$$\frac{\partial S^-}{\partial x_q} = \sqrt{2S}\frac{\partial a^\dagger}{\partial x_q} = \frac{\sqrt{2S}}{\sqrt{N}} \sum_{\vec{k}} a^\dagger_{\vec{k}} \frac{\partial}{\partial x_q} e^{i\vec{k}\vec{r}} = i\frac{\sqrt{2S}}{\sqrt{N}} \sum_{\vec{k}} a^\dagger_{\vec{k}} k_q e^{i\vec{k}\vec{r}} \tag{B.45}$$

$$\frac{\partial S_z}{\partial x_q} = -\frac{\partial a^\dagger a}{\partial x_q} = -\frac{1}{N} \sum_{\vec{k}\vec{k}'} a_{\vec{k}} a^\dagger_{\vec{k}'} \frac{\partial}{\partial x_q} e^{-i\vec{k}\vec{r}} e^{i\vec{k}'\vec{r}} = i\frac{1}{N} \sum_{\vec{k}\vec{k}'} a_{\vec{k}} a^\dagger_{\vec{k}'} (k_q - k'_q) e^{-i(\vec{k}-\vec{k}')\vec{r}}\,. \tag{B.46}$$

Now, we neglect higher order terms with more than two annihilation or creation operators. Thus, we find

$$\begin{aligned}U_{\text{mel}} =&\frac{a_1 S}{N}\sum_{q,l=1,l\neq q}^{3}\sum_{\vec{k}\vec{k}'} e_{ql}\left(a_{\vec{k}}a^{\dagger}_{\vec{k}'}k_q k'_l e^{-i(\vec{k}-\vec{k}')\vec{r}} + a^{\dagger}_{\vec{k}}a_{\vec{k}'}k_q k'_l e^{i(\vec{k}-\vec{k}')\vec{r}}\right)\\ &+\frac{a_2 S}{N}\sum_{q=1}^{3}\sum_{\vec{k}\vec{k}'} e_{qq}\left(a_{\vec{k}}a^{\dagger}_{\vec{k}'}k_q k'_q e^{-i(\vec{k}-\vec{k}')\vec{r}} + a^{\dagger}_{\vec{k}}a_{\vec{k}'}k_q k'_q e^{i(\vec{k}-\vec{k}')\vec{r}}\right)\\ &+\frac{a_3 S}{N}\sum_{q,l=1,l\neq q}^{3}\sum_{\vec{k}\vec{k}'} e_{ll}\left(a_{\vec{k}}a^{\dagger}_{\vec{k}'}k_q k'_q e^{-i(\vec{k}-\vec{k}')\vec{r}} + a^{\dagger}_{\vec{k}}a_{\vec{k}'}k_q k'_q e^{i(\vec{k}-\vec{k}')\vec{r}}\right).\end{aligned} \tag{B.47}$$

The symmetric strain tensor needs to be rewritten in terms of phonon operators

$$e_{ij} = \frac{1}{2}\left(-i\sum_{\vec{p}} p_j\sqrt{\frac{\hbar}{2mN\omega_p}}(b_{\vec{p}} + b^{\dagger}_{-\vec{p}})\, e_{\vec{p},i}\, e^{-i\vec{p}\vec{r}} - i\sum_{\vec{p}} p_i\sqrt{\frac{\hbar}{2mN\omega_p}}(b_{\vec{p}} + b^{\dagger}_{-\vec{p}})\, e_{\vec{p},j}\, e^{-i\vec{p}\vec{r}}\right). \tag{B.48}$$

Thus, we find

$$\begin{aligned}H =&\int_V d^3\vec{x}\, U_{\text{mel}}\\ =&\frac{1}{N}\int_V d^3\vec{x}\, a_1 S\sum_{p,l=1,l\neq p}^{3}\sum_{\vec{k}\vec{k}'} e_{pl}\left(a_{\vec{k}}a^{\dagger}_{\vec{k}'}k_p k'_l e^{-i(\vec{k}-\vec{k}')\vec{r}} + a^{\dagger}_{\vec{k}}a_{\vec{k}'}k_p k'_l e^{i(\vec{k}-\vec{k}')\vec{r}}\right)\\ &+\frac{1}{N}\int_V d^3\vec{x}\, a_2 S\sum_{p=1}^{3}\sum_{\vec{k}\vec{k}'} e_{pp} 2a_{\vec{k}}a^{\dagger}_{\vec{k}'}k_p k'_p e^{-i(\vec{k}-\vec{k}')\vec{r}}\\ &+\frac{1}{N}\int_V d^3\vec{x}\, a_3 S\sum_{p,l=1,l\neq p}^{3}\sum_{\vec{k}\vec{k}'} e_{ll} 2a_{\vec{k}}a^{\dagger}_{\vec{k}'}k_p k'_p e^{-i(\vec{k}-\vec{k}')\vec{r}}.\end{aligned} \tag{B.49}$$

We are making use of

$$\int_V d^3\vec{x} e^{-i\vec{Q}\vec{r}} = (2\pi)^3\delta(\vec{Q}) \tag{B.50}$$

$$\sum_{\vec{k}'} = \frac{3a^3N}{4\pi^4}\int d^3\vec{k}', \tag{B.51}$$

and find

$$\begin{aligned}H =&\frac{a_1}{2i}\frac{S}{N}\int_V d^3\vec{x}\sum_{q,l=1,l\neq q}^{3}\sum_{\vec{k}\vec{k}'\vec{p}}\sqrt{\frac{\hbar}{2mN\omega_p}}a_{\vec{k}}a^{\dagger}_{\vec{k}'}\left(k_q k'_l + k'_q k_l\right)\\ &\times\left(p_l(b_{\vec{p}} + b^{\dagger}_{-\vec{p}})\, e_{\vec{p},q} + p_q(b_{\vec{p}} + b^{\dagger}_{-\vec{p}})\, e_{\vec{p},l}\right)e^{-i(\vec{k}-\vec{k}'+\vec{p})\vec{r}}\\ &+\frac{a_2}{i}\frac{S}{N}\int_V d^3\vec{x}\sum_{q=1}^{3}\sum_{\vec{k}\vec{k}'\vec{p}}\sqrt{\frac{\hbar}{2mN\omega_p}}2a_{\vec{k}}a^{\dagger}_{\vec{k}'}(b_{\vec{p}} + b^{\dagger}_{-\vec{p}})\, e_{\vec{p},q}\, p_q k_q k'_q e^{-i(\vec{k}-\vec{k}'+\vec{p})\vec{r}}\\ &+\frac{a_3}{i}\frac{S}{N}\int_V d^3\vec{x}\sum_{q,l=1,l\neq q}^{3}\sum_{\vec{k}\vec{k}'\vec{p}}\sqrt{\frac{\hbar}{2mN\omega_p}}2a_{\vec{k}}a^{\dagger}_{\vec{k}'}(b_{\vec{p}} + b^{\dagger}_{-\vec{p}})\, e_{\vec{p},l}\, p_l k_q k'_q e^{-i(\vec{k}-\vec{k}'+\vec{p})\vec{r}}.\end{aligned} \tag{B.52}$$

Now, we evaluate the integral and find

$$\begin{aligned}
H =&\frac{6a^3}{\pi}\frac{a_1 S}{2i}\sum_{q,l=1,l\neq q}^{3}\sum_{\vec{k}\vec{p}}\sqrt{\frac{\hbar}{2mN\omega_p}}a_{\vec{k}}a^\dagger_{\vec{k}+\vec{p}}(k_q(k_l+p_l)+k_l(k_q+p_q))\\
&\qquad\times\left(p_l(b_{\vec{p}}+b^\dagger_{-\vec{p}})\,e_{\vec{p},q}+p_q(b_{\vec{p}}+b^\dagger_{-\vec{p}})\,e_{\vec{p},l}\right)\\
&+\frac{6a^3}{\pi}\frac{2a_2 S}{i}\sum_{q=1}^{3}\sum_{\vec{k}\vec{q}}\sqrt{\frac{\hbar}{2mN\omega_p}}a_{\vec{k}}a^\dagger_{\vec{k}+\vec{p}}(b_{\vec{p}}+b^\dagger_{-\vec{p}})\,e_{\vec{p},q}\,p_q k_q(k_q+p_q)\\
&+\frac{6a^3}{\pi}\frac{2a_3 S}{i}\sum_{q,l=1,l\neq q}^{3}\sum_{\vec{k}\vec{p}}\sqrt{\frac{\hbar}{2mN\omega_p}}a_{\vec{k}}a^\dagger_{\vec{k}+\vec{p}}(b_{\vec{p}}+b^\dagger_{-\vec{p}})\,e_{\vec{p},l}\,p_l k_q(k_q+p_q)\\
=&\frac{6a^3}{\pi}\frac{a_1 S}{i}\sum_{q,l=1,l\neq q}^{3}\sum_{\vec{k}\vec{p}}\sqrt{\frac{\hbar}{2mN\omega_p}}a_{\vec{k}}a^\dagger_{\vec{k}+\vec{p}}(k_q(k_l+p_l)+k_l(k_q+p_q))\,p_l(b_{\vec{p}}+b^\dagger_{-\vec{p}})\,e_{\vec{p},q}\\
&+\frac{6a^3}{\pi}\frac{2a_2 S}{i}\sum_{q=1}^{3}\sum_{\vec{k}\vec{p}}\sqrt{\frac{\hbar}{2mN\omega_p}}a_{\vec{k}}a^\dagger_{\vec{k}+\vec{p}}(b_{\vec{p}}+b^\dagger_{-\vec{p}})\,e_{\vec{p},q}\,p_q k_q(k_q+p_q)\\
&+\frac{6a^3}{\pi}\frac{2a_3 S}{i}\sum_{q,l=1,l\neq q}^{3}\sum_{\vec{k}\vec{p}}\sqrt{\frac{\hbar}{2mN\omega_p}}a_{\vec{k}}a^\dagger_{\vec{k}+\vec{p}}(b_{\vec{p}}+b^\dagger_{-\vec{p}})\,e_{\vec{p},l}\,p_l k_q(k_q+p_q)\,. \qquad \text{(B.53)}
\end{aligned}$$

If one assumes $a_2 = a_1$ (cf. Eq. (2) of Ref. [51]), then one finds

$$\begin{aligned}
H =&\frac{6a^3}{\pi}\frac{a_1 S}{i}\sum_{q=1}^{3}\sum_{\vec{k}\vec{p}}\sqrt{\frac{\hbar}{2mN\omega_p}}a_{\vec{k}}a^\dagger_{\vec{k}+\vec{p}}\left(k_q((\vec{k}+\vec{p})\cdot\vec{p})+(\vec{k}\cdot\vec{p})(k_q+p_q)\right)(b_{\vec{p}}+b^\dagger_{-\vec{p}})\,e_{\vec{p},q}\\
&+\frac{6a^3}{\pi}\frac{2a_3 S}{i}\sum_{q=1}^{3}\sum_{\vec{k}\vec{p}}\sqrt{\frac{\hbar}{2mN\omega_p}}a_{\vec{k}}a^\dagger_{\vec{k}+\vec{p}}p_q((\vec{k}+\vec{p})\cdot\vec{k})(b_{\vec{p}}+b^\dagger_{-\vec{p}})\,e_{\vec{p},q}\,. \qquad \text{(B.54)}
\end{aligned}$$

Let us assume $a_3 = a_1$ for simplicity. We have three phonon modes (one for each spatial dimension). Thus, we find three coupling parameters

$$V_{\text{ex,x}} = \frac{6a^3}{\pi}\frac{a_1 S}{i}\sqrt{\frac{\hbar}{2mN\omega_p}}\left(k_x((\vec{k}+\vec{p})\cdot\vec{p})+(\vec{k}\cdot\vec{p})(k_x+p_x)+2p_x((\vec{k}+\vec{p})\cdot\vec{k})\right) \qquad \text{(B.55)}$$

$$V_{\text{ex,y}} = \frac{6a^3}{\pi}\frac{a_1 S}{i}\sqrt{\frac{\hbar}{2mN\omega_p}}\left(k_y((\vec{k}+\vec{p})\cdot\vec{p})+(\vec{k}\cdot\vec{p})(k_y+p_y)+2p_y((\vec{k}+\vec{p})\cdot\vec{k})\right) \qquad \text{(B.56)}$$

$$V_{\text{ex,z}} = \frac{6a^3}{\pi}\frac{a_1 S}{i}\sqrt{\frac{\hbar}{2mN\omega_p}}\left(k_z((\vec{k}+\vec{p})\cdot\vec{p})+(\vec{k}\cdot\vec{p})(k_z+p_z)+2p_z((\vec{k}+\vec{p})\cdot\vec{k})\right). \qquad \text{(B.57)}$$

Because these three interactions are different, the squares of absolute value are added in the collision integral

$$\begin{aligned}|V_{\mathrm{ex,ges}}|^2 =&|V_{\mathrm{ex,x}}|^2 + |V_{\mathrm{ex,y}}|^2 + |V_{\mathrm{ex,z}}|^2\\ =&\frac{36a^6}{\pi^2}\frac{\hbar A_1^2}{2mNS^2\omega_p}\left((\vec{k}\cdot\vec{k})((\vec{k}+\vec{p})\cdot\vec{p})^2 + (\vec{k}\cdot\vec{p})^2(\vec{k}+\vec{p})^2 + 4(\vec{p}\cdot\vec{p})((\vec{k}+\vec{p})\cdot\vec{k})^2\right)\\ &+\frac{36a^6}{\pi^2}\frac{\hbar A_1^2}{2mNS^2\omega_p}\left(10(\vec{k}\cdot(\vec{k}+\vec{p}))((\vec{k}+\vec{p})\cdot\vec{p})(\vec{k}\cdot\vec{p})\right)\\ =&V_{\mathrm{ex}}^2k^2p(4k^2+p^2+20kp\cos(\vartheta)+(12k^2+15p^2)\cos^2(\vartheta)+12kp\cos^3(\vartheta))\,. \end{aligned} \tag{B.58}$$

The average can be calculated in the following way. Let $k' = |\vec{k}+\vec{p}|$, $\vartheta_1 = \measuredangle(\vec{p},\vec{k}+\vec{p})$ and $\vartheta_2 = \measuredangle(\vec{k},\vec{k}+\vec{p})$. Then

$$\begin{aligned}|V_{\mathrm{ex,ges}}|^2 =&\frac{36a^6}{\pi^2}\frac{\hbar A_1^2}{2mNS^2\omega_p}\left(kk(k'p\cos(\vartheta_1))^2 + (kp\cos(\vartheta_1+\vartheta_2))^2k'k' + 4pp(k'k\cos(\vartheta_2))^2\right.\\ &\left.+\,10(kk'\cos(\vartheta_2))(k'p\cos(\vartheta_1))(kp\cos(\vartheta_1+\vartheta_2))\right)\,. \end{aligned} \tag{B.59}$$

The average coupling parameter read

$$\begin{aligned}|V_{\mathrm{ex,ges,av}}|^2 &= \frac{1}{(4\pi)^2}\int_0^{2\pi}\int_0^{2\pi}\int_0^{\pi}\int_0^{\pi} sin(\vartheta_1)sin(\vartheta_2)|V_{\mathrm{ex,ges}}|^2\,d\vartheta_1\,d\vartheta_2\,d\varphi_1\,d\varphi_2\\ &= \frac{36a^6}{\pi^2}\frac{\hbar A_1^2}{2mNS^2\omega_p}\frac{10}{3}k^2k'^2p^2\\ &= \frac{A}{N}k^2k'^2p\,. \end{aligned} \tag{B.60}$$

For calculating the numeric parameters, we use an identity out of [43, p. 333]. This is

$$\left|\frac{V_{\mathrm{ex,ges,av}}}{V_{\mathrm{Sc,av}}}\right| \propto \frac{M_0Dk^2}{B} \propto 1\,, \tag{B.61}$$

for $k = k' \approx 10^6\mathrm{cm}^{-1}$. We make use of Eq. (B.33). From there, we get for $k = k'$

$$\frac{|V_{\mathrm{ex,ges,av}}|^2}{|V_{\mathrm{Sc,av}}|^2} = \frac{(A/N)k^2k'^2p}{4\cdot(1/N)\cdot 4.95482\cdot 10^{-8}\,\mathrm{GHz}^2\,\mathrm{cm}\,p} = \frac{Ak^4}{4\cdot 4.95482\cdot 10^{-8}\,\mathrm{GHz}^2\,\mathrm{cm}} = 1\,, \tag{B.62}$$

for $k \approx 10^6\mathrm{cm}^{-1}$. Thus, we get

$$A = \frac{4\cdot 4.95482\cdot 10^{-8}\,\mathrm{GHz}^2\,\mathrm{cm}}{(10^6\mathrm{cm}^{-1})^4} = 1.98197\cdot 10^{-31}\,\mathrm{GHz}^2\,\mathrm{cm}^5\,. \tag{B.63}$$

C Collision integral for magnon-magnon interaction

In this appendix, we will calculate the collision integral in the Boltzmann equation for the magnon-magnon interaction in detail. First, we consider dipolar magnons in section C.1 and after that exchange magnons in section C.2. In sections 5.1 and 5.2, we already presented the short calculation. The collision integral will be used in chapter 5 to calculate the wave number dependent magnon temperature.

Here, we consider a thin film out of a thin magnetic insulator (YIG, $Y_3Fe_5O_{12}$) on top of the GGG substrate ($Gd_3Ga_5O_{12}$). Since the thickness of the GGG substrate is much thicker than the thickness of the YIG film, the phonons are rarely influenced by the magnons. Thus, the phonon temperature profile out of chapter 3 will be used as an input parameter. In chapter 4, we derived the collision integral for the magnon-phonon interaction. With these ingredients and the collision integral for the magnon-magnon interactions, we calculate the wave number dependent magnon temperature in chapter 5.

C.1 Three particle interaction - dipole-dipole-interaction

C.1.1 Collision integral

We set up the collision integral for three particle magnon-magnon interaction. The corresponding third order collision integral reads (see Eq. (5.7) in this thesis or see Eq. (11.9) on page 289 in Ref. [43])

$$\begin{aligned}
\left.\frac{\partial f_{\vec{k}}}{\partial t}\right|_{\mathrm{St},3} =& \sum_{\vec{k}'} \Big\{ \frac{1}{2} W(\mathrm{M}_{\vec{k}+\vec{k}'} \to \mathrm{M}_{\vec{k}} + \mathrm{M}_{\vec{k}'}) + \frac{1}{2} W(\mathrm{M}_{\vec{k}'} \to \mathrm{M}_{\vec{k}'-\vec{k}} + \mathrm{M}_{\vec{k}}) \\
&+ \frac{1}{2} W(\mathrm{M}_{\vec{k}'} + \mathrm{M}_{\vec{k}-\vec{k}'} \to \mathrm{M}_{\vec{k}}) - \frac{1}{2} W(\mathrm{M}_{\vec{k}} + \mathrm{M}_{\vec{k}'} \to \mathrm{M}_{\vec{k}+\vec{k}'}) \\
&- \frac{1}{2} W(\mathrm{M}_{\vec{k}'-\vec{k}} + \mathrm{M}_{\vec{k}} \to \mathrm{M}_{\vec{k}'}) - \frac{1}{2} W(\mathrm{M}_{\vec{k}} \to \mathrm{M}_{\vec{k}'} + \mathrm{M}_{\vec{k}-\vec{k}'}) \Big\} \\
=& \frac{1}{2} \frac{2\pi}{\hbar} \sum_{\vec{k}'} |V|^2 \delta(\epsilon_{\vec{k}+\vec{k}'} - \epsilon_{\vec{k}} - \epsilon_{\vec{k}'}) \cdot 4 \cdot \Big[f_{\vec{k}+\vec{k}'}(1+f_{\vec{k}})(1+f_{\vec{k}'}) - f_{\vec{k}} f_{\vec{k}'}(1+f_{\vec{k}+\vec{k}'}) \Big] \\
&+ \frac{1}{2} \frac{2\pi}{\hbar} \sum_{\vec{k}'} |V|^2 \delta(\epsilon_{\vec{k}'} - \epsilon_{\vec{k}'-\vec{k}} - \epsilon_{\vec{k}}) \cdot 4 \cdot \Big[f_{\vec{k}'}(1+f_{\vec{k}'-\vec{k}})(1+f_{\vec{k}}) - f_{\vec{k}} f_{\vec{k}'-\vec{k}}(1+f_{\vec{k}'}) \Big] \\
&+ \frac{1}{2} \frac{2\pi}{\hbar} \sum_{\vec{k}'} |V|^2 \delta(\epsilon_{\vec{k}-\vec{k}'} + \epsilon_{\vec{k}'} - \epsilon_{\vec{k}}) \cdot 4 \cdot \Big[f_{\vec{k}-\vec{k}'} f_{\vec{k}'}(1+f_{\vec{k}}) - f_{\vec{k}}(1+f_{\vec{k}-\vec{k}'})(1+f_{\vec{k}'}) \Big] \,.
\end{aligned} \tag{C.1}$$

The term $W(\mathrm{M}_{\vec{k}+\vec{k}'} \to \mathrm{M}_{\vec{k}} + \mathrm{M}_{\vec{k}'})$ denotes the probability for the transformation of one magnon with wave vector $\vec{k}+\vec{k}'$ into one magnon with wave vector $\vec{k}$ and one magnon with wave vector $\vec{k}'$. Again, $f_{\vec{k}}$ denotes the magnon density with wave vector $\vec{k}$ and $\epsilon_{\vec{k}}$ denotes the magnon energy for magnons with wave vector $\vec{k}$. The term $|V|^2$ denotes the matrix-element of the transition and will be determined later. The result can be found in Eq. (5.29) or in Eq. (C.33). The factor 1/2 occurs, because scattering processes are double counted. The

equivalences read

$$W(\mathrm{M}_{\vec{k}+\vec{k}'} \to \mathrm{M}_{\vec{k}} + \mathrm{M}_{\vec{k}'}) \mathrel{\hat{=}} W(\mathrm{M}_{\vec{k}+\vec{k}'} \to \mathrm{M}_{\vec{k}'} + \mathrm{M}_{\vec{k}}) \tag{C.2}$$

$$W(\mathrm{M}_{\vec{k}'} \to \mathrm{M}_{\vec{k}'-\vec{k}} + \mathrm{M}_{\vec{k}}) \mathrel{\hat{=}} W(\mathrm{M}_{\vec{k}'} \to \mathrm{M}_{\vec{k}} + \mathrm{M}_{\vec{k}'-\vec{k}}) \tag{C.3}$$

$$W(\mathrm{M}_{\vec{k}'} + \mathrm{M}_{\vec{k}-\vec{k}'} \to \mathrm{M}_{\vec{k}}) \mathrel{\hat{=}} W(\mathrm{M}_{\vec{k}-\vec{k}'} + \mathrm{M}_{\vec{k}'} \to \mathrm{M}_{\vec{k}})\,. \tag{C.4}$$

Now, we perform a first order Taylor expansion for the temperatures and find:

$$\begin{aligned}
\left.\frac{\partial f_{\vec{k}}}{\partial t}\right|_{\mathrm{St},3} \approx & \frac{4\pi}{\hbar} \sum_{\vec{k}'} |V|^2 \delta(\epsilon_{\vec{k}+\vec{k}'} - \epsilon_{\vec{k}} - \epsilon_{\vec{k}'}) f^0_{\vec{k}+\vec{k}'} (1 + f^0_{\vec{k}})(1 + f^0_{\vec{k}'}) \frac{1}{k_\mathrm{B} T_0^2} \\
& \times \left[(\epsilon_{\vec{k}} + \epsilon_{\vec{k}'}) T_\mathrm{M}(\vec{k} + \vec{k}') - \epsilon_{\vec{k}'} T_\mathrm{M}(\vec{k}') - \epsilon_{\vec{k}} T_\mathrm{M}(\vec{k}) \right] \\
& + \frac{4\pi}{\hbar} \sum_{\vec{k}'} |V|^2 \delta(\epsilon_{\vec{k}'} - \epsilon_{\vec{k}'-\vec{k}} - \epsilon_{\vec{k}}) f^0_{\vec{k}'} (1 + f^0_{\vec{k}'-\vec{k}})(1 + f^0_{\vec{k}}) \frac{1}{k_\mathrm{B} T_0^2} \\
& \times \left[-\epsilon_{\vec{k}} T_\mathrm{M}(\vec{k}) + \epsilon_{\vec{k}'} T_\mathrm{M}(\vec{k}') + (\epsilon_{\vec{k}} - \epsilon_{\vec{k}'}) T_\mathrm{M}(\vec{k}' - \vec{k}) \right] \\
& + \frac{4\pi}{\hbar} \sum_{\vec{k}'} |V|^2 \delta(\epsilon_{\vec{k}-\vec{k}'} + \epsilon_{\vec{k}'} - \epsilon_{\vec{k}}) f^0_{\vec{k}-\vec{k}'} f^0_{\vec{k}'} (1 + f^0_{\vec{k}}) \frac{1}{k_\mathrm{B} T_0^2} \\
& \times \left[-\epsilon_{\vec{k}} T_\mathrm{M}(\vec{k}) + \epsilon_{\vec{k}'} T_\mathrm{M}(\vec{k}') + (\epsilon_{\vec{k}} - \epsilon_{\vec{k}'}) T_\mathrm{M}(\vec{k} - \vec{k}') \right].
\end{aligned} \tag{C.5}$$

In this expression, the wave number dependent magnon temperature occurs as a linear parameter. Later, we will discretize the magnon temperature and the summation. Thus, we will get a system of linear equations for the magnon temperature. By now, we introduce abbreviations

$$0 = \left.\frac{\partial f_{\vec{k}}}{\partial t}\right|_{\mathrm{St}} = \sum_{\vec{k}'} \left(\frac{|V|^2}{\tau_A^{mm}} \frac{T_\mathrm{M}(\vec{k})}{T_0} + \frac{|V|^2}{\tau_B^{mm}} \frac{T_\mathrm{M}(\vec{k}')}{T_0} + \frac{|V|^2}{\tau_C^{mm}} \frac{T_\mathrm{M}(\vec{k} \pm \vec{k}')}{T_0} \right), \tag{C.6}$$

with

$$\begin{aligned}
\frac{1}{\tau_A^{mm}} = & \frac{4\pi}{\hbar} \delta(\epsilon_{\vec{k}+\vec{k}'} - \epsilon_{\vec{k}} - \epsilon_{\vec{k}'}) f^0_{\vec{k}+\vec{k}'} (1 + f^0_{\vec{k}})(1 + f^0_{\vec{k}'}) \frac{-\epsilon_{\vec{k}}}{k_\mathrm{B} T_0} \\
& + \frac{4\pi}{\hbar} \delta(\epsilon_{\vec{k}'} - \epsilon_{\vec{k}'-\vec{k}} - \epsilon_{\vec{k}}) f^0_{\vec{k}'} (1 + f^0_{\vec{k}'-\vec{k}})(1 + f^0_{\vec{k}}) \frac{-\epsilon_{\vec{k}}}{k_\mathrm{B} T_0} \\
& + \frac{4\pi}{\hbar} \delta(\epsilon_{\vec{k}-\vec{k}'} + \epsilon_{\vec{k}'} - \epsilon_{\vec{k}}) f^0_{\vec{k}-\vec{k}'} f^0_{\vec{k}'} (1 + f^0_{\vec{k}}) \frac{-\epsilon_{\vec{k}}}{k_\mathrm{B} T_0},
\end{aligned} \tag{C.7}$$

and

$$\begin{aligned}
\frac{1}{\tau_B^{mm}} = & \frac{4\pi}{\hbar} \delta(\epsilon_{\vec{k}+\vec{k}'} - \epsilon_{\vec{k}} - \epsilon_{\vec{k}'}) f^0_{\vec{k}+\vec{k}'} (1 + f^0_{\vec{k}})(1 + f^0_{\vec{k}'}) \frac{-\epsilon_{\vec{k}'}}{k_\mathrm{B} T_0} \\
& + \frac{4\pi}{\hbar} \delta(\epsilon_{\vec{k}'} - \epsilon_{\vec{k}'-\vec{k}} - \epsilon_{\vec{k}}) f^0_{\vec{k}'} (1 + f^0_{\vec{k}'-\vec{k}})(1 + f^0_{\vec{k}}) \frac{+\epsilon_{\vec{k}'}}{k_\mathrm{B} T_0} \\
& + \frac{4\pi}{\hbar} \delta(\epsilon_{\vec{k}-\vec{k}'} + \epsilon_{\vec{k}'} - \epsilon_{\vec{k}}) f^0_{\vec{k}-\vec{k}'} f^0_{\vec{k}'} (1 + f^0_{\vec{k}}) \frac{+\epsilon_{\vec{k}'}}{k_\mathrm{B} T_0},
\end{aligned} \tag{C.8}$$

and

$$\begin{aligned}\frac{1}{\tau_C^{mm}} =& \frac{4\pi}{\hbar}\delta(\epsilon_{\vec{k}+\vec{k}'} - \epsilon_{\vec{k}} - \epsilon_{\vec{k}'}) f^0_{\vec{k}+\vec{k}'}(1+f^0_{\vec{k}})(1+f^0_{\vec{k}'})\frac{(\epsilon_{\vec{k}}+\epsilon_{\vec{k}'})}{k_\mathrm{B}T_0} \\ &+ \frac{4\pi}{\hbar}\delta(\epsilon_{\vec{k}'} - \epsilon_{\vec{k}'-\vec{k}} - \epsilon_{\vec{k}}) f^0_{\vec{k}'}(1+f^0_{\vec{k}'-\vec{k}})(1+f^0_{\vec{k}})\frac{(\epsilon_{\vec{k}}-\epsilon_{\vec{k}'})}{k_\mathrm{B}T_0} \\ &+ \frac{4\pi}{\hbar}\delta(\epsilon_{\vec{k}-\vec{k}'} + \epsilon_{\vec{k}'} - \epsilon_{\vec{k}}) f^0_{\vec{k}-\vec{k}'} f^0_{\vec{k}'}(1+f^0_{\vec{k}})\frac{(\epsilon_{\vec{k}}-\epsilon_{\vec{k}'})}{k_\mathrm{B}T_0}\,. \end{aligned} \tag{C.9}$$

C.1.2 Numerical treatment

For avoiding some difficulties, we perform a transformation of the integration procedure. We start with introducing some abbreviations

$$\frac{1}{\tau_A^{mm}} = \frac{1}{\tau_{A1}^{mm}}\delta(\epsilon_{\vec{k}+\vec{k}'} - \epsilon_{\vec{k}} - \epsilon_{\vec{k}'}) + \frac{1}{\tau_{A2}^{mm}}\delta(\epsilon_{\vec{k}'} - \epsilon_{\vec{k}'-\vec{k}} - \epsilon_{\vec{k}}) + \frac{1}{\tau_{A3}^{mm}}\delta(\epsilon_{\vec{k}-\vec{k}'} + \epsilon_{\vec{k}'} - \epsilon_{\vec{k}}) \tag{C.10}$$

$$\frac{1}{\tau_{A1}^{mm}} = \frac{4\pi}{\hbar} f^0_{\vec{k}+\vec{k}'}(1+f^0_{\vec{k}})(1+f^0_{\vec{k}'})\frac{-\epsilon_{\vec{k}}}{k_\mathrm{B}T_0} \tag{C.11}$$

$$\frac{1}{\tau_{A2}^{mm}} = \frac{4\pi}{\hbar} f^0_{\vec{k}'}(1+f^0_{\vec{k}'-\vec{k}})(1+f^0_{\vec{k}})\frac{-\epsilon_{\vec{k}}}{k_\mathrm{B}T_0} \tag{C.12}$$

$$\frac{1}{\tau_{A3}^{mm}} = \frac{4\pi}{\hbar} f^0_{\vec{k}-\vec{k}'} f^0_{\vec{k}'}(1+f^0_{\vec{k}})\frac{-\epsilon_{\vec{k}}}{k_\mathrm{B}T_0}\,, \tag{C.13}$$

and

$$\frac{1}{\tau_B^{mm}} = \frac{1}{\tau_{B1}^{mm}}\delta(\epsilon_{\vec{k}+\vec{k}'} - \epsilon_{\vec{k}} - \epsilon_{\vec{k}'}) + \frac{1}{\tau_{B2}^{mm}}\delta(\epsilon_{\vec{k}'} - \epsilon_{\vec{k}'-\vec{k}} - \epsilon_{\vec{k}}) + \frac{1}{\tau_{B3}^{mm}}\delta(\epsilon_{\vec{k}-\vec{k}'} + \epsilon_{\vec{k}'} - \epsilon_{\vec{k}}) \tag{C.14}$$

$$\frac{1}{\tau_{B1}^{mm}} = \frac{4\pi}{\hbar} f^0_{\vec{k}+\vec{k}'}(1+f^0_{\vec{k}})(1+f^0_{\vec{k}'})\frac{-\epsilon_{\vec{k}'}}{k_\mathrm{B}T_0} \tag{C.15}$$

$$\frac{1}{\tau_{B2}^{mm}} = \frac{4\pi}{\hbar} f^0_{\vec{k}'}(1+f^0_{\vec{k}'-\vec{k}})(1+f^0_{\vec{k}})\frac{+\epsilon_{\vec{k}'}}{k_\mathrm{B}T_0} \tag{C.16}$$

$$\frac{1}{\tau_{B3}^{mm}} = \frac{4\pi}{\hbar} f^0_{\vec{k}-\vec{k}'} f^0_{\vec{k}'}(1+f^0_{\vec{k}})\frac{+\epsilon_{\vec{k}'}}{k_\mathrm{B}T_0}\,, \tag{C.17}$$

and

$$\frac{1}{\tau_C^{mm}} = \frac{1}{\tau_{C1}^{mm}}\delta(\epsilon_{\vec{k}+\vec{k}'} - \epsilon_{\vec{k}} - \epsilon_{\vec{k}'}) + \frac{1}{\tau_{C2}^{mm}}\delta(\epsilon_{\vec{k}'} - \epsilon_{\vec{k}'-\vec{k}} - \epsilon_{\vec{k}}) + \frac{1}{\tau_{C3}^{mm}}\delta(\epsilon_{\vec{k}-\vec{k}'} + \epsilon_{\vec{k}'} - \epsilon_{\vec{k}}) \tag{C.18}$$

$$\frac{1}{\tau_{C1}^{mm}} = \frac{4\pi}{\hbar} f^0_{\vec{k}+\vec{k}'}(1+f^0_{\vec{k}})(1+f^0_{\vec{k}'})\frac{(\epsilon_{\vec{k}}+\epsilon_{\vec{k}'})}{k_\mathrm{B}T_0} \tag{C.19}$$

$$\frac{1}{\tau_{C2}^{mm}} = \frac{4\pi}{\hbar} f^0_{\vec{k}'}(1+f^0_{\vec{k}'-\vec{k}})(1+f^0_{\vec{k}})\frac{(\epsilon_{\vec{k}}-\epsilon_{\vec{k}'})}{k_\mathrm{B}T_0} \tag{C.20}$$

$$\frac{1}{\tau_{C3}^{mm}} = \frac{4\pi}{\hbar} f^0_{\vec{k}-\vec{k}'} f^0_{\vec{k}'}(1+f^0_{\vec{k}})\frac{(\epsilon_{\vec{k}}-\epsilon_{\vec{k}'})}{k_\mathrm{B}T_0}\,, \tag{C.21}$$

and

$$T_1(\vec{k},\vec{k}',\vec{k}+\vec{k}') = \left(\frac{1}{\tau_{A1}^{mm}}\frac{T_\mathrm{M}(\vec{k})}{T_0} + \frac{1}{\tau_{B1}^{mm}}\frac{T_\mathrm{M}(\vec{k}')}{T_0} + \frac{1}{\tau_{C1}^{mm}}\frac{T_\mathrm{M}(\vec{k}+\vec{k}')}{T_0}\right) \tag{C.22}$$

$$T_2(\vec{k},\vec{k}',\vec{k}-\vec{k}') = \left(\frac{1}{\tau_{A2}^{mm}}\frac{T_\mathrm{M}(\vec{k})}{T_0} + \frac{1}{\tau_{B2}^{mm}}\frac{T_\mathrm{M}(\vec{k}')}{T_0} + \frac{1}{\tau_{C2}^{mm}}\frac{T_\mathrm{M}(\vec{k}-\vec{k}')}{T_0}\right) \tag{C.23}$$

$$T_3(\vec{k},\vec{k}',\vec{k}-\vec{k}') = \left(\frac{1}{\tau_{A3}^{mm}}\frac{T_\mathrm{M}(\vec{k})}{T_0} + \frac{1}{\tau_{B3}^{mm}}\frac{T_\mathrm{M}(\vec{k}')}{T_0} + \frac{1}{\tau_{C3}^{mm}}\frac{T_\mathrm{M}(\vec{k}-\vec{k}')}{T_0}\right). \tag{C.24}$$

These abbreviations we insert in Eq. (C.6) and find

$$0 = \sum_{\vec{k}'} |V|^2\, T_1(k,k',|\vec{k}+\vec{k}'|)\delta(\epsilon_{\vec{k}+\vec{k}'} - \epsilon_{\vec{k}} - \epsilon_{\vec{k}'}) \tag{C.25}$$

$$+ \sum_{\vec{k}'} |V|^2\, T_2(k,k',|\vec{k}-\vec{k}'|)\delta(\epsilon_{\vec{k}'} - \epsilon_{\vec{k}'-\vec{k}} - \epsilon_{\vec{k}}) \tag{C.26}$$

$$+ \sum_{\vec{k}'} |V|^2\, T_3(k,k',|\vec{k}-\vec{k}'|)\delta(\epsilon_{\vec{k}-\vec{k}'} + \epsilon_{\vec{k}'} - \epsilon_{\vec{k}}). \tag{C.27}$$

Since the functions T_1, T_2 and T_3 only depend on absolute values of the wave vectors, we can write the integration in spherical coordinates. We rewrite the sum into an integral and introduce an integration over

$$k_m = |\vec{k} \pm \vec{k}'| = \sqrt{k^2 + k'^2 \pm 2kk'(\cos(\vartheta)\cos(\vartheta') + \sin(\vartheta)\sin(\vartheta')\cos(\varphi-\varphi'))}\,. \tag{C.28}$$

In our calculation, we are interested in the equation integrated over ϑ and φ (cf. Eq. (5.2)). It is

$$\begin{aligned}
0 =& \int \frac{d\Omega}{4\pi}\frac{3a^3N}{4\pi^4}\int d^3\vec{k}'\int_0^{2k_\mathrm{F}} dk_m \delta(k_m - |\vec{k}+\vec{k}'|)\,|V|^2\,T_1(k,k',|\vec{k}+\vec{k}'|)\,\delta(\epsilon_{\vec{k}+\vec{k}'} - \epsilon_{\vec{k}} - \epsilon_{\vec{k}'}) \\
&+ \int \frac{d\Omega}{4\pi}\frac{3a^3N}{4\pi^4}\int d^3\vec{k}'\int_0^{2k_\mathrm{F}} dk_m \delta(k_m - |\vec{k}-\vec{k}'|)\,|V|^2\,T_2(k,k',|\vec{k}-\vec{k}'|)\,\delta(\epsilon_{\vec{k}'} - \epsilon_{\vec{k}'-\vec{k}} - \epsilon_{\vec{k}}) \\
&+ \int \frac{d\Omega}{4\pi}\frac{3a^3N}{4\pi^4}\int d^3\vec{k}'\int_0^{2k_\mathrm{F}} dk_m \delta(k_m - |\vec{k}-\vec{k}'|)\,|V|^2\,T_3(k,k',|\vec{k}-\vec{k}'|)\,\delta(\epsilon_{\vec{k}-\vec{k}'} + \epsilon_{\vec{k}'} - \epsilon_{\vec{k}}),
\end{aligned} \tag{C.29}$$

with the Fermi wave number $k_\mathrm{F} = k_\mathrm{max} = 3.10{\cdot}10^7{\cdot}\mathrm{cm}^{-1}$. We introduce spherical coordinates and find

$$\begin{aligned}
0 =& \frac{3a^3N}{16\pi^5}\int_0^\pi d\vartheta\sin(\vartheta)\int_0^{2\pi}d\varphi\int_0^{k_\mathrm{F}}dk'\,k'^2\int_0^\pi d\vartheta'\,\sin(\vartheta')\int_0^{2\pi}d\varphi'\int_0^{2k_\mathrm{F}}dk_m \\
&\quad\times\delta(k_m - |\vec{k}+\vec{k}'|)\,|V|^2\,T_1(k,k',k_m)\,\delta(\epsilon_{k_m} - \epsilon_k - \epsilon_{k'}) \\
&+ \frac{3a^3N}{16\pi^5}\int_0^\pi d\vartheta\sin(\vartheta)\int_0^{2\pi}d\varphi\int_0^{k_\mathrm{F}}dk'\,k'^2\int_0^\pi d\vartheta'\,\sin(\vartheta')\int_0^{2\pi}d\varphi'\int_0^{2k_\mathrm{F}}dk_m \\
&\quad\times\delta(k_m - |\vec{k}-\vec{k}'|)\,|V|^2\,T_2(k,k',k_m)\,\delta(\epsilon_{k'} - \epsilon_{k_m} - \epsilon_k) \\
&+ \frac{3a^3N}{16\pi^5}\int_0^\pi d\vartheta\sin(\vartheta)\int_0^{2\pi}d\varphi\int_0^{k_\mathrm{F}}dk'\,k'^2\int_0^\pi d\vartheta'\,\sin(\vartheta')\int_0^{2\pi}d\varphi'\int_0^{2k_\mathrm{F}}dk_m \\
&\quad\times\delta(k_m - |\vec{k}-\vec{k}'|)\,|V|^2\,T_3(k,k',k_m)\,\delta(\epsilon_{k_m} + \epsilon_{k'} - \epsilon_k).
\end{aligned} \tag{C.30}$$

Now, we use Eq. (C.28) to solve the angular integration. First, we relocate the term in the delta-distribution.

$$
\begin{aligned}
=&\frac{3a^3N}{16\pi^5}\int_0^{\pi} d\vartheta\sin(\vartheta)\int_0^{2\pi} d\varphi\int_0^{k_\mathrm{F}} dk'\,k'^2\int_0^{\pi} d\vartheta'\,\sin(\vartheta')\int_0^{2\pi} d\varphi'\int_0^{2k_\mathrm{F}} dk_m\left|\frac{k_m}{kk'}\right||V|^2\,T_1(k,k',k_m)\\
&\times\delta(\epsilon_{k_m}-\epsilon_k-\epsilon_{k'})\,\delta\left(\cos(\vartheta)\cos(\vartheta')+\sin(\vartheta)\sin(\vartheta')\cos(\varphi-\varphi')-\frac{k_m^2-k^2-k'^2}{2kk'}\right)\\
+&\frac{3a^3N}{16\pi^5}\int_0^{\pi} d\vartheta\sin(\vartheta)\int_0^{2\pi} d\varphi\int_0^{k_\mathrm{F}} dk'\,k'^2\int_0^{\pi} d\vartheta'\,\sin(\vartheta')\int_0^{2\pi} d\varphi'\int_0^{2k_\mathrm{F}} dk_m\left|\frac{k_m}{kk'}\right||V|^2\,T_2(k,k',k_m)\\
&\times\delta(\epsilon_{k'}-\epsilon_{k_m}-\epsilon_k)\,\delta\left(\cos(\vartheta)\cos(\vartheta')+\sin(\vartheta)\sin(\vartheta')\cos(\varphi-\varphi')+\frac{k_m^2-k^2-k'^2}{2kk'}\right)\\
+&\frac{3a^3N}{16\pi^5}\int_0^{\pi} d\vartheta\sin(\vartheta)\int_0^{2\pi} d\varphi\int_0^{k_\mathrm{F}} dk'\,k'^2\int_0^{\pi} d\vartheta'\,\sin(\vartheta')\int_0^{2\pi} d\varphi'\int_0^{2k_\mathrm{F}} dk_m\left|\frac{k_m}{kk'}\right||V|^2\,T_3(k,k',k_m)\\
&\times\delta(\epsilon_{k_m}+\epsilon_{k'}-\epsilon_k)\,\delta\left(\cos(\vartheta)\cos(\vartheta')+\sin(\vartheta)\sin(\vartheta')\cos(\varphi-\varphi')+\frac{k_m^2-k^2-k'^2}{2kk'}\right).
\end{aligned}
\tag{C.31}
$$

We again relocate the angular delta function. It is

$$
\begin{aligned}
=&\frac{3a^3N}{16\pi^5}\int_0^{\pi} d\vartheta\sin(\vartheta)\int_0^{2\pi} d\varphi\int_0^{k_\mathrm{F}} dk'\,k'^2\int_0^{\pi} d\vartheta'\,\sin(\vartheta')\int_0^{2\pi} d\varphi'\int_0^{2k_\mathrm{F}} dk_m\left|\frac{k_m}{kk'}\right||V|^2\,T_1(k,k',k_m)\\
&\times\delta(\epsilon_{k_m}-\epsilon_k-\epsilon_{k'})\,\delta\left(\cos(\varphi-\varphi')+\frac{\cos(\vartheta)\cos(\vartheta')}{\sin(\vartheta)\sin(\vartheta')}-\frac{k_m^2-k^2-k'^2}{2kk'\sin(\vartheta)\sin(\vartheta')}\right)\frac{1}{\sin(\vartheta)\sin(\vartheta')}\\
+&\frac{3a^3N}{16\pi^5}\int_0^{\pi} d\vartheta\sin(\vartheta)\int_0^{2\pi} d\varphi\int_0^{k_\mathrm{F}} dk'\,k'^2\int_0^{\pi} d\vartheta'\,\sin(\vartheta')\int_0^{2\pi} d\varphi'\int_0^{2k_\mathrm{F}} dk_m\left|\frac{k_m}{kk'}\right||V|^2\,T_2(k,k',k_m)\\
&\times\delta(\epsilon_{k'}-\epsilon_{k_m}-\epsilon_k)\,\delta\left(\cos(\varphi-\varphi')+\frac{\cos(\vartheta)\cos(\vartheta')}{\sin(\vartheta)\sin(\vartheta')}+\frac{k_m^2-k^2-k'^2}{2kk'\sin(\vartheta)\sin(\vartheta')}\right)\frac{1}{\sin(\vartheta)\sin(\vartheta')}\\
+&\frac{3a^3N}{16\pi^5}\int_0^{\pi} d\vartheta\sin(\vartheta)\int_0^{2\pi} d\varphi\int_0^{k_\mathrm{F}} dk'\,k'^2\int_0^{\pi} d\vartheta'\,\sin(\vartheta')\int_0^{2\pi} d\varphi'\int_0^{2k_\mathrm{F}} dk_m\left|\frac{k_m}{kk'}\right||V|^2\,T_3(k,k',k_m)\\
&\times\delta(\epsilon_{k_m}+\epsilon_{k'}-\epsilon_k)\,\delta\left(\cos(\varphi-\varphi')+\frac{\cos(\vartheta)\cos(\vartheta')}{\sin(\vartheta)\sin(\vartheta')}+\frac{k_m^2-k^2-k'^2}{2kk'\sin(\vartheta)\sin(\vartheta')}\right)\frac{1}{\sin(\vartheta)\sin(\vartheta')}.
\end{aligned}
\tag{C.32}
$$

Kaganov *et al.* [56] made calculations on the Hamilton operator for different magnon-magnon scattering processes. We take Eq. (39) out of [56]

$$
\begin{aligned}
|V|^2=&\frac{1}{N}V_{\mathrm{abs}}^2\,|\cos(\vartheta)\sin(\vartheta)(\cos(\varphi)+i\sin(\varphi))+\cos(\vartheta')\sin(\vartheta')(\cos(\varphi')+i\sin(\varphi'))|^2\\
=&\frac{1}{N}V_{\mathrm{abs}}^2\left(\cos^2(\vartheta)\sin^2(\vartheta)+\cos^2(\vartheta')\sin^2(\vartheta')+\cos(\vartheta)\sin(\vartheta)\cos(\vartheta')\sin(\vartheta')\left(e^{i(\varphi-\varphi')}+e^{i(\varphi'-\varphi)}\right)\right)\\
=&\frac{1}{N}V_{\mathrm{abs}}^2\left(\cos^2(\vartheta)\sin^2(\vartheta)+\cos^2(\vartheta')\sin^2(\vartheta')+2\cos(\vartheta)\sin(\vartheta)\cos(\vartheta')\sin(\vartheta')\cos(\varphi-\varphi')\right)
\end{aligned}
\tag{C.33}
$$

$$
V_{\mathrm{abs}}^2=\frac{(2\pi\mu_\mathrm{B})^2\,2\mu_0\mu_\mathrm{B}M_0}{a^3}=52.1824\cdot\mathrm{GHz}^2\,,
\tag{C.34}
$$

while the constant $\mu_\mathrm{B}=9.2740154\cdot10^{-24}J/T$ denotes the Bohr magneton. Additionally, the constant $\mu_0=12.566370614\cdot10^{-7}T^2\cdot m^3/J$ denotes the vacuum permeability, and

$M_0 = 139\,\mathrm{G} = 0.0139\,\mathrm{T}$ [43, p. 182] is the magnetic saturation. The lattice constant for YIG is $a = 1.2376\,\mathrm{nm}$ [52, 53]. The upper expression will be set in into the collision integral term. Thus, we find

$$
\begin{aligned}
0 =& \frac{3a^3}{16\pi^5} \int_0^{\pi} d\vartheta \sin(\vartheta) \int_0^{2\pi} d\varphi \int_0^{k_{\max}} dk'\, k'^2 \int_0^{\pi} d\vartheta'\, \sin(\vartheta') \int_0^{2\pi} d\varphi' \int_0^{\infty} dk_m \left|\frac{k_m}{kk'}\right| V_{\mathrm{abs}}^2\, T_1(k,k',k_m) \\
&\times \left(\cos^2(\vartheta)\sin^2(\vartheta) + \cos^2(\vartheta')\sin^2(\vartheta') + 2\cos(\vartheta)\sin(\vartheta)\cos(\vartheta')\sin(\vartheta')\cos(\varphi-\varphi')\right) \\
&\times \delta(\epsilon_{k_m} - \epsilon_k - \epsilon_{k'})\, \delta\left(\cos(\varphi-\varphi') + \frac{\cos(\vartheta)\cos(\vartheta')}{\sin(\vartheta)\sin(\vartheta')} - \frac{k_m^2 - k^2 - k'^2}{2kk'\sin(\vartheta)\sin(\vartheta')}\right) \frac{1}{\sin(\vartheta)\sin(\vartheta')} \\
&+ \frac{3a^3}{16\pi^5} \int_0^{\pi} d\vartheta \sin(\vartheta) \int_0^{2\pi} d\varphi \int_0^{k_{\max}} dk'\, k'^2 \int_0^{\pi} d\vartheta'\, \sin(\vartheta') \int_0^{2\pi} d\varphi' \int_0^{\infty} dk_m \left|\frac{k_m}{kk'}\right| V_{\mathrm{abs}}^2\, T_2(k,k',k_m) \\
&\times \left(\cos^2(\vartheta)\sin^2(\vartheta) + \cos^2(\vartheta')\sin^2(\vartheta') + 2\cos(\vartheta)\sin(\vartheta)\cos(\vartheta')\sin(\vartheta')\cos(\varphi-\varphi')\right) \\
&\times \delta(\epsilon_{k'} - \epsilon_{k_m} - \epsilon_k)\, \delta\left(\cos(\varphi-\varphi') + \frac{\cos(\vartheta)\cos(\vartheta')}{\sin(\vartheta)\sin(\vartheta')} + \frac{k_m^2 - k^2 - k'^2}{2kk'\sin(\vartheta)\sin(\vartheta')}\right) \frac{1}{\sin(\vartheta)\sin(\vartheta')} \\
&+ \frac{3a^3}{16\pi^5} \int_0^{\pi} d\vartheta \sin(\vartheta) \int_0^{2\pi} d\varphi \int_0^{k_{\max}} dk'\, k'^2 \int_0^{\pi} d\vartheta'\, \sin(\vartheta') \int_0^{2\pi} d\varphi' \int_0^{\infty} dk_m \left|\frac{k_m}{kk'}\right| V_{\mathrm{abs}}^2\, T_3(k,k',k_m) \\
&\times \left(\cos^2(\vartheta)\sin^2(\vartheta) + \cos^2(\vartheta')\sin^2(\vartheta') + 2\cos(\vartheta)\sin(\vartheta)\cos(\vartheta')\sin(\vartheta')\cos(\varphi-\varphi')\right) \\
&\times \delta(\epsilon_{k_m} + \epsilon_{k'} - \epsilon_k)\, \delta\left(\cos(\varphi-\varphi') + \frac{\cos(\vartheta)\cos(\vartheta')}{\sin(\vartheta)\sin(\vartheta')} + \frac{k_m^2 - k^2 - k'^2}{2kk'\sin(\vartheta)\sin(\vartheta')}\right) \frac{1}{\sin(\vartheta)\sin(\vartheta')}\,.
\end{aligned}
\tag{C.35}
$$

Now, we substitute $\varphi \to \varphi + \varphi'$.

$$
\begin{aligned}
0 =& \frac{3a^3}{16\pi^5} \int_0^{\pi} d\vartheta \sin(\vartheta) \int_0^{2\pi} d\varphi \int_0^{k_{\max}} dk'\, k'^2 \int_0^{\pi} d\vartheta'\, \sin(\vartheta') \int_0^{2\pi} d\varphi' \int_0^{\infty} dk_m \left|\frac{k_m}{kk'}\right| V_{\mathrm{abs}}^2\, T_1(k,k',k_m) \\
&\times \left(\cos^2(\vartheta)\sin^2(\vartheta) + \cos^2(\vartheta')\sin^2(\vartheta') + 2\cos(\vartheta)\sin(\vartheta)\cos(\vartheta')\sin(\vartheta')\cos(\varphi)\right) \\
&\times \delta(\epsilon_{k_m} - \epsilon_k - \epsilon_{k'})\, \delta\left(\cos(\varphi) + \frac{\cos(\vartheta)\cos(\vartheta')}{\sin(\vartheta)\sin(\vartheta')} - \frac{k_m^2 - k^2 - k'^2}{2kk'\sin(\vartheta)\sin(\vartheta')}\right) \frac{1}{\sin(\vartheta)\sin(\vartheta')} \\
&+ \frac{3a^3}{16\pi^5} \int_0^{\pi} d\vartheta \sin(\vartheta) \int_0^{2\pi} d\varphi \int_0^{k_{\max}} dk'\, k'^2 \int_0^{\pi} d\vartheta'\, \sin(\vartheta') \int_0^{2\pi} d\varphi' \int_0^{\infty} dk_m \left|\frac{k_m}{kk'}\right| V_{\mathrm{abs}}^2\, T_2(k,k',k_m) \\
&\times \left(\cos^2(\vartheta)\sin^2(\vartheta) + \cos^2(\vartheta')\sin^2(\vartheta') + 2\cos(\vartheta)\sin(\vartheta)\cos(\vartheta')\sin(\vartheta')\cos(\varphi)\right) \\
&\times \delta(\epsilon_{k'} - \epsilon_{k_m} - \epsilon_k)\, \delta\left(\cos(\varphi) + \frac{\cos(\vartheta)\cos(\vartheta')}{\sin(\vartheta)\sin(\vartheta')} + \frac{k_m^2 - k^2 - k'^2}{2kk'\sin(\vartheta)\sin(\vartheta')}\right) \frac{1}{\sin(\vartheta)\sin(\vartheta')} \\
&+ \frac{3a^3}{16\pi^5} \int_0^{\pi} d\vartheta \sin(\vartheta) \int_0^{2\pi} d\varphi \int_0^{k_{\max}} dk'\, k'^2 \int_0^{\pi} d\vartheta'\, \sin(\vartheta') \int_0^{2\pi} d\varphi' \int_0^{\infty} dk_m \left|\frac{k_m}{kk'}\right| V_{\mathrm{abs}}^2\, T_3(k,k',k_m) \\
&\times \left(\cos^2(\vartheta)\sin^2(\vartheta) + \cos^2(\vartheta')\sin^2(\vartheta') + 2\cos(\vartheta)\sin(\vartheta)\cos(\vartheta')\sin(\vartheta')\cos(\varphi)\right) \\
&\times \delta(\epsilon_{k_m} + \epsilon_{k'} - \epsilon_k)\, \delta\left(\cos(\varphi) + \frac{\cos(\vartheta)\cos(\vartheta')}{\sin(\vartheta)\sin(\vartheta')} + \frac{k_m^2 - k^2 - k'^2}{2kk'\sin(\vartheta)\sin(\vartheta')}\right) \frac{1}{\sin(\vartheta)\sin(\vartheta')}\,.
\end{aligned}
\tag{C.36}
$$

Thus, we are able to perform the integration via φ'. For the φ-integration, the term does only depend on $\cos(\varphi)$. Thus, we can separate the integration into 0 to π and π to 2π.

$$\begin{aligned}
0 =& \frac{3a^3}{16\pi^5} 4\pi \int_0^\pi d\vartheta \sin(\vartheta) \int_0^\pi d\varphi \int_0^{k_\mathrm{max}} dk'\, k'^2 \int_0^\pi d\vartheta'\, \sin(\vartheta') \int_0^\infty dk_m \left|\frac{k_m}{kk'}\right| V_\mathrm{abs}^2\, T_1(k,k',k_m) \\
&\times \left(\cos^2(\vartheta)\sin^2(\vartheta) + \cos^2(\vartheta')\sin^2(\vartheta') + 2\cos(\vartheta)\sin(\vartheta)\cos(\vartheta')\sin(\vartheta')\cos(\varphi)\right) \\
&\times \delta(\epsilon_{k_m} - \epsilon_k - \epsilon_{k'})\, \delta\left(\cos(\varphi) + \frac{\cos(\vartheta)\cos(\vartheta')}{\sin(\vartheta)\sin(\vartheta')} - \frac{k_m^2 - k^2 - k'^2}{2kk'\sin(\vartheta)\sin(\vartheta')}\right) \frac{1}{\sin(\vartheta)\sin(\vartheta')} \\
&+ \frac{3a^3}{16\pi^5} 4\pi \int_0^\pi d\vartheta \sin(\vartheta) \int_0^\pi d\varphi \int_0^{k_\mathrm{max}} dk'\, k'^2 \int_0^\pi d\vartheta'\, \sin(\vartheta') \int_0^\infty dk_m \left|\frac{k_m}{kk'}\right| V_\mathrm{abs}^2\, T_2(k,k',k_m) \\
&\times \left(\cos^2(\vartheta)\sin^2(\vartheta) + \cos^2(\vartheta')\sin^2(\vartheta') + 2\cos(\vartheta)\sin(\vartheta)\cos(\vartheta')\sin(\vartheta')\cos(\varphi)\right) \\
&\times \delta(\epsilon_{k'} - \epsilon_{k_m} - \epsilon_k)\, \delta\left(\cos(\varphi) + \frac{\cos(\vartheta)\cos(\vartheta')}{\sin(\vartheta)\sin(\vartheta')} + \frac{k_m^2 - k^2 - k'^2}{2kk'\sin(\vartheta)\sin(\vartheta')}\right) \frac{1}{\sin(\vartheta)\sin(\vartheta')} \\
&+ \frac{3a^3}{16\pi^5} 4\pi \int_0^\pi d\vartheta \sin(\vartheta) \int_0^\pi d\varphi \int_0^{k_\mathrm{max}} dk'\, k'^2 \int_0^\pi d\vartheta'\, \sin(\vartheta') \int_0^\infty dk_m \left|\frac{k_m}{kk'}\right| V_\mathrm{abs}^2\, T_3(k,k',k_m) \\
&\times \left(\cos^2(\vartheta)\sin^2(\vartheta) + \cos^2(\vartheta')\sin^2(\vartheta') + 2\cos(\vartheta)\sin(\vartheta)\cos(\vartheta')\sin(\vartheta')\cos(\varphi)\right) \\
&\times \delta(\epsilon_{k_m} + \epsilon_{k'} - \epsilon_k)\, \delta\left(\cos(\varphi) + \frac{\cos(\vartheta)\cos(\vartheta')}{\sin(\vartheta)\sin(\vartheta')} + \frac{k_m^2 - k^2 - k'^2}{2kk'\sin(\vartheta)\sin(\vartheta')}\right) \frac{1}{\sin(\vartheta)\sin(\vartheta')}\,.
\end{aligned} \tag{C.37}$$

Additionally, we perform a transformation $p = \cos(\varphi)$ of the angular delta-function and find

$$\begin{aligned}
0 =& \frac{3a^3}{16\pi^5} 4\pi \int_0^\pi d\vartheta \int_1^{-1} dp \int_0^{k_\mathrm{max}} dk'\, k'^2 \int_0^\pi d\vartheta' \int_0^\infty dk_m \left|\frac{k_m}{kk'}\right| V_\mathrm{abs}^2\, T_1(k,k',k_m) \\
&\times \left(\cos^2(\vartheta)\sin^2(\vartheta) + \cos^2(\vartheta')\sin^2(\vartheta') + 2\cos(\vartheta)\sin(\vartheta)\cos(\vartheta')\sin(\vartheta')\, p\right) \\
&\times \delta(\epsilon_{k_m} - \epsilon_k - \epsilon_{k'})\, \delta\left(p + \frac{\cos(\vartheta)\cos(\vartheta')}{\sin(\vartheta)\sin(\vartheta')} - \frac{k_m^2 - k^2 - k'^2}{2kk'\sin(\vartheta)\sin(\vartheta')}\right) \frac{1}{-\sin(\arccos(p))} \\
&+ \frac{3a^3}{16\pi^5} 4\pi \int_0^\pi d\vartheta \int_1^{-1} dp \int_0^{k_\mathrm{max}} dk'\, k'^2 \int_0^\pi d\vartheta' \int_0^\infty dk_m \left|\frac{k_m}{kk'}\right| V_\mathrm{abs}^2\, T_2(k,k',k_m) \\
&\times \left(\cos^2(\vartheta)\sin^2(\vartheta) + \cos^2(\vartheta')\sin^2(\vartheta') + 2\cos(\vartheta)\sin(\vartheta)\cos(\vartheta')\sin(\vartheta')\, p\right) \\
&\times \delta(\epsilon_{k'} - \epsilon_{k_m} - \epsilon_k)\, \delta\left(p + \frac{\cos(\vartheta)\cos(\vartheta')}{\sin(\vartheta)\sin(\vartheta')} + \frac{k_m^2 - k^2 - k'^2}{2kk'\sin(\vartheta)\sin(\vartheta')}\right) \frac{1}{-\sin(\arccos(p))} \\
&+ \frac{3a^3}{16\pi^5} 4\pi \int_0^\pi d\vartheta \int_1^{-1} dp \int_0^{k_\mathrm{max}} dk'\, k'^2 \int_0^\pi d\vartheta' \int_0^\infty dk_m \left|\frac{k_m}{kk'}\right| V_\mathrm{abs}^2\, T_3(k,k',k_m) \\
&\times \left(\cos^2(\vartheta)\sin^2(\vartheta) + \cos^2(\vartheta')\sin^2(\vartheta') + 2\cos(\vartheta)\sin(\vartheta)\cos(\vartheta')\sin(\vartheta')\, p\right) \\
&\times \delta(\epsilon_{k_m} + \epsilon_{k'} - \epsilon_k)\, \delta\left(p + \frac{\cos(\vartheta)\cos(\vartheta')}{\sin(\vartheta)\sin(\vartheta')} + \frac{k_m^2 - k^2 - k'^2}{2kk'\sin(\vartheta)\sin(\vartheta')}\right) \frac{1}{-\sin(\arccos(p))}\,.
\end{aligned} \tag{C.38}$$

We solve the p-integral

$$\begin{aligned}
0 =& \frac{3a^3N}{16\pi^5} 4\pi \int_0^\pi d\vartheta \int_0^{k_{\max}} dk'\, k'^2 \int_0^\pi d\vartheta' \int_0^\infty dk_m \left|\frac{k_m}{kk'}\right| V_{\text{abs}}^2\, T_1(k,k',k_m) \\
&\times \left(\cos^2(\vartheta)\sin^2(\vartheta) + \cos^2(\vartheta')\sin^2(\vartheta') - 2\cos(\vartheta)\sin(\vartheta)\cos(\vartheta')\sin(\vartheta')\,\beta^-\right) \\
&\times \delta(\epsilon_{k_m} - \epsilon_k - \epsilon_{k'})\,\Theta(1-\beta^-)\,\Theta(1+\beta^-)\,\frac{1}{\sqrt{1-(\beta^-)^2}} \\
&+ \frac{3a^3N}{16\pi^5} 4\pi \int_0^\pi d\vartheta \int_0^{k_{\max}} dk'\, k'^2 \int_0^\pi d\vartheta' \int_0^\infty dk_m \left|\frac{k_m}{kk'}\right| V_{\text{abs}}^2\, T_2(k,k',k_m) \\
&\times \left(\cos^2(\vartheta)\sin^2(\vartheta) + \cos^2(\vartheta')\sin^2(\vartheta') - 2\cos(\vartheta)\sin(\vartheta)\cos(\vartheta')\sin(\vartheta')\,\beta^+\right) \\
&\times \delta(\epsilon_{k'} - \epsilon_{k_m} - \epsilon_k)\,\Theta(1-\beta^+)\,\Theta(1+\beta^+)\,\frac{1}{\sqrt{1-(\beta^+)^2}} \\
&+ \frac{3a^3N}{16\pi^5} 4\pi \int_0^\pi d\vartheta \int_0^{k_{\max}} dk'\, k'^2 \int_0^\pi d\vartheta' \int_0^\infty dk_m \left|\frac{k_m}{kk'}\right| V_{\text{abs}}^2\, T_3(k,k',k_m) \\
&\times \left(\cos^2(\vartheta)\sin^2(\vartheta) + \cos^2(\vartheta')\sin^2(\vartheta') - 2\cos(\vartheta)\sin(\vartheta)\cos(\vartheta')\sin(\vartheta')\,\beta^+\right) \\
&\times \delta(\epsilon_{k_m} + \epsilon_{k'} - \epsilon_k)\,\Theta(1-\beta^+)\,\Theta(1+\beta^+)\,\frac{1}{\sqrt{1-(\beta^+)^2}}\,,
\end{aligned} \tag{C.39}$$

with

$$\beta^+ = \frac{\cos(\vartheta)\cos(\vartheta') + \alpha}{\sin(\vartheta)\sin(\vartheta')} \qquad \beta^- = \frac{\cos(\vartheta)\cos(\vartheta') - \alpha}{\sin(\vartheta)\sin(\vartheta')} \qquad \alpha = \frac{k_m^2 - k^2 - k'^2}{2kk'}\,. \tag{C.40}$$

Now, we want to handle the integration via ϑ and ϑ' in Eq. (C.39). Since, it is not possible to solve the resulting integral of ϑ and ϑ', one has to perform it numerically. This we can treat by performing an approximation of the solution to the integral dependent on the parameter α out of Eq. (C.40). Because of Eq. (C.28), it is $0 \leq k \leq k_{\max}$ and $0 \leq k' \leq k_{\max}$, the parameter α is limited to $-1 \leq \alpha \leq 1$. We can write down the integral

$$\begin{aligned}
h(\alpha) =& \int d\vartheta \int d\vartheta'\, \Theta(1-\beta^\pm)\,\Theta(1+\beta^\pm)\,\frac{1}{\sqrt{1-(\beta^\pm)^2}} \\
&\times \left(\cos^2(\vartheta)\sin^2(\vartheta) + \cos^2(\vartheta')\sin^2(\vartheta') - 2\cos(\vartheta)\sin(\vartheta)\cos(\vartheta')\sin(\vartheta')\,\beta^\pm\right)\,.
\end{aligned} \tag{C.41}$$

At the end, the result can be approximated in the following way

$$h(\alpha) \approx \Theta(1-|\alpha|)\left(c_1 + c_2\,\alpha^2 + c_3\,\alpha^4\right)\,. \tag{C.42}$$

One finds

$$c_1 = 0.838041 \tag{C.43}$$
$$c_2 = 2.49346 \tag{C.44}$$
$$c_3 = 0.0113386\,. \tag{C.45}$$

In figure 53, the accordance of the approximation is shown.

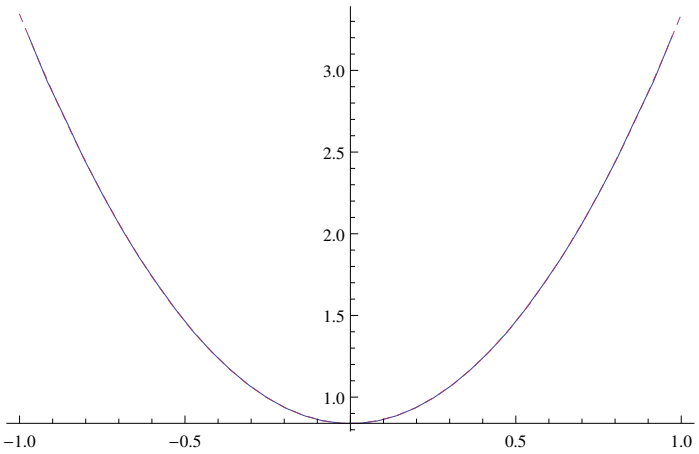

Figure 53: Plot of function $h(\alpha)$. The blue and solid line describes the numeric evaluation of Eq. (C.41). The red and dashed line denotes the approximated function out of Eq. (C.42)

Including this approximation, we find for the collision integral

$$\begin{aligned}0 =&\frac{3a^3N}{4\pi^4}\int_0^{k_{\max}} dk'\,k'^2\int_0^{\infty} dk_m \left|\frac{k_m}{kk'}\right| V_{\text{abs}}^2\, T_1(k,k',k_m)\,\delta(\epsilon_{k_m}-\epsilon_k-\epsilon_{k'})\,h\left(\frac{k_m^2-k^2-k'^2}{2kk'}\right)\\ &+\frac{3a^3N}{4\pi^4}\int_0^{k_{\max}} dk'\,k'^2\int_0^{\infty} dk_m \left|\frac{k_m}{kk'}\right| V_{\text{abs}}^2\, T_2(k,k',k_m)\,\delta(\epsilon_{k'}-\epsilon_{k_m}-\epsilon_k)\,h\left(\frac{k_m^2-k^2-k'^2}{2kk'}\right)\\ &+\frac{3a^3N}{4\pi^4}\int_0^{k_{\max}} dk'\,k'^2\int_0^{\infty} dk_m \left|\frac{k_m}{kk'}\right| V_{\text{abs}}^2\, T_3(k,k',k_m)\,\delta(\epsilon_{k_m}+\epsilon_{k'}-\epsilon_k)\,h\left(\frac{k_m^2-k^2-k'^2}{2kk'}\right).\end{aligned} \tag{C.46}$$

Since k_m is no longer dependent on k', it is now very simple to solve the energy-delta-distribution for the k'-integration. One still has to consider, that the k'-integration only takes place in the first Brillouin zone. It is $k_{\max}=k_{\text{F}}$. We set the energy dispersion for the magnons [43, p. 181] for $k\le k_F$

$$\epsilon_k=\omega_H+D_{\text{ex}}k^2\,, \tag{C.47}$$

and for $k>k_{\text{F}}\wedge k\le 2k_{\text{F}}$

$$\epsilon_k=\omega_H+D_{\text{ex}}(2k_{\text{F}}-k)^2\,. \tag{C.48}$$

Now, we separate the calculation into normal processes N_p and Umklapp processes U. Here, we regard the Umklapp processes of k, k' and k_m. It is

$$0=N_p+U\,. \tag{C.49}$$

Thus

$$\begin{aligned}N_p =&\frac{3a^3}{4\pi^4}\frac{1}{2D_{\text{ex}}}\int_0^{k_{\text{F}}} dk_m\,\frac{k_m}{k}\,h\left(\frac{k_m^2-k^2-k'^2}{2kk'}\right) V_{\text{abs}}^2\,\Theta(k_{\text{F}}-k')\,\Theta(k')\,T_1(k,k',k_m)\Big|_{k'=\sqrt{\frac{\epsilon_{k_m}-\epsilon_k-\epsilon_0}{D_{\text{ex}}}}}\\ &+\frac{3a^3}{4\pi^4}\frac{1}{2D_{\text{ex}}}\int_0^{k_{\text{F}}} dk_m\,\frac{k_m}{k}\,h\left(\frac{k_m^2-k^2-k'^2}{2kk'}\right) V_{\text{abs}}^2\,\Theta(k_{\text{F}}-k')\,\Theta(k')\,T_2(k,k',k_m)\Big|_{k'=\sqrt{\frac{\epsilon_{k_m}+\epsilon_k-\epsilon_0}{D_{\text{ex}}}}}\\ &+\frac{3a^3}{4\pi^4}\frac{1}{2D_{\text{ex}}}\int_0^{k_{\text{F}}} dk_m\,\frac{k_m}{k}\,h\left(\frac{k_m^2-k^2-k'^2}{2kk'}\right) V_{\text{abs}}^2\,\Theta(k_{\text{F}}-k')\,\Theta(k')\,T_3(k,k',k_m)\Big|_{k'=\sqrt{\frac{\epsilon_k-\epsilon_{k_m}-\epsilon_0}{D_{\text{ex}}}}}.\end{aligned} \tag{C.50}$$

For the Umklapp processes we choose a symmetrized way. It is

$$\begin{aligned} U =& \frac{1}{3} N_p \left(k_m \in [k_\mathrm{F}, 2k_\mathrm{F}]\right) + \frac{1}{3} \frac{k'}{|2k_\mathrm{F} - k'|} N_p \left(k' \in [k_\mathrm{F}, 2k_\mathrm{F}]\right) \\ &+ \frac{1}{3} N_p \left(k \in [k_\mathrm{F}, 2k_\mathrm{F}]\right) . \end{aligned} \tag{C.51}$$

The extra factor in the second summand arises from a different algebraic term of the energy dispersion $\epsilon_{\vec{k}'} = \omega_H + D_\mathrm{ex}(2k_\mathrm{F} - k')^2$ for $k' \in [k_\mathrm{F}, 2k_\mathrm{F}]$.

C.2 Four particle interaction - exchange interaction

C.2.1 Hamilton operator

Now, we consider the exchange interaction between magnons. We write down the following Hamilton operator for the magnons

$$\hat{H}_\mathrm{Heisenberg} = -J \sum_{\langle mn \rangle} \vec{S}_m \vec{S}_n \,, \tag{C.52}$$

while J denotes the coupling constant or exchange energy and where $\langle mn \rangle$ denotes the summation over the nearest neighbors. We introduce raising and lowering operators

$$S^+_{\vec{m}} = S^x_{\vec{m}} + iS^y_{\vec{m}} \qquad S^-_{\vec{m}} = S^x_{\vec{m}} - iS^y_{\vec{m}} \qquad S^z_{\vec{m}} = S^z_{\vec{m}} \,, \tag{C.53}$$

while $S^\pm_m$ denote the lowering (-) and raising (+) operators. The commutator relations are [54, p. 76]

$$\left[S^i_{\vec{m}}, S^j_{\vec{n}}\right] = i\delta_{\vec{m},\vec{n}} \epsilon^{ijk} S^k_{\vec{m}} \qquad \left[S^z_{\vec{m}}, S^\pm_{\vec{n}}\right] = \pm\delta_{\vec{m},\vec{n}} S^\pm_{\vec{m}} \qquad \left[S^+_{\vec{m}}, S^-_{\vec{n}}\right] = 2\delta_{\vec{m},\vec{n}} S^z_{\vec{m}} \,. \tag{C.54}$$

We perform the Holstein-Primakoff-transformation [43, p. 207] and rewrite the Hamilton operator. The simple case of the calculation can be found in Ref. [54, p. 77 ff]. The Holstein-Primakoff-transformation is performed by introducing the following operators

$$S^-_{\vec{m}} = a^\dagger_{\vec{m}} \sqrt{2S - a^\dagger_{\vec{m}} a_{\vec{m}}} \qquad S^+_m = \sqrt{2S - a^\dagger_{\vec{m}} a_{\vec{m}}}\, a_m \qquad S^z_{\vec{m}} = S - a^\dagger_{\vec{m}} a_{\vec{m}} \,. \tag{C.55}$$

The operators $a_{\vec{m}}$ and $a^\dagger_{\vec{m}}$ denote the annihilation and the creation of one magnon at position $\vec{m}$, respectively. All operators fulfill the common commutation relations.

$$[a_{\vec{m}}, a_{\vec{n}}] = 0 \qquad \left[a^\dagger_{\vec{m}}, a^\dagger_{\vec{n}}\right] = 0 \qquad \left[a_{\vec{m}}, a^\dagger_{\vec{n}}\right] = \delta_{\vec{m},\vec{n}} \,. \tag{C.56}$$

Since $S = 14.2$ (cf. Eq. (B.28)), the above operators may be approximated as

$$S^-_{\vec{m}} \approx \sqrt{2S} a^\dagger_{\vec{m}} - \frac{1}{\sqrt{8S}} a^\dagger_{\vec{m}} a^\dagger_{\vec{m}} a_{\vec{m}} \qquad S^+_{\vec{m}} \approx \sqrt{2S} a_{\vec{m}} - \frac{1}{\sqrt{8S}} a^\dagger_{\vec{m}} a_{\vec{m}} a_{\vec{m}} \,. \tag{C.57}$$

One finds the following expansion of the operator product

$$\hat{H}_{\text{Heisenberg}} = -J\sum_{\vec{m},i}\vec{S}_{\vec{m}}\vec{S}_{\vec{m}+\vec{e}_i} = -J\sum_{\vec{m},i}\left(S^z_{\vec{m}}S^z_{\vec{m}+\vec{e}_i}+\frac{1}{2}\left(S^+_{\vec{m}}S^-_{\vec{m}+\vec{e}_i}+S^-_{\vec{m}}S^+_{\vec{m}+\vec{e}_i}\right)\right) \tag{C.58}$$

$$\begin{aligned}
&= -JNS^2 - JS\sum_{\vec{m},i}\left(-2a^\dagger_{\vec{m}}a_{\vec{m}}+a^\dagger_{\vec{m}}a_{\vec{m}+\vec{e}_i}+a_{\vec{m}}a^\dagger_{\vec{m}+\vec{e}_i}\right)\\
&\quad-\frac{J}{4}\sum_{\vec{m},i}\left(4a^\dagger_{\vec{m}}a_{\vec{m}}a^\dagger_{\vec{m}+\vec{e}_i}a_{\vec{m}+\vec{e}_i}-a^\dagger_{\vec{m}}a_{\vec{m}}a_{\vec{m}}a^\dagger_{\vec{m}+\vec{e}_i}-a_{\vec{m}}a^\dagger_{\vec{m}+\vec{e}_i}a^\dagger_{\vec{m}+\vec{e}_i}a_{\vec{m}+\vec{e}_i}\right)\\
&\quad-\frac{J}{4}\sum_{\vec{m},i}\left(-a^\dagger_{\vec{m}}a^\dagger_{\vec{m}}a_{\vec{m}}a_{\vec{m}+\vec{e}_i}-a^\dagger_{\vec{m}}a^\dagger_{\vec{m}+\vec{e}_i}a_{\vec{m}+\vec{e}_i}a_{\vec{m}+\vec{e}_i}\right).
\end{aligned} \tag{C.59}$$

Hence, we find

$$\begin{aligned}
\hat{H}_{\text{Heisenberg}} &= -JNS^2 - JS\sum_{\vec{m},i}\left(-2a^\dagger_{\vec{m}}a_{\vec{m}}+a^\dagger_{\vec{m}}a_{\vec{m}+\vec{e}_i}+a_{\vec{m}}a^\dagger_{\vec{m}+\vec{e}_i}\right)\\
&\quad-\frac{J}{4}\sum_{\vec{m},i}\left(4a^\dagger_{\vec{m}}a^\dagger_{\vec{m}+\vec{e}_i}a_{\vec{m}}a_{\vec{m}+\vec{e}_i}\right)\\
&\quad-\frac{J}{4}\sum_{\vec{m},i}\left(-a^\dagger_{\vec{m}}a^\dagger_{\vec{m}+\vec{e}_i}a_{\vec{m}}a_{\vec{m}}-a^\dagger_{\vec{m}+\vec{e}_i}a^\dagger_{\vec{m}}a_{\vec{m}}a_{\vec{m}}-a^\dagger_{\vec{m}}a^\dagger_{\vec{m}}a_{\vec{m}}a_{\vec{m}+\vec{e}_i}-a^\dagger_{\vec{m}}a^\dagger_{\vec{m}}a_{\vec{m}+\vec{e}_i}a_{\vec{m}}\right),
\end{aligned} \tag{C.60}$$

while $\vec{e}_i$ denotes the vector in direction i with length of the lattice constant. Let us now perform a Fourier transformation. We use

$$a_{\vec{k}} = \frac{1}{\sqrt{N}}\sum_{m_1,m_2,m_3=1}^{\sqrt[3]{N}} e^{i\vec{k}\vec{m}}a_{\vec{m}} \qquad a_{\vec{m}} = \frac{1}{\sqrt{N}}\sum_{\vec{k}}^{\text{B.Z.}} e^{-i\vec{k}\vec{m}}a_{\vec{k}}\,. \tag{C.61}$$

The operators $a_{\vec{k}}$ and $a^\dagger_{\vec{k}}$ denote the annihilation and the creation of one magnon with wave vector $\vec{k}$, respectively. The commutator relations are still fulfilled in the reciprocal case. It is

$$\left[a_{\vec{k}},a_{\vec{k}'}\right]=0 \qquad \left[a^\dagger_{\vec{k}},a^\dagger_{\vec{k}'}\right]=0 \qquad \left[a_{\vec{k}},a^\dagger_{\vec{k}'}\right]=\delta_{\vec{k},\vec{k}'}\,. \tag{C.62}$$

After set in the transformation, we perform the sum over m which leads to delta-distributions. We introduce the abbreviations $\vec{k}_3=\vec{k}-\vec{q}$ and $\vec{k}_4=\vec{k}'+\vec{q}$. A symmetrized version can be written down

$$\begin{aligned}
&= -JNS^2 - JS\sum_{\vec{k},i}^{\text{B.Z.}}\left(-2a^\dagger_{\vec{k}}a_{\vec{k}}+e^{-ik_i}a^\dagger_{\vec{k}}a_{\vec{k}}+e^{+ik_i}a^\dagger_{\vec{k}}a_{\vec{k}}\right)\\
&\quad-\frac{J}{4N}\sum_{\vec{k}\vec{k}'\vec{q},i}^{\text{B.Z.}}\frac{1}{2}4\left(e^{iq'_i}+e^{-iq'_i}\right)a^\dagger_{\vec{k}}a^\dagger_{\vec{k}'}a_{\vec{k}-\vec{q}}a_{\vec{k}'+\vec{q}}\\
&\quad-\frac{J}{4N}\sum_{\vec{k}\vec{k}'\vec{q},i}^{\text{B.Z.}}\frac{1}{2}\left(-e^{ik'_i}-e^{-ik'_i}-e^{ik_i}-e^{-ik_i}-e^{ik_{4,i}}-e^{-ik_{4,i}}-e^{ik_{3,i}}-e^{-ik_{3,i}}\right)a^\dagger_{\vec{k}}a^\dagger_{\vec{k}'}a_{\vec{k}-\vec{q}}a_{\vec{k}'+\vec{q}}.
\end{aligned} \tag{C.63}$$

This is

$$
\begin{aligned}
&= - JNS^2 - JS \sum_{\vec{k},i}^{\text{B.Z.}} \left(-2 + 2\cos(k_i)\right) a^\dagger_{\vec{k}} a_{\vec{k}} \\
&\quad - \frac{J}{4N} \sum_{\vec{k}\vec{k}'\vec{q},i}^{\text{B.Z.}} \left(4\cos(q_i) - \cos(k_i) - \cos(k_i') - \cos(k_{3,i}) - \cos(k_{4,i})\right) a^\dagger_{\vec{k}} a^\dagger_{\vec{k}'} a_{\vec{k}-\vec{q}} a_{\vec{k}'+\vec{q}} \qquad \text{(C.64)} \\
&\approx - JNS^2 + \sum_{\vec{k},i}^{\text{B.Z.}} D_{\text{ex}} k^2 a^\dagger_{\vec{k}} a_{\vec{k}} \\
&\quad - \frac{J}{4N} \sum_{\vec{k}\vec{k}'\vec{q},i}^{\text{B.Z.}} \frac{a^2}{2} \left(k_i^2 + k_i'^2 + k_{3,i}^2 + k_{4,i}^2 - 4q_i^2\right) a^\dagger_{\vec{k}} a^\dagger_{\vec{k}'} a_{\vec{k}-\vec{q}} a_{\vec{k}'+\vec{q}}, \qquad \text{(C.65)}
\end{aligned}
$$

with

$$\vec{k}_3 = \vec{k} - \vec{q} \qquad \vec{k}_4 = \vec{k}' + \vec{q}. \qquad \text{(C.66)}$$

We can read out the interaction prefactor for the exchange-interaction

$$|V_{\text{ex}}| = \frac{Ja^2}{8N}(k^2 + k'^2 + k_3^2 + k_4^2 - 4q^2)\,. \qquad \text{(C.67)}$$

To calculate the coupling parameter J, we use an identity from [43, p. 210]. If one only includes first nearest neighbor hopping, one finds for a simple cubic lattice

$$J \approx \frac{D_{\text{ex}}}{Sa^2}\,. \qquad \text{(C.68)}$$

It is

$$
\begin{aligned}
\hbar &= 1.05457266 \cdot 10^{-34}\,\text{Js} && \text{(C.69)} \\
S &= 14.2\,[53] && \text{(C.70)} \\
D_{\text{ex}} &= 9.16 \cdot 10^{-11}\,\text{GHz cm}^2 [43, p.\ 182] && \text{(C.71)} \\
a &= 1.2376\,\text{nm}\,[52,\ 53]\,. && \text{(C.72)}
\end{aligned}
$$

Thus, we find

$$J = 421.159\,\text{GHz}\,. \qquad \text{(C.73)}$$

C.2.2 Collision integral

Now, we set up the collision integral of the Boltzmann equation (see Eq. (11.22) on page 294 in Ref. [43] or Eq. (5.61))

$$
\begin{aligned}
\left.\frac{\partial f_{\vec{k}}}{\partial t}\right|_{\text{St}} =& \frac{1}{2} \sum_{\vec{q}\vec{k}'} \Big\{ W(\text{M}_{\vec{k}-\vec{q}} + \text{M}_{\vec{k}'+\vec{q}} \to \text{M}_{\vec{k}} + \text{M}_{\vec{k}'}) + W(\text{M}_{\vec{k}'+\vec{q}} + \text{M}_{\vec{k}-\vec{q}} \to \text{M}_{\vec{k}} + \text{M}_{\vec{k}'}) \\
& - W(\text{M}_{\vec{k}} + \text{M}_{\vec{k}'} \to \text{M}_{\vec{k}-\vec{q}} + \text{M}_{\vec{k}'+\vec{q}}) - W(\text{M}_{\vec{k}} + \text{M}_{\vec{k}'} \to \text{M}_{\vec{k}'+\vec{q}} + \text{M}_{\vec{k}-\vec{q}}) \Big\} \qquad \text{(C.74)} \\
=& \frac{1}{2} \frac{2\pi}{\hbar} \sum_{\vec{q}\vec{k}'} |V|^2 \delta(\epsilon_{\vec{k}} + \epsilon_{\vec{k}'} - \epsilon_{\vec{k}-\vec{q}} - \epsilon_{\vec{k}'+\vec{q}}) \cdot 16 \cdot f_{\vec{k}-\vec{q}} f_{\vec{k}'+\vec{q}} (1 + f_{\vec{k}})(1 + f_{\vec{k}'}) \\
& - \frac{1}{2} \frac{2\pi}{\hbar} \sum_{\vec{q}\vec{k}'} |V|^2 \delta(\epsilon_{\vec{k}} + \epsilon_{\vec{k}'} - \epsilon_{\vec{k}-\vec{q}} - \epsilon_{\vec{k}'+\vec{q}}) \cdot 16 \cdot (1 + f_{\vec{k}-\vec{q}})(1 + f_{\vec{k}'+\vec{q}}) f_{\vec{k}} f_{\vec{k}'}\,. \qquad \text{(C.75)}
\end{aligned}
$$

We perform a first order Taylor expansion for the temperatures and find:

$$\begin{aligned}\left.\frac{\partial f_{\vec{k}}}{\partial t}\right|_{\mathrm{St}} \approx & \frac{16\pi}{\hbar}\sum_{\vec{q}\vec{k}'}|V|^2\delta(\epsilon_{\vec{k}}+\epsilon_{\vec{k}'}-\epsilon_{\vec{k}-\vec{q}}-\epsilon_{\vec{k}'+\vec{q}})\cdot f^0_{\vec{k}-\vec{q}}f^0_{\vec{k}'+\vec{q}}(1+f^0_{\vec{k}})(1+f^0_{\vec{k}'})\frac{1}{k_BT_0^2} \\ & \times\left[-\epsilon_{\vec{k}}T_{\mathrm{M}}(\vec{k})-\epsilon_{\vec{k}'}T_{\mathrm{M}}(\vec{k}')+\epsilon_{\vec{k}-\vec{q}}T_{\mathrm{M}}(\vec{k}-\vec{q})+\epsilon_{\vec{k}'+\vec{q}}T_{\mathrm{M}}(\vec{k}'+\vec{q})\right]. \qquad \text{(C.76)}\end{aligned}$$

At the end, the collision integral can be written in relaxation time notation

$$\left.\frac{\partial f_{\vec{k}}}{\partial t}\right|_{\mathrm{St}} \approx \sum_{\vec{q}\vec{k}'}\left\{\frac{|V|^2}{\tau_{M1}}\frac{T_{\mathrm{M}}(\vec{k})}{T_0}+\frac{|V|^2}{\tau_{M2}}\frac{T_{\mathrm{M}}(\vec{k}')}{T_0}+\frac{|V|^2}{\tau_{M3}}\frac{T_{\mathrm{M}}(\vec{k}-\vec{q})}{T_0}+\frac{|V|^2}{\tau_{M4}}\frac{T_{\mathrm{M}}(\vec{k}'+\vec{q})}{T_0}\right\}, \qquad \text{(C.77)}$$

with

$$\frac{1}{\tau_{M1}} = \frac{1}{\tilde{\tau}_{M1}}\delta(\epsilon_{\vec{k}}+\epsilon_{\vec{k}'}-\epsilon_{\vec{k}-\vec{q}}-\epsilon_{\vec{k}'+\vec{q}}) \qquad \text{(C.78)}$$

$$\frac{1}{\tau_{M2}} = \frac{1}{\tilde{\tau}_{M2}}\delta(\epsilon_{\vec{k}}+\epsilon_{\vec{k}'}-\epsilon_{\vec{k}-\vec{q}}-\epsilon_{\vec{k}'+\vec{q}}) \qquad \text{(C.79)}$$

$$\frac{1}{\tau_{M3}} = \frac{1}{\tilde{\tau}_{M3}}\delta(\epsilon_{\vec{k}}+\epsilon_{\vec{k}'}-\epsilon_{\vec{k}-\vec{q}}-\epsilon_{\vec{k}'+\vec{q}}) \qquad \text{(C.80)}$$

$$\frac{1}{\tau_{M4}} = \frac{1}{\tilde{\tau}_{M4}}\delta(\epsilon_{\vec{k}}+\epsilon_{\vec{k}'}-\epsilon_{\vec{k}-\vec{q}}-\epsilon_{\vec{k}'+\vec{q}}), \qquad \text{(C.81)}$$

and

$$\frac{1}{\tilde{\tau}_{M1}} = \frac{16\pi}{\hbar}\cdot f^0_{\vec{k}-\vec{q}}f^0_{\vec{k}'+\vec{q}}(1+f^0_{\vec{k}})(1+f^0_{\vec{k}'})\frac{1}{k_BT_0}(-\epsilon_{\vec{k}}) \qquad \text{(C.82)}$$

$$\frac{1}{\tilde{\tau}_{M2}} = \frac{16\pi}{\hbar}\cdot f^0_{\vec{k}-\vec{q}}f^0_{\vec{k}'+\vec{q}}(1+f^0_{\vec{k}})(1+f^0_{\vec{k}'})\frac{1}{k_BT_0}(-\epsilon_{\vec{k}'}) \qquad \text{(C.83)}$$

$$\frac{1}{\tilde{\tau}_{M3}} = \frac{16\pi}{\hbar}\cdot f^0_{\vec{k}-\vec{q}}f^0_{\vec{k}'+\vec{q}}(1+f^0_{\vec{k}})(1+f^0_{\vec{k}'})\frac{1}{k_BT_0}(+\epsilon_{\vec{k}-\vec{q}}) \qquad \text{(C.84)}$$

$$\frac{1}{\tilde{\tau}_{M4}} = \frac{16\pi}{\hbar}\cdot f^0_{\vec{k}-\vec{q}}f^0_{\vec{k}'+\vec{q}}(1+f^0_{\vec{k}})(1+f^0_{\vec{k}'})\frac{1}{k_BT_0}(+\epsilon_{\vec{k}'+\vec{q}}), \qquad \text{(C.85)}$$

with

$$|V| = |V_{\mathrm{ex}}| = \frac{Ja^2}{8N}(k^2+k'^2+k_3^2+k_4^2-4q^2). \qquad \text{(C.86)}$$

C.2.3 Numerical treatment

For avoiding some difficulties, we perform a transformation of the integration procedure. We start with introducing some abbreviations

$$0 = \sum_{\vec{q}\vec{k}'}|V_{\mathrm{ex}}|^2\cdot T_1(k,k',|\vec{k}-\vec{q}|,|\vec{k}'+\vec{q}|)\delta(\epsilon_{\vec{k}}+\epsilon_{\vec{k}'}-\epsilon_{\vec{k}-\vec{q}}-\epsilon_{\vec{k}'+\vec{q}}), \qquad \text{(C.87)}$$

with

$$T_1(k,k',|\vec{k}-\vec{q}|,|\vec{k}'+\vec{q}|) = \left\{\frac{1}{\tilde{\tau}_{M1}}\frac{T_{\mathrm{M}}(|\vec{k}|)}{T_0}+\frac{1}{\tilde{\tau}_{M2}}\frac{T_{\mathrm{M}}(|\vec{k}'|)}{T_0}+\frac{1}{\tilde{\tau}_{M3}}\frac{T_{\mathrm{M}}(|\vec{k}-\vec{q}|)}{T_0}+\frac{1}{\tilde{\tau}_{M4}}\frac{T_{\mathrm{M}}(|\vec{k}'+\vec{q}|)}{T_0}\right\}. \qquad \text{(C.88)}$$

Because the function T_1 only depends on absolute values, we can write the integration in spherical coordinates. We rewrite the sum into an integral and introduce an integration over

$$k_m = |\vec{k} - \vec{q}| = \sqrt{k^2 + q^2 - 2kq\cos(\sphericalangle(\vec{k}, \vec{q}))} \tag{C.89}$$

$$k_p = |\vec{k}' + \vec{q}| = \sqrt{k'^2 + q^2 + 2k'q\cos(\sphericalangle(\vec{k}', \vec{q}))}\,. \tag{C.90}$$

We are making use of Eq. (B.51). It is

$$\begin{aligned}
0 =& \frac{3Na^3}{4\pi^4}\int d^3\vec{k}' \frac{3Na^3}{4\pi^4}\int d^3\vec{q} \int_0^{2k_{max}} dk_m \int_0^{2k_{max}} dk_p\, \delta(k_m - |\vec{k} - \vec{q}|) \\
& \times \delta(k_p - |\vec{k}' + \vec{q}|) \cdot |V_{\mathrm{ex}}|^2 \cdot T_1(k, k', k_m, k_p)\, \delta(\epsilon_{\vec{k}} + \epsilon_{\vec{k}'} - \epsilon_{\vec{k}-\vec{q}} - \epsilon_{\vec{k}'+\vec{q}}) \\
=& \frac{3Na^3}{4\pi^4}\int d^3\vec{k}' \frac{3Na^3}{4\pi^4}\int d^3\vec{q} \int_0^{2k_{max}} dk_m \int_0^{2k_{max}} dk_p\, \delta(k_m - \sqrt{k^2 + q^2 - 2kq\cos(\sphericalangle(\vec{k}, \vec{q}))}) \\
& \times \delta(k_p - \sqrt{k'^2 + q^2 + 2k'q\cos(\sphericalangle(\vec{k}', \vec{q}))}) \cdot |V_{\mathrm{ex}}|^2 \cdot T_1(k, k', k_m, k_p)\, \delta(\epsilon_{\vec{k}} + \epsilon_{\vec{k}'} - \epsilon_{\vec{k}-\vec{q}} - \epsilon_{\vec{k}'+\vec{q}}) \\
=& \frac{3Na^3}{4\pi^4}\int d^3\vec{k}' \frac{3Na^3}{4\pi^4}\int d^3\vec{q} \int_0^{2k_{max}} dk_m \int_0^{2k_{max}} dk_p\, \delta\left(\cos(\sphericalangle(\vec{k}, \vec{q})) + \frac{k_m^2 - k^2 - q^2}{2kq}\right) \frac{k_m}{k\,q} \\
& \times \delta\left(\cos(\sphericalangle(\vec{k}', \vec{q})) - \frac{k_p^2 - k'^2 - q^2}{2k'q}\right) \frac{k_p}{k'\,q} \cdot |V_{\mathrm{ex}}|^2 \cdot T_1(k, k', k_m, k_p)\, \delta(\epsilon_{\vec{k}} + \epsilon_{\vec{k}'} - \epsilon_{\vec{k}-\vec{q}} - \epsilon_{\vec{k}'+\vec{q}})\,.
\end{aligned} \tag{C.91}$$

We have to divide the calculation into normal processes N_p and Umklapp processes U. Here, we regard the Umklapp processes of k, k', k_m and k_p. For the vector $\vec{q}$, we do not consider Umklapp processes. Thus, we find

$$0 = N_p + U\,, \tag{C.92}$$

while N_p denotes the sum for normal processes and U the sum for Umklapp processes. The delta function which contains the energy dispersion relations can be solved in two different ways. One may relocate the equation for k_m, k_p or k'. Since k_m and k_p are on an equal footing, we change the equation of the energy dispersions for k_m on the one hand and for k' on the other hand. At the end we sum up both contributions with a weighting factor of $1/2$ for both contributions respectively. Additionally, we rotate the $\vec{q}$ coordinate system in that way, that its z-axis is parallel to the vector $\vec{k}$. In the same way, we rotate the $\vec{k}'$ coordinate system in that way, that its z-axis is parallel to the vector $\vec{q}$. Thus, we can set $\sphericalangle(\vec{k}, \vec{q}) = \alpha$ and $\sphericalangle(\vec{k}', \vec{q}) = \vartheta$. Since the resulting integrand does no longer depend on the φ-angle of the

$\vec{k}'$ and $\vec{q}$ coordinate system, their integral reduces to 2π. It is

$$\begin{aligned}
N_p =& \frac{1}{2}\frac{9N^2a^6}{16\pi^8}(2\pi)^2 \int_0^{k_{max}} dk' \int_0^{k_{max}} dq \int_0^{k_{max}} dk_m \int_0^{k_{max}} dk_p \int_{-1}^{1} d\cos(\vartheta) \int_{-1}^{1} d\cos(\alpha)\, k'^2\, q^2 \\
&\times \delta\left(\cos(\alpha) + \frac{k_m^2 - k^2 - q^2}{2kq}\right) \delta\left(\cos(\vartheta) - \frac{k_p^2 - k'^2 - q^2}{2k'q}\right) \frac{k_m}{k\,q}\,\frac{k_p}{k'\,q} \\
&\times |V_{\mathrm{ex}}|^2 \cdot T_1(k,k',k_m,k_p)\,\frac{1}{2D_{ex}k_m}\,\delta\left(k_m - \sqrt{\frac{\epsilon_k + \epsilon_{k'} - \epsilon_{\vec{k}_p} - \epsilon_0}{D_{ex}}}\right) \\
&+ \frac{1}{2}\frac{9N^2a^6}{16\pi^8}(2\pi)^2 \int_0^{k_{max}} dk' \int_0^{k_{max}} dq \int_0^{k_{max}} dk_m \int_0^{k_{max}} dk_p \int_{-1}^{1} d\cos(\vartheta) \int_{-1}^{1} d\cos(\alpha)\, k'^2\, q^2 \\
&\times \delta\left(\cos(\alpha) + \frac{k_m^2 - k^2 - q^2}{2kq}\right) \delta\left(\cos(\vartheta) - \frac{k_p^2 - k'^2 - q^2}{2k'q}\right) \frac{k_m}{k\,q}\,\frac{k_p}{k'\,q} \\
&\times |V_{\mathrm{ex}}|^2 \cdot T_1(k,k',k_m,k_p)\,\frac{1}{2D_{ex}k'}\,\delta\left(k' - \sqrt{\frac{\epsilon_{k_p} + \epsilon_{k_m} - \epsilon_{\vec{k}} - \epsilon_0}{D_{ex}}}\right) \\
=& \frac{1}{2}\frac{9N^2a^6}{4\pi^6}\frac{1}{2D_{ex}} \int_0^{k_{max}} dk' \int_0^{k_{max}} dq \int_0^{k_{max}} dk_p\, k'^2\, q^2\, \Theta(k_m)\,\Theta(k_{max} - k_m)\,\Theta\left(1 - \left|\frac{k_m^2 - k^2 - q^2}{2kq}\right|\right) \\
&\times \Theta\left(1 - \left|\frac{k_p^2 - k'^2 - q^2}{2k'q}\right|\right) \frac{1}{k_m}\,\frac{k_m}{k\,q}\,\frac{k_p}{k'\,q} \cdot |V_{\mathrm{ex}}|^2 \cdot T_1(k,k',k_m,k_p)\Big|_{k_m = \sqrt{\frac{\epsilon_k + \epsilon_{k'} - \epsilon_{\vec{k}_p} - \epsilon_0}{D_{ex}}}} \\
&+ \frac{1}{2}\frac{9N^2a^6}{4\pi^6}\frac{1}{2D_{ex}} \int_0^{k_{max}} dk_m \int_0^{k_{max}} dq \int_0^{k_{max}} dk_p\, k'^2\, q^2\, \Theta(k_m)\,\Theta(k_{max} - k_m)\,\Theta\left(1 - \left|\frac{k_m^2 - k^2 - q^2}{2kq}\right|\right) \\
&\times \Theta\left(1 - \left|\frac{k_p^2 - k'^2 - q^2}{2k'q}\right|\right) \frac{1}{k'}\,\frac{k_m}{k\,q}\,\frac{k_p}{k'\,q} \cdot |V_{\mathrm{ex}}|^2 \cdot T_1(k,k',k_m,k_p)\Big|_{k' = \sqrt{\frac{\epsilon_{k_p} + \epsilon_{k_m} - \epsilon_{\vec{k}} - \epsilon_0}{D_{ex}}}} .
\end{aligned} \tag{C.93}$$

Now, we use the identities

$$\begin{aligned}
&\int_0^{k_{max}} dq\, \Theta\left(1 - \left|\frac{k_m^2 - k^2 - q^2}{2kq}\right|\right) \Theta\left(1 - \left|\frac{k_p^2 - k'^2 - q^2}{2k'q}\right|\right) \\
&\quad = \min\left[k_{max}, \min\left(k_m + k, k_p + k'\right)\right] \\
&\qquad - \min\left[k_{max}, \max\left(|k_m - k|, |k_p - k'|\right), \min\left(k_m + k, k_p + k'\right)\right]
\end{aligned} \tag{C.94}$$

$$\begin{aligned}
&\int_0^{k_{max}} dq\, q^2\, \Theta\left(1 - \left|\frac{k_m^2 - k^2 - q^2}{2kq}\right|\right) \Theta\left(1 - \left|\frac{k_p^2 - k'^2 - q^2}{2k'q}\right|\right) \\
&\quad = \frac{\left(\min\left[k_{max}, \min\left(k_m + k, k_p + k'\right)\right]\right)^3}{3} \\
&\qquad - \frac{\left(\min\left[k_{max}, \max\left(|k_m - k|, |k_p - k'|\right), \min\left(k_m + k, k_p + k'\right)\right]\right)^3}{3}
\end{aligned} \tag{C.95}$$

$$\begin{aligned}\int_0^{k_{max}} dq\, q^4\, \Theta\left(1-\left|\frac{k_m^2-k^2-q^2}{2kq}\right|\right)\, \Theta\left(1-\left|\frac{k_p^2-k'^2-q^2}{2k'q}\right|\right)\\ =&\frac{(\min\left[k_{max},\min\left(k_m+k,k_p+k'\right)\right])^5}{5}\\ &-\frac{(\min\left[k_{max},\max\left(|k_m-k|,|k_p-k'|\right),\min\left(k_m+k,k_p+k'\right)\right])^5}{5}\,. \end{aligned} \tag{C.96}$$

We define

$$|V_{\text{ex}}|^2 = |V_{\text{ex,abs}}|^2 \frac{1}{N^2} a^4 (k^2+k'^2+k_3^2+k_4^2-4q^2)^2 \tag{C.97}$$

$$|V_{\text{ex,abs}}| = \frac{J}{8} = \frac{D_{\text{ex}}}{8Sa^2}\,, \tag{C.98}$$

and

$$\begin{aligned} Q(k,k',k_m,k_p) =& a^4\cdot(k^2+k'^2+k_3^2+k_4^2)^2\cdot\left(\min\left[k_{max},\min\left(k_m+k,k_p+k'\right)\right]\right.\\ &\left.-\min\left[k_{max},\max\left(|k_m-k|,|k_p-k'|\right),\min\left(k_m+k,k_p+k'\right)\right]\right)\\ &-8a^4\cdot(k^2+k'^2+k_3^2+k_4^2)\cdot\left(\frac{(\min\left[k_{max},\min\left(k_m+k,k_p+k'\right)\right])^3}{3}\right.\\ &\left.-\frac{(\min\left[k_{max},\max\left(|k_m-k|,|k_p-k'|\right),\min\left(k_m+k,k_p+k'\right)\right])^3}{3}\right)\\ &+16a^4\cdot\left(\frac{(\min\left[k_{max},\min\left(k_m+k,k_p+k'\right)\right])^5}{5}\right.\\ &\left.-\frac{(\min\left[k_{max},\max\left(|k_m-k|,|k_p-k'|\right),\min\left(k_m+k,k_p+k'\right)\right])^5}{5}\right)\,. \end{aligned} \tag{C.99}$$

Thus, we get

$$\begin{aligned} N_p =& \frac{1}{2}\frac{9a^6}{4\pi^6}\frac{1}{2D_{ex}}\int_0^{k_{max}} dk' \int_0^{k_{max}} dk_p\, \frac{k'\,k_p}{k}\, T_1(k,k',k_m,k_p)\,\Theta(k_m)\,\Theta(k_{max}-k_m)\\ &\times |V_{\text{ex,abs}}|^2\cdot Q(k,k',k_m,k_p)\Big|_{k_m=\sqrt{\frac{\epsilon_k+\epsilon_{k'}-\epsilon_{\vec{k}_p}-\epsilon_0}{D_{ex}}}}\\ &+\frac{1}{2}\frac{9a^6}{4\pi^6}\frac{1}{2D_{ex}}\int_0^{k_{max}} dk_m \int_0^{k_{max}} dk_p\, \frac{k_m\,k_p}{k}\, T_1(k,k',k_m,k_p)\,\Theta(k_m)\,\Theta(k_{max}-k_m)\\ &\times |V_{\text{ex,abs}}|^2\cdot Q(k,k',k_m,k_p)\Big|_{k'=\sqrt{\frac{\epsilon_{k_p}+\epsilon_{k_m}-\epsilon_{\vec{k}}-\epsilon_0}{D_{ex}}}}\,. \end{aligned} \tag{C.100}$$

This expression (cf. Eq. (5.80)) will be evaluated numerically in section 7. For the Umklapp processes we choose a symmetrized way. It is

$$\begin{aligned} U =& \frac{1}{2}\,N_p\left(k_p\in[k_{max},2k_{max}]\right)+\frac{1}{2}\,\frac{k_m}{|2k_{max}-k_m|}\,N_p\left(k_m\in[k_{max},2k_{max}]\right)\\ &+\frac{1}{2}\,\frac{k_m}{|2k_{max}-k_m|}\,N_p\left(k_p\in[k_{max},2k_{max}]\wedge k_m\in[k_{max},2k_{max}]\right)\\ &+\frac{1}{2}\,N_p\left(k'\in[k_{max},2k_{max}]\right)+\frac{1}{2}\,N_p\left(k\in[k_{max},2k_{max}]\right)\\ &+\frac{1}{2}\,N_p\left(k\in[k_{max},2k_{max}]\wedge k'\in[k_{max},2k_{max}]\right)\,. \end{aligned} \tag{C.101}$$

The extra factor in the second and third summand arises from a different algebraic term of the energy dispersion $\epsilon_{\vec{k}_m} = \omega_H + D_{ex}(2k_{max} - k_m)^2$ for $k_m \in [k_{max}, 2k_{max}]$.

Acknowledgments

First of all I would like to thank and express my deep gratitude to Tamara S. Nunner for supervising my thesis. I am very thankful, that she spent a lot of time for our joint research and supervising my thesis. I am also very appreciative of her scientific enthusiasm and endurance in uncountable discussions that have inspired me for my/our work and my/our calculations throughout the past years. Her support and careful guidance was very helpful for writing the thesis.

Furthermore, I would like to thank Piet W. Brouwer for co-referring this thesis. I have greatly benefited from and I am grateful for the collaborations with Rico Schmidt and Clemens Meyer zu Rheda. Furthermore I would like to thank the members of the Dahlem Center for Complex Quantum Systems for various discussions and providing such a friendly and inspiring atmosphere. For creating this inspiring atmosphere, I am grateful to Piet W. Brouwer and Felix von Oppen. I have taken great benefit and pleasure from scientific as well as non-scientific interaction with numerous present and former members. Moreover, I would like to thank Brigitte Odeh for her administrative support.

I also would like to show gratitude to my parents, who supported and encouraged my development since I was born. They are likable and caring people and spend much time with me growing up. Of course, I would like to thank all my friends. Friendship is the most important existing lifeblood.

I am grateful that I have studied at the Christian Albrechts-Universität zu Kiel and Freie Universität Berlin. In both institutions, I had many motivating, committed and instructive lecturers, who also made possible to write this thesis.

Finally, I acknowledge funding by the Deutsche Forschungsgemeinschaft through the priority program 1538 "Spin Caloric Transport".

Curriculum Vitae

For reasons of data protection,
the *curriculum vitae* is not included in the online version of this thesis.

Literature

[1] P. Grünberg, R. Schreiber, Y. Pang, M. B. Brodsky and H. Sowers. Layered Magnetic Structures: Evidence for Antiferromagnetic Coupling of Fe Layers across Cr Interlayers. *Phys. Rev. Lett.* 57, 2442 (1986).

[2] M. N. Baibich, J. M. Broto, A. Fert, F. Nguyen Van Dau, F. Petroff, P. Eitenne, G. Creuzet, A. Friederich, and J. Chazelas. Giant Magnetoresistance of (001)Fe/(001)Cr Magnetic Snperlattices. *Phys. Rev. Lett.* 61, 2472 (1988).

[3] G. Binasch, P. Grünberg, F. Saurenbach and W. Zinn. Enhanced magnetoresistance in layered magnetic structures with antiferromagnetic interlayer exchange. *Phys. Rev. B* 39, 4828 (1989).

[4] M. I. D'yakonov and V. I. Perel'. Possibility of Orienting Electron Spins with Current. *Sov. Phys. JETP Lett.* 13, 467 (1971).

[5] M. I. D'yakonov and V. I. Perel'. Current-induced spin orientation of electrons in semiconductors. *Phys. Lett. A* 35, 459 (1971).

[6] J. E. Hirsch. Spin Hall Effect. *Phys. Rev. Lett.* 83, 1834 (1999).

[7] Y. K. Kato, R. C. Myers, A. C. Gossard and D. D. Awschalom. Observation of the Spin Hall Effect in Semiconductors. *Science* 306 (5703), 1910 (2004).

[8] J. Wunderlich, B. Kaestner, J. Sinova and T. Jungwirth. Experimental Observation of the Spin-Hall Effect in a Two-Dimensional Spin-Orbit Coupled Semiconductor System. *Phys. Rev. Lett.* 94, 047204 (2005).

[9] V. Sih, R. C. Myers, Y. K. Kato, W. H. Lau, A. C. Gossard and D. D. Awschalom. Spatial imaging of the spin Hall effect and current-induced polarization in two-dimensional electron gases. *Nat. Phys.* 1, 31 (2005).

[10] A. A. Bakun, B. P. Zakharchenya, A. A. Rogachev, M. N. Tkachuk and V. G. Fleisher. Observation of a surface photocurrent caused by optical orientation of electrons in a semiconductor. *Sov. Phys. JETP Lett.* 40, 1293 (1984).

[11] H. Zhao, E. J. Loren, H. M. van Driel and A. L. Smirl. Coherence Control of Hall Charge and Spin Currents. *Phys. Rev. Lett.* 96, 246601 (2006).

[12] E. Saitoh, M. Ueda, H. Miyajima and G. Tatara. Conversion of spin current into charge current at room temperature: Inverse spin-Hall effect. *Appl. Phys. Lett.* 88 (18), 182509 (2006).

[13] S. O. Valenzuela and M. Tinkham. Direct electronic measurement of the spin Hall effect. *Nature* 442, 176 (2006).

[14] T. Kimura, Y. Otani, T. Sato, S. Takahashi and S. Maekawa. Room-Temperature Reversible Spin Hall Effect. *Phys. Rev. Lett.* 98, 156601 (2007).

[15] W. Mathis. Seebeck, Thomas Johann. *Neue Deutsche Biographie* 24 (2010), S. 132-133 [Onlinefassung]; URL: http://www.deutsche-biographie.de/ppn117654698.html

[16] R. D. Barnard. Thermoelectricity in metals and alloys. *Taylor & Francis* (1972).

[17] K. Uchida, S. Takahashi, K. Harii, J. Ieda, W. Koshibae, K. Ando, S. Maekawa and E. Saitoh. Observation of the spin Seebeck effect. *Nat. Lett.* 455, 778 (2008).

[18] K. Uchida, T. Ota, K. Harii, S. Takahashi, S. Maekawa, Y. Fujikawa and E. Saitoh. Spin-Seebeck effects in $Ni_{81}Fe_{19}$ films. *Solid State Commun.* 150, 524 (2010).

[19] C. M. Jaworski, J. Yang, S. Mack, D. D. Awschalom, J. P. Heremans and R. C. Myers. Observation of the spin-Seebeck effect in a ferromagnetic semiconductor. *Nat. Mater.* 9, 898 (2010).

[20] K. Uchida, T. Ota, H. Adachi, J. Xiao, T. Nonaka, Y. Kajiwara, G. E. W. Bauer, S. Maekawa and E. Saitoh. Thermal spin pumping and magnon-phonon-mediated spin-Seebeck effect. *J. Appl. Phys.* 111, 103903 (2012).

[21] K. Uchida, J. Xiao, H. Adachi, J. Ohe, S. Takahashi, J. Ieda, T. Ota, Y. Kajiwara, H. Umezawa, H. Kawai, G. E. W. Bauer, S. Maekawa and E. Saitoh. Spin Seebeck insulator. *Nat. Mater.* 9, 894 (2010).

[22] K. Uchida, H. Adachi, T. An, T. Ota, M. Toda, B. Hillebrands, S. Maekawa, and E. Saitoh. Long-range spin Seebeck effect and acoustic spin pumping. *Nat. Mater.* 10, 737 (2011). on MgO substrates. *J. Appl. Phys.* 111, 07B106 (2012).

[23] J. Xiao, G. E. W. Bauer, K. Uchida, E. Saitoh, and S. Maekawa. Theory of magnon-driven spin Seebeck effect. *Phys. Rev. B* 81, 214418 (2010).

[24] D. J. Sanders and D. Walton. Effect of magnon-phonon thermal relaxation on heat transport by magnons. *Phys. Rev. B* 15, 1489 (1977).

[25] H. Adachi, K. Uchida, E. Saitoh, J. Ohe, S. Takahashi and S. Maekawa. Gigantic enhancement of spin Seebeck effect by phonon drag. *Appl. Phys. Lett.* 97, 252506 (2010).

[26] H. Adachi, J. Ohe, S. Takahashi and S. Maekawa. Linear-response theory of spin Seebeck effect in ferromagnetic insulators. *Phys. Rev. B* 83, 094410 (2011).

[27] J. Ohe, H. Adachi, S. Takahashi and S. Maekawa. Numerical study on the spin Seebeck effect. *Phys. Rev. B* 83, 115118 (2011).

[28] K. Uchida, H. Adachi, T. Ota, H. Nakayama, S. Maekawa and E. Saitoh. Observation of longitudinal spin-Seebeck effect in magnetic insulators. *Appl. Phys. Lett.* 97, 172505 (2010).

[29] K. Uchida, T. Nonaka, T. Ota and E. Saitoh. Longitudinal spin-Seebeck effect in sintered polycrystalline (Mn,Zn)Fe_2O_4. *Appl. Phys. Lett.* 97, 262504 (2010).

[30] C. M. Jaworski, J. Yang, S. Mack, D. D. Awschalom, R. C. Myers and J. P. Heremans. Spin-Seebeck Effect: A Phonon Driven Spin Distribution. *Phys. Rev. Lett.* 106, 186601 (2011).

[31] M. Agrawal, V. I. Vasyuchka, A. A. Serga, A. D. Karenowska, G. A. Melkov and B. Hillebrands. Direct Measurement of Magnon Temperature: New Insight into Magnon-Phonon Coupling in Magnetic Insulators. *Phys. Rev. Lett.* 111, 107204 (2013).

[32] K. S. Tikhonov, J. Sinova and A. M. Finkel'stein. Spectral non-uniform temperature and non-local heat transfer in the spin Seebeck effect. *Nat. Comm.* 4, 1945 (2013).

[33] M. Schmid, S. Srichandan, D. Meier, T. Kuschel, J.-M. Schmalhorst, M. Vogel, G. Reiss, C. Strunk and C. H. Back. Transverse Spin Seebeck Effect versus Anomalous and Planar Nernst Effects in Permalloy Thin Films. *Phys. Rev. Lett.* 111, 187201 (2013).

[34] S. Y. Huang, W. G. Wang, S. F. Lee, J. Kwo and C. L. Chien. Intrinsic Spin-Dependent Thermal Transport. *Phys. Rev. Lett.* 107, 216604 (2011).

[35] A. D. Avery, M. R. Pufall and B. L. Zink. Observation of the Planar Nernst Effect in Permalloy and Nickel Thin Films with In-Plane Thermal Gradients. *Phys. Rev. Lett.* 109, 196602 (2012).

[36] D. Meier, D. Reinhardt, M. Schmid, C. H. Back, J.-M. Schmalhorst, T. Kuschel and G. Reiss. Influence of heat flow directions on Nernst effects in Py/Pt bilayers. *Phys. Rev. B* 88, 184425 (2013).

[37] C. T. Bui and F. Rivadulla. Anomalous and planar Nernst effects in thin films of the half-metallic ferromagnet $La_{2/3}Sr_{1/3}MnO_3$. *Phys. Rev. B* 90, 100403(R) (2014).

[38] I. V. Soldatov, N. Panarina, C. Hess, L. Schultz and R. Schäfer. Thermoelectric effects and magnetic anisotropy of $Ga_{1-x}Mn_xAs$ thin films. *Phys. Rev. B* 90, 104423 (2014).

[39] D. Meier, D. Reinhardt, M. van Straaten, C. Klewe, M. Althammer, M. Schreier, S. T. B. Goennenwein, A. Gupta, M. Schmid, C. H. Back, J.-M. Schmalhorst, T. Kuschel and G. Reiss. Longitudinal spin Seebeck effect contribution in transverse spin Seebeck effect experiments in Pt/YIG and Pt/NFO. *Nat. Comm.* 6, 8211 (2015).

[40] A. S. Shestakov, M. Schmid, D. Meier, T. Kuschel and C. H. Back. Dependence of transverse magneto-thermoelectric effects on inhomogeneous magnetic fields. arXiv:cond-mat/1510.07241v1 (2015)

[41] G. P. Srivastava. The physics of phonons. *Adam Hilger*, (1990)

[42] N. W. Ashcroft and N. D. Mermin. Solid State Physics. *Cengage Learning*, (1976).

[43] A. G. Gurevich and G. A. Melkov. Magnetization Oscillations and Waves. *CRC Press*, Inc. (1996).

[44] L. Boltzmann. Weitere Studien über das Wärmegleichgewicht unter Gasmolekülen. Wiener Berichte 66, 275 (1872).

[45] P. W. Brouwer. Theoretical Solid State Physics. *Lecture notes of summer semester 2015, Freie Universität Berlin*, (2015)

[46] J. M. Ziman. Electrons and phonons. *Clarendon Press*, (1972).

[47] O. Madelung. Festkörpertheorie 2 - Wechselwirkungen. *Heidelberger Taschenbücher*, (1972).

[48] Neelmani and G. S. Verma. Phonon Conductivity of Trivalent Rare-Earth-Doped Gallium and Aluminium Garnets. *Phys. Rev. B* 6, 3509 (1972).

[49] J. Callaway. Model for Lattice Thermal Conductivity at Low Temperatures. *Phys. Rev* 113, 1046 (1959).

[50] M. Abramowitz and I. A. Stegun. Handbook of mathematical functions. *Dover New York*, tenth edition, 1972.

[51] M. I. Kaganov and V. M. Tsukernik. Phenomenological theory of kinetic processes in ferromagnetic dielectric. Pt. 2. Interaction of spin waves with phonons. *Sov. Phys. JETP* 9, 151 (1959).

[52] M. A. Gilleo and S. Geller. Magnetic and Crystallographic Properties of Substituted Yttrium-Iron Garnet, $3Y_2O_3{\cdot}x\ M_2O_3{\cdot}$ (5-x) Fe_2O_3. *Phys. Rev.* 110, 73 (1958).

[53] A. Kreisel, F. Sauli, L. Bartosch and P. Kopietz. Microscopic spin-wave theory for yttrium-iron garnet films. *Eur. Phys. J. B* 71, 59-68 (2009).

[54] A. Altland and B. Simons. Condensed Matter Field Theory. *Cambridge university press* Second edition (2010).

[55] M. Schreier, A. Kamra, M. Weiler, J. Xiao, G. E. W. Bauer, R. Gross and S. T. B. Goennenwein. Magnon, phonon, and electron temperature profiles and the spin Seebeck effect in magnetic insulator/normal metal hybrid structures. *Phys. Rev. B* 88, 094410 (2013).

[56] M. I. Kaganov and V. M. Tsukernik. Phenomenological theory of kinetic processes in ferromagnetic dielectrics. *Sov. Phys. JETP* 7, No. 6, 1107 (1958).

[57] R. Schmidt, F. B. Wilken and T. S. Nunner. *unpublished*

[58] S. Gangadharaiah and A. L. Chernyshev. Thermal drag revisited: Boltzmann versus Kubo. *Phys. Rev. B* 82, 134421 (2010).

[59] W. Strauss. Magnetoelastic Properties of Yttrium-Iron Garnet. *Physical Acoustics, Principles and Methods* Vol. 4, Pt. B, Applications to Quantum and Solid State Physics, Academic Press, New York, 211-268 (2009).

[60] K. Uchida, A. Kirihara, M. Ishida, R. Takahashi and E. Saitoh. Local Spin-Seebeck Effect Enabling Two-Dimensional Position Sensing. *Jpn. J. Appl. Phys.* 50, 120211 (2011).

Abstract

In the present theoretical thesis, we analyze the influence of quasiballistic phonons to the transverse spin Seebeck effect by making use of the Boltzmann equation.

The setup for the transverse spin Seebeck effect consists of an insulating and non magnetic GGG-substrate ($Gd_3Ga_5O_{12}$), where a temperature gradient is applied. On top of the substrate, there is evaporated a thin film out of a ferrimagnetic and here insulating YIG ($Y_3Fe_5O_{12}$). The temperature gradient is applied parallel to the surface of the YIG-film. The heat reservoirs are modeled as ideal heat reservoirs. On top of the YIG-film, there are platinum stripes to detect the transverse spin Seebeck voltage.

The first experimental observation of the transverse spin Seebeck effect was made by Uchida *et al.* as reported in 2008 [17] and on YIG as reported in 2010 [21]. Agrawal *et al.* [31] as reported in 2013 and later other groups made contradictory observations to the transverse spin Seebeck effect. This motivates us to perform a wave-vector dependent calculation of the phonon temperature and the magnon temperature in the YIG-film based on local interactions. Because the thickness of the YIG-film is much smaller than the thickness of the GGG substrate, we start our calculation by calculating the wave number dependent phonon temperature profile in the GGG substrate. Therefore, we set up a Boltzmann equation and perform a relaxation time approximation. Phonons with a large wave number have a small relaxation length and thus take the temperature of the phonons in the proximity. In contrast, phonons with a small wave number have a long relaxation length and scatter nearly hitchless in the substrate. Thus, the slope of the temperature profile is smaller for small wave number phonons.

To calculate the wave number dependent magnon temperature in the YIG-film, we set up a Boltzmann equation for the magnons. Here, we consider phonon-magnon interaction and magnon-magnon interaction as well. The wave number dependent phonon temperature is taken as an input parameter. For the magnons, we include exchange magnons and dipolar magnons. Umklapp processes are neglected for magnons. After some analytic transformations and approximations, we end up with a system of linear equations for the wave number dependent magnon temperature and solve this system. For large wave number magnons we find a large slope in the temperature profile, while for small wave number magnons we find a small slope in the temperature profile.

Furthermore, we analyze the spin pumping mechanism between an insulating ferromagnet and a normal metal by making use of the Boltzmann equation. In our theory, we assume an intermediate layer between the ferromagnet and the normal metal, where the sd-interaction between magnons and electrons takes place. At the end, we find a spin current induced in the normal metal, which is proportional to the temperature difference between magnons in the ferromagnet and electrons in the normal metal.

At the end we calculate the transverse spin Seebeck voltage by using three different theories. For overall average temperatures much smaller than room temperature, we find a larger value as for room temperature. For small temperatures, we find a result in the order of nanovolts or tenth of nanovolts.

Kurzfassung

In der vorliegenden Arbeit haben wir den Einfluss von quasi-ballistisch propagierenden Phononen auf den transversalen Spin Seebeck Effekt untersucht. Hierbei haben wir die Boltzmann-Gleichung verwendet.

Der experimentelle Aufbau für den transversalen Spin Seebeck Effekt besteht aus einem isolierenden nicht magnetischen GGG-Substrat ($Gd_3Ga_5O_{12}$), an dem ein Temperatur-Gradient angelegt ist. Obenauf befindet sich eine aufgedampfte Schicht aus einem ferrimagnetischem und hier isolierenden YIG ($Y_3Fe_5O_{12}$). Der Temperatur-Gradient ist parallel zur Oberfläche des YIG-Films angelegt und die Wärmebäder werden als ideale Wärmebäder modelliert. Auf dem YIG-Film befinden sich Platin-Streifen, um die transversale Spin Seebeck Spannung zu detektieren.

Über die erste experimentelle Entdeckung des transversalen Spin Seebeck Effekt wurde von Uchida *et al.* im Jahr 2008 [17] und mit YIG im Jahr 2010 [21] berichtet. Agrawal *et al.* [31] und später auch andere Gruppen haben widersprüchliche experimentelle Beobachtungen zum transversalen Spin Seebeck Effekt gemacht. Dieses motiviert uns dazu, eine Wellenvektor-abhängige Rechnung von der Phonon-Temperatur und der Magnon-Temperatur durchzuführen, welche auf lokalen Wechselwirkungen basiert. Weil die Dicke des YIG-Filmes sehr viel kleiner gegenüber der Dicke des GGG-Substrates ist, beginnen wir mit der Berechnung der Wellenvektor-abhängigen Phonon-Temperatur im GGG-Substrat. Dafür stellen wir eine Boltzmann-Gleichung auf und führen eine Relaxationszeit-Näherung durch. Phononen mit einer hohen Wellenzahl haben eine kleine Relaxationslänge und nehmen deswegen die Temperatur der Phononen in der Umgebung an. Hingegen nehmen Phononen mit einer kleinen Wellenzahl eine lange Relaxationslänge an und streuen fast gar nicht im Substrat. Daher ist die Steigung des Temperatur-Profiles für kleine Wellenzahl-Phononen kleiner.

Um die Wellenvektor-abhängige Magnon-Temperatur im YIG-Film auszurechnen, stellen wir eine Boltzmann-Gleichung für Magnonen auf. Hier berücksichtigen wir Phonon-Magnon- und Magnon-Magnon-Wechselwirkungen. Die Wellenvektor-abhängige Phonon-Temperatur wird hier als Input verwendet. Für die Magnonen berücksichtigen wir sowohl Austausch-Magnonen ebenso wie dipolare Magnonen. Umklapp-Prozesse sind bei Magnonen vernachlässigt. Nach analytischen Term-Umformungen und Näherungen gelangen wir zu einem linearen Gleichungssystem für die Wellenzahl-abhängige Magnon-Temperatur und lösen dieses Gleichungssystem. Für Magnonen mit einer hohen Wellenzahl finden wir eine große Steigung im Temperatur-Profil, wohingegen wir eine flache Steigung im Temperatur-Profil für Magnonen mit einer kleinen Wellenzahl finden.

Darüber hinaus analysieren wir den Spin-Pump-Mechanismus zwischen einem isolierenden Ferromagneten und einem normal leitendem Metall, wobei wir die Boltzmann-Gleichung verwenden. In unserer Theorie nehmen wir an, dass sich zwischen dem Ferromagneten und dem normalem Metall eine dünne Schicht befindet, in der die SD-Wechselwirkung zwischen Magnonen und Elektronen stattfinden kann. Am Ende finden wir einen im normalen Metall induzierten Spin-Strom, welcher proportional zur Temperatur-Differenz zwischen den Magnonen im Ferromagneten und den Elektronen im normalen Metall ist.

Am Ende rechnen wir die transversale Spin Seebeck Spannung aus, wobei wir hierfür drei verschiedene Theorien verwenden. Für Gesamt-Mittelwert-Temperaturen, welche viel kleiner als Zimmertemperatur sind, finden wir einen größeren Wert als bei Zimmertemperatur. Für entsprechend kleine Temperaturen finden wir Spannungen in der Größe von Nanovolt oder Zehntel-Nanovolt.